ISSN 2075-8545 (online)
ASI • CAS • CrossRef • CNKI • DOAJ • EBSCO Publishing • ESCI Web of Science • EZB • eLIBRARY.RU • Google Scholar • HEAL Link
ICI Journals Master List • Metaphora • OAJI • ProQuest • Readera • ResearchBib • ResearchGate • Scopus • Ulrich's Periodicals Directory

NANOTECHNOLOGIES IN CONSTRUCTION
NANOTEKHNOLOGII V STROITEL'STVE
A Scientific Internet-Journal
2026 • Tom 18 • No. 5



IN THE ISSUE:

- SCALING UP THE APPLICATION PROCESS OF "NI–SIC" METAL-MATRIX COMPOSITE COATING
- CHOICE OF A METHOD FOR ASSESSING THE DEPTH OF THE TEMPERED LAYER IN A MARTENSITIC STEEL WELDED JOINT
- ANALYSIS OF THE OWLv2 MODEL USAGE FOR REAL-TIME OBJECT DETECTION
- STUDY OF THE EFFECT OF PART GEOMETRY ON THE PRESSURE RISE LAW OF THE FORMING GAS USING COMPUTER SIMULATION

www.nanobuild.ru e-mail: info@nanobuild.ru

ISSUED WITH SUPPORT OF

РОССИЙСКАЯ ИНЖЕНЕРНАЯ АКАДЕМИЯ
RUSSIAN ACADEMY OF ENGINEERING

NANOTECHNOLOGIES IN CONSTRUCTION
NANOTEKHNOLOGII V STROITEL'STVE
НАНОТЕХНОЛОГИИ В СТРОИТЕЛЬСТВЕ: НАУЧНЫЙ ИНТЕРНЕТ-ЖУРНАЛ

ISSN 2075-8545 (online)

«Nanotechnologies in Construction» is a peer-reviewed journal.

The Journal's main objectives are:

- to provide information support for the development and implementation of knowledge-intensive technologies and new materials in construction, housing and utilities, mechanical engineering, energy, and other fields;
- to improve the scientometric indicators of authors (citation counts, h-index, number of publications, etc.).

The main tasks:

- Providing scientists and specialists from different countries with the opportunity to publish the results of their research and receive information about modern technologies and materials, high-performance equipment in construction, communal and housing services, joint areas (industry, power et al.).
- To provide information support and participate in the events (forums, conferences, symposia, workshops, exhibitions,round tables etc) devoted to nanoindustry and problems of application of nanoindustry in construction and housing and communal services, which are perspective and of great importance.

The Journal has been published since 2009. Frequency: bimonthly.

These are the topics of the papers published in the journal: creation of new functional materials; nanostructured systems strength and penetrability formation theory development; the problems of nanomaterials and nanotechnologies implementation in construction and building materials; diagnostics of building systems nanostructures and nanomaterials; technologies aimed at studying nanomaterial properties; technological principles of nanostructures creation (liquid melts, sol and gel synthesis). The topics may be different, directly or indirectly related to the areas mentioned above.

The journal publishes: original papers; reviews; discussing materials, comments, other information materials.

The language of publication: English; Russian.

The edition's readers and authors are:

- students, lecturers, post-graduates and people working for doctor's degree;
- scientists and specialists of research institutes and nanotechnological centers;
- heads and specialists of the institutions, organizations and factories from the sphere of construction and housing and communal services;
- scientists and specialists of the industries which are adjacent to construction;
- experts of the enterprise-producers manufacturing nanoindustrial output.

EDITORS

EDITOR-IN-CHIEF – Boris V. GUSEV, Dr. Sci. (Eng.), Professor, Corresponding Member of the Russian Academy of Sciences, Academician of the Russian Academy of Engineering and the International Academy of Engineering, President, Russian Academy of Engineering, Gazetny per., 9, bldg. 4, Moscow, 125009, Russian Federation, SPIN: 3578-5498, AuthorID: 14638, ResearcherID: J-3271-2017, Scopus Author ID: 7006276535, https://orcid.org/0000-0003-2718-9539
Contacts: e-mail: info@nanobuild.ru, info-rae@mail.ru

EXECUTIVE EDITORIAL SECRETARY – Vladimir I. VEDENYAPIN, Moscow, Russian Federation
Contacts: e-mail: pr@nanobuild.ru, info@nanobuild.ru

DEPUTY EDITOR-IN-CHIEF – Leonid A. IVANOV, Dr. (Inf. Tech.), Cand. Sci. (Eng.), Senior Researcher, Academician of the Russian Academy of Engineering and the International Academy of Engineering, Visiting Professor at Wuhan University of Technology, China, Honorary Professor at Shantou University, China, Honorary Professor of University of Electronic Science and Technology of China (UESTC), First Vice-President – Chief Scientific Secretary, Russian Academy of Engineering, Gazetny per., 9, bldg. 4, Moscow, 125009, Russian Federation, AuthorID: 876704, ResearcherID: J-3885-2017, Scopus Author ID: 57220927491, https://orcid.org/0000-0001-9513-8712
Contacts: e-mail: info@nanobuild.ru, l.a.ivanov@mail.ru

EXECUTIVE EDITOR – Yulia A. EVSTIGNEEVA, Member of the Russian Association of Journalists, Moscow, Russian Federation
Contacts: e-mail: info@nanobuild.ru, evstigneeva.ju@yandex.ru

HEAD OF DESIGN DEPARTMENT – Andrey S. REZNICHENKO, Businessman, Moscow, Russian Federation
Contacts: e-mail: info@nanobuild.ru, ras77222@yandex.ru

CHIEF FOR FOREIGN RELATIONS – Zhanna V. PISARENKO, Doctor of Economics, Professor assistant, Corresponding member of the Russian Academy of Engineering, Member of the International Expert Public Advisory Council of the Basic Organization of the CIS Member States for Training, Professional Retraining and Advanced Training of Personnel in the Field of Insurance (Dushanbe, Tajikistan), Chairman of the Scientific Commission in Economics and Business, St Petersburg University, Professor of the Department of Risk Management and Insurance, St. Petersburg State University, 7/9, Universitetskaya Embankment, Saint Petersburg, 199034, Russian Federation, SPIN: 3850-0954, AuthorID: 409029, ResearcherID: R-5567-2016, Scopus Author ID: 57190213592, https://orcid.org/0000-0002-9082-2897
Contacts: e-mail: info@nanobuild.ru, z.pisarenko@spbu.ru

EDITORIAL BOARD

CHAIRMAN OF THE EDITORIAL BOARD – EDITOR-IN-CHIEF OF THE JOURNAL

Boris V. GUSEV – Dr. Sci. (Eng.), Professor, Corresponding Member of the Russian Academy of Sciences, Academician of the Russian Academy of Engineering and the International Academy of Engineering, President, Russian Academy of Engineering, Gazetny per., 9, bldg. 4, Moscow, 125009, Russian Federation, SPIN: 3578-5498, AuthorID: 14638, ResearcherID: J-3271-2017, Scopus Author ID: 7006276535, info-rae@mail.ru, https://orcid.org/0000-0003-2718-9539

MEMBERS OF THE EDITORIAL BOARD

Sergey M. ABRAMOV – Dr. Sci. (Phys.-Math.), Corresponding Member of the Russian Academy of Sciences, Chief Researcher, Program Systems Institute named after A. K. Ailamazyan of the Russian Academy of Science, Peter Great street, 4A, Veskovo Village, Pereslavsky District, Yaroslavl region, 152021, Russian Federation, SPIN: 4196-5775, AuthorID: 1927, ResearcherID: AAW-1963-2021, Scopus Author ID: 7005979792, abram@botik.ru, https://orcid.org/0000-0001-6603-7971

ISSN 2075-8545 (online)

Nanotechnologies in construction
Нанотехнологии в строительстве

2026; 18 (5):
576–577

Nanobuild.ru

Leonid A. IVANOV – Dr. (Inf. Tech.), Cand. Sci. (Eng.), Senior Researcher, Academician of the Russian Academy of Engineering and the International Academy of Engineering, Visiting Professor at Wuhan University of Technology, China, Honorary Professor at Shantou University, China, Honorary Professor of University of Electronic Science and Technology of China (UESTC), First Vice-President – Chief Scientific Secretary, Russian Academy of Engineering, Gazetny per., 9, bldg. 4, Moscow, 125009, Russian Federation, AuthorID: 876704, ResearcherID: J-3885-2017, Scopus Author ID: 57220927491, l.a.ivanov@mail.ru, ORCID: https://orcid.org/0000-0001-9513-8712

Evgeny N. KABLOV – Dr. Sci. (Eng.), Professor, Academician of the Russian Academy of Sciences, Deputy President, Russian Academy of Sciences, Leninsky Prospect, build. 32-A, Moscow, 119334, Russian Federation, ENKablov@pran.ru

Evgeny V. KOROLEV – Dr. Sci. (Eng.), Professor, Academician of the Russian Academy of Engineering, Vice-Rector for Research, St. Petersburg State University of Architecture and Civil Engineering, 4, 2nd Krasnoarmeiskaya Str., Saint Petersburg, 190005, Russian Federation, SPIN: 1249-6325, AuthorID: 351849, ResearcherID: Q-4873-2019, Scopus Author ID: 37099331400, prorector_nr@spbgasu.ru, https://orcid.org/0000-0003-3600-812X

Vladimir A. LABUNOV – Dr. Sci. (Eng.), Professor, Foreign Member of the Russian Academy of Sciences, Academician of National Academy of Sciences of Belarus, Academician of International Academy of Informatization and of Belarusian Engineering-Technological Academy, Head of the Scientific-Research LAB of the Belarusian State University of Informatics and Radioelectronics, 220013, Minsk, P.Brovki str. 6, Republic of Belarus, V.labunov@bsuir.by

Polad MALKIN – Dr. Sci. (Phys.-Math.), Professor, Foreign Member of the Russian Academy of Engineering, Member of the Association of Engineers and Architects, Israel, Managing Director, Construction Project Office, M-Group / E. Weisberg, 10 Jerusalem St., Haifa 3313218, Israel, SPIN: 4040-5244, Polad.malkin@gmail.com, https://orcid.org/0000-0001-7995-7662

Zhanna V. PISARENKO – Doctor of Economics, Professor assistant, Corresponding member of the Russian Academy of Engineering, Member of the International Expert Public Advisory Council of the Basic Organization of the CIS Member States for Training, Professional Retraining and Advanced Training of Personnel in the Field of Insurance (Dushanbe, Tajikistan), Chairman of the Scientific Commission in Economics and Business, St. Petersburg University, Professor of the Department of Risk Management and Insurance, St. Petersburg State University, 7/9, Universitetskaya Embankment, Saint Petersburg, 199034, Russian Federation, SPIN: 3850-0954, AuthorID: 409029, ResearcherID: R-5567-2016, Scopus Author ID: 57190213592, z.pisarenko@spbu.ru, https://orcid.org/0000-0002-9082-2897

Leonid S. RATKIN – Cand. Sci. (Eng.), Professor at the Academy of Military Sciences, Academician of the Russian Academy of Engineering and the International Academy of Engineering, Full member of International Academy of Transport, International Communication Academy, Scientific Secretary of Council of Veterans of Russian Academy of Sciences, Leninsky Prospect, build. 74, Moscow, 119991, Russian Federation, SPIN-код: 4298-7150, AuthorID: 1078615, Scopus Author ID: 359201511000, Rathkeen@bk.ru, https://orcid.org/0000-0003-4193-5075

Alexander S. SIGOV – Dr. Sci. (Phys.-Math.), Professor, Academician of the Russian Academy of Sciences, member: MRS, IOP, IET, IEEE, EPS; President, MIREA – Russian Technological University, Moscow, Vernadsky Avenue 78, 119454, Russian Federation, AuthorID: 17622, ResearcherID: U-2545-2019, Scopus Author ID: 35557510600, assigov@yandex.ru, https://orcid.org/0000-0002-1216-3339

Konstantin SOBOLEV – Ph.D. in Construction Materials, Professor, Member, Mexican Academy of Sciences, Fellow and active committee member, American Concrete Institute (ACI), Founding Chair, ACI 241/236D Nanotechnology of Concrete, Co-founder & Vice President, Concrete Nanotechnology and Nanoscience Society (CNNS), Professor, Department of Civil and Environmental Engineering, College of Engineering and Applied Science, University of Wisconsin-Milwaukee, P.O. Box 784, Milwaukee, WI 53201, USA, sobolev@uwm.edu

Li D. XU – Ph.D., Professor, Foreign Member of the Russian Academy of Sciences and the Russian Academy of Engineering, Academician of the European Academy of Sciences, Fellow of the Institute of Electrical and Electronics Engineers (IEEE), Professor, Department of Information Technology Old Dominion University, Norfolk, VA, 23529, USA, lxu@odu.edu, https://orcid.org/0000-0002-3263-5217

Larisa A. URKHANOVA – Dr. Sci. (Eng.), Professor, Academic Advisor of the Russian Academy of Engineering, Professor, Department «Transport construction», National research Moscow state university of civil engineering, 26, Yaroslavskoye Shosse, Moscow, 129337, Russian Federation, SPIN: 8925-0385, AuthorID: 457981, ResearcherID: U-1352-2017, Scopus Author ID: 6505603130, urkhanova@mail.ru, https://orcid.org/0000-0002-2716-2144

Vyacheslav R. FALIKMAN – Dr. Sci (Materials), PhD (Chem.), Senior Researcher, Full member of the Russian Academy of Engineering, Full member of the International Academy of Engineering, Honorary Life Member of the International Federation for Structural Concrete (fib), Honorary Member of the International Union of Laboratories and Experts in Construction Materials, Systems and Structures (RILEM), Fellow of the Asian Concrete Federation, Member of the American Concrete Institute, Head of the Center for Scientific and Technical Support of Complex Construction Projects, Scientific Research Center "Construction", 6, 2nd Institutskaya St., Moscow, 109428, Russian Federation, SPIN: 3437-6962, Scopus Author ID: 6507014269, vfalikman@yandex.ru, https://orcid.org/0000-0001-6232-9862

Oleg L. FIGOVSKY – Dr. Sci. (Eng.), Professor, Foreign Member of the Russian Academy of Engineering and Russian Academy of Architecture and Construction Sciences, Academician of the European Academy of Sciences, He has served as the chairman of the UNESCO "Green Chemistry," founder and director of International Nanotechnology Research Center Polymate (1998–2018), Director of R&D at Eurotech, Ltd. (1998–2008), President, Israel Inventors Association,Dr. Shimkin street, Haifa, 26110, Israel, figovsky@gmail.com

Vadim G. KHOZIN – Dr. Sci. (Eng.), Professor, Head of Department, Kazan State University of Architecture and Engineering, Kazan, 1 Zelenaya St., Kazan, 420043, Russian Federation, SPIN: 3825-6514, AuthorID: 43534, khozin.vadim@yandex.ru, https://orcid.org/0000-0003-0874-316X

Vyacheslav I. CHERNOIVANOV – Dr. Sci. (Eng.), Professor, Academician of the Russian Academy of Sciences, Russian Academy of Engineering and International Academy of Engineering, Scientific consultant, Federal Scientific Agroengineering Center VIM, Moscow, 1st Institutsky Proezd, house 5,109428, Russian Federation, SPIN: 1618-4796, AuthorID: 251571, vichernoivanov@mail.ru

The Journal is registered as an independent mass media in the Ministry of Communication and Mass Media of the Russian Federation. (Registration Certificate Эл № ФС77 – 35813 of 31 March 2009 issued by the Federal Service on Supervision in the Sphere of Connection and Mass Communications).

Founder and Publisher – Center for New Technologies «Nanostroitel'stvo», Korolev, Moscow region, Russian Federation
Contacts: e-mail: l.a.ivanov@mail.ru

Address of edition: Russian Federation, 125009, Moscow, Gazetny per., bld. 9, str. 4
Contacts: e-mail: info@nanobuild.ru

Website: http://nanobuild.ru/

Release date of № 5 Vol. 18 is 21.10.2026

ISSUED WITH SUPPORT OF

RUSSIAN ACADEMY OF ENGINEERING

ISSN 2075-8545 (online)

NANOTECHNOLOGIES IN CONSTRUCTION: A Scientific Internet-Journal 2026 • Vol. 18 • No. 5
NANOTEKHNOLOGII V STROITEL'STVE

CONTENTS

PUBLISHER INFORMATION 576

TO THE AUTHORS AND READERS 579

CONSTRUCTION MATERIALS SCIENCE

Kiseleva S.K., Akhmerov L.D., Khusnutdinova A.Z., Kandarov I.V.
Scaling up the application process of "Ni–SiC" metal-matrix composite coating 580

Mazidullin D.N., Tregubov P.P., Demchenko M.V., Akhmerov L.D., Arslanov A.A.
Assessment of the processability of applying a metal matrix coating by electrochemical deposition on an internal combustion engine cylinder 591

THE RESULTS OF THE SPECIALISTS' AND SCIENTISTS' RESEARCHES

Latypov O.R., Kim K.V., Lukyanov V.V., Latypova D.R., Daminev R.R., Khusnutdinova A.Z.
Assessment of the potential application of thermoplastic polymers for insulating the electrodes of high-temperature cartridge-type electric heaters 601

Artemenko S.O., Zhukov A.D., Medvedev A.A., Bobrova E.Yu., Pilipenko A.S.
Energy efficiency for pitched roof insulation system 609

Latypov O.R., Kim K.V., Lukyanov V.V., Latypova D.R., Daminev R.R., Ahmadullina A.F.
Creating a technology to coat the insulating material on the "cold" section of a cartridge-style electric heater for operation in aggressive environments 621

APPLICATION OF NANOMATERIALS AND NANOTECHNOLOGIES IN CONSTRUCTION

Rubin O.D., Antonov A.S., Almasri A. Experimental studies of reinforced concrete structures in the "HPP supporting piers – power-house headwall" system strengthened with prestressed basalt composite reinforcement. Part II 627

SYSTEM SOLUTIONS FOR TECHNOLOGICAL PROBLEMS

Stepanenko N.Yu., Chertovskikh S.V., Kandarov I.V., Rubtsov A.V. Study of the effect of part geometry on the pressure rise law of the forming gas using computer simulation 657

Ustyuzhanin K.Yu., Ziganshina F.T., Sadykova R.R.
Analysis of the OWLv2 model usage for real-time object detection 673

Kulakov P.A., Afanasenko V.G. Inverse kinematics algorithm for trajectories with specified tool orientation 681

Fayrushin A.M., Tumanova E.Yu., Sobachkin A.S., Imayev M.F., Tokarev A.S., Musina D.R.
Choice of a method for assessing the depth of the tempered layer in a martensitic steel welded joint 691

Stepanenko N.Yu., Chertovskikh S.V., Rubtsov A.V., Ivanov N.E.
Study of the flow characteristics of a shut-off and control device for generating a controlled gas flow 701

PUBLISHING ETHICS 713

AUTHOR GUIDELINES 717

TO AUTHORS AND READERS

Dear colleagues!

The administration of Ufa State Petroleum Technological University (USPTU) requested that the editorial board of the electronic journal Nanotechnology in Construction: Scientific Internet Journal highlight, in Issue No. 5, 2026, the key achievements of leading scientists in developing and implementing advanced technologies in construction, housing and utilities, and related sectors (industry, energy, etc.).

Currently, USPTU includes four faculties, five institutes, four higher schools, a lyceum, an Institute of Additional Professional Education, and an Engineering Center. The university also has three branches, in the cities of Oktyabrsky, Salavat, and Sterlitamak. USPTU offers a full cycle of education: general education (grades 10–11), secondary vocational education, higher education (bachelor's, specialist's, and master's degrees), training of highly qualified personnel (postgraduate studies), and additional education and vocational training programs.

In 2026, Ufa State Petroleum Technological University was ranked among the top three universities in the federal project "TOP-IT START" and received a grant to implement advanced educational programs in information technology: "Advanced Technologies for the Development and Testing of Information Systems" and "Business and System Analyst." The first program was developed and will be delivered jointly with Gazpromneft – Digital Solutions; the second, jointly with Rostelecom.

The university is actively expanding its international activities, broadening international cooperation in scientific and technical development, promoting active student and teacher exchange through academic mobility programs, and delivering a wide range of professional training and retraining programs for international specialists. More than 2,000 international students' study at the university.

In terms of research output, USPTU ranks highest in the Volga Federal District. The university participates in the federal program "Priority 2030," which supports university development programs and focuses on three strategic technological projects for the university: "Chemistry of the New Economy," "Technological Engineering and Autonomization of Production Processes in the Fuel and Energy Complex," and "New Technologies, Technical and Intelligent Systems in Mechanical Engineering." The university is actively developing scientific schools, which are rightly proud to include the names of renowned scientists—among them full members and corresponding members of the Russian Academy of Sciences and the Academy of Sciences of the Republic of Bashkortostan, as well as honored workers in education, science, technology, construction, and architecture. An integral part of the work of faculty and students is publishing articles in leading Russian and international journals.

It is gratifying to note that the editorial board of Nanotechnologies in Construction: Scientific Internet Journal met us half way and prepared an issue focused primarily on USPTU's developments. We are grateful to the editorial board for its work on this issue!

Sincerely, Vice-Rector for Research and Innovation
Denis Alekseevich Gulin

ISSN 2075-8545 (online)

Nanotechnologies in construction
Нанотехнологии в строительстве

2026; 18 (5):
580–590

Nanobuild.ru

CONSTRUCTION MATERIALS SCIENCE

CC BY 4.0

Original article
https://doi.org/10.15828/2075-8545-2026-18-5-580-590

Scaling up the application process of "Ni–SiC" metal-matrix composite coating

Svetlana K. Kiseleva[1, 2*], **Linar D. Akhmerov**[1, 2], **Aliyana Z. Khusnutdinova**[1, 2], **Irek V. Kandarov**[1, 2]

[1] Ufa State Petroleum Technological University, Ufa, Kosmonavtov str. 1, 450064, Russian Federation
[2] Scientific and Production Association "Technopark of Aviation Technologies", Ufa, Tramvaynaya str. 5, building 1, 450112, Russian Federation

* Corresponding author: e-mail: kiseleva_s2018@mail.ru

ABSTRACT

Introduction. Today, metal-matrix composite coatings are widely in demand due to the possibility of combining the properties of both the metal base and their reinforcing particles. The simplest and most technologically advanced method of coating is electrodeposition. One of the key parameters that determines the quality of the coating formed and the electrodeposition rate is current density. The literature presents opposing views on how current density affects the quality of composite coatings. The primary criterion is the volume fraction of reinforcing particles. The use of nanoparticles (less than 100 nm in size) as a hardener makes it possible to significantly increase the hardness and wear resistance of the matrix due to dispersion hardening, however, they have a high tendency to agglomeration and require more careful control of electrodeposition modes. It is important during electrodeposition to form a coating with a uniform distribution of particles in the metal matrix over the entire working area of the workpiece to ensure stability of mechanical and functional properties, which will subsequently determine the durability of the parts. From this point of view, it is of interest to scale the electrodeposition process and switch to model samples, the long size of which imitates the maximum height of a real axisymmetric part, for example, a cylinder, which will allow reproducing coating conditions close to production ones. The aim of the research is to study the homogeneity of the structure and properties of the Ni–SiC coating containing a fraction of particles larger than 2 μm and formed on long workpieces (with an area of 0.2 dm^2) in the process of electrodeposition depending on the current density. **Methods and materials.** Cast aluminum alloy AK7 was used as the substrate material for forming the Ni–SiC composite coating. The dimensions of the substrate samples were 70×20×4 mm. Electrodeposition mode: current density of 0.5 A/dm^2, 10 A/dm^2, 20 A/dm^2; duration 60 minutes; temperature 60 °C. The microstructure of the coatings was examined using a JSM-6490 LV scanning electron microscope at a magnification of ×500. Microhardness was estimated using a TBM Tochline microhardness tester at a load of 50 g. Wear resistance tests were performed on a Nanovea tribometer using the ball-on-disk method. **Results and discussion.** The technology of electrodeposition of the matrix composite coating "Ni–SiC" on long flat samples (0.2 dm^2) of aluminum alloy AK7 was developed and the optimal process parameters were selected. The possibility of forming a homogeneous coating based on a nickel matrix containing large SiC particles on flat long samples (0.2 dm^2) of aluminum alloy AK7, simulating a sector of an axisymmetric part, was demonstrated. **Conclusion.** The metal-matrix composite coating "Ni–SiC", formed on flat long samples (with an area of 0.2 dm^2) of aluminum alloy AK7 as a result of electrodeposition, is characterized by uniformity of thickness, volume fraction of silicon carbide particles and microhardness in three control zones for each current density. The higher the current density during electrodeposition, the higher the thickness of the formed Ni–SiC metal matrix composite coating, the volume fraction of reinforcing particles and the microhardness.

KEYWORDS: metal matrix composite coatings, electrodeposition, microhardness, silicon carbide, mass loss

SOURCES OF FUNDING FOR THE SCIENTIFIC WORK THAT RESULTED IN THE PUBLICATION: This work was conducted as part of the Strategic Project "New technologies, technical, and intelligent systems in mechanical engineering" of the Ufa State Petroleum Technological University Development Program for 2021–2030 in accordance with the Priority 2030 Strategic Academic Leadership Program.

ACKNOWLEDGEMENTS: The authors are grateful for the financial support of this project.

FOR CITATION:
Kiseleva S.K., Akhmerov L.D., Khusnutdinova A.Z., Kandarov I.V. Scaling up the application process of "Ni–SiC" metal-matrix composite coating. *Nanotechnologies in Construction.* 2026;18(5):580–590. https://doi.org/10.15828/2075-8545-2026-18-5-580-590. – EDN: SJSTWL.

© Kiseleva S.K., Akhmerov L.D., Khusnutdinova A.Z., Kandarov I.V., 2026

ISSN 2075-8545 (online)

Nanotechnologies in construction
Нанотехнологии в строительстве

2026; 18 (5):
580–590

Nanobuild.ru

CONSTRUCTION MATERIALS SCIENCE

Масштабирование процесса нанесения металломатричного композиционного покрытия «Ni–SiC»

Светлана Камильевна Киселева[1,2*], Линар Динарович Ахмеров[1,2], Алияна Зенфировна Хуснутдинова[1,2], Ирек Вилевич Кандаров[1,2]

[1] Уфимский государственный нефтяной технический университет, 450064, Уфа, ул. Космонавтов, 1, Российская Федерация

[2] Научно-производственная ассоциация «Технопарк Авиационных Технологий», 450112, Уфа, ул. Трамвайная 5, к. 1, Российская Федерация

* Автор, ответственный за переписку: e-mail: kiseleva_s2018@mail.ru

АННОТАЦИЯ

Введение. На сегодняшний день металломатричные композиционные покрытия являются широко востребованными благодаря возможности сочетания в себе свойств как металлической основы, так и упрочняющих их частиц. Наиболее простым и технологичным способом нанесения покрытия является электроосаждение. Одним из фундаментальных параметров, определяющим качество формируемого покрытия и скорость электроосаждения, является плотность тока. В литературе имеются противоположные мнения о влиянии плотности тока на качество композитного покрытия. Основным критерием выбирают содержание объемной доли упрочняющих частиц. Использование наночастиц (размером менее 100 нм) в качестве упрочнителя позволяет значительно повысить твердость и износостойкость матрицы за счет дисперсионного твердения, однако они обладают высокой склонностью к агломерации и требуют более тщательного контроля режимов электроосаждения. Немаловажно при электроосаждении сформировать покрытие с равномерным распределением частиц в металлической матрице по всей рабочей площади заготовки для обеспечения стабильности механических и функциональных свойств, что в дальнейшем будет определять долговечность работы деталей. С этой точки зрения представляет интерес масштабирование процесса электроосаждения и переход на модельные образцы, длинновой размер которых имитирует максимальную высоту реальной осесимметричной детали, например цилиндр, что позволит воспроизвести условия нанесения покрытия, приближённые к производственным. Цель работы – исследование однородности структуры и свойств покрытия «Ni–SiC», содержащего фракцию частиц размером более 2 мкм и сформированного на длинномерных заготовках (площадью 0,2 дм^2) в процессе электроосаждения в зависимости от плотности тока. **Методы и материалы.** В качестве материала подложки для формирования композиционного покрытия «Ni–SiC» использовали литейный алюминиевый сплав АК7. Размеры образцов подложки 70×20×4 мм. Режим электроосаждения: плотность тока 0,5 А/дм^2, 10 А/дм^2, 20 А/дм^2; продолжительность 60 минут; температура 60 °С. Микроструктуру покрытий исследовали с помощью растрового электронного микроскопа «JSM-6490 LV» при увеличении ×500. Микротвердость оценивали с использованием микротвердомера «TBM Tochline» при нагрузке 50 г. Испытания на износостойкость проводили на трибометре «Nanovea» методом «шарик-по-диску». **Результаты и обсуждение.** Проведена отработка технологии электроосаждения матричного композиционного покрытия «Ni–SiC» на длинномерные плоские образцы (0,2 дм^2) из алюминиевого сплава АК7 и подбор оптимальных параметров процесса. Продемонстрирована возможность формирования однородного покрытия на основе никелевой матрицы, содержащей крупные частицы SiC на плоских длинномерных образцах (0,2 дм^2) из алюминиевого сплава АК7, имитирующих сектор осесимметричной детали. **Выводы.** Металломатричное композитное покрытие «Ni–SiC», сформированное на плоских длинномерных образцах (площадью 0,2 дм^2) из алюминиевого сплава АК7 в результате электроосаждения, характеризуется однородностью толщины, объемной долей частиц карбида кремния и микротвердости в трех контрольных зонах для каждой плотности тока. Чем выше плотность тока при электроосаждении, тем выше толщина формируемого металломатричного композитного покрытия «Ni–SiC», объемная доля упрочняющих частиц и микротвердость.

КЛЮЧЕВЫЕ СЛОВА: металломатричные композиционные покрытия, электроосаждение, микротвердость, карбид кремния, унос массы

ИСТОЧНИКИ ФИНАНСИРОВАНИЯ НАУЧНОЙ РАБОТЫ, РЕЗУЛЬТАТОМ КОТОРОЙ СТАЛА ПУБЛИКАЦИЯ: Работа проводилась в рамках реализации Стратегического проекта «Новые технологии, технические и интеллектуальные системы в машиностроении» программы развития ФГБОУ ВО «Уфимский государственный нефтяной технический университет» на 2021–2030 годы в соответствии с программой стратегического академического лидерства «Приоритет 2030».

БЛАГОДАРНОСТИ: Авторы выражают благодарность за финансовую поддержку проекта.

ДЛЯ ЦИТИРОВАНИЯ:

Киселева С.К., Ахмеров Л.Д., Хуснутдинова А.З., Кандаров И.В. Масштабирование процесса нанесения металломатричного композиционного покрытия «Ni–SiC». *Нанотехнологии в строительстве.* 2026;18(5):580–590. https://doi.org/10.15828/2075-8545-2026-18-5-580-590. – EDN: SJSTWL.

ISSN 2075-8545 (online)

Nanotechnologies in construction
Нанотехнологии в строительстве

2026; 18 (5):
580–590

Nanobuild.ru

CONSTRUCTION MATERIALS SCIENCE

INTRODUCTION

Today, metal-matrix composite coatings (MMCCs) are widely in demand due to the possibility of combining the properties of both the metal base and their reinforcing particles. The introduction of reinforcing particles improves the mechanical properties of the coatings, their corrosion resistance, and expands their applications [1, 2].

The development of various methods for introducing particles into a metal matrix is gaining significant importance due to the potential for synthesizing a wide range of materials with unique functional properties. The simplest and most technologically advanced coating method is electrodeposition [3], which involves the reduction of metal ions from an electrolyte based on salt solutions under the influence of an electric current. The workpiece acts as a cathode and is connected to the negative pole of the power source, while the anode, typically an electrode in an electrolyte solution of the same metal, is connected to the positive pole. The physicochemical principles of electrodeposition are well known in electroplating.

Of particular interest among the MMCCs obtained by electrodeposition are nickel composite coatings. The introduction of solid particles of SiC [4], Al_2O_3 [5], ZrO_2 [4], WC [6] and TiO_2 [7] leads to a significant improvement in the mechanical properties of the coatings, such as strength, hardness and wear resistance, and determines their potential application.

The most extensive research has been conducted on nickel-matrix composites containing embedded silicon carbide (SiC) particles. For components operating under conditions of intense friction and mechanical stress, and used in the automotive, aerospace, and manufacturing industries, the Ni–SiC system is indispensable as a protective coating [8, 9]. Previously, galvanic chromium plating was used to harden the surface of components such as aluminum cylinders and piston rings. However, switching to a Ni–SiC coating reduces environmental pollution and avoids negative impacts on human health [10].

As is known, the advantage of the Ni–SiC coating electrodeposition process is the ability to control the structure and properties by changing such process parameters as electrolyte composition, temperature, stirring speed and particle content [1, 9], as well as the relative position of the cathode and anode during electrodeposition [11, 12]. The latter parameter becomes most significant in the development of a technology for electrodeposition of a coating containing a large fraction of particles larger than 2 μm. The authors [12] note that the horizontal position of the treated surface allows for the stable production of a Ni–SiC composite coating characterized by good adhesion. It is worth noting that in these studies the coating was formed on flat samples with an area of 0.1 dm^2. Another fundamental parameter determining the quality of the formed coating and the electrodeposition rate is the current density ρ. It is noted [ ] that there is an optimal range of ρ, in which a coating with the maximum particle content is formed. For example, for nanosized SiC particles this range is from 40 to 60 mA/cm^2.

During electrodeposition, it's crucial to form a coating with a uniform particle distribution in the metal matrix across the entire working surface of the workpiece to ensure stable mechanical and functional properties, which will ultimately determine the longevity of the components. From this perspective, it's of interest to scale up the electrodeposition process and switch to model samples whose lengths mimic the maximum height of a real axisymmetric component, such as a cylinder, allowing for the reproduction of coating application conditions similar to those in production.

Thus, the aim of this work is to study the homogeneity of the structure and properties of the Ni–SiC coating containing a fraction of particles larger than 2 μm and formed on long workpieces (0.2 cm^2 area) in the process of electrodeposition depending on the current density.

MATERIALS AND METHODS

Raw material

Cast aluminum alloy AK7 (GOST 30620-98) was used as the substrate material for the Ni–SiC composite coating. Its microhardness was 58HV. The size of the flat samples was chosen to match the linear dimension of a sector of an axisymmetric cylindrical part and was 70 mm long, 20 mm wide, and 4 mm thick.

The chemical element content of the substrate material was assessed using an INCA-Energy X-ray microanalyzer and an Inca X-Act energy-dispersive spectrometer, both of which are equipped with a JSM-6490 LV scanning electron microscope (SEM). Analysis of five spectra taken from the sample surface revealed the following average component content (wt %): Al – 81.0; Si – 18.0; Mg – 0.1.

Surface preparation of samples before coating

Surface preparation was performed to improve adhesion of the coating to the substrate material. It included several steps:

- degreasing in an ultrasonic bath with acetone for 2 minutes;
- rinsing in warm distilled water;
- etching in a solution of hydrofluoric (HF) and nitric acids (HNO_3) for 3 minutes;
- rinsing twice in distilled water at room temperature.

After rinsing, the flat samples were immediately mounted in the setup to prevent the substrate surface

ISSN 2075-8545 (online)

from drying out and the re-formation of the natural oxide film due to interaction with atmospheric oxygen.

Electrodeposition

For coating application, a Watts sulfamate electrolyte was used, the composition of which is presented in Table 1 [14].

The electrolyte for Ni–SiC deposition was prepared as follows. Boric acid, nickel chloride, nickel sulfate, and sodium lauryl sulfate were dissolved sequentially in a glass container filled with distilled water to $^3/_4$ of the required volume at a temperature of up to 70 °C. The electrolyte was then topped up to the required volume and silicon carbide was added.

Table 1. Electrolyte composition and electrodeposition parameters

Components	Concentration, g/l
Single nickel salt ($Ni_2SO_4 \cdot 7H_2O$)	300l
Nickel chloride ($NiCl_2$)	30
Boric acid (H_3BO_3)	30
Sodium lauryl sulfate ($C_{12}H_{25}SO_4Na$)	1.5
Silicon carbide (SiC)	150
Electrodeposition parameters	**Value**
Temperature (°C)	60±1
Ph	3.5…4.0
Processing duration τ, min	60
Stirring speed n, rpm	from 1 to 300
Current density j, A/dm^2	0.5; 10,0; 20.0

An NPA2 electrolytic nickel rod (GOST 492-2006) was used as the anode.

The apparatus for electrodepositing a composite coating is shown in Fig. 1 and consists of a cylindrical bath 1 and two funnel-shaped end caps 2 and 3, which cover the ends of the bath with a cylindrical nickel anode 4 placed therein. A flat sample is attached to the inner wall of the bath. The bath with the caps is mounted in a movable frame 6 capable of rotation around an axis of symmetry to transmit centrifugal forces to the electrolyte (7 in Fig. 1) with SiC particles (8 in Fig. 1). A fixed frame 9 allows the position of the bath 1 to be changed relative to the vector of the earth's gravitational field. Sample 5 made of aluminum alloy, which serves as the cathode, and cylindrical nickel anode 4 are connected to a DC source.

The electrodeposition mode was selected based on the experimental results obtained earlier [12, 13]: the electrolyte temperature was 60 °C, the stirring speed varied depending on the position of the bath relative to the vector of the gravitational field of the earth's attraction (from 1 to 300 rpm), and the treatment duration was 60 minutes (Table 1).

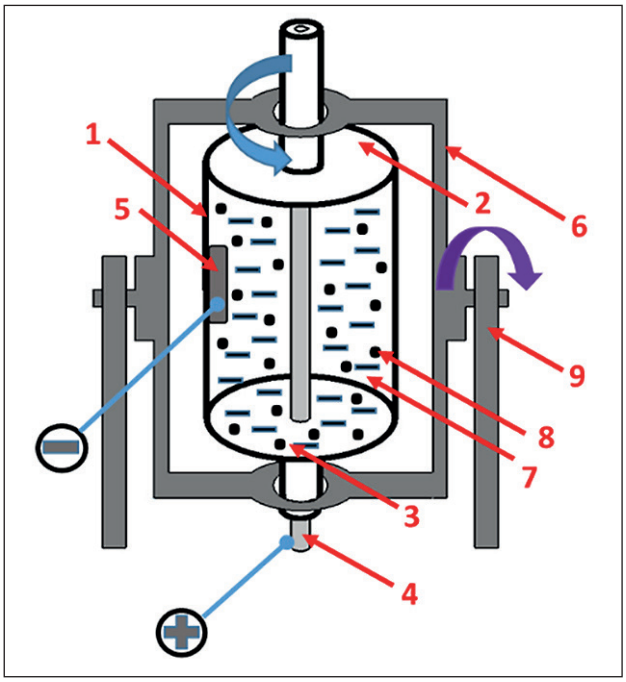


Fig. 1. Device for electrodeposition of Ni–SiC coating

Preparing samples for research

Electrodeposition of the composite coating was carried out on three samples. Electrodeposition modes differed in current density according to Table 1. To carry out metallographic studies, microsections were prepared in the following sequence: cutting blanks for transverse microsections on an electric spark machine; mechanical grinding using abrasives with a grain size up to P2000 (10 microns) and subsequent polishing using polishing suspensions on grinding and polishing equipment.

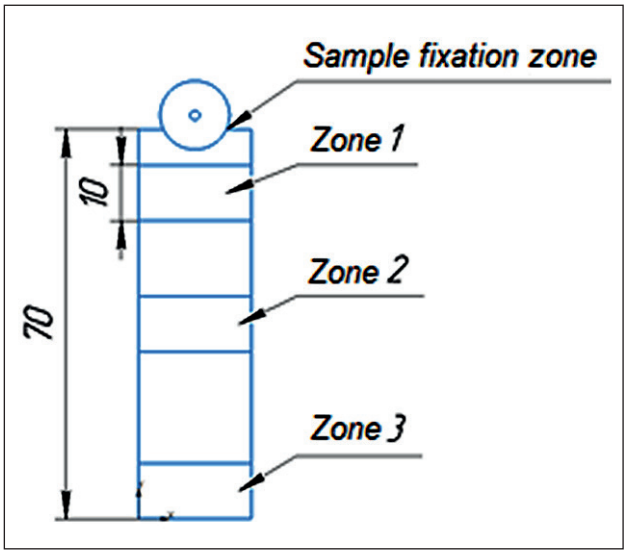


Fig. 2. Scheme of cutting samples for research

ISSN 2075-8545 (online)

Microstructural analysis technique

JSM-6490 LV scanning electron microscope (SEM) at ×500 magnification was used to determine the coating thickness and quantify the silicon carbide content. The volume fraction of silicon carbide in the coating was determined using the grid overlay method [1].

The chemical element content of the coating was assessed using an INCA-Energy X-ray microanalyzer and an Inca X-Act energy-dispersive spectrometer, both of which are equipped with JSM-6490 LV scanning electron microscope (SEM).

Test methods for wear resistance and microhardness

Wear resistance tests in zone 2 were carried out on a Nanovea tribometer using the ball-on-disk method in the following modes: rotation speed – 286 rpm; friction circle radius – 5 mm; linear velocity – 0.063 m/s; force – 2 N; friction type – dry; maximum track length – 1000 m; counterbody – steel ball with a diameter of 6.3 mm. Three parameters were selected as wear characteristics: the magnitude of mass wear of the sample (W), the magnitude of mass wear of the counterbody (Wb) and the wear track width (*b*).

The value of mass wear of the sample was calculated using the formula:

$$W = (m_0 - m_k/m_0) \times 100\%, \quad (1)$$

where m_0 – sample weight before testing, kg;
m_k – sample weight after testing, kg.

The magnitude of mass wear of the counterbody was determined by the formula:

$$W_ш = (m_0^ш - m_k^ш/m_0^ш) \times 100\%, \quad (2)$$

where m_0^b – mass of the ball before testing, kg;
m_k^b – mass of the ball after testing, kg.

The microhardness (HV) in the cross section was assessed using a TBM Tochline microhardness tester with a load of 50 g and an indentation time of 10 s.

RESULTS

Coating microstructure

Electrodeposition resulted in coatings on samples of AK18 aluminum alloy. Visual inspection of the sample surfaces revealed no delamination of the coating from the substrate or any defects such as discontinuities.

The microstructure of cross-sections of the electrodeposited samples is shown in Figure 3. The coatings formed intact without cracks, and good adhesion to the substrate is evident. No defects, such as pores, were observed along the transition zone from the base material to the coating. The coating consists of a nickel matrix with embedded silicon carbide particles, as clearly demonstrated by the elemental composition of the coating (Fig. 4).

A comparative analysis of the coating morphology (Fig. 3) and thickness assessment in different zones (Fig. 5a) indicate uniform formation across the entire surface of the samples. At low current densities (j = 0.5 A/dm²), the coating thickness varies from 17 to 25 μm depending on the zone. As the current density increases to 10 and then to 20 A/dm², the coating thickness increases by almost two and four times compared to j = 0.5 A/dm². Thickness uniformity is maintained across different zones and is within the error margin.

The volume fraction of silicon carbide particles increases with increasing current density (Fig. 5b) from 10% at 0.5 A/dm² to 15% (j = 10.0 A/dm²) and 16% (j = 20.0 A/dm²). Despite the fact that the coating thickness increases significantly with increasing current density, a similar multiple increase in the volume fraction of silicon carbide particles is not observed.

Coating microhardness

As shown in Figure 6, the coating microhardness depends on current density. At low current density (0.5 A/dm²), microhardness reaches no more than 250 HV. As j increases to 10.0 A/dm², microhardness increases almost threefold (637 HV for zone 2). A further increase in current density to 20 A/dm² does not result in an increase in HV.

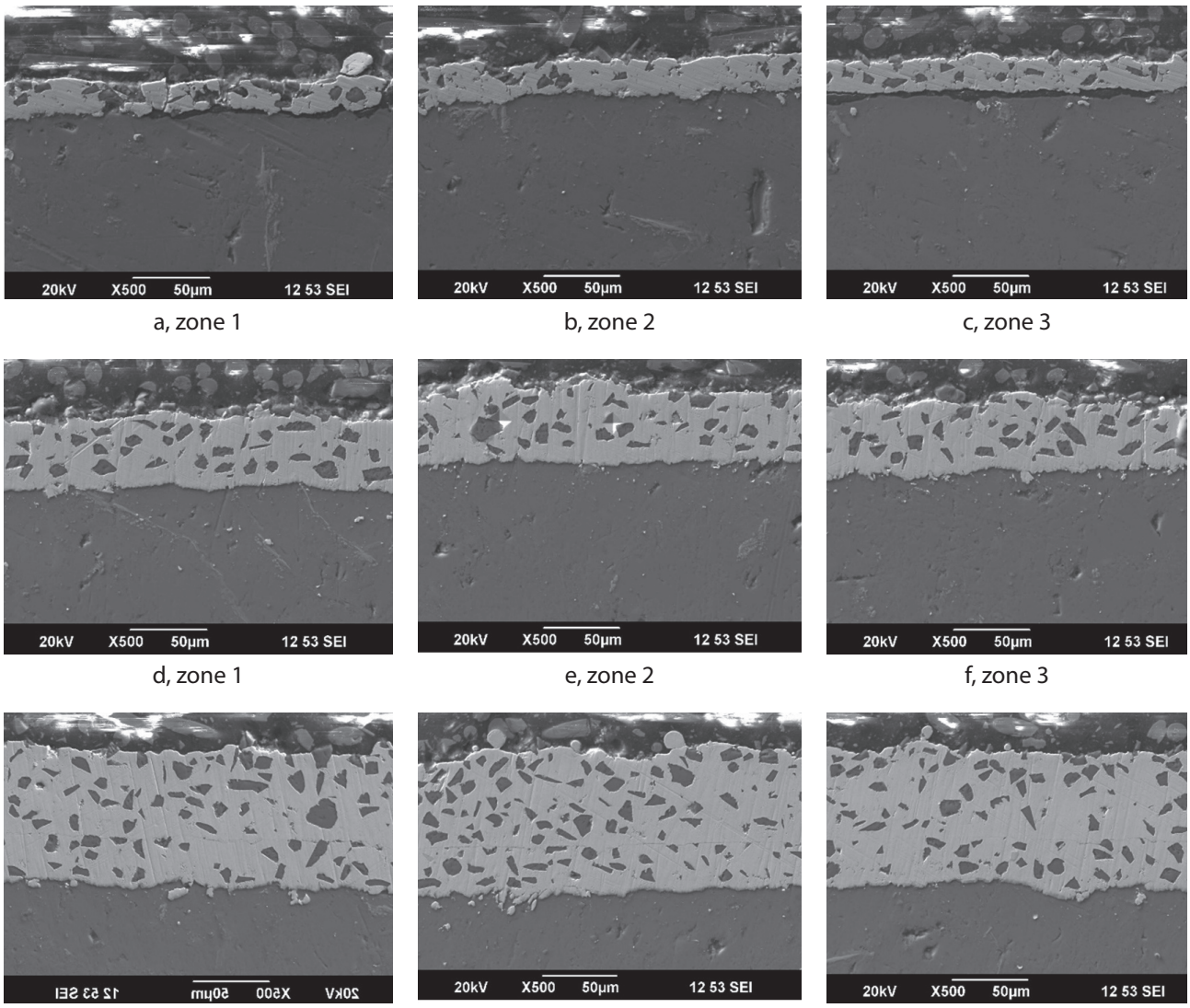
For j = 0.5 A/dm², the coating microhardness in zones 1, 2, and 3 (according to the cutting diagram in Fig. 2) varies within the error limits. Similar uniformity of coating microhardness in different zones of the samples is observed for the electrodeposition mode at current densities of 10 and 20 A/dm².

Coating wear resistance

Tribometer testing is used to evaluate the adhesion quality of coatings to the substrate surface. No delamination or failure of coatings formed at different current densities was observed in tribological tests. The wear tracks [16] formed during the tests are shown in Figure 7. Table 2 shows the specimen wear (W), the counterface wear (Wb), and the wear track width (b). These characteristics, as is well known, can be used to assess the intensity of surface damage.

The obtained data indicate increased wear resistance compared to the substrate material. The sample obtained at a current density of 0.5 A/dm² exhibited the highest wear resistance, corresponding to the lowest mass loss. As the current density increased to 10 A/dm² and 20 A/dm²,

ISSN 2075-8545 (online)

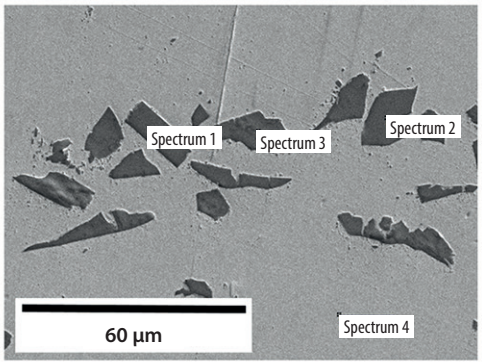


a, zone 1 b, zone 2 c, zone 3

d, zone 1 e, zone 2 f, zone 3

g, zone 1 h, zone 2 k, zone 3

Fig. 3. Microstructure of cross-sections of coated samples, SEM: a, b, c – 0.5 A/dm^2; d, e, f – 10.0 A/dm^2; g, h, k – 20.0 A/dm^2



№ spectrum	C	Si	Ni
spectrum 1	40,7	58,2	1,0
spectrum 2	41,6	57,1	1,2
spectrum 3	39,8	57,7	1,3
spectrum 4	-	-	100

Fig. 4. Elemental composition of the coating

ISSN 2075-8545 (online)

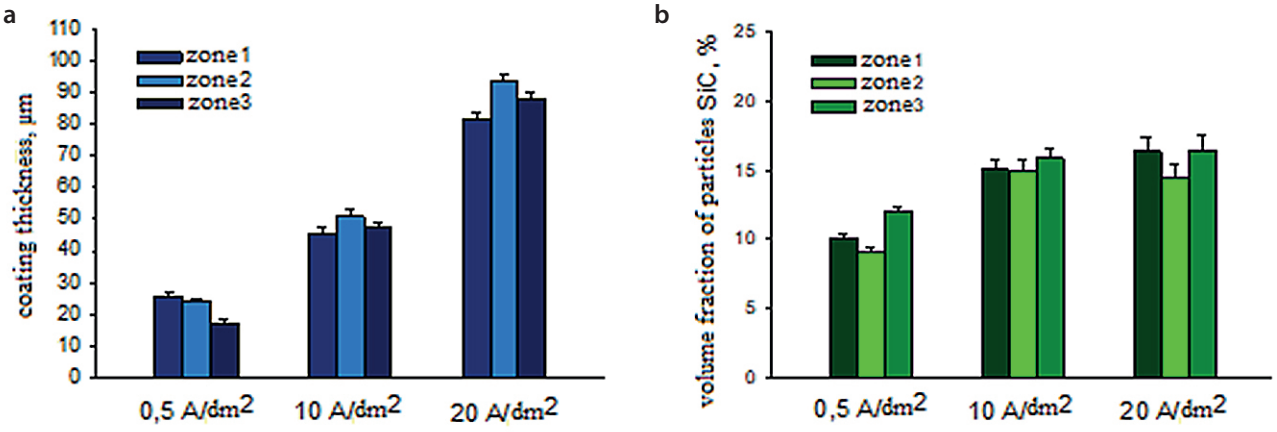


Fig. 5. Comparative analysis of coatings obtained at different current densities: coating thickness (a); volume fraction of SiC particles (b)

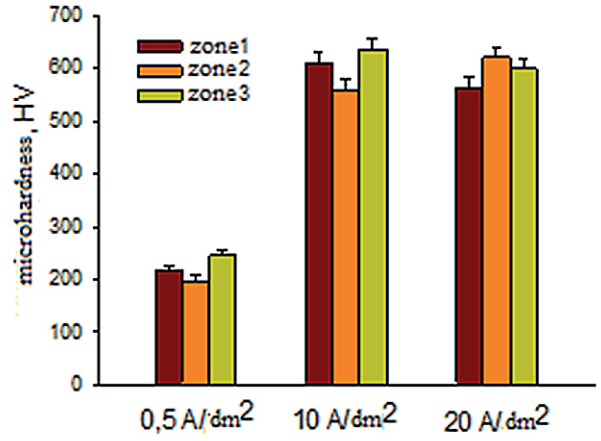


Fig. 6. Microhardness of coatings

mass loss increased, but remained 2.5–3.5 times higher than that of AK7. The samples obtained at a current density of 0.5 A/dm² and 20 A/dm² exhibited the smallest wear track widths, indicating good adhesion strength.

Thus, the coatings formed on flat samples of AK7 aluminum alloy are characterized by homogeneity over the entire area, while their structure and properties depend on the current density.

DISCUSSION

Electrodeposition is known to be one of the most common methods for producing composite coatings based on a metal matrix on the surface of components [17]. A basic electrodeposition setup consists of two conductive electrodes immersed in an electrolyte bath. One working electrode is connected to the negative pole and serves as the cathode, while the other is connected to the positive pole. When an external electric field is applied, cations move toward the cathode, discharge, and are deposited as a metallic layer [18, 19]. To date, sufficient laboratory experience has been accumulated in forming composite coatings reinforced with particles such as SiC, Al_2O_3, WC, TiO_2, and others. However, the transition from laboratory samples to product processing presents a challenge, primarily related to the need to form coatings exclusively on the working surfaces. Ensuring uniformity of coating formation is also crucial.

As a result of the conducted research, the possibility of obtaining a Ni–SiC composite coating on model samples, the long dimension of which simulates

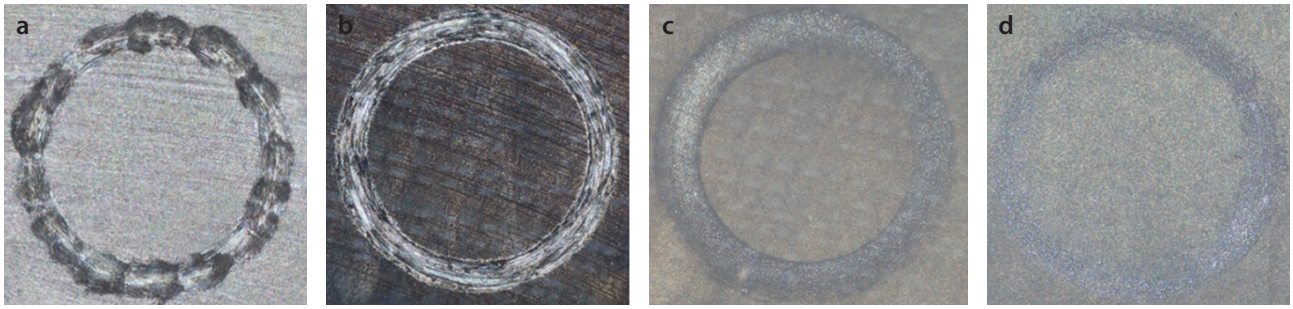


Fig. 7. Wear tracks: AK18 (a); 0.5 A/dm² (b), 10 A/dm² (c), 20 A/dm² (d)

ISSN 2075-8545 (online)

Table 2. Results of tribological tests

	W, %	W_b, %	b, microns
AK18	$9.0 \cdot e^{-3}$	0.01	452±5
coating (j = 0,5 A/dm²)	$1.4 \cdot e^{-3}$	0.21	446±
coating (j = 10 A/dm²)	$5.0 \cdot e^{-3}$	0.26	566±
coating (j = 20 A/dm²)	$5.0 \cdot e^{-3}$	0.24	445±

the maximum height of a cylinder (20×70×2 mm) was demonstrated.

Current density is considered a key factor that directly affects the quality of the composite coating formed on the base metal substrate [20]. The mechanism of inclusion of SiC into the nickel matrix, and, consequently, the rate of incorporation, at low current densities is determined by adsorption, and at high current densities by the transport of second-phase particles [21]. The literature contains conflicting opinions on the effect of current density on the quality of composite coatings. The primary criterion is the volume fraction of reinforcing particles. In most cases, an increase in the particle fraction is observed with increasing current density [3, 20, 22]. However, there are publications whose authors demonstrate the opposite effect – a decrease in the volume fraction with an increase in current density [23]. In [13], it is noted that with increasing current density, an increase in the volume fraction of particles is initially observed, followed by a decrease with further increases in current density. This discrepancy can be explained by the fact that the authors use different methods of mixing the electrolyte, different sizes of reinforcing particles (from nanoscale to micron-scale), and different relative positions of the cathode and anode.

It should be noted that when using nanoscale SiC particles, a more pronounced dependence of the content of the hardener on the current density is observed. Studies show that nanoparticles are characterized by a decrease in switching efficiency at high current densities, which is associated with increased competition between nickel ion discharge processes and electrophoretic particle transfer [24, 25]. In addition, nanoparticles are critically important to prevent their agglomeration in the electrolyte, which can be achieved by using ultrasonic mixing [26]. Unlike micron particles, for which convection is the determining mechanism of delivery to the cathode, nanoparticles are more susceptible to the influence of electrokinetic phenomena and require more careful control of deposition parameters [27].

In the current study, increasing the current density resulted in an increase in both the volume fraction of silicon carbide particles and an increase in the thickness of the formed coating (Fig. 5). Silicon carbide particles are known to have a negative charge. In the electrolyte solution, nickel ions are adsorbed onto the particle surface, and due to the positive charge, they are incorporated into the coating [28, 29, 30]. Electrodeposition processes are known to obey Faraday's first law [31]. It can be assumed that with increasing current density, a larger mass of nickel is adsorbed on the silicon carbide particles and, with their further deposition on the base metal substrate, a coating of greater thickness is formed.

The performance characteristics of coatings for practical applications are determined by mechanical properties such as microhardness and adhesion. These properties determine the quality of the coating and may vary depending on its structure.

Metal-matrix composites are characterized by higher microhardness values compared to coatings based on pure metal. This is explained by the mechanism of dispersion strengthening of the matrix by inclusions of co-precipitated strengthening particles, which act as barriers to dislocation movement [32, 33, 34]. It is known that the microhardness of metal-matrix composites depends not only on the mechanical characteristics of the matrix nickel phase, particles, and interphase boundaries, but also on the amount of the dispersed phase [3, 7]. The obtained results confirm this trend. When evaluating the microhardness, a greater consistency was revealed with the volume fraction of silicon carbide particles in the coating composition than with its thickness (compare Fig. 5 and Fig. 6).

The wear resistance of Ni–SiC composite coatings depends on the current density through the thickness and volume fraction of embedded solid particles in the coating. As with microhardness, the volume fraction of particles has a more pronounced effect than the coating thickness. The best wear resistance was achieved for a coating containing 10% SiC, obtained at a density of 0.5 A/dm². The increase in mass loss and the resulting decrease in wear resistance at current densities of 10 and 20 A/dm² can be associated with the tearing out of particles during friction, which leads to additional wear of the coating surface. In the literature, the term "third-body wear" is used to describe this process [35]. In this case, scratches are observed on the wear tracks of the Ni–SiC composite coating and their absence on the wear tracks of the pure nickel-based coating. With increasing coating thickness, the volume fraction of particles increases, consequently, the percentage of particles torn out of the

ISSN 2075-8545 (online)

metal matrix increases. For nanocomposite coatings, the wear mechanisms may differ: the uniform distribution of nanoparticles in the matrix contributes to a more stable formation of the protective layer and a reduction in abrasive wear [27, 36].

CONCLUSION

Thus, this study demonstrates the feasibility of scaling up the process of electrodeposition of "Ni–SiC" metal-matrix composite coating on long, flat specimens of AK7 aluminum alloy. The following conclusions can be drawn from this work:

1. The metal-matrix composite coating "Ni–SiC", formed on flat long samples (0.2 cm^2 area) of AK7 aluminum alloy as a result of electrodeposition, is characterized by uniformity of thickness, volume fraction of silicon carbide particles and microhardness in three control zones for each current density.

2. The higher the current density during electrodeposition, the higher the thickness of the formed Ni–SiC metal-matrix composite coating, the volume fraction of reinforcing particles and the microhardness.

3. Mass loss during tribological tests for a sample coated with "Ni–SiC" composite coating is lower than for an uncoated sample.

REFERENCES

1. Saini A., Singh G., Mehta S., Singh H., Dixit S. A review on mechanical behaviour of electrodeposited Ni-composite coatings. *Int J Interact Des Manuf.* 2023;17:2247–2258.

3. Walsh F.C., Ponce de Leon C. Towards improved electroplating of metal-particle composite coatings. *Trans IMF.* 2020;98(6):288–299. https://doi.org/10.1080/00202967.2020.1819022

3. Burzyńska L., Rudnik E., Koza J., Błażc L., Szymański W. Electrodeposition and heat treatment of nickel/silicon carbide composites. *Surf Coat Technol.* 2008;202:2545–2556. https://doi.org/10.1016/j.surfcoat.2007.09.020

4. Zellele D.M, Yar-Mukhamedova G.S., Rutkowska-Gorczyca M. A review on properties of electrodeposited nickel composite coatings: Ni–Al_2O_3, Ni–SiC, Ni–ZrO_2, Ni–TiO_2 and Ni–WC. *Materials.* 2024;17:5715. https://doi.org/10.3390/ma17235715

5. Steinbach J., Ferkel H. Nanostructured Ni-Al_2O_3 films prepared by dc and pulsed dc electroplating. *Scripta Mater.* 2001;44:1813–1816.

6. Mohajeri S., Dolati A., Rezagholibeiki S. Electrodeposition of Ni/WC nano composite in sulfate solution. *Mater Chem Phys.* 2011;129:746–750.

7.Yılmaz G., Hapçi G., Orhan G. Properties of Ni/nano-TiO_2 composite coatings prepared by direct and pulse current electroplating. *J. Mater Eng Perform.* 2015;24:709–720. https://doi.org/10.1007/s11665-014-1346-4

8. Jenczyk P., Gawrońska M., Dera W., Chrzanowska-Giżyńska J., Denis P., Jarząbek D.M. Application of SiC particles coated with a protective Ni layer for production of Ni/SiC co-electrodeposited composite coatings with enhanced tribological properties. *Ceram Int.* 2019;45(17B):23540–23547. https://doi.org/10.1016/j.ceramint.2019.08.063

9. Ariffin I.A., Kamdi Z. A review on wear behavior of nickel-silicon carbide electrodeposition coating. *Res Prog Mech Manuf Eng.* 2022;3(1):377–384.

10. Zhang F., Wang Q., Shen H., Bai C., Li C., Tian D., Wang B. Effect of SiC concentration on the microstructure and anti-wear performance of electrodeposited Ni-SiC composite coatings constructed for piston ring application. *Materials (Basel).* 2025;18(5):1117. https://doi.org/10.3390/ma18051117

11. Kiseleva S. K., Akhmerov L. D., Mustafin R. F., Lukyanov V. V., Astanin V. V. Formation of nickel-silicon carbide composite coating. *Materials. Technologies. Design.* 2025;7(1):36–44. https://doi.org/10.54708/26587572_2025_712036

12. Kiseleva S. K., Akhmerov L. D., Lukyanov V. V., Kandarov I. V. Installation for applying Ni-SiC composite coating. *Materials. Technologies. Design.* 2025;7(3):21–31. https://doi.org/10.54708/26587572_2025_732221

13. Walsh F.C., Ponce de Leon C. A review of the electrodeposition of metal matrix composite coatings by inclusion of particles in a metal layer: an established and diversifying technology. *Trans IMF.* 2014;92(2):83–98.

14. Huang P.-C., Hou K.-H., Hong J.-J., Lin M.-H., Wang G.-L. *Study of fabrication and wear properties of Ni–SiC composite coatings on A356 aluminum alloy.* Patent CN № 113061890A. 2021.

15. Saltykov S. A. *Stereometric metallography.* Moscow: Metallurgiya; 1976: 270. (In Russian).

16. Nemane V., Chatterjee S. Effect of silicon carbide incorporation and heat treatment on tribological properties of electroless Ni-BW alloy coating. *Mater Chem Phys.* 2024;311:128500. https://doi.org/10.1016/j.matchemphys.2023.128500

ISSN 2075-8545 (online)

17. Kamel M.M., Alzahrani E., Ibrahim I.S., et al. Electrodeposition of well-crystalline Ni-Co alloy thin films on steel substrates from aqueous solutions containing citrate anions. *Int J Electrochem Sci.* 2021;16:1–22. https://doi.org/10.20964/2021.09.18

18. Liu W., Jiang K., Li Q., Ma C., Xia F. Jet pulse electrodeposited Ni-SiC thin coatings by using experimental system designed for potential industrial application. *Int J Electrochem Sci.* 2021;16:21044. https://doi.org/10.20964/2021.04.23

19. Guan T., Zhang N. Recent advances in electrodeposition of nickel based nanocomposites enhanced with lubricating nanoparticles. *Nanomanuf Metrol.* 2024;7:25. https://doi.org/10.1007/s41871-024-00245-6

20. Kumar D., Shree G. Wear and hardness evaluation of electrodeposited Ni-SiC nanocomposite coated copper. *Int J Microstruct Mater Prop.* 2020;15(2):88–106.

21. Ovchinnikova K.V. *Technology of composite electrolytic coatings of nickel-cobalt-aluminum oxide and nickel-cobalt-diamond* [dissertation for the degree of candidate of technical sciences]. Novocherkassk. South-Russian State Polytechnical University named after M.I. Platov; 2021.

22. Vaezi M.R., Sadrnezhaad S.K., Nikzad L. Electrodeposition of Ni–SiC nano composite coatings and evaluation of wear and corrosion resistance and electroplating characteristics. *Colloids Surf A Physicochem Eng Aspects.* 2008;315(1–3):176–182.

23. Krasikova A.V., Agafonov D.V., Markova M.A., Bykova A.D., Belyakov A.N., Kravchenko I.N., et al. Electrodeposition of a Ni–SiC composite coating from a vibration-stabilized electrolyte–suspension. *Russ Metall (Metally).* 2023;(6):796–802. https://doi.org/10.1134/s0036029523060241

24. Dobosz I. Codeposition of SiC particles with electrolytic nickel. *Arch Met Mater.* 2011. https://doi.org/10.2478/v10172-011-0072-2

25. Rao H., Li W., Luo Z., Liu H., Zhu L., Chen H. Nucleation and growth mechanism of Ni/SiC composite coatings electrodeposited with micro- and nano-SiC particles. *J Mater Res Technol.* 2024;30:3079–3091. https://doi.org/10.1016/j.jmrt.2024.04.008

26. Cai C., Zhu X.B., Zheng G.Q., Yuan Y., Huang X., Cao F., Yang J.F., Zhang Z. Electrodeposition and characterization of nano-structured Ni–SiC composite films. *Surf Coat Technol.* 2011;205(11):3448–3454. https://doi.org/10.1016/j.surfcoat.2010.12.002

27. Krasikov A.B., Markov M.A., Krasikov V.L., Kravchenko I.N., Staritsyn M.V., Bykova A.D., Belyakov A.N. Influence of vibration parameters during electrodeposition of Ni–SiC composite coatings from a vibration-stabilized suspension. *Problems of mechanical engineering and machine reliability.* 2022;(4):21-27. https://doi.org/10.31857/S0235711922040113

28. Mingazova G.G., Fomina R.E., Vodopyanova S.V., Saifullin R.S., Zhilyakov V.V. Physico-chemical properties of nickel composite coatings. *Bull Tech Univ.* 2017;20(15):42–44. (In Russian)

29. Tseluikin V.N., Yakovlev A.V. On electrochemical deposition and properties of nickel-based composite coatings. *Phys Chem Surf Prot Mater.* 2020;56(2):197–201. (In Russian). https://doi.org/10.31857/s004418562002028x

30. Tseluikin V.N., Vasilenk E.A., Nevernaya O. G., Tseluikina G. V., Surmenko E. L. Physico mechanical properties of composite coatings based on a nickel chromium alloy. *Condensed media and interphase boundaries.* 15(2) 156–159. (In Russian)

31. Zhachkin S.Yu., Trifonov G.I., Sidorkin O.A., Pustovetov A.V. Wear Resistance of Nickel Composite Coatings with Micron-Sized and Submicron-Sized Particles of SiC. *Engineering Technologies and Systems.* 2024;34(4):629–647. https://doi.org/10.15507/2658-4123.034.202404.629-647

32. Nemane V., Chatterjee S. Evaluation of microstructural, mechanical, and tribological characteristics of Ni–B–W–SiC electroless composite coatings involving multi-pass scratch test. *Materials Characterization.* 2021;180:111414. https://doi.org/10.1016/j.matchar.2021.111414

33. Wang F., Fu X., Shen M., Xu Y., Duan S., Wang Q., Cao H., Lin J. Preparation of Ni-P-SiC composite coatings by magnetic field enhanced jet electrodeposition. *Int J Electrochem Sci.* 2020;15:10432–10452. https://doi.org/10.20964/2020.10.13

34. Lv Q., Fu X., Chen X., Lin J., Cao H. Investigating the effects of the current density on the properties of Ni–P–La_2O_3 composite coatings. *Int J Electrochem Sci.* 2020;15:11250–11264. https://doi.org/10.20964/2020.11.76

35. Huang P.C., Hou K.H., Hong J.J., Lin M.H., Wang G.L. Study of fabrication and wear properties of Ni–SiC composite coatings on A356 aluminum alloy. *Wear.* 2021;476–477:203772. https://doi.org/10.1016/j.wear.2021.203772

36. Piñate S., Ghassemali E., Zanella C. Strengthening mechanisms and wear behavior of electrodeposited Ni–SiC nanocomposite coatings. *J Mater Sci.* 2022;57:16632–16648. https://doi.org/10.1007/s10853-022-07655-1

ISSN 2075-8545 (online)

ADDITIONAL INFORMATION

The authors declare that generative artificial intelligence technologies and technologies based on artificial intelligence were not used in the preparation of the article.

INFORMATION ABOUT THE AUTHORS

Svetlana K. Kiseleva – Cand. Sci. (Tech.), Associate Professor Ufa State Petroleum Technological University, Ufa, Kosmonavtov str. 1, 450064, Republic of Bashkortostan, Russian Federation; Senior Researcher at the Center for Intelligent Mechanical Engineering, Ufa State Petroleum Technological University; researcher, Technopark of Aviation Technologies, Ufa, Tramvaynaya str. 5, building 1, 450112, Republic of Bashkortostan, Russian Federation, kiseleva_s2018@mail.ru, https://orcid.org/0000-0003-1819-247X

Linar D. Akhmerov – laboratory assistant of Center for Intelligent Engineering of Ufa State Petroleum Technological University, Ufa, Kosmonavtov str. 1, 450064, Republic of Bashkortostan, Russian Federation, laboratory assistant, Technopark of Aviation Technologies, Ufa, Tramvaynaya str. 5, building 1, 450112, Republic of Bashkortostan, Russian Federation, linarakhmerov2@gmail.com, https://orcid.org/0009-0002-9825-2697

Aliyana Z. Khusnutdinova - Research Engineer at the Center for Intelligent Mechanical Engineering, Ufa State Petroleum Technological University, Ufa, Kosmonavtov str. 1, 450064, Republic of Bashkortostan, Russian Federation; Metallographic Engineer, Technopark of Aviation Technologies, Ufa, Tramvaynaya str. 5, building 1, 450112, Republic of Bashkortostan, Russian Federation, aliyana.husnutdinova@yandex.ru, https://orcid.org/0009-0006-0072-9792

Irek V. Kandarov – Cand. Sci. (Tech.), Associate Professor, Acting Head of the Department of "Intelligent Systems and Equipment in Mechanical Engineering" Ufa State Petroleum Technological University, Ufa, Kosmonavtov str. 1, 450064, Republic of Bashkortostan, Russian Federation; Leading Engineer at the Center for Intelligent Mechanical Engineering, Ufa State Petroleum Technological University; Director of Technopark AT, Ufa, Tramvaynaya str. 5, building 1, 450112, Republic of Bashkortostan, Russian Federation, https://orcid.org/0009-0009-6330-8524

CONTRIBUTION OF THE AUTHORS

Svetlana K. Kiseleva – scientific supervision; development of the concept and methodology of the research; analysis of the research results; writing the article; drawing up final conclusions.

Linar D. Akhmerov – editing and data processing.

Aliyana Z. Khusnutdinova – preparation and writing of the text of the section «Methods and Materials»; data processing.

Irek V. Kandarov – scientific supervision, scientific editing of the text, participation in scientific discussion.

The authors declare no conflicts of interests.

The article was submitted 18.06.2026; approved after reviewing 30.09.2026; accepted for publication 05.10.2026.

ISSN 2075-8545 (online)

Nanotechnologies in construction
Нанотехнологии в строительстве

2026; 18 (5):
591–600

Nanobuild.ru

CONSTRUCTION MATERIALS SCIENCE

Original article
https://doi.org/10.15828/2075-8545-2026-18-5-591-600

CC BY 4.0

Assessment of the processability of applying a metal matrix coating by electrochemical deposition on an internal combustion engine cylinder

Denis N. Mazidullin[1], Pavel P. Tregubov[1], Maria V. Demchenko[1]*, Linar D. Akhmerov[1, 2], Azamat A. Arslanov[1, 2]

[1] Ufa State Petroleum Technological University, Ufa, Kosmonavtov str. 1, 450064, Russian Federation
[2] Scientific and Production Association "Technopark of Aviation Technologies," Ufa, Tramvaynaya str. 5, building 1, 450112, Russian Federation

* Corresponding author: e-mail: m.v.demchenko@yandex.ru

ABSTRACT

Introduction. Weight optimization of internal combustion engines is achieved through the use of aluminum alloys. In order to increase the wear resistance of surfaces, functional coatings are used – including those with the inclusion of nanoparticles. Nanoparticles are incorporated into the coating to substantially improve performance properties such as hardness and wear resistance, also to form a more uniform structure. To maintain the gap in the piston-cylinder group, it is important to assess the current state of the surface of the parts and the method of preparing them for applying a metal-matrix wear-resistant coating. **Methods and materials.** During the study, an integral analysis of the microgeometry of the piston and cylinder surfaces was carried out using a laser scanner (measurement accuracy – 10 microns). Surface of cylinder is coated with Ni–SiC by electrochemical deposition. Samples from different sectors of the inner surface of the cylinder were cut to evaluate the coating. The microhardness was determined using a TBM Tochline microhardness meter at a load of 50 g. The microstructure and chemical composition of the coating were examined using a JSM-6490 LV scanning electron microscope at a magnification of x500. **Results and discussion.** Analysis of the cylinder and piston microgeometry revealed a nominal radial gap of 250 μm. Deviations of the cylinder dimensions correspond to the 5th degree of accuracy of castings, for the piston – to the 3rd. Bore diameter in cylinder цилиндре $39^{+0,146}_{+0,000}$, piston diameter $38{,}5^{-0,038}_{-0,150}$. Thickness of coating layer including series-formed main nickel layer with strengthening phase SiC ≈ 900 nm is 160±10 mcm. Average microhardness of the applied coating 420 HV. The cylinder depth variation does not exceed 10 HV, which characterizes the uniformity of the formed nickel-strengthening phases SiC. **Conclusion.** Before coating, machining of the inner surface of the cylinder is required to equalize the radial gap to 400+10 μm, ensuring a $39^{+0,40}_{+0,39}$ mm. The developed coater ensures geometric and structural uniformity of the coating with a thickness of 160±10 microns. The coated surface shall be finished. In the future, bench tests of the wear resistance of the coating will be carried out. Subsequent studies will be aimed at optimizing the technology of its application in order to achieve an indicator of operating time of 500 hours before overhaul.

KEYWORDS: internal combustion engine cylinder, 3D digitization, 3D inspection, 3D modeling, reverse engineering, electronic product model, preliminary design, wear-resistant metal-matrix coatings, electrochemical deposition

SOURCES OF FUNDING FOR THE SCIENTIFIC WORK THAT RESULTED IN THE PUBLICATION: The study was carried out within the framework of the PRIORITY 2030 program of the Ministry of Science and Higher Education of the Russian Federation.

ACKNOWLEDGEMENTS: The authors are grateful for the financial support of the project.

FOR CITATION:
Mazidullin D.N., Tregubov P.P., Demchenko M.V., Akhmerov L.D., Arslanov A.A. Assessment of the processability of applying a metal matrix coating by electrochemical deposition on an internal combustion engine cylinder. *Nanotechnologies in Construction.* 2026;18(5):591–600. https://doi.org/10.15828/2075-8545-2026-18-5-591-600. – EDN: SMLGUZ.

© Mazidullin D.N., Tregubov P.P., Demchenko M.V., Akhmerov L.D., Arslanov A.A., 2026

ISSN 2075-8545 (online)

Nanotechnologies in construction
Нанотехнологии в строительстве

2026; 18 (5):
591–600

Nanobuild.ru

CONSTRUCTION MATERIALS SCIENCE

Оценка технологичности нанесения металломатричного покрытия методом электрохимического осаждения на цилиндр ДВС

Денис Нарисович Мазидуллин[1], **Павел Павлович Трегубов**[1], **Мария Вячеславовна Демченко**[1]*, **Линар Динарович Ахмеров**[1, 2], **Азамат Альфизович Арсланов**[1, 2]

[1] Уфимский государственный нефтяной технический университет, 450064, Уфа, ул. Космонавтов, 1, Российская Федерация

[2] Научно-производственная ассоциация «Технопарк Авиационных Технологий», Россия, Республика Башкортостан, 450112, Уфа, ул. Трамвайная 5, к. 1, Российская Федерация

* Автор, ответственный за переписку: e-mail: m.v.demchenko@yandex.ru

АННОТАЦИЯ

Введение. Оптимизация массы двигателей внутреннего сгорания достигается путем применения алюминиевых сплавов. С целью повышения износостойкости поверхностей применяются функциональные покрытия – в том числе, с включением наночастиц. Наночастицы вводят в состав покрытия, чтобы существенно улучшить такие эксплуатационные свойства, как твердость и износостойкость, также для формирования более однородной структуры. Для сохранения зазора в группе поршень-цилиндр важно оценить текущее состояние поверхности деталей и методику их подготовки для нанесения металломатричного износостойкого покрытия. **Методы и материалы.** В ходе исследования проведен интегральный анализ микрогеометрии поверхности поршня и цилиндра с применением лазерного сканера (точность измерений – 10 мкм). На поверхность цилиндра путем электрохимического осаждения нанесено покрытие Ni–SiC. Для оценки покрытия были вырезаны образцы с разных секторов внутренней поверхности цилиндра. Микротвердость определяли с использованием микротвердомера «TBM Tochline» при нагрузке 50 г. Микроструктуру и химический состав покрытия исследовали с помощью растрового электронного микроскопа «JSM-6490 LV» при увеличении x500. **Результаты и обсуждение.** Анализ микрогеометрии цилиндра и поршня выявил номинальный радиальный зазор 250 мкм. Отклонения размеров цилиндра соответствуют 5-й степени точности отливок, для поршня – 3-й. Диаметр отверстия в цилиндре $39^{+0,146}_{+0,000}$, диаметр поршня $38{,}5^{-0,038}_{-0,150}$. Толщина слоя покрытия, включающего последовательно формируемый основной никелевый слой с упрочняющей фазой SiC ≈ 900 нм, составляет 160±10 мкм. Среднее значение микротвердости нанесенного покрытия 420 HV. По глубине цилиндра разброс значений не превышает 10 HV, что характеризует однородность сформированного слоя никель – упрочняющие фазы SiC. **Заключение.** Перед нанесением покрытия требуется механическая обработка внутренней поверхности цилиндра для выравнивания радиального зазора до 400+10 мкм с обеспечением размера $39^{+0,40}_{+0,39}$ мм. Разработанная установка для нанесения покрытия обеспечивает геометрическую и структурную однородность покрытия с толщиной 160±10 мкм. Поверхность с нанесенным покрытием следует подвергать финишной обработке. В дальнейшем будут проведены стендовые испытания износостойкости покрытия. Последующие исследования будут направлены на оптимизацию технологии его нанесения с целью достижения показателя в наработке 500 часов до капитального ремонта.

КЛЮЧЕВЫЕ СЛОВА: цилиндр двигателя внутреннего сгорания, 3д-оцифровка, 3д-инспекция, 3д-моделирование, реверс-инжиниринг, электронная модель изделия, эскизное проектирование, износостойкие металломатричные покрытия, элкетрохимическое осаждение

ИСТОЧНИКИ ФИНАНСИРОВАНИЯ НАУЧНОЙ РАБОТЫ, РЕЗУЛЬТАТОМ КОТОРОЙ СТАЛА ПУБЛИКАЦИЯ: Исследование выполнено в рамках программы Министерства науки и высшего образования Российской Федерации «ПРИОРИТЕТ 2030».

БЛАГОДАРНОСТИ: Авторы выражают благодарность за финансовую поддержку проекта.

ДЛЯ ЦИТИРОВАНИЯ:
Мазидуллин Д.Н., Трегубов П.П., Демченко М.В., Ахмеров Л.Д., Арсланов А.А. Оценка технологичности нанесения металломатричного покрытия методом электрохимического осаждения на цилиндр ДВС. *Нанотехнологии в строительстве.* 2026;18(5):591–600. https://doi.org/10.15828/2075-8545-2026-18-5-591-600. – EDN: SMLGUZ.

INTRODUCTION

According to an analytical report [1], the engine market is expected to grow from $84 billion in 2022 to $115 billion in 2027. There is an increase in interest in hybrid-electric and all-electric power plants, but traditional internal combustion engines (ICEs) continue to dominate the market due to the existing infrastructure and maintenance

ISSN 2075-8545 (online)

networks. To reduce the development time of domestic engines, reverse engineering is used [2]. When creating competitive mechanical engineering products, it is important to improve their technical characteristics. One of the main causes of failure of machines with reciprocating movement of working elements is wear of pistons and mating surfaces of cylinders. Modern approaches to improving the wear resistance of the cylinder-piston group include the use of wear-resistant coatings, optimization of materials, additives to oils, as well as innovative surface treatment technologies. The group of promising coatings includes composite coatings with a metal matrix. One of the types of composite coatings of cylinder working surfaces that are in demand on the market is the Ni–SiC system – nikasil [3, 4], which is widely used to reduce the wear of engine parts. Silicon carbide SiC nanoparticles play a key role in the effectiveness of such a coating: due to their small size, they provide dispersion hardening of the matrix, contribute to the formation of a denser and more uniform layer structure, reduce porosity and increase the hardness of the coating. In addition, due to the high specific surface of the nanoparticles, adhesion to the matrix is improved, which prevents the coating from chipping under intense cyclic loads characteristic of the cylinder-piston group. USPTU has developed a technology and an installation for applying Ni–SiC coating to flat samples made of aluminum alloys AK7 by electrochemical deposition [5-7] with the prospect of improvement for application to axisymmetric surfaces.

The purpose of this work is to evaluate the manufacturability of the developed method of coating the inner surface of an ICE cylinder with a volume of 40 cm^3. Tasks are integral analysis of microgeometry of surfaces of parts in cylinder-piston group by method of reverse engineering, evaluation of gaps, evaluation of formed coating, development of recommendations for preparation of inner surface of cylinder under consideration for application of coating with specified thickness and evaluation of non-uniformity of application.

METHODS

Data on the geometry of the product were collected using an AtlaScan ZG Tech laser scanner with an accuracy of ± 0.01 mm. The device is included in the state register of measuring instruments [8]. For the collection, digitization and processing of geometry, licensed software (software) was used for the reverse engineering of pointshape-design by DREAMTNS [9]. GOM Inspect software was used for 3D inspection and work with digitization results [10]. Compass-3D computer-aided design (CAD) system was used to correct the models [11].

The chemical composition of the base metal was studied using the Olympus Innov-X Delta Premium portable XRF spectrometer in accordance with [12].

Coating microstructure studies were performed on a JSM 6490 LV scanning electron microscope (SEM). The chemical content of the coating was determined using an INCA Energy X-ray microanalyzer and an Inca X Act energy dispersive spectrometer.

Coating thickness was measured using the Altami Studio 4.0 software "MET 1C" Altami microscope.

Metal matrix composite coating "Ni–SiC" was applied electrochemically on a specially designed installation. The design of the installation [6] (on flat samples) provides for the possibility of coating the inner surfaces of cylindrical parts. The design feature of the installation is a cylindrical bath on a rotary base, providing both horizontal and vertical position of the part. The vertical position makes it possible to form a pure nickel layer, while the horizontal position makes it possible to obtain a composite Ni–SiC coating. The technological effectiveness of the installation is due to the following factors: the design of the installation does not require complex systems for forced mixing of the electrolyte, using the force of gravity for electrodeposition of particles; at one installation it is possible to obtain coating both on experimental samples and on full-size parts; positive results on flat samples confirm the technological heritability when switching to real axisymmetric parts.

To confirm the technological heritability of the installation, a cylindrical part with an internal cavity diameter of 39 mm was coated. In this case, when applying the coating, the part itself serves as a cylindrical bath. The deposition mode and composition of the electrolyte were the same as for the flat samples [5], but the fraction of silicon carbide particles was about 900 nm. Samples were then cut for metallographic studies (Fig. 1).

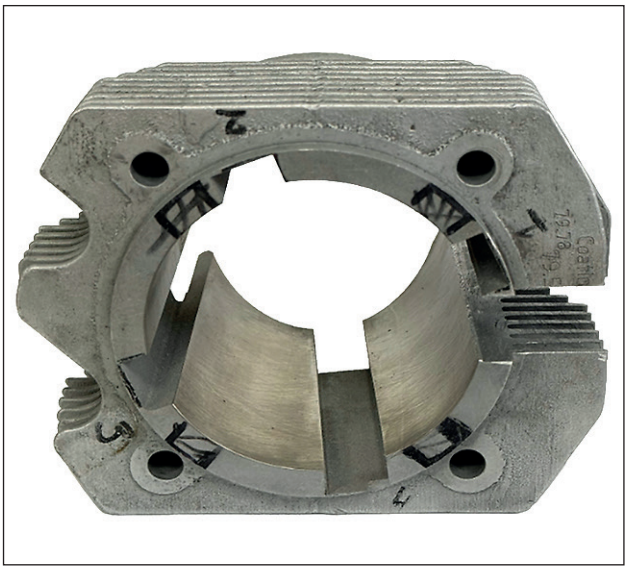


Fig. 1. Sample cutting areas

ISSN 2075-8545 (online)

Nanotechnologies in construction
Нанотехнологии в строительстве

2026; 18 (5):
591–600

RESULTS AND DISCUSSION

1. Microgeometry of piston-cylinder surfaces

When evaluating the geometry of the inner cavity of the coating cylinder, several types of internal combustion engines with a volume of 40 cm^3 were considered as prototypes: GTT70 from NGH and 70SS HARBIN BIN-AU TECHNOLOGY DEVELOPMENT CO., LTD.

3D digitization of cylinder-piston group parts was performed. Workflow for Creating an Electronic Geometric Product Model (EGMI) as a Solid State Computer Model (SM) includes aligning a polygonal surface model of a part with a global assembly coordinate system, splitting model surfaces, defining base surfaces for geometry analysis, sketching on base surfaces, – building a solid CAD model, performing an inspection (comparison) of the obtained solid KM relative to the polygonal surface model, export the model in .STEP format for further work in CAD. The results of inspection of the digitized housing of the cylinder of the internal combustion engine and KM are shown in Figure 2.

Inspection results reflect deviations of solid model geometry from polygonal surface model. Deviations in plus are indicated in red. Deviations in minus are indicated in blue. The most significant deviations of the cylinder CM after editing in ESCS are the muffler connection flange (its thickness was rounded to an integer) and the location of the cooling ribs in the lower part of the cylinder. Maximum deviations are 0.5 mm (Fig. 2), which corresponds to the 5th degree of accuracy in accordance with [13].

The interior of the cylinder is machined. Machining is performed to ensure accurate geometry, removal of the surface layer of the casting, as well as to prepare the surface for the application of a wear-resistant coating. To determine the degree of dimensional accuracy, an analysis of the microgeometry of the inner surface of the cylinder was carried out, as well as diagrams of profile deviations in three sections (Fig. 3). The nominal diameter of the section is 39 mm. The results of analysis of section profile deviations from the nominal diameter size are presented in Table 1.

The results of inspection of the digitized ICE and KM piston are shown in Figure 4.

Deviations of the piston dimensions do not exceed 0.23 mm in the base and 0.08 mm near the hemispherical end part, which corresponds to 3 degrees of accuracy [13]. The layout of the planes for the analysis of the microgeometry of the outer surface of the piston is shown in Figure 5.

The nominal diameter of the section is 38.9 mm. The results of analysis of section profile deviations from the nominal diameter size are presented in Table 2.

Thus, the nominal radial clearance is 250 μm. There are no regulatory documents to ensure gaps in the piston-cylinder pair, the manufacturer installs them himself, depending on many factors. When applying the coating, we focus on maintaining the nominal gap. The results of the cylinder and piston geometry study showed that the hole diameter in the cylinder e $39^{+0.146}_{+0.00}$, the piston diameter $38{,}5^{-0.038}_{-0.15}$. Analysis of the microgeometry of the ICE under consideration showed that the minimum radial gap was 269 microns, the maximum radial gap was 398 microns. The manufacturing accuracy depends on the field of application of the internal combustion engine. The measured values of the gaps are typical for non-response devices.

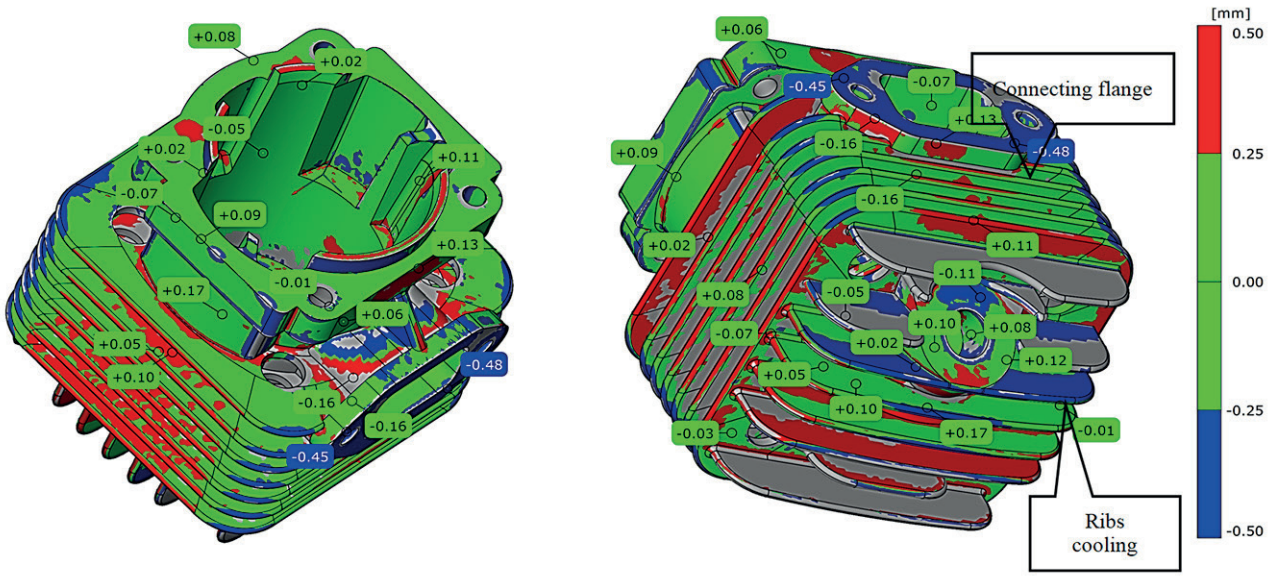


Fig. 2. Results of inspection of "Cylinder" part

ISSN 2075-8545 (online)

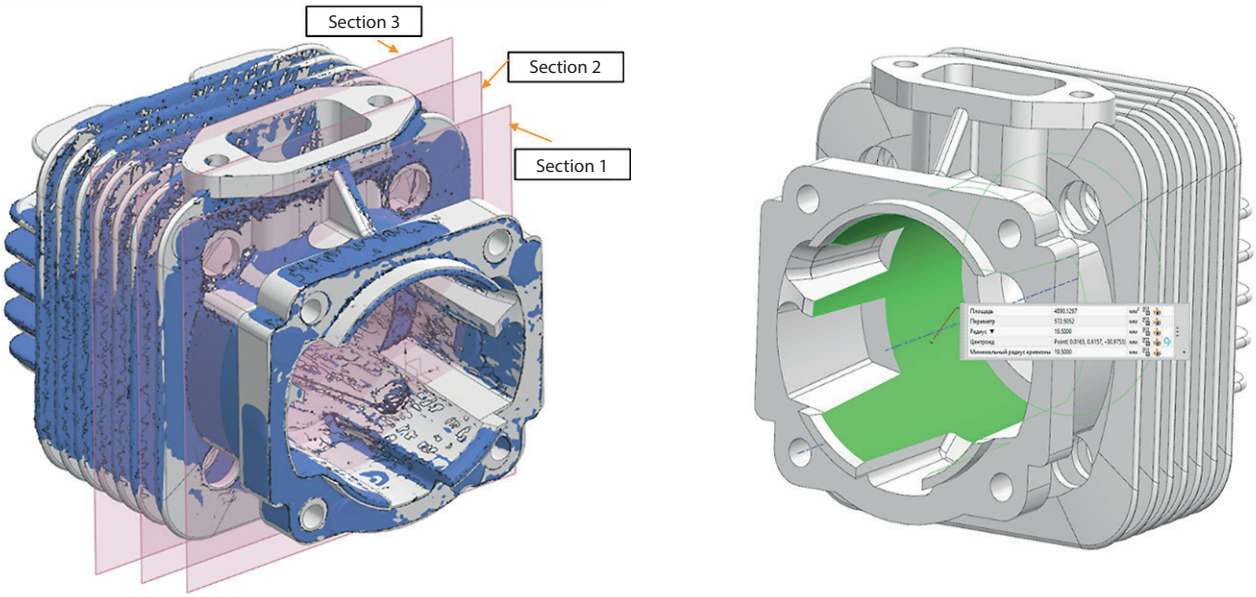
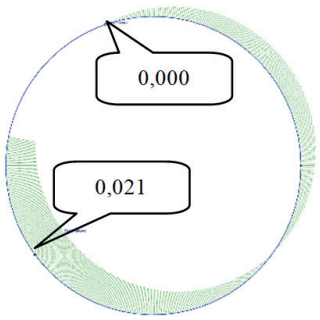
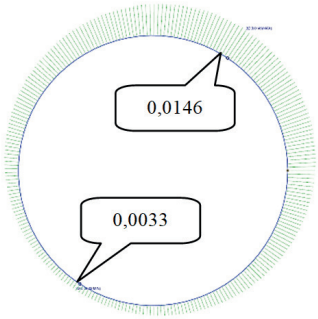
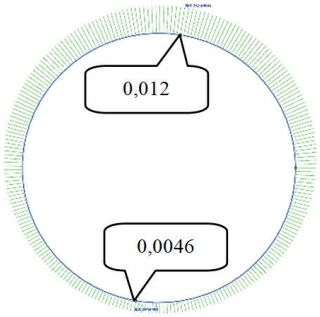


Fig. 3. Location of "Cylinder" part profile microgeometry analysis planes

Table 1. Results of microgeometry analysis of the cylinder inner surface profile

Section 1		Minimum deviation 0.00 mm Maximum deviation 0.021 mm
Section 2		Minimum deviation 0.0033 mm Maximum deviation 0.0146 mm
Section 3		Minimum deviation 0.0046 mm Maximum deviation 0.012 mm

ISSN 2075-8545 (online)

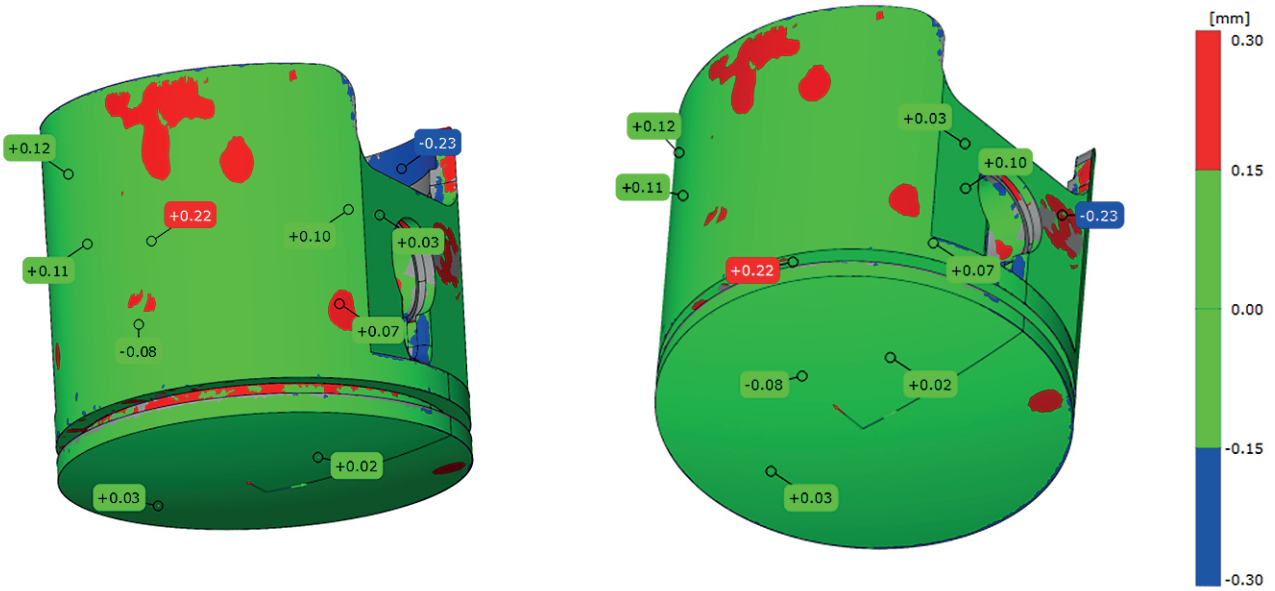


Fig. 4. "Piston" part inspection results

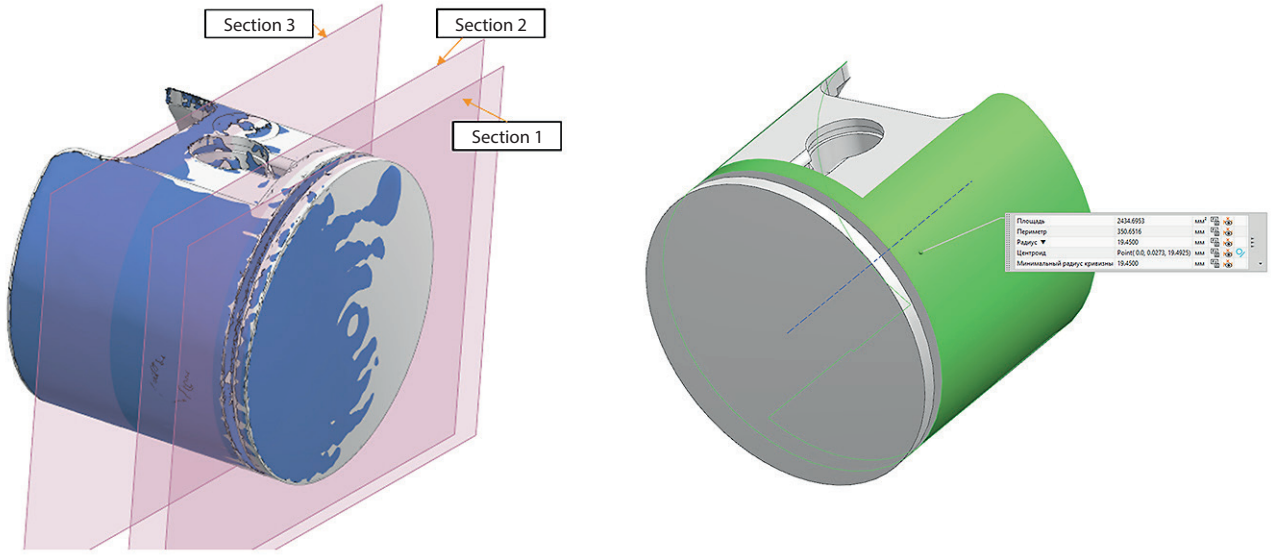


Fig. 5. Location of planes of "Piston" part profile microgeometry analysis

2. Chemical composition of piston-cylinder parts

In the case of machining of the housing for coating, repair of the worn coating and the cylinder itself, the material of the parts should be determined. The results of the study of the chemical composition of the main parts of the internal combustion engine are presented in Table 3.

Aluminum deformable alloy AMg4.5 State Standard 4784-2019 [15] is the closest in composition to the material of the parts of the cylinder body, body cover and cylinder piston. This alloy contains 3.5–4.5% magnesium, which provides the necessary balance between strength and ductility of the material.

3. Analysis of Nikasil coating properties on the inner surface of the cylinder

Figure 6 shows a typical microstructure of a Ni SiC composite coating applied to a cylinder. It can be seen from the figure that silicon carbide nanoparticles are uniformly distributed throughout the matrix. Table 4 shows the results of the selected local power dispersion analysis zones.

ISSN 2075-8545 (online)

Table 2. Results of microgeometry analysis of piston outer surface profile

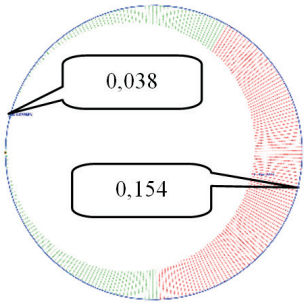
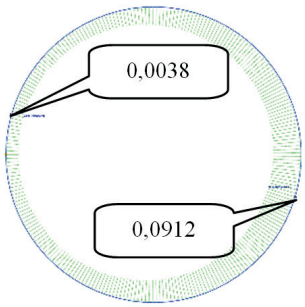
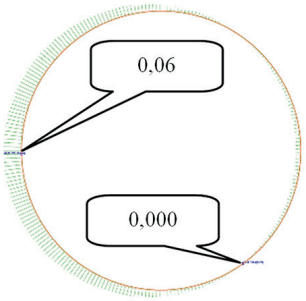
Section 1		Minimum deviation 0.038 mm Maximum deviation 0.154 mm
Section 2		Minimum deviation 0.0038 mm Maximum deviation 0.0912 mm
Section 3		Minimum deviation 0.00 mm Maximum deviation 0.06 mm

Table 3. Results of spectral analysis of internal combustion engine parts

Details	Al	Cu	Fe	Zn	Mn	Ni	Mg	Si	Cr	Ti
Cylinder housing	93.84± 0.80	0.05± 0.006	0.01± 0.003	0.01± 0.003	0.50± 0.005	-	5.20± 0.05	0.35± 0.04	0.02± 0.001	0.02± 0.001
Housing cover	93.48± 0.80	0.04± 0.005	0.02± 0.003	0.01± 0.003	0.53± 0.005	-	5.50± 0.05	0.38± 0.04	0.02± 0.001	0.02± 0.001
Piston	98.50± 0.90	0.633± 0.006	0.282± 0.007	0.015± 0.003	0.45± 0.005	0.578± 0.006	5.30± 0.05	0.30± 0.04	0.01± 0.001	0.015± 0.001

Spectra 1, 3–5 correspond to the main coverage area, spectra 2, 6, 7 – to the cylinder material.

In order to verify the uniformity of the coating over the entire surface, control measurements were carried out in three characteristic zones: at the upper edge of the cylinder, in the middle part and at the lower edge (from section 1 to section 3 according to Fig. 3). In each of these zones, the thickness of the coating in the cross-section was determined, and the Vickers microhardness was evaluated. The results obtained are shown in Table 5.

Recommended values of Nikasil layer thickness are 100–200 μm [16–17]. The thickness of the formed coating (Table 5) was 160±10 μm.

When assessing the uniformity of the coating (Table 5), a slight decrease in thickness is noted from the upper to the lower edge of the cylinder (from section 1 to section 3 according to Fig. 3). This is due to the pecu-

ISSN 2075-8545 (online)

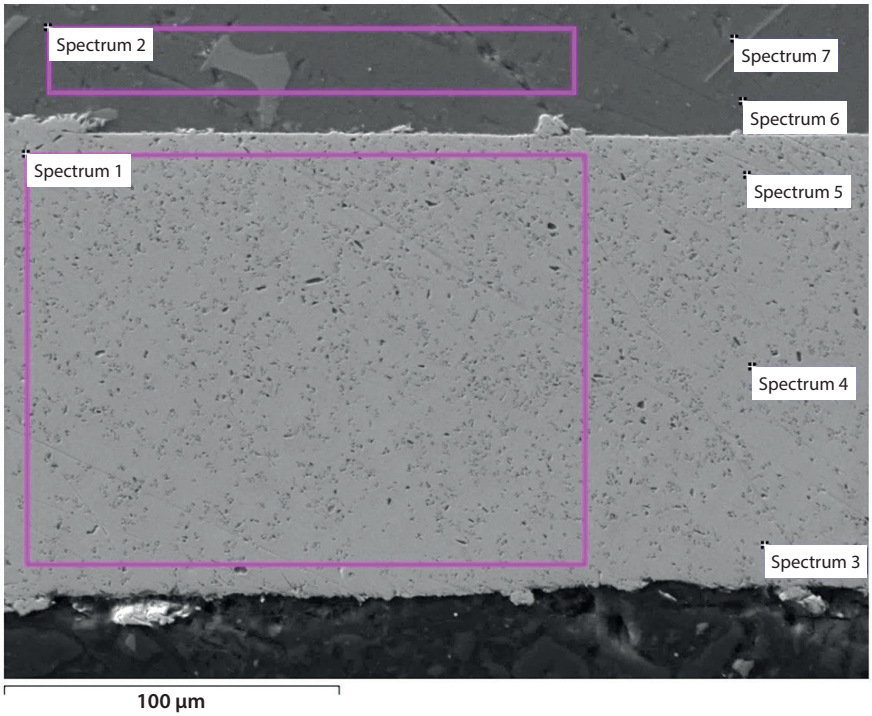


Fig. 6. Ni–SiC coating microstructure

Table 4. Elemental composition of the coating according to Figure 6

Spectrum	In stat.	C	Mg	Al	Si	Fe	Ni	Cu	Zn	Result
Spectrum 1	Yes	3.23			2.82		93.95			100.00
Spectrum 2	Yes	4.90	0.49	86.87	3.46	1.44	0.60	1.65	0.59	100.00
Spectrum 3	Yes				0.62		99.38			100.00
Spectrum 4	Yes	7.22			7.77		85.01			100.00
Spectrum 5	Yes	2.55			0.60		96.85			100.00
Spectrum 6	Yes		0.54	95.29	0.75		0.66	2.06	0.70	100.00
Spectrum 7	Yes		0.57	87.94	0.97	0.44	3.78	5.80	0.50	100.00
Max.		7.22	0.57	95.29	7.77	1.44	99.38	5.80	0.70	
Min.		2.55	0.49	86.87	0.60	0.44	0.60	1.65	0.50	
All results are reported in weight percent (wt%)										

Table 5. Coating thickness and hardness

	Upper edge Section 1	Middle Section 2	Bottom Edge Section 3
Thickness, µm	170±5	158±5	150±5
Hardness HV	429±5	411±5	420±5

liarities of the hydrodynamics of the electrolyte with the horizontal arrangement of the bath.

Deviations in the microhardness values of the composite coating along the entire length of the cylinder do not exceed 5%, which indicates the technological uniformity of the applied composition.

CONCLUSION

The nominal radial clearance in the cylinder-piston group is 250 µm. According to the results of evaluation of microgeometry of the cylinder-piston pair profiles, the radial clearance on the ICE under consideration is from

ISSN 2075-8545 (online)

269 μm to 398 μm, which is critical for critical devices. Before coating, machining of the inner surface of the cylinder is required to equalize the radial gap to 400+10 μm, ensuring a $39^{+0,40}_{+0,39}$ mm.

The developed coater ensures geometric and structural uniformity of the coating with a thickness of 160±10 microns. The thickness error is explained by the peculiarities of the electrolyte hydrodynamics with the horizontal arrangement of the bath. The coated surface shall be finished.

In the future, bench tests of the wear resistance of the coating will be carried out. Subsequent studies will be aimed at optimizing the technology of its application in order to achieve an indicator of operating time of 500 hours before overhaul.

REFERENCES

1. Borovkov A.I. *Aircraft and UAV engines market in 2023: Trends and scenarios. An Expert and Research Report*. POLYTECH-PRESS; 2023. https://doi.org/10.18720/SPBPU/2/i24-126 (in Russ.).

2. Aviation of Russia: 16 December 2023. Available at: https://aviation21.ru/turbovintovoj-dvigatel-dlya-tvs-2ms-sozdadut-metodom-revers-inzhiniringa (accessed: 15.10.2025). (in Russ.).

3. Zhachkin S., Trifonov G., Sidorkin O., Pustovetov A. Wear resistance of nickel composite coatings with micron and submicron SiC particles. *Engineering technologies and systems*. 2024; 34 (4):629–647. https://doi.org/10.15507/2658-4123.034.202404 (in Russ.).

4. Hui F. Electroplating of Compound Ni–SiC Coatings and Improvement of Wear Resistance. *Key Engineering Materials*. 2010; 426-427:399–402. https://doi.org/ 10.4028/www.scientific.net/kem.426-427.399

5. Kiseleva S., Akhmerov L. Lukyanov V., Kandarov I. Ni-SiC composite coating obtained by electrodeposition. *Nanotechnology in construction*. 2025; 17 (4): 446-454. https://doi.org/10.15828/2075-8545-2025-17-4-446-454 (in Russ.).

6. Kiseleva S., Akhmerov L., Lukyanov V., Kandarov I. Ni-SiC composite coating unit. *Materials. Technologies. Design*. 2025;7:3(22):21–31. https://doi.org/10.54708/26587572_2025_732221 (in Russ.).

7. Lukyanov V. Kiseleva S., Berdin V., Akhmerov L. *Device for galvanic deposition of composite Ni-SiC* (Patent No. RU 243 639 U1). Ufa State Petroleum Technological University; 2025.

8. *Approved types of measuring instruments*. Available at: https://fgis.gost.ru/fundmetrology/cm/mits/6cb239e1-aac1-81c4-554d-d02da8d636b9 (accessed: 15.10.2025). (in Russ.).

9. *PointShape Design*. Available at: https://www.pointshape.online/#design (accessed: 15.10.2025). (in Russ.).

10. *Zeiss inspect: One Metrology Software*. Available at: https://www.gom.com/en/products/gom-suite/gom-inspect-pro?msclkid=f0dfe046d54f11c8780081b88e0cb936 (accessed: 15.10.2025).

11. *Russian engineering software ASCON*. Available at: https://ascon.ru/ (accessed: 15.10.2025). (in Russ.).

12. *Non-ferrous metals and their alloys. General requirements for analytical methods*. Edition 1 2026-03. Read sample. GOST 25086:2025. (in Russ.).

13. *Castings made of metals and alloys. Dimensional tolerances, weights and machining allowances*. Edition 1 2009-12. Read sample. GOST R 53464-2009. (in Russ.).

14. *General tolerances. Tolerances for linear and angular dimensions without individual tolerance indications*. Edition 2004-01. Read sample. GOST 30893.1-2002. (in Russ.).

15. *Aluminium and aluminium deformable alloys. Stamps*. Edition 2019-01. Read sample. GOST 4784-2019. (in Russ.).

17. *Nicosil coating and chromium plating of chainsaw cylinder*. Available at: https://web.archive.org/web/20171130175221/ http://chainsaws-portal.ru/benzopila/nikosilovoe-pokrtie-i-hromirovanie-tsilindra-benzopil.html (accessed: 15.10.2025). (in Russ.).

18. *Unified corrosion and ageing protection system. Metallic and non-metallic inorganic coatings. General selection requirements*. Edition 1985-01. Read sample. GOST 9.303-84. (in Russ.).

ISSN 2075-8545 (online)

Nanotechnologies in construction
Нанотехнологии в строительстве

2026; 18 (5):
591–600

Nanobuild.ru

CONSTRUCTION MATERIALS SCIENCE

ADDITIONAL INFORMATION

The authors declare that during the preparation of the article did not use technologies of generative artificial intelligence and technologies based on artificial intelligence.

INFORMATION ABOUT THE AUTHORS

Denis N. Mazidullin – engineer, Center for reverse engineering, senior lecturer, Mechanics and machine design department, Ufa state petroleum technological university, Ufa, Kosmonavtov str. 1, 450064, Russian Federation, mazidullindenis@mail.ru, https://orcid.org/0009-0009-0225-3814

Pavel P. Tregubov – engineer, Reverse engineering center, assistant, Technological machines and equipment department, Ufa state petroleum technological university, Ufa, Kosmonavtov str. 1, 450064, Russian Federation, tregubov@tpaha.ru, https://orcid.org/0009-0000-4962-7160

Maria V. Demchenko – Can.Sci. (Eng.), Associate Professor, Technological machines and equipment department, director of the Reverse engineering center, Ufa state petroleum technological university, Ufa, Kosmonavtov str. 1, 450064, Russian Federation, m.v.demchenko@yandex.ru, https://orcid.org/0000-0002-6950-5811

Linar D. Akhmerov – laboratory assistant, Intelligent engineering center, Ufa state petroleum technological university, Kosmonavtov str. 1, 450064, Russian Federation; laboratory assistant Technopark AT, Ufa, Tramvaynaya str. 5, building 1, 450112, Russian Federation, linarakhmerov2@gmail.com, https://orcid.org/0009-0002-9825-2697

Azamat A. Arslanov – engineer, Intelligent engineering center, Ufa state petroleum technological university, Ufa, Kosmonavtov str. 1, 450064, Russian Federation; design engineer Technopark AT, Ufa, Tramvaynaya str. 5, building 1, 450112, Russian Federation, texnopark_arslanov_2024@mail.ru, https://orcid.org/0009-0004-8893-9764

CONTRIBUTION OF THE AUTHORS

D.N. Mazidullin – analysis of the microgeometry of the surfaces of parts, calculation of the degree of accuracy of the surfaces of castings and mechanical processing of parts by reverse engineering.

P.P. Tregubov – 3D digitization of internal combustion engine parts, processing and stitching of scans, development of solid-state models, 3D inspection of models relative to scans.

M.V. Demchenko – substantiation of the relevance and purpose of ICE reverse engineering, setting research objectives, analysis and interpretation of results taking into account the subsequent application of metal-matrix coating.

L.D. Akhmerov – coating the cylinder by electrodeposition.

A.A. Arslanov – analysis of the research results.

The authors declare no conflicts of interest

The article was submitted 06.07.2026; approved after reviewing 05.10.2026; accepted for publication 10.10.2026.

ISSN 2075-8545 (online)

Nanotechnologies in construction
Нанотехнологии в строительстве

2026; 18 (5):
601–608

Nanobuild.ru

THE RESULTS OF THE SPECIALISTS' AND SCIENTISTS' RESEARCHES

Original article
https://doi.org/10.15828/2075-8545-2026-18-5-601-608

CC BY 4.0

Assessment of the potential application of thermoplastic polymers for insulating the electrodes of high-temperature cartridge-type electric heaters

Oleg R. Latypov[1]*, Karina V. Kim[1, 2], Vasily V. Lukyanov[1, 2], Dina R. Latypova[1], Rustem R. Daminev[1], Aliyana Z. Khusnutdinova[1, 2]

[1] Ufa State Petroleum Technological University, 450064, Ufa, Kosmonavtov street, 1, Russian Federation
[2] Scientific and Production Association "Technopark of Aviation Technologies", Tramvaynaya str. 5, building 1, 450112, Russian Federation

* Corresponding author: e-mail: o.r.latypov@mail.ru

ABSTRACT

Introduction. Tubular electric heaters are widely used in industrial and domestic heating applications. Structurally, tubular electric heaters consist of a metal shell housing a heating element, with the space between them filled with a high-temperature, heat-conducting dielectric material. A tubular electric heater is divided into several zones: the active (heating) zone, the cold zone (contact terminal zone), and the transition zone. The "cold" sections of the tubular electric heater, where the contact rods connected to the terminal wires are located, are the most critical in terms of electrical safety and durability. This zone requires reliable electrical insulation, sealing from the external environment (moisture, corrosive environments, dust, aggressive vapors), and mechanical fixation of the current-carrying elements. The aim of this study was to develop and optimize the composition of a sealing material for the cold section of a tubular electric heater. **Materials and Methods.** To achieve this goal, a series of pilot samples of sealing materials for protective insulating coatings were manufactured by modifying their compositional components: the polymer base, plasticizer, and filler. Samples of sealing materials for the cold section of tubular electric heaters were subjected to a comprehensive evaluation of their adhesive strength, oil-and-petrol resistance, dielectric and mechanical properties, and chemical resistance. **Results.** The paper presents an analysis of the feasibility of using an insulating nanomaterial for the cold section of a tubular electric heater. The results of a study of materials with various compositions, including Ammerheim Phenol Epoxy phenol-epoxy coating, T-111 epoxy resin, F-4D fluoroplastic suspension with nanoscale particles, one-component silicone sealant, ethyl cellulose, VIKSINT PK-68 organosilicon rubber, and SEDM-6 epoxy resin, showed that the most promising material for sealing the "cold" section of a tubular electric heater is F-4D fluoroplastic, which exhibits unique chemical resistance to gasoline, oils, and aggressive environments, a wide operating temperature range (from –190 to 250 °C), and excellent dielectric properties. **Conclusion.** Based on the results of the tests, fluoroplastic F-4D was selected as the sealing dielectric material for the "cold" section of the cartridge electric heater. This material possesses the necessary properties for operation: heat resistance, oil-and- petrol resistance, dielectric strength, high ductility, and chemical resistance. However, the fluoroplastic F-4D-based composition requires additional modification to improve adhesion to the metal surface of the tubular electric heater.

KEYWORDS: tubular electric heater, dielectric resistance, heat resistance, oil-and-petrol resistance, chemical resistance, fluoroplastic

SOURCES OF FUNDING FOR THE SCIENTIFIC WORK THAT RESULTED IN THE PUBLICATION: This work was conducted as part of the Strategic Project "New technologies, technical, and intelligent systems in mechanical engineering" of the Ufa State Petroleum Technological University Development Program for 2021–2030 in accordance with the Priority 2030 Strategic Academic Leadership Program.

ACKNOWLEDGEMENTS: The authors are grateful for the financial support of this project.

FOR CITATION:
Latypov O.R., Kim K.V., Lukyanov V.V., Latypova D.R., Daminev R.R., Khusnutdinova A.Z. Assessment of the potential application of thermoplastic polymers for insulating the electrodes of high-temperature cartridge-type electric heaters. *Nanotechnologies in Construction*. 2026;18(5):601–608. https://doi.org/10.15828/2075-8545-2026-18-5-601-608. – EDN: SOFXUR.

© Latypov O.R., Kim K.V., Lukyanov V.V., Latypova D.R., Daminev R.R., Khusnutdinova A.Z., 2026

ISSN 2075-8545 (online)

Nanotechnologies in construction
Нанотехнологии в строительстве

2026; 18 (5):
601–608

Nanobuild.ru

THE RESULTS OF THE SPECIALISTS' AND SCIENTISTS' RESEARCHES

Анализ возможности применения термопластичных полимеров для изоляции электродов высокотемпературных патронных электрических нагревателей

Олег Ренатович Латыпов[1]*, Карина Вадимовна Ким[1, 2], Василий Васильевич Лукьянов[1, 2], Дина Ринатовна Латыпова[1], Рустем Рифович Даминев[1], Алияна Зенфировна Хуснутдинова[1, 2]

[1] Уфимский государственный нефтяной технический университет, 450064, Уфа, улица Космонавтов, 1, Российская Федерация

[2] Научно-производственная ассоциация «Технопарк Авиационных технологий», 450112, Уфа, ул. Трамвайная 5, к. 1, Российская Федерация

* Автор, ответственный за переписку: e-mail: o.r.latypov@mail.ru

АННОТАЦИЯ

Введение. Трубчатые электронагреватели нашли широкое применение в промышленных и бытовых нагревательных устройствах. Конструктивно трубчатые электронагреватели представляет собой металлическую оболочку, внутри которой расположен нагревательный элемент, а пространство между ними заполнено высокотемпературным теплопроводящим диэлектрическим материалом. В конструкции трубчатого электронагревателя выделяют несколько зон: активную (нагревательную), холодную зону (зону вывода контактов) и переходную область. Наиболее ответственными с точки зрения электрической безопасности и долговечности являются «холодные» части трубчатого электронагревателя, где располагаются контактные стержни, соединенные с выводными проводами. Именно в этой зоне необходимо обеспечить надежную электроизоляцию, герметизацию от внешней среды (влаги, коррозионной среды, пыли, агрессивных паров) и механическую фиксацию токоведущих элементов. Целью работы являлась разработка и оптимизация состава герметизирующего материала для холодной части трубчатого электронагревателя. **Материалы и методы.** Для достижения цели были изготовлены серии опытных образцов герметизирующих материалов для защитного изоляционного покрытия путем модифицирования их компонентов состава: полимерной основы, пластификатора и наполнителя. Образцы из герметизирующих материалов для холодной части трубчатого электронагревателя подвергли комплексной оценке на их адгезионную прочность, маслобензостойкость, диэлектрические и механические характеристики, а также химическую стойкость. **Результаты.** В работе приведен анализ возможности применения изолирующего наноматериала на холодную часть трубчатого электронагревателя. Результаты исследования материалов различных составов: фенол-эпоксидного покрытия «Аммерхайм Фенол Эпокси», эпоксидной смолы Т-111, фторопластовой суспензии Ф-4Д с наноразмерными частицами, однокомпонентного силиконового герметика, этилцеллюлозы, кремнийорганического каучука ВИКСИНТ ПК-68, эпоксидной смолы СЭДМ-6 – показали, что наиболее перспективными материалами для герметизации «холодной» части трубчатого электронагревателя является фторопласт Ф-4Д, который обладает уникальной химической стойкостью к бензину, маслам и агрессивным средам, широким диапазоном рабочих температур (от –190 до 250 °С) и превосходными диэлектрическими свойствами. **Заключение.** В результате проведенных испытаний выбран герметизирующий диэлектрический материал фторопласт Ф-4Д для «холодной» части патронного электрического нагревателя. Этот материал обладает необходимыми для эксплуатации свойствами: термостойкостью, маслобензостойкостью, диэлектрической прочностью, имеет высокую пластичность и химическую стойкость. Однако композиция на основе фторопласт Ф-4Д требует дополнительной модификации для повышения адгезии к металлической поверхности трубчатого электронагревателя.

КЛЮЧЕВЫЕ СЛОВА: трубчатый электронагреватель, диэлектрическая стойкость, термостойкость, маслобензостойкость, химическая стойкость, фторопласт

ИСТОЧНИКИ ФИНАНСИРОВАНИЯ НАУЧНОЙ РАБОТЫ, РЕЗУЛЬТАТОМ КОТОРОЙ СТАЛА ПУБЛИКАЦИЯ: Работа проводилась в рамках реализации Стратегического проекта «Новые технологии, технические и интеллектуальные системы в машиностроении» программы развития ФГБОУ ВО «Уфимский государственный нефтяной технический университет» на 2021-2030 годы в соответствии с программой стратегического академического лидерства «Приоритет 2030».

БЛАГОДАРНОСТИ: Авторы выражают благодарность за финансовую поддержку проекта.

ДЛЯ ЦИТИРОВАНИЯ:

Латыпов О.Р., Ким К.В., Лукьянов В.В., Латыпова Д.Р., Даминев Р.Р., Хуснутдинова А.З. Анализ возможности применения термопластичных полимеров для изоляции электродов высокотемпературных патронных электрических нагревателей. *Нанотехнологии в строительстве*. 2026;18(5):601–608. https://doi.org/10.15828/2075-8545-2026-18-5-601-608. – EDN: SOFXUR.

ISSN 2075-8545 (online)

INTRODUCTION

Cartridge tubular electric heaters are widely used for heating casting molds and press forms, as well as various liquids, such as water, fats and oils, and acid and alkali solutions. These products serve as components in industrial installations and household heating appliances [1–3]. A promising area of application may be the oil and gas production industry. However, oil field environments are characterized by high aggressiveness. The corrosive aggressiveness of oil field environments is caused by the presence of dissolved acidic gases (CO_2, O_2 and H_2S), abrasive particles, basic salt ions (Mg^{2+}, Ca^{2+}, Na^+, SO_4^{2-}, Cl^-), water-soluble mineral and organic acids and bases, as well as the presence of anaerobic and aerobic microorganisms, the metabolic products of which provoke microbiological corrosion of metal and biofouling [4–7]. The cold section of a tubular electric heater is an unheated section near the terminals of electrical wires, the length of which varies depending on the heater design, and the cross-section and diameter of the resistive heating element are determined based on the specific power permissible for the material under the given operating conditions [2]. The sealing zone of the cold section is critical in terms of thermal and chemical effects. The destruction of the sealed layer and subsequent diffusion of moisture contributes to the saturation of the heat-conducting insulating material of the inner part of the cartridge electric heater, which can lead to its destruction and electrical breakdown on the housing [8].

Electrical strength and high insulation resistance are fundamental to ensuring electrical safety when operating a cartridge heater. Cold insulation resistance must be at least 0.5 megohms at 500 VDC. Leakage current, in turn, is standardized to no more than 0.75 mA/kW at 127–380 V, 50 Hz. The recommended test voltage for polymer insulation can reach 2500 V. Insulation resistance must be at least 20 megohms. However, increasing temperature can reduce the resistance of the insulating material, so heat resistance is also important – this is the material's ability to withstand elevated temperatures without deteriorating its properties for a period equal to its normal service life [9]. Insulation resistance depends on temperature, electrical and mechanical stress, vibration, environmental aggressiveness, chemical influences, and humidity [10]. To insulate the cold section of the heater, it is necessary to use insulating materials of heat resistance class F (155 °C) or H (180 °C). Moreover, the product must withstand short-term overheating up to 200 °C. In addition to high-temperature resistance, the insulation must maintain elasticity and integrity under cyclic temperature changes and not cause cracking of the coating.

Contact between the cold section of a cartridge heater and hydrocarbon liquids (oil, gasoline, and lubricants) is inevitable when operating heaters in the oil industry. Therefore, the insulation material for the cold section of a cartridge heater must be sufficiently oil-and-petrol resistance.

In the oil and gas industry, wire insulation must withstand a range of aggressive factors: natural gas and its components, hydrogen sulfide (H_2S), carbon dioxide (CO_2), formation waters with a high salt content, acids and alkalis used in well treatment, solvents used in cleaning equipment, as well as other process fluids [5–6].

In this regard, specific requirements are imposed on the insulating material for the cold section of the cartridge electric heater: a wide operating temperature range: from –60 °C to +180 °C; resistance to hydrocarbon environments (oil and gasoline resistance); high dielectric properties; good adhesion to metal substrates; chemical resistance to aggressive environments – acidic gases, salts, acids and alkalis.

MATERIALS AND RESEARCH METHODS

Polymer compositions that are already in use or are considered the most promising for the operation of the cold section of a cartridge electric heater in aggressive conditions were selected as test objects [11–14].

Ammerheim Phenol Epoxy coating is a two-component phenol-epoxy composition based on novolac resin. According to the manufacturer's technical documentation, the coating is designed for the anti-corrosion protection of metal structures operating at temperatures up to 220 °C. It is resistant to sudden temperature changes and chemically resistant to hydrocarbons, acids, and alkalis.

T-111 resin is an epoxy resin modified with polyorganosiloxane. It is designed for the production of heat-resistant adhesives, in particular K-400 adhesive, which operates in temperatures ranging from –196 °C to 400 °C for short periods and for up to 1000 hours at 200 °C.

SDM-6 epoxy resin, which is a component of K-300-61 adhesive, can be used in temperatures ranging from –196 °C to 300 °C for 1 minute, and at 200 °C for 1000 hours.

Ethyl cellulose is a cellulose derivative in which some hydroxyl groups are replaced by ethyl groups. It forms strong, durable, and elastic films. It has low hygroscopicity. It is compatible with many plasticizers, resins, and oils.

A one-component silicone sealant designed for sealing, bonding, and sealing joints and components, heating panels, and other elements exposed to high temperatures. It features excellent adhesion to most building materials. It offers high performance characteristics: it maintains elasticity under continuous thermal loads of up to 300 °C and is non-corrosive to metals.

Fluoroplast-4D is a product of tetrafluoroethylene polymerization, produced in an aqueous environment under pressure. Fluoroplast has high dielectric properties

ISSN 2075-8545 (online)

and is resistant to aggressive environments. The operating temperature of fluoroplastic films ranges from –60 °C to 250 °C.

VIKSINT PK-68 organosilicon rubber is an organosilicon compound designed to protect electronic and radio-technical equipment operating for extended periods in air and high-humidity conditions at temperatures ranging from –60 °C to 200 °C. The compound's softness and elasticity make it suitable for sealing ferrite and permalloy components.

To produce free-standing films (for tensile testing and oil and petrol resistance), fluoroplastic-4 plates measuring 200×200×3 mm, according to GOST 10007-80, were used. The film was separated from the fluoroplastic mechanically after complete curing.

For adhesion testing, we used 50×50×2 mm plates made of 12Kh18N10T corrosion-resistant steel. Before coating application, the plate surface was sanded with 120–150 μm abrasive paper to achieve a roughness of Ra 1.6–3.2 μm. A two-stage degreasing process was then performed: first with acetone, then with isopropyl alcohol. The plates were wiped with lint-free cloths, changing them at each stage.

Oil-and-petrol resistance tests were conducted on the materials using a methodology adapted from GOST 12020-2018. Thickness swelling and mass changes of the material samples were calculated. For this purpose, 50×50 mm specimens were cut from loose films of the material, their thickness was measured at five points with a micrometer to an accuracy of 0.01 mm, and weighed on an analytical balance. The specimens were completely immersed in gasoline at a temperature of (22±2) °C for periods of 1, 3, 24, 48, and 196 hours. After removal, the specimens were blotted with filter paper, re-weighed, and their thickness was measured. The appearance of cracks, bubbles, cloudiness, delamination, and other defects was also visually noted, and the change in area due to warping was determined.

Adhesion was tested using the normal pull-off method according to GOST 32299-2025 (ISO 4624:2023) on a REM-U-A universal testing machine (Russia) with a maximum load of 50 kN. The loading rate was 1 mm/min. Steel cylindrical caps were glued to the coating with KD-19 epoxy adhesive. The adhesive was cured for 24 hours at a temperature of (22±5) °C in fixtures for centering the cylindrical caps to the coating. After curing, the sample was secured in the machine grips and loaded until failure. The failure mode was assessed visually: adhesive (peeling off from the substrate), cohesive (rupture within the coating), mixed (peeling off the cap from the coating or a combination of both).

Tensile properties were determined in accordance with GOST 11262-2017. The method involves stretching a specimen at a specified strain rate until failure, determining the ultimate strength and relative elongation. Type 2 (blade) specimens were cut from loose films in accordance with GOST 11262-2017. Tests were conducted on a REM-U-A universal testing machine (Russia) at a temperature of 23±2 °C. The specimen was clamped in wedge or screw grips of the machine such that its longitudinal axis coincided with the loading direction, and the working part was positioned between the grips without distortion. During testing, the load-displacement diagram was automatically recorded using the built-in software. At least three specimens for each composition were tested. The final result was taken as the arithmetic mean; the measurement error according to GOST 11262-2017 for the load should not exceed 1% of the measured value.

The thermal stability of the coatings was assessed by annealing in a KS-18 furnace (Russia) at elevated temperatures. The annealing temperatures were 150, 180, and 200 °C. The coatings were held at these temperatures for 1 hour, and cooled in air at room temperature until completely cooled. Color change, cracks, and warpage of the samples were assessed.

The volume and surface electrical resistance of the insulating coatings were measured with a megohmmeter. The voltage was applied for 60 seconds – the time required for the current to reach a steady state due to polarization processes in the dielectric. The steady-state resistance was recorded.

RESULTS AND DISCUSSION

Due to the promising use of cartridge heaters in the oil and gas industry, oil and gasoline resistance tests were initially conducted. The worst results were observed for ethyl cellulose films. During the preparation and application of the composition to steel samples, a highly porous structure was observed due to incomplete dissolution of the ethyl cellulose powder in the ketone solvent, leading to particle agglomeration and clump formation. The experiment revealed that the developed porosity of the resulting film resulted in its poor barrier properties, specifically, a lack of oil-and-petrol resistance.

Testing of the coating formed using VIKSINT PK-68 organosilicon rubber also revealed its unsuitability for hydrocarbon-containing environments. When a steel plate coated with this coating was immersed in gasoline, swelling resulted in adhesion failure and subsequent peeling.

SEDM-6 and T-11 epoxy resins tested in gasoline for 24 hours showed satisfactory results: swelling resulted in a weight increase of 18 to 20%.

Test results of a single-component silicone sealant showed that the material is resistant to hydrocarbon environments, with no visible signs of degradation, cracking, or adhesion loss. Therefore, this silicone sealant has been established to have sufficient oil-and-petrol resistance for use in contact with gasoline and oils.

ISSN 2075-8545 (online)

The two-component phenol-epoxy coating "Ammerheim Phenol Epoxy" demonstrated the best results. Visual and instrumental analysis revealed no noticeable changes in the linear dimensions of the sample (no swelling). After 96 hours of exposure to gasoline, the coating's adhesion to the substrate remained unchanged, with no signs of delamination or degradation.

Test results of a fluoroplastic coating made from F-4D suspension showed that fluoroplastic exhibits virtually no interaction with hydrocarbons. No visible surface changes, warping, or loss of transparency were observed. The films remained flexible and elastic.

Thus, VIKSINT PK-68 materials, one-component silicone sealant, SEDM-6 and T-11 epoxy resins, Ammerheim Phenol Epoxy phenol-epoxy coating, and F-4D fluoroplastic passed the oil-and-petrol resistance tests.

Next, adhesion strength tests were conducted. Table 1 summarizes the test results for the materials under consideration.

It was noted that all test samples exhibited cohesive or mixed peel strength, indicating adequate adhesion to the metal surface. However, even with the use of adhesive underlayers, the fluoroplastic coating does not achieve the adhesion strength typical of phenolic epoxy materials (8–10 MPa) and remains susceptible to failure during multilayer application (Fig. 1).

The next test involved stretching the insulating films to assess their strength properties. Films made from Ammerheim Phenol Epoxy demonstrated a tensile strength of (10±1) MPa at a relative elongation of 30–33%. This level of strength is sufficient to prevent the coating from breaking when the heater is pressed into the mounting hole. An elongation of 30% indicates moderate ductility –

Table 1. Adhesive strength of coatings to a metal substrate

	Ammerheim Phenol Epoxy	Suspension F-4D with nanoscale particles	Primer + F-4D suspension with nanoscale particles	Ammerheim Phenol Epoxy + T-111 Epoxy Resin
Max. load, N	8198 ± 1	716 ± 1	1807 ± 1	6476 ± 1
Max. deformation, mm	4 ± 1	6 ± 1	4 ± 1	6 ± 1
Ultimate tensile strength, MPa	8 ± 1	1± 1	3 ± 1	6 ± 1
Nature of separation	mixed	cohesive	cohesive	mixed

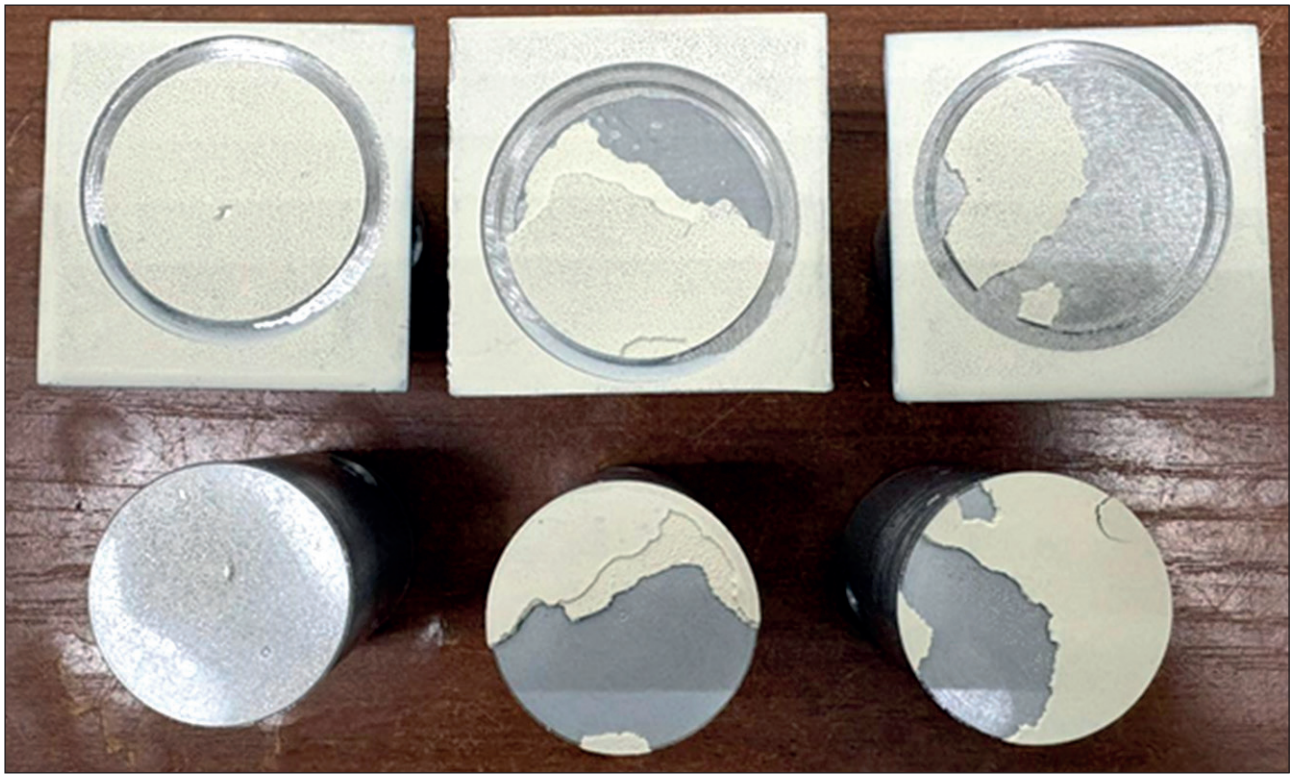


Fig. 1. Cohesive-adhesive peel strength of Ammerheim Phenol Epoxy films + T-111 epoxy resin after testing

ISSN 2075-8545 (online)

the material can be deformed without cracking – but is not highly elastic, which may limit its use in conditions with alternating temperatures.

To assess resistance to elevated temperatures, the coatings were briefly heat-treated to 300 °C. It was found that heating the Ammerheim Phenol Epoxy film to 180 °C and above resulted in irreversible embrittlement. For this material, with the addition of 5–10% plasticizer, heating resulted in a loss of ductility and the appearance of microcracks on the surface.

Films made from T-111 resin exhibited significantly lower strength – (4±1) MPa – but elongation at break reached 49–52%. This is typical behavior for epoxy resins with siloxane modification: they become soft and ductile, but lose strength.

The tensile strength of films made from Ammerheim Phenol Epoxy and T-111 epoxy resin was (6±1) MPa, and the relative elongation was 70.8%. Compared to pure Ammerheim Phenol Epoxy, the strength decreased by approximately 25%, while elasticity more than doubled. This combination of properties is optimal for coatings operating under alternating temperatures: the highly elastic film will follow the deformations of the metal shell without cracking.

Based on the results of measurements and visual inspection of fluoroplast-4 samples, it was established that the material retains its functionality up to 250 °C, and short-term heating up to 300 °C, which allows this limit to be considered acceptable for short-term operating modes (Fig. 2).

One of the key requirements for the insulating material of the "cold" section of a cartridge heater is high electrical resistance, ensuring safe operation at voltages up to 2500 V. According to industry standards, the insulation resistance in the cold state must be at least 1 megohm. The test results are presented in Table 2.

All materials tested showed high insulation resistance, significantly exceeding the required values.



Fig. 2. The appearance of the fluoroplastic-4 coating after heat treatment

CONCLUSION

During the selection of an insulating material for the cold section of a tubular electric cartridge heater, experimental studies were conducted on the following materials: Ammerheim Phenol Epoxy phenol-epoxy coating, T-111 epoxy resin, F-4D fluoroplastic suspension, one-component silicone sealant, ethyl cellulose, VIKSINT PC-68 organosilicon rubber, and SEDM-6 epoxy resin. The experimental results showed:

1.Ammerheim Phenol Epoxy coating exhibits strong adhesion to metal substrates (8–10 MPa), high oil and petrol resistance, high electrical resistance (greater than 2.5 TOhms at 2500 V), and heat resistance up to 200 °C. Based on its combined properties, Ammerheim Phenol Epoxy is recognized as the most balanced material for insulating the cold section of cartridge heaters.

2.T-111 resin demonstrated high elasticity (elongation up to 70%), good dielectric properties (11.57 GOhm), and resistance to short-term overheating up to 400 °C. The main drawback was the difficulty of forming a continuous coating on a metal substrate. However, due to its high elasticity and heat resistance, it can be used as a component in composite compounds.

3.Fluoroplastic F-4D exhibits exceptional chemical resistance to gasoline, oils, and aggressive environments,

Table 2. Results of electrical resistance measurements

Material	Measured resistance, Ohm
Ammerheim Phenol Epoxy	$>2.5 \cdot 10^{12}$ (> 2.5 TOhm)
T-111 Epoxy Resin	$1.157 \cdot 10^{10}$ (11.57 GOhm)
Ammerheim Phenol Epoxy + T-111 Epoxy Resin	$2.3 \cdot 10^{12}$ (2.3 TOhm)
Fluoroplastic F-4D	$>2.5 \cdot 10^{12}$ (> 2.5 TOhm)
One-Component Silicone Sealant	$>2.5 \cdot 10^{12}$ (> 2.5 TOhm)
VIKSINT PK-68 Organosilicon Rubber	$>2.5 \cdot 10^{12}$ (> 2.5 TOhm)

ISSN 2075-8545 (online)

a wide operating temperature range (from –190 °C to +250 °C), and excellent dielectric properties. However, poor adhesion to metal surfaces and cracking during multilayer baking were noted. The use of a primer based on chromium oxide and phosphoric acid increased adhesion to 1.1 MPa, but this is insufficient for direct application to a cold surface. Nevertheless, the material itself is considered promising with further optimization of the adhesive sublayers.

4. This one-component silicone sealant has demonstrated good heat resistance (up to 300 °C) and oil-and-petrol resistance. Silicone sealants maintain their functionality over a wide temperature range and are resistant to hydrocarbons, making them suitable for cold-side insulation, provided adhesion is improved.

The most suitable of the materials studied is fluoroplastic F-4D. It possesses a combination of properties (heat resistance, oil-and-petrol resistance, and dielectric strength) that make it suitable for further development as an insulating coating for the cold section of cartridge heaters.

REFERENCES

1. *GOST 8865-93. Electrical insulation systems. Evaluation of heat resistance and classification*. Introduced on 1994-06-02. Moscow: Standartinform; 1994.

2. Latypov O.R., Cherepashkin S.E., Latypova D.R. The use of the method of controlling the electrochemical parameters of aqueous solutions to combat complications in the operation of oil field pipelines. *Corrosion in the Oil & Gas Industry 2020: E3S Web of Conferences 2021;225:01008*. https://doi.org/10.1051/e3sconf/202122501008. – EDN: LCTAJM.

3. Ustinovskaya M.A. Features of Epoxy-Phenol Compositions for Protecting Canned Containers / M.A. Ustinovskaya, M.V. Krylovskaya. *Advances in Chemistry and Chemical Technology*. 2018; 32: 13 (209):68-70. EDN: VPMKQW.

4. Latypov O.R., Bugai D.E., Boev E.V. Method of Controlling Electrochemical Parameters of Oil Industry Processing Liquids. *Chemical and Petroleum Engineering*. 2015;51(3):283-285. https://doi.org/10.1007/s10556-015-0038-8. – EDN: WTLZMZ.

5. Pechenkina M.Yu., Latypov O.R., Bugai D.E. Increasing the corrosion resistance of the material of oil and gas equipment in water-salt solutions by changing the electrochemical parameters. *IOP Conf. Series: Earth and Environmental Science*. 720;(2021):012142. https://doi.org/10.1088/1755-1315/720/1/012142. – EDN: VVRZLQ.

6. Latypov Oleg, Tyusenkov Anton. Evaluation of corrosion resistance of low alloy steel in catholyte solution. *AIP Conference Proceedings*. 2022; *2467*:020037. https://doi.org/10.1063/5.0092422. – EDN: IRJZNF.

7. Shevlyakov F.B., Latypov O.R. The stability constant of the protective film of corrosion inhibitors. *Int. J. Corros. Scale Inhib*. 2023;12(3):825–841. https://doi.org/10.17675/2305-6894-2023-12-3-2. – EDN: EUJXRW.

8. Bredikhin S.I., Zhigachev A.O., Matveyev D.V., Agarkova E.A. *High-Temperature Sealant for Solid-Oxide Fuel Cells*. Patent RU 2822175C1; 2024.

9. Wang T. *Organic silicone sealant with high thermal conductivity*. Patent CN 101054507 A; 2007.

10. Evstigneev M.A., Bykova T.I. *The method of sealing tubular electric heaters*. Patent SU 972669 A1. No. 3309435/24-07; filed 30.06.1987; published 07.11.1982.

11. Kuznetsova V.A., Zheleznyak V.G., Kurshev E.V., Emelyanov V.V. Study of fuel and water resistance of coatings based on filled epoxy-thiokol polymer compositions. *Aviation materials and technologies*. 2021; 2 (63).

12. Gerasimov D.M., Ilyukhina M.A., Glazov P.A. Low-molecular organosilicon rubbers in sealing compositions (review). *Aviation materials and technologies*. 2020;8:35-45. https://doi.org/10.18577/2307-6046-2020-0-8-35-45. – EDN: NCDFGT.

13.Sukanto H., Raharjo W.W., Ariawan D., Triyono J., Kaavesina M. Epoxy resins thermosetting for mechanical engineering. *Open Engineering*. 2021; 11(1):797–814. https://doi.org/10.1515/eng-2021-0078. – EDN: QYSCSO.

14. Li B., Zhang X., Qi G., Wang X., Zhang J., Han P., Ru Y., Qiao J. A rubber-modified epoxy composite with very high toughness and heat resistance. *Polymers and Polymer Composites*. 2019;27(9):582–586. https://doi.org/10.1177/0967391119854649.

ISSN 2075-8545 (online)

ADDITIONAL INFORMATION

The authors declare that generative artificial intelligence (AI) and AI-based technologies were not used in the preparation of this article.

INFORMATION ABOUT THE AUTHORS

Oleg R. Latypov – Dr. Sci. (Eng.), Professor, Head of the Department of Materials Science and Corrosion Protection, Institute of Oil and Gas Engineering and Digital Technologies, Ufa State Petroleum Technological University, Ufa, Kosmonavtov str. 1, 450064, Republic of Bashkortostan, Russian Federation, o.r.latypov@mail.ru, https://orcid.org/0000-0002-4487-1516

Karina V. Kim – Institute of Oil and Gas Engineering and Digital Technologies, Ufa State Petroleum Technological University, Ufa, Russia; Engineer, Center for Intelligent Mechanical Engineering, Ufa State Petroleum Technological University, Ufa, Kosmonavtov str. 1, 450064, Republic of Bashkortostan, Russian Federation; Laboratory Assistant, Technopark AT, Ufa, Tramvaynaya str. 5, building 1, 450112, Republic of Bashkortostan, Russian Federation, vadimovnakk@gmail.com, https://orcid.org/0009-0004-9434-0408

Vasily V. Lukyanov – Cand. Sci. (Eng.), Associate Professor, Department of Intelligent Systems, Technologies and Equipment in Mechanical Engineering, Institute of Oil and Gas Engineering and Digital Technologies, Ufa State Petroleum Technological University, Ufa, Russia; Senior Researcher, Center for Intelligent Mechanical Engineering, Ufa State Petroleum Technological University, Ufa, Kosmonavtov str. 1, 450064, Republic of Bashkortostan, Russian Federation; Head of Department, Development Management of Special Technologies and Equipment, Technopark AT, Ufa, Tramvaynaya str. 5, building 1, 450112, Republic of Bashkortostan, Russian Federation, lukianovv@bk.ru, https://orcid.org/0009-0006-3621-3966

Dina R. Latypova – Cand. Sci. (Eng.), Associate Professor, Associate Professor of the Department of Materials Science and Corrosion Protection, Institute of Oil and Gas Engineering and Digital Technologies, Ufa State Petroleum Technological University, Ufa, Kosmonavtov str. 1, 450064, Republic of Bashkortostan, Russian Federation, d.r.latypova@mail.ru, https://orcid.org/0000-0002-0637-3313

Rustem R. Daminev – Dr. Sci. (Eng.), Professor, Director of the Institute of Oil and Gas Engineering and Digital Technologies, Ufa State Petroleum Technological University, Ufa, Kosmonavtov str. 1, 450064, Republic of Bashkortostan, Russian Federation, daminew@mail.ru, https://orcid.org/0000-0001-8673-5240

Aliyana Z. Khusnutdinova – Research Engineer, Center for Intelligent Mechanical Engineering, Ufa State Petroleum Technological University, Ufa, Kosmonavtov str. 1, 450064, Republic of Bashkortostan, Russian Federation; Metallurgical Engineer, Technopark AT, Ufa, Tramvaynaya str. 5, building 1, 450112, Republic of Bashkortostan, Russian Federation, aliyana.husnutdinova@yandex.ru, https://orcid.org/0009-0006-0072-9792

CONTRIBUTION OF THE AUTHORS

Oleg R. Latypov – conceptualization (formulation of the research idea and objectives), scientific supervision, review and editing.

Karina V. Kim – conducting experiments and data collection, data processing and curation, visualization of results.

Vasily V. Lukyanov – methodology development, provision of resources (equipment, materials), data analysis, review and editing.

Dina R. Latypova – methodology development, conducting experiments, validation of results, drafting of the manuscript, review and editing.

Rustem R. Daminev – project administration, provision of resources, scientific supervision, review and editing.

Aliyana Z. Khusnutdinova – conducting experiments, data collection, visualization, preparation of illustrations.

The authors declare no conflicts of interest.

The article was submitted 04.07.2026; approved after reviewing 03.10.2026; accepted for publication 09.10.2026.

ISSN 2075-8545 (online)

Nanotechnologies in construction
Нанотехнологии в строительстве

2026; 18 (5):
609–620

Nanobuild.ru

THE RESULTS OF THE SPECIALISTS' AND SCIENTISTS' RESEARCHES

CC BY 4.0

Original article
https://doi.org/10.15828/2075-8545-2026-18-5-609-620

Energy efficiency for pitched roof insulation system

Saveliy O. Artemenko[1], Alexey D. Zhukov[1], Andrey A. Medvedev[1, 3], Ekaterina Yu. Bobrova[2*], Anton S. Pilipenko[1]

[1] National Research Moscow State University of Civil Engineering, 129337, Yaroslavskoye shosse, 26, Moscow, Russian Federation
[2] National Research University "Higher School of Economics", 109028, Pokrovsky Blvd., 11 pp. 10, Moscow, Russian Federation
[3] Russian State University for Geological Prospecting, 117485, Miklukho-Maklaya st., 23, Moscow, Russian Federation

* Corresponding author: e-mail: mla-gasis@mail.ru

ABSTRACT

Introduction. Energy efficiency is a comprehensive criterion that accounts for both manufacturing and installation costs of products, as well as resource savings during structure operation. Optimizing energy costs in product manufacturing and material selection becomes essential, considering the specific operational characteristics of individual construction systems. **Methods and Materials.** Soft stone wool slabs, glass mesh, and modified epoxy resin-based adhesive served as starting materials. The structure was examined using a FEI Quanta 200 scanning electron microscope. Product properties were determined following standard methods. Operational durability assessment employed an accelerated hydrothermal treatment method applied to mineral wool cylinder fragments using a setup developed by Moscow State University of Civil Engineering (MGSU)–GASIS(HSE)–MAXMIR, evaluating changes in product compressibility. **Results.** Thermo-humid exposure had minimal impact on changes in average product density, with variations within experimental error. The binder type showed no significant influence on product characteristics across all stages of temperature-humidity exposure. However, sample mass loss due to thermo-humid exposure and airflow was substantial, necessitating slab reinforcement on surfaces contacting the ventilated space of pitched roofs to resist airflow. **Discussion.** Properties of mineral wool products with reinforced outer layers fully satisfy the operating conditions of thermal insulation materials in pitched roof systems, which experience temperature and humidity fluctuations, as well as dynamic loads from airflow in ventilated spaces. Conclusion. The research resulted in the development and testing of a novel product: soft and semi-rigid mineral wool slabs reinforced with glass mesh. These slabs maintain equivalent thermal characteristics and manufacturing costs to conventional analogs while exhibiting significantly enhanced operational stability, thereby ensuring greater overall system durability. Product energy efficiency was comprehensively evaluated.

KEYWORDS: energy efficiency, comfort conditions, lightweight mineral wool slabs, modified epoxy binder, operational durability

SOURCES OF FUNDING FOR THE SCIENTIFIC WORK THAT RESULTED IN THE PUBLICATION: The studies were conducted on an initiative basis at the experimental facility of ROKCVOOL. Part of the research was carried out at the National Research University Moscow State University of Civil Engineering as part of the implementation of the university's development program "PRIORITY 2030". Project 3.1 "Scientific breakthrough in the construction industry – new technologies, new materials, new methods."

FOR CITATION:
Artemenko S.O., Zhukov A.D., Medvedev A.A., Bobrova E.Yu., Pilipenko A.S. Energy efficiency for pitched roof insulation system. *Nanotechnologies in Construction.* 2026;18(5):609–620. https://doi.org/10.15828/2075-8545-2026-18-5-609-620. – EDN: EETPWG.

© Artemenko S.O., Zhukov A.D., Medvedev A.A., Bobrova E.Yu., Pilipenko A.S., 2026

ISSN 2075-8545 (online)

Nanotechnologies in construction
Нанотехнологии в строительстве

2026; 18 (5):
609–620

Nanobuild.ru

THE RESULTS OF THE SPECIALISTS' AND SCIENTISTS' RESEARCHES

Системы изоляции скатной кровли и их энергетическая эффективность

Савелий Олегович Артеменко[1], Алексей Дмитриевич Жуков[1], Андрей Александрович Медведев[1, 3], Екатерина Юрьевна Боброва[2*], Антон Сергеевич Пилипенко[1]

[1] Национальный исследовательский Московский государственный строительный университет, 129337, Москва, Ярославское шоссе, 26, Российская Федерация

[2] Национальный исследовательский университет Высшая школа экономики, 109028, Москва, Покровский бул., 11, стр. 10, Российская Федерация

[3] Российский государственный геологоразведочный университет им. С. Орджоникидзе, 117485, Москва, ул. Миклухо-Маклая, 23, Российская Федерация

* Автор, ответственный за переписку: e-mail: mla-gasis@mail.ru

АННОТАЦИЯ

Введение. Энергетическая эффективность является комплексным критерием, учитывающим как затраты при изготовлении и монтаже изделий, так и экономию ресурсов при эксплуатации конструкции. Становится целесообразным оптимизация энергетических затрат при изготовлении изделий и использования материалов с учетом особенностей функционирования конкретной строительной системы. **Методы и материалы.** В качестве исходного материала использовались мягкие плиты на основе каменной ваты, стеклянная сетка и клей на основе модифицированной эпоксидной смолы. Изучение структуры осуществлялось с помощью растрового электронного микроскопа FEI Quanta 200. Свойства изделий определялись по нормативным методикам. Оценка эксплуатационной стойкости осуществлялась по ускоренному методу путем гидротермальной обработки фрагментов минераловатных цилиндров на установке, разработанной МГСУ(МИСИ)–ГАСИС(ВШЭ))–МАКСМИР по изменению сжимаемости изделий. **Результаты.** Установлено, что тепловлажностное воздействие незначительно влияет на изменение средней плотности изделий, а вид связующего незначительно влияет на характеристики изделий и их изменение на всех этапах температурно-влажностного воздействия. Потеря массы образцов в результате тепловлажностного воздействия и воздействия потоков воздуха весьма значима. Это делает необходимым усиление плит по поверхностям, контактирующим с вентилируемым пространством скатной кровли, для противодействия воздушному потоку. **Обсуждение.** Увеличение теплопроводности и плотности коррелированы между собой и обусловлены некоторым уплотнением минераловатных изделий в результате вибрационных испытаний. Причиной уплотнения может рассматриваться как смятие волокон, в рамках предложенной теории прочности, так и ослабление омоноличенных контактов между волокнами. **Заключение.** В результате исследований протестирован новый вид продукции – мягкие и полужесткие минераловатные плиты, упрочненные стеклянной сеткой, которые при тех же тепловых характеристиках и стоимости изготовления, что и их аналоги, обладают значительно более высокой эксплуатационной стабильностью, обеспечивая большую долговечность системы в целом. Осуществлена оценка энергетической эффективности изделий.

КЛЮЧЕВЫЕ СЛОВА: энергетическая эффективность, условия комфорта, легкие минераловатные плиты, модифицированное эпоксидное связующее, эксплуатационная стойкость

ИСТОЧНИКИ ФИНАНСИРОВАНИЯ НАУЧНОЙ РАБОТЫ, РЕЗУЛЬТАТОМ КОТОРОЙ СТАЛА ПУБЛИКАЦИЯ: Исследования проводились в инициативном порядке на экспериментальной базе ЗАО РОКВУЛ. Часть исследований выполнена в НИУ МГСУ в рамках реализации Программы развития университета «ПРИОРИТЕТ 2030». Проект 3.1 «Научный прорыв в строительной отрасли – новые технологии, новые материалы, новые методы».

ДЛЯ ЦИТИРОВАНИЯ:
Артеменко С.О., Жуков А.Д., Медведев А.А., Боброва Е.Ю., Пилипенко А.С. Системы изоляции скатной кровли и их энергетическая эффективность. *Нанотехнологии в строительстве.* 2026;18(5):609–620. https://doi.org/10.15828/2075-8545-2026-18-5-609-620. – EDN: EETPWG.

INTRODUCTION

Building systems, as a defining factor in forming the insulation envelope of buildings of any purpose, began to develop in Russia in the mid-1990s. The goal of introducing such systems was, first and foremost, energy savings, and second, increased structural durability, the creation of an optimal indoor microclimate, and similar benefits. A distinctive feature of the building system was the use of a specific material for specific operating conditions. At the same time, replacing that material with another one with similar properties no longer guaranteed a comparable result.

In the early 2010s, a broader concept began to be used: energy efficiency. In this case, not only the use of building systems forming the building's insulation envelope was con-

ISSN 2075-8545 (online)

sidered, but also the costs of material production, logistics, installation, and, in some cases, dismantling structures at the end of their service life and disposing of the remaining materials [5–7]. Inevitably, the issue of investment payback arose, which could be achieved only through energy savings during operation of the insulated structure and by extending its maintenance-free service life.

The maintenance-free service life of a building structure depends on many factors, including the type of structure, operating conditions, material quality, exposure to the external environment, and protective measures. It should be noted that the timing of both routine and major repairs is regulated by regional programs and can range from 20 to 50 years. Monetary energy savings are determined both by energy consumption and by the cost of the energy source, such as gas. The cost of 1 cubic meter of gas in Russia and Belarus in the second half of 2025 was 8–10 rubles, while in Germany or France it was about 130–150 rubles. The cost of the structure included in the insulation envelope system falls within a common range for all countries: from 4,000 to 8,000 rubles per 1 m². At present, amid the energy crisis, the price of gas under long-term contracts has increased by a factor of 1.2 to 1.8. Therefore, if the payback period for investments in an insulation system in Europe begins after 15–20 years of operation, then in Russia this period is about 100 years or more.

Therefore, the following criteria have become relevant today: reducing energy costs at the manufacturing stage, improving indoor comfort, and increasing structural durability through the use of effective insulation systems and improved operational stability [10–12]. Technological aspects related to environmental protection and minimizing negative impacts on the environment throughout the material life cycle also remain significant [13–15].

Thermal insulation materials largely determine structural durability because of their low strength and high thermal performance. These materials protect structures and indoor spaces from cold and overheating, but they themselves require protection from mechanical loads and atmospheric effects [16–18]. Materials may be based on synthetic (polymeric) or mineral matrices, but regardless of their structure and the building systems in which they are used, special requirements are imposed on thermal resistance, thermal conductivity, and operational stability [19–21].

The subject of the research presented in the article is a pitched-roof insulation system using lightweight stone-wool slabs and the properties of these slabs. From the standpoint of mechanical loads (compression or delamination), the thermal insulation in this system is not mechanically loaded, while the main loads are carried by the rafter system and sheathing, i.e., the roof's load-bearing structure. This makes it possible to use lightweight (soft and semi-rigid) thermal insulation slabs with a density of up to 70 kg/m³ in the insulation envelope.

Loads acting on the insulation envelope are shown in Fig. 1. Firstly, this is an intense dynamic load formed by air flows in the ventilated space. The airflow creates a vacuum above the surface (negative pressure) and, on one hand, promotes a reduction in the humidity of the thermal insulation envelope and its thermal conductivity, thereby increasing thermal resistance. On the other hand, this same factor initiates the movement of the vapor-air mixture and contributes to the carry-out of fibers and binder from the material. Such loads can lead to the deg-

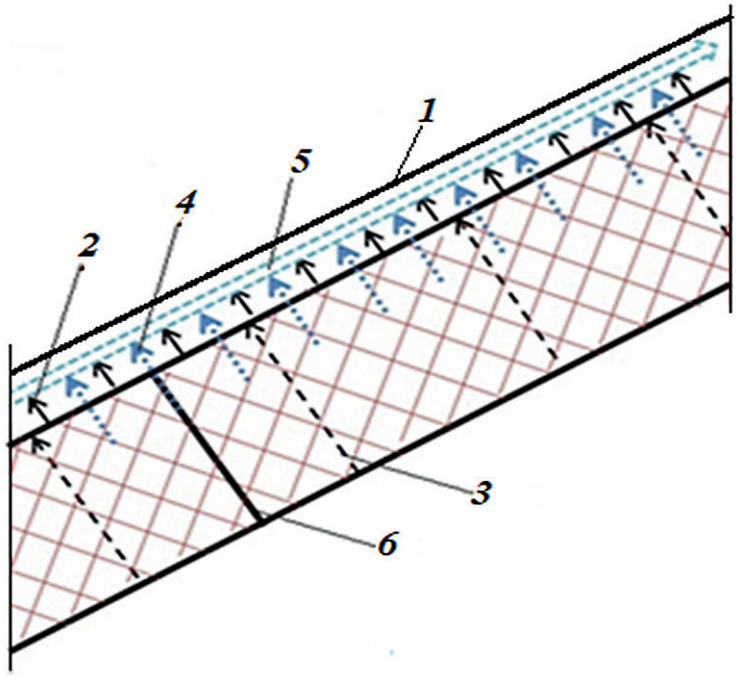


Fig. 1. Loads on thermal insulation in a pitched roof structure: 1 – roof covering; 2 – distributed pull-off load; 3 – movement of air and water vapor in the insulation layer; 4 – air exfiltration; 5 – airflow in the ventilated space; 6 – joint of insulation slabs

ISSN 2075-8545 (online)

radation of the properties of mineral wool slabs. The effects of temperature, humidity, and air flows determine the gradual carry-out of fibers and binder from the slabs: thermal conductivity increases, while cohesion decreases. As a result, disruption of the continuity of the insulation covering and failure of the system as a whole may occur. The pitched roof system must be designed taking into account comprehensive temperature effects and the possibility of periodic moistening of the insulation.

Lightweight (soft or semi-rigid) stone wool-based slabs with an innovative binder based on modified epoxy resins were adopted as the basis for the pitched roof insulation system. Typically, phenol-formaldehyde-based binders are used in mineral wool products. Such a binder has satisfactory characteristics and cures at temperatures of 240–280 °C. However, like any phenol-containing substance, it is toxic during incomplete polycondensation of the binder. Various synthetic materials with high adhesion to mineral surfaces and resistance to temperature-humidity effects can be used as binders in mineral and fibrous composites [26–28]. Modified epoxy compounds have a lower curing temperature, are less toxic, and, as previous studies have shown, are fully applicable for curing mineral fibrous materials in terms of their properties [29–31]. From a production standpoint, products based on modified epoxy binder exhibit better energy efficiency characteristics.

As a result of analyzing a priori information, it was established that the most significant criteria are ecological stability, operational durability, the ability to create an optimal thermo-humidity regime in premises, as well as lower energy costs in manufacturing. The use of lightweight mineral wool products is promising provided their operational durability is improved.

The goal of the research is to study the properties of stone wool-based products using modified epoxy binder and surface reinforcement, analyze the applicability of such products in pitched roof structures, and assess the energy efficiency of the adopted solutions.

MATERIALS AND METHODS

Soft stone wool slabs, glass mesh, and modified epoxy resin-based adhesive were used as starting materials. The epoxy adhesive composition was based on previous studies [34–36]. The base was ED-20 epoxy resin. The modifier consumption was 6.0% of the binder mass, and the plasticizer consumption was 3.0% of the binder mass. The heat treatment temperature was 150–154 °C. After binder curing, the adhesion strength was 58.4 MPa, and the adhesion strength after climatic tests was 29.1 MPa.

Lightweight mineral wool slabs on synthetic (phenol-formaldehyde resin) and modified epoxy binder were considered as research objects. The average density range of the studied slabs was from 32 to 68 kg/m³ (soft slabs 32–36 kg/m³; semi-rigid 64–68 kg/m³).

The structure was studied using a FEI Quanta 200 scanning electron microscope. Product properties were determined according to standard methods: GOST 17177-94 and GOST 9573-2002, as well as SP 50.13330.2010, SP 23-101-2004, SP 17.13330.2017. Operational durability was assessed using an accelerated method through hydrothermal treatment of mineral wool cylinder fragments on a setup developed by Moscow State University of Civil Engineering (MGSU)–GASIS(HSE)–MAXMIR based on changes in product compressibility.

RESULTS AND DISCUSSION

Changes in compressibility and thermal conductivity of mineral wool slabs were evaluated using an express method. The average density of the slabs was taken as 34 kg/m³ (soft slabs) and 66 kg/m³ (semi-rigid slabs). Products on two types of binders were considered: phenol-formaldehyde resins and modified epoxy binder.

The following patterns were established as a result of express tests. First, thermo-humid exposure has little effect on changes in the average density of products, and variations do not exceed experimental error. Second, the type of binder does not significantly affect the characteristics of products and their changes at all stages of temperature-humidity exposure. This allows the conclusion that replacing classical resins with a modified binder has an insignificant impact on product properties.

Third, the mass loss of samples due to thermo-humid exposure and air flow exposure is quite significant for slabs of different average densities and for slabs on different binders (Fig. 2). Mass losses for samples on modified epoxy binder are slightly, but higher, than for samples on synthetic resins. This may be due to the fact that the cured phenolic binder has greater adhesive cohesion with the surface of amorphous mineral fibers, and the binder itself is more resistant to temperature-humidity effects.

Regardless of slab density and the type of binder used, all lightweight slabs exhibit significant mass loss due to temperature-humidity exposure complicated by airflow effects. This necessitates reinforcing the slabs on surfaces in contact with the ventilated space of the pitched roof to counteract the airflow.

Since the samples are pre-dried to near-zero humidity, the mass loss of the slabs is associated with the carry-out of the matrix substance, specifically loosely fixed fibers (due to monolithization of contacts with the binder). This factor is more pronounced in ultra-lightweight (soft) slabs, as these materials have a lower degree of volumetric fiber interlacing and binder content compared to slabs with an average density approaching 70 kg/m³.

The solution to this problem is the use of soft or semi-rigid mineral wool slabs with reinforcement of their outer layer (Fig. 3). The technology for manufacturing stone wool-based slabs remains unchanged but is supplemented

ISSN 2075-8545 (online)

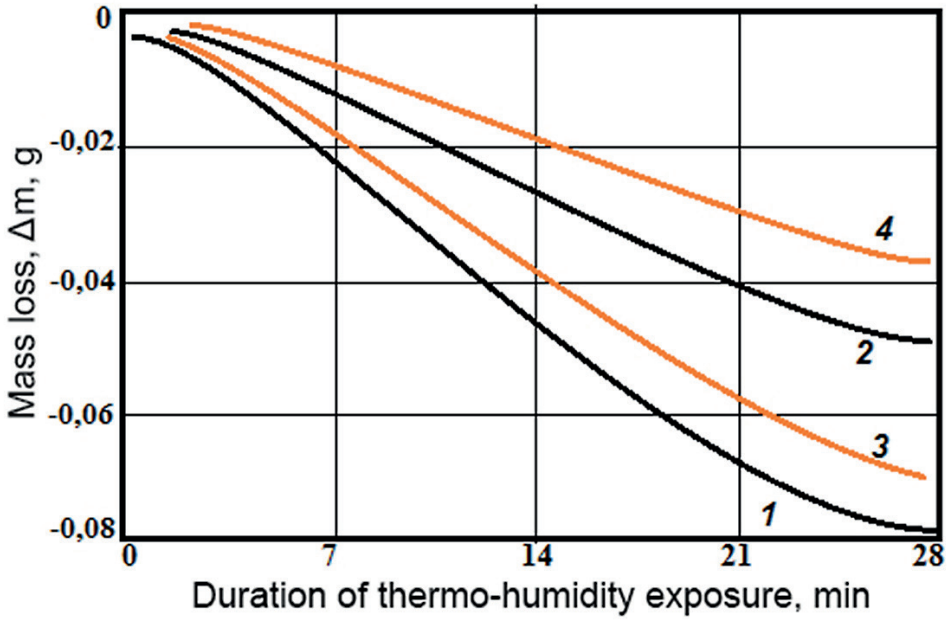


Fig. 2. Mass loss at an air flow velocity of 6 m/s for slabs of average density, kg/m^3: 1, 3 – 32–36; 2, 4 – 64–68; binder: 1, 2 – modified epoxy; 2, 4 – synthetic resins



Fig. 3. Mineral wool slabs with reinforced surface layer (a, b) and slabs with glued glass mesh in the structure (c, d)

with operations for laying the reinforcement material, which is mechanically fixed to the carpet surface (similar to the technology of stitched mats) or glued using modified epoxy adhesive.

These mineral wool slabs are recommended for use in structures where the insulation does not bear significant mechanical loads: in pitched roofs (when laid between rafters), in frame wall structures (when insulation is placed between frame posts), and in floor structures (when insulation is laid between joists).

The protective layer consists of a fiberglass mesh fixed to the material during its manufacturing process. In the products, the protective and thermal insulation layers form a single whole. The properties of the products are presented in Table 1.

For all types of plates: vapor permeability coefficient of at least 0.30 mg/(m·h·Pa); humidity by weight of not more than 0.5%; water absorption by volume of 1.5–2%.

The usage of mineral wool products with a reinforced outer layer eliminates one technological operation: the laying and fixing of the windproof layer. The use of products with large lengths (up to 6 m) allows for faster installation of the thermal insulation layer.

The assessment of the operational durability of the products was carried out based on a standard method with the generation of impacts in a climatic chamber. Additional loads such as vibration, salt fog, and air blow-through of the material were used to evaluate fiber emission. The studies used fragments of mineral wool slabs on modified epoxy binder: soft and semi-rigid, with average

ISSN 2075-8545 (online)

Table 1. Characteristics of mineral wool products with a reinforced layer

Name of characteristic	Medium density of slabs, kg/m³	
	32–36	64–68
Compressibility, %, not more than	30	20
Thermal conductivity at 25 °C, W/(m·°C), not more than	0.036–0.037	0.037–0.038
Thermal conductivity under service conditions A, W/(m·K)	0.038–0.039	0.039–0.040
Thermal conductivity under service conditions B, W/(m·K)	0.039–0.040	0.041–0.042

densities of 32-36 kg/m³ (average 34 kg/m³); 48–52 kg/m³ (average 50 kg/m³); 64-68 kg/m³ (average 66 kg/m³).

The test cycle in the climatic chamber was carried out in the following mode: cooling samples to –20 °C – 1 hour; holding at –20 °C – 1 hour; temperature rise to 20 °C – 2 hours; holding at 20 °C – 1 hour; cooling to –20 °C – 1 hour, and then the cycles were repeated. Samples were taken after every 10 cycles, and basic properties were determined, with graphs constructed for changes in thermal conductivity, compressibility, and air permeability depending on the number of «freeze-thaw» cycles (z).

The results of the active experiments were subjected to statistical processing, which allowed approximating the real values with systems of straight lines with the introduction of confidence intervals: permissible deviation from the mean (mathematical expectation) within the statistical interval. It was assumed that the distribution of results at each experimental point follows a distribution close to the Gaussian distribution.

It was found that thermal conductivity increases with the passage of climatic cycles (Fig. 4); however, the presence of a protective coating has an insignificant effect on thermal conductivity (within experimental error).

The change in the air permeability coefficient i, kg/(m²·hour·Pa), at Dp = 10 Pa depending on the number of «freeze-thaw-heating» cycles of mineral wool slabs (Fig. 5) is due to changes in the hydraulic resistance of the products. As a result of climatic effects on products with a volume-oriented structure, some settling (i.e., compaction of the products) becomes possible.

Analysis of the graphs (Fig. 4 and 5) shows that the dependence of thermal conductivity and air permeability coefficient of mineral wool slabs (for each average density) on the number of «freeze-thaw-heating» cycles can be represented by dependencies close to linear (taking into account experimental error) and can be approximated by linear equations. This significantly simplifies the practical use of the results, but is valid only for the average density ranges of slabs studied in the experiment.

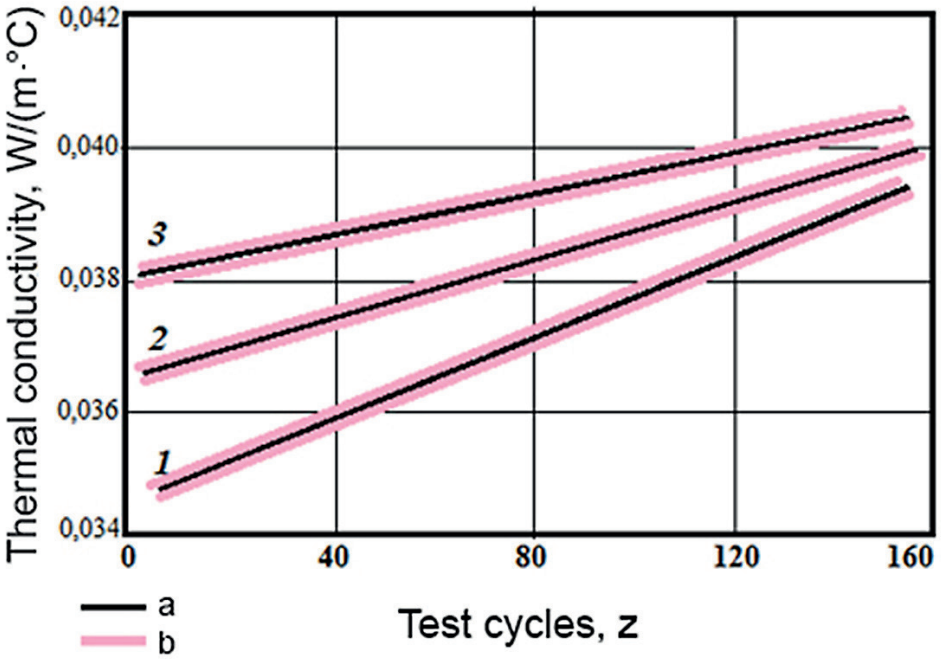


Fig. 4. Dependence of thermal conductivity of mineral wool products on cyclic effects at average density, kg/m³: 1 – 32–36; 2 – 48–52; 3 – 64–68: a – average value; b – deviation from the average value

ISSN 2075-8545 (online)

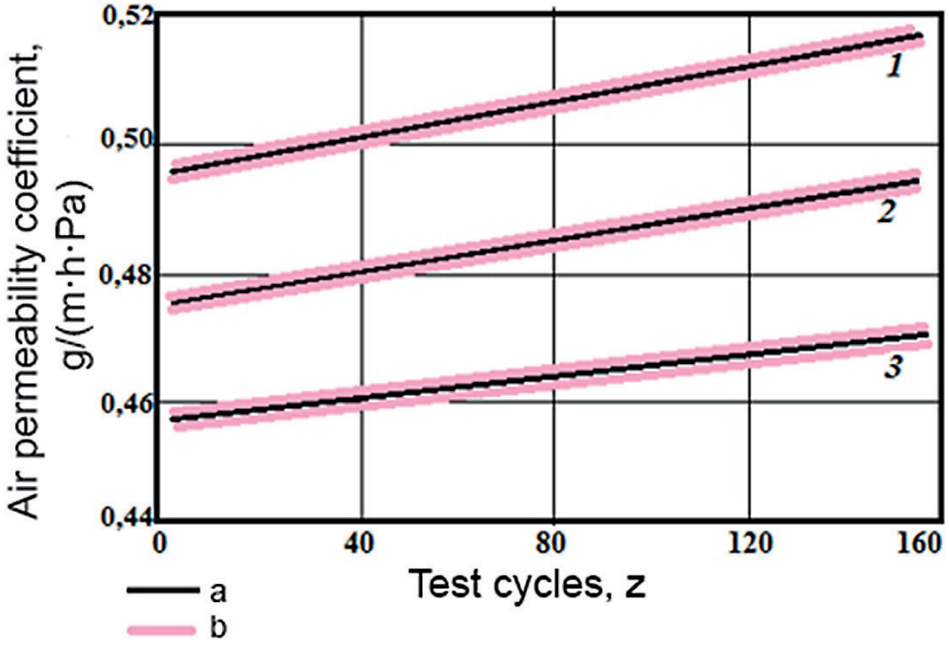


Fig. 5. Dependence of air permeability of mineral wool slabs on cyclic effects at average density, kg/m^3: 1 – 32–36; 2 – 48–52; 3 – 64–68: a – average value; b – deviation from the average value

The test results for slab compressibility depending on the number of «freeze-thaw-heating» cycles of mineral wool slabs of different densities (soft and semi-rigid) are shown in Fig. 6.

The increase in compressibility of mineral wool slabs on modified epoxy binder as a result of cyclic tests is associated with the material structure, fiber properties, and binder properties. Climatic effects most strongly influence the properties of the cured binder: its strength, brittleness, and adhesion to the surface of mineral fibers. Secondly, with significant test cycles, the properties of the mineral fiber may change, including its strength characteristics;

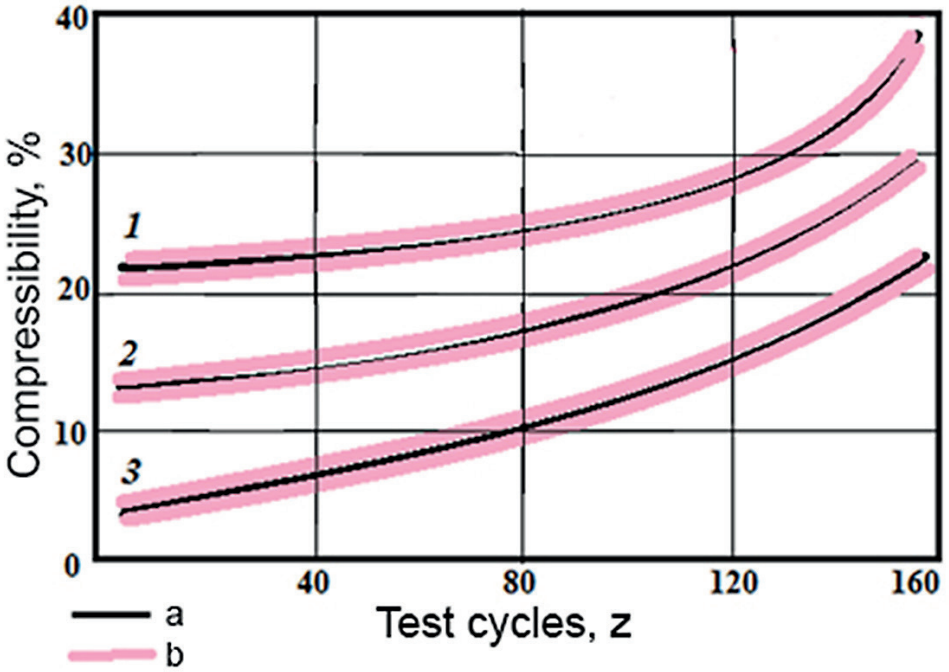


Fig. 6. Dependence of compressibility of mineral wool slabs on cyclic effects at average density, kg/m^3: 1 – 32–36; 2 – 48–52; 3 – 64–68: a – average value; b – deviation from the average value

ISSN 2075-8545 (online)

temperature deformation of fibers, caused by the difference in thermal expansion between the amorphous mineral fiber structure and the cured synthetic binder, can also affect properties and adhesion.

The combined effect of these factors leads to a weakening of the structure characteristics and, consequently, an increase in product compressibility. This must be taken into account when predicting the durability of the insulation envelope of building structures.

As already noted, in addition to durability, comfort, and environmental conditions, energy costs in material manufacturing affect the energy efficiency of building systems. Replacing phenol-containing binder with modified epoxy allows significantly reducing the heat treatment temperature without fundamental changes in technology and process implementation (Table 2).

When using phenol-formaldehyde binder cured at 250-300 °C, the heat content of the heat flow is:

$$10000 \times 300 \times 1.315 / 3600 = 1095 \text{ kW}.$$

When using modified epoxy binders cured at 100–150 °C, the heat content of the heat flow is:

$$10000 \times 150 \times 1.315 / 3600 = 548 \text{ kW}.$$

Reduction in heat losses due to changes in heat treatment temperature (resulting from changes in binder curing temperature), and consequently in the temperature of the heat transfer medium. The total calculated economic (energy) effect of reducing the heat treatment temperature by 150 °C is estimated at 30–40%.

The ecological efficiency of thermal insulation materials or pitched roof systems using them depends on the following factors:

Energy savings achieved through the use of insulated structures, i.e., fuel savings, reduced harmful emissions from fuel combustion into the atmosphere, and, consequently, reduced environmental impact.

Durability of the building system itself, which determines the maintenance-free service life. Durability depends on the operational stability of the materials, as well as on design and installation quality. All else being equal, the determining factor can be considered the «weak link,» i.e., the operational stability of the thermal insulation material.

Energy costs for material manufacturing, primarily insulation, taking into account the specific consumption of thermal insulation material per unit area of the roof, i.e., insulation thickness.

There are various methods for assessing the environmental friendliness of building systems. The system under consideration combines pitched roofing, vapor and waterproofing materials, thermal insulation material, and sheathing and rafter materials made of wood. Wood and metal are always considered materials that do not create negative environmental impacts. Polymeric membranes and metal coatings can be regarded as inert materials. Accordingly, the thermal insulation material can be considered the main factor of influence. In this case, these are products based on stone wool, basalt fiber, or foam glass, as well as lightweight mineral wool products of comparable density (up to 70 kg/m³) with epoxy and phenolic binders.

The assessment of insulation efficiency presented in the previous section showed that the energy efficiency of mineral wool products is approximately 1.2 times higher than that of basalt fiber products and 1.1 times higher than that of foam glass-based products. In addition, due to the lower heat treatment temperature of the synthetic binder, the effectiveness of mineral fiber insulation increases by 20–30%.

The properties of fibrous materials are practically identical, while the environmental impact of producing stone wool products is significantly lower, which allows them to be rated as a more environmentally friendly material. Foam glass, due to its cellular porosity, is a more stable material than fibrous ones, but its much higher density leads to additional costs during installation and operation of structures.

The voluntary EcoMaterial certification system operating in the Russian Federation consists of three sections. The first section assesses how safe the material is for humans. The second section evaluates the overall impact of the material and its production on the environment. The third section contains criteria for promoting green solutions and trends, supporting social eco-projects, and so on.

There are several certification levels: EcoMaterial Basis – material safe for humans; EcoMaterial Green – material safe for humans and the environment; EcoMaterial Absolut – environmentally clean material; EcoMaterial

Table 2. Efficiency indicators of mineral wool slabs

Indicator	Binder type	
	phenol-formaldehyde	modified epoxy
Heat treatment energy costs, kW	1095	548
Reduction in heat consumption for heat treatment, %	–	50
Energy effect, %	–	20–30

ISSN 2075-8545 (online)

Natural – absolutely natural material, the highest-rated category. The certification results show that stone wool-based products belong to the EcoMaterial Green level, while the others can presumably be classified as EcoMaterial Basis.

CONCLUSION

In pitched roof systems, the presence of a load-bearing rafter structure minimizes direct mechanical loads on the insulation envelope, making it possible to use lightweight and compressible mineral wool slabs; soft or semi-rigid. On the other hand, in these systems, the thermal insulation material comes into direct contact with the environment due to open access through ventilation cavities, as well as air flows in the ventilated space.

Research has established that lightweight (soft and semi-rigid) reinforced slabs based on stone wool and using modified epoxy binder can be used in pitched roof structures without the risk of disruption to the continuity of the insulation covering. Glass mesh is used as a reinforcement element, fixed to the slab surface with adhesive or mechanically by stitching with the base material.

The conducted research allows formulating a general concept for improving the energy efficiency of pitched roof insulation systems, including criteria for material operational stability, structure durability, and reduction of negative environmental impacts.

REFERENCES

1. Gagarin V.G. Macroeconomic aspects of the justification of energy-saving measures in improving the thermal protection of building enclosing structures. *Building materials.* 2010;3:8-16. (In Russ.)

2. Lesovik V.S., Gridchin A.M., Alfimova N.I. Building materials and products: textbook for the direction 270100 "Construction" [Text]. Belgorod: Publishing house of BSTU; 2011. 222 p. (In Russ.)

3. Kudryavtsev P.G. Composition and structure of porous heat-resistant inorganic composite materials. *Nanotechnologies in construction*. 2018;10(4):75-100. https://doi.org/10.15828/2075-8545-2018-10-4-75-100

4. Bessonov I.V., Zhukov A.D., Bobrova E.Yu., Govryakov I.S., Gorbunova E.A. Optimization of properties and structure of extra-light materials using digital methods. *Nanotechnologies in construction*. 2025;17(2):109-118. https://doi.org/10.15828/2075-8545-2025-17-2-109-118. – EDN: WXZIJJ

5. Baykov I.R., Smorodova O.V., Trofimov A.Yu., Kuznetsova E.V. Experimental study of thermal insulation nano materials based on aerogels. *Nanotechnologies in construction*. 2019;11(4):462-477. https://doi.org/10.15828/2075-8545 2019-11-4-462-477

6. Kazbek Ivanov and Boris Efimov Modeling of the structure and properties of a mineral wool cylinders. / *MATEC Web of Conferences*. Vol. 298 (2019) IC-MTMTE 2019. Published online: 18 November 2019. https://doi.org/10.1051/matecconf/201929800096

7. Ter-Zakaryan K.A.; Zhukov A.D.; Bessonov I.V.; Bobrova E.Y.; Pshunov T.A.; Dotkulov, K.T. Modified polyethylene foam for critical environments. *polymers.* 2022;14:4688. https://doi.org/10.3390/polym14214688

8. Zhukov A.D., Bobrova E.Yu., Bessonov I.V., Mednikova E.A. *Energy efficiency of building systems*: a monograph. Moscow: INFRA-M;2022.

9. Sinitsin D.A., Shayakhmetov U.S., Rakhimova O.N. Khalikov R.M., Nedoseko I.V. Nanostructured foam ceramics for construction purposes: production technology and applications. *Nanotechnologies in construction*. 2021;13(4):213-221. https://doi.org/10.15828/2075-8545-2021-13-4-213-221

10. İhsan Türkel, İffet Gamze Mütevelli Özkan, Esmanur Baltaoğlu, Ahmet Benli, Oğuzhan Yavuz Bayraktar, Halil Barış Özel, et al. Enhancing thermal insulation, mechanical strength, and durability of one-part fly ash-based geopolymer foam concrete using lime and mahogany sawdust. *Construction and Building Materials*. 2025;491:142656. https://doi.org/10.1016/j.conbuildmat.2025.142656

11. Parracha João L., Veiga Rosário, Nunes Lina, Flores-Colen Inês. Effects of hygrothermal and natural aging on the durability of multilayer insulation systems incorporating thermal mortars with EPS and aerogel // *Cement and Concrete Composites*. 2024;148:105483. https://doi.org/10.1016/j.cemconcomp.2024.105483

12. Parracha J.L., Borsoi G., Veiga R., Flores-Colen I., Nunes L., Viegas C.A., et al. Durability assessment of external thermal insulation composite systems in urban and maritime environment. *Science of the total environment*. 2022;849:157828. https://doi.org/10.1016/j.scitotenv.2022.157828

13. Zhuk P.M., Zhukov A.D. Normative Legal Base for the Environmental Assessment of Building Materials: Prospects for Improvement. *Ecology and industry of Russia*. 2018;22(4):52-57. https://doi.org/10.184 12/1816-0395-2018-4-52-57

14. Zhuk P.M. Evaluation system of ecological safety on life cycle of inorganic fibrous heat-insulating materials. *Bulletin of MGSU* [Proceedings of Moscow State University of Civil Engineering]. 2013;12:118-122. eLibrary ID: 20931013

15.Yongpeng Song, Caihong Xue, Weichao Guo, Yanying Bai, Yuxuan Shi, Qingxin Zhao. Foamed geopolymer insulation materials: Research progress on insulation performance and durability. *Journal of cleaner production*. 2024;444:140991. https://doi.org/10.1016/j.jclepro.2024.140991

16. Kudryavtsev P.G. Composition and structure of porous heat-resistant inorganic composite materials. *Nanotechnologies in construction*. 2018;10(4):75-100. https://doi.org/10.15828/2075-8545-2018-10-4-75-100

17. Shengkun Sun, Shui Yu, Jianyu An, Fuhong Han. Research on thermal performance and durability of ETICS under wind load in severe cold area. *Applied thermal engineering*. 2025;281(1):128530. https://doi.org/10.1016/j.applthermaleng.2025.128530

18. Gang Wu, Tao Li, Maohua Zhang, Jiyin Cui, Jiamin Li. Durability and thermal insulation properties of glazed hollow bead concrete with nanoparticles in marine atmospheric environment. *Journal of building engineering*. 2024;110071. https://doi.org/10.1016/j.jobe.2024.110071

19. Moganraj Nagapan, Soon Poh Yap, Kim Hung Mo, Beng Fye Lau, Nur Arina Mohd Rohaizad. Recycling spent mushroom substrate as a partial fine aggregate substitute in cement brick Production: Evaluating mechanical, durability, and thermal insulation properties. *Sustainable chemistry and pharmacy*. 2025;46:102050. https://doi.org/10.1016/j.scp.2025.102050

20. Zhukov A., Bobrova E., Medvedev A., Ushakov N., Beniya D., Poserenin A Modelling of Technology of Mineral Wool Products. *EMMFT 2018. Advances in intelligent systems and computing*. 2018;983. Springer, Cham. https://doi.org/10.1007/978-3-030-19868-8_81

21. Yawen He, Som Shrestha, Hongyu Zhou. Integrating greenery systems and active insulation into adaptive building envelopes for enhanced sustainability and thermal resilience. *Energy and buildings*. 2026;354; 116940. https://doi.org/10.1016/j.enbuild.2025.116940

22. Zhukov A.D., Bobrova E.Yu., Zinovieva E.A., Ivanov K.K. Thermal insulation: operational properties and methods of research. *IPICSE*. 2018. https://doi.org/10.1051/ matecconf/201825101016

23. Ivanov K.K. Thermal insulation shaped mineral wool products with effective binder. / K.K. Ivanov, A.D. Zhukov, E.Yu. Bobrova, E.Yu. Zhukova. *E3S Web of Conferences*. 2019; 110:02024. *ISC SPbWOSCE-2018*. https://doi.org/10.1051/e3sconf/201911002024

24. Mukhametov A.P., Petrova A.P. Thermosetting binders for polymer composite materials (review). *Aviation Materials and Technologies*. 2019;3:56-58. https://doi.org/10.18577/2071-9140-2019-0-3-48-58

25. Rudawská A., Sarna-Boś K., Rudawska A., Olewnik-Kruszkowska E., & Frigione, M. Biological effects and toxicity of compounds based on cured epoxy resins. *Polymers. 2022;*14. https://doi.org/10.3390/polym14224915

26. Drozdyuk T.A., Eisenstadt A.M., Korolev E.V. High-temperature modification of saponite-containing material. *Building materials*. 2021;11:30-35. https://doi.org/10.31659/0585-430X-2021-797-11-30-35

27. Eremeeva N.M., Nikiforov A.V. Investigation of the properties of epoxy compositions based on modified cellulose-containing materials. *The journal «Young Scientist»*. 2015;24.1:20-23. URL: https://moluch.ru/archive/104/24030 (date of notification: 12/15/2024).

28. Merkulova Yu.I., Mukhametov R.R., Dolgova E.V., Akhmadieva K.R. Polycyanurate binder for obtaining composites by impregnation under pressure. *Proceedings of VIAM: electron. scientific and technical journal*. 2016;11(47):05. https://doi.org/10.18577/2307-6046-2016-0-11-5-5

ISSN 2075-8545 (online)

29. Zagora A., Tkachuk A., Terekhov I., Mukhametov R. Methods of chemical modification of epoxy oligomers (review). *Proceedings of VIAM*. 2021. https://doi.org/10.18577/2307-6046-2021-0-7-73-85

30. Zheleznyak V.G., Chursova L.V. Modification of binders and matrices based on them in order to increase the fracture toughness. *Aviation Materials and Technologies*. 2014;1:47-50. https://doi.org/10.18577/2071- 9140-2014-0-1-47-50

31. Kalenda P., Kalendová A. Improved chemical resistance of epoxy resin-based coating compositions. *Dyes and Pigments* 1995; 27:305-312. https://doi.org/10.1016/0143-7208(94)00070-I

32. Nakamura S., Yamamoto S., Tsuji Y., Tanaka K., Yoshizawa K. Theoretical study on the contribution of interfacial functional groups to the adhesive interaction between epoxy resins and aluminum surfaces. *Langmuir: the ACS journal of surfaces and colloids*. 2022. https://doi.org/10.1021/acs.langmuir.2c00529

33. Li R., Leng Z., Zhang Y., Xu X. Preparation and characterization of waterborne epoxy modified bitumen emulsion as a potential high-performance cold binder. *Journal of Cleaner Production*. 2019; 235(14). https://doi.org/10.1016/j.jclepro.2019.06.267

34. Artemenko S.O., Bobrova E.Yu., Zhukov A.D. Studies of the properties and structure of mineral wool energy-efficient products. *Scientific research of the SCO countries: synergy and integration*. Beijing, China, Scientific publishing house Infinity. 2024: 152-157.

35. Bobrova E.Yu., Popov I.I., Gandzhuntscev M.I., Zhukov A.D. Thermosetting binder for fibrous insulating materials. *Russian Journal of Building Construction and Architecture*. 2021;44-52. https://doi.org/10.36622/VSTU.2021.52.4.004

36. Zhukov A.D., Artemenko S.O., Bobrova E.Yu., Medvedev A.A. Low-energy binder for products based on rock wool. *Nanotechnologies in construction*. 2025;17(4):377-388. https://doi.org/10.15828/2075-8545-2025-17-4-377-388. – EDN: BORGVT

ADDITIONAL INFORMATION

The authors state that generative artificial intelligence and artificial intelligence-based technologies were not used in the preparation of the article.

INFORMATION ABOUT THE AUTHORS

Savely O. Artemenko – postgraduate student, Department of Building Materials Science at the National Research Moscow State University of Civil Engineering; 129337, Moscow, Yaroslavskoe Highway, 26, Russian Federation; specialist in the development of the facade direction of LLC «ROCKWOOL». 115230. Moscow, Kashirskoye Highway, house 3, building 2, structure 9, floor 2, office No. A206, Russian Federation, art.savely@yandex.ru, https://orcid.org/0009-0001-5584-680X

Alexey D. Zhukov – Cand. Sci. (Eng.), Associate Professor, Associate Professor of the Department of Building Materials Science at the National Research Moscow State University of Civil Engineering, 129337, Moscow, Yaroslavskoe Highway, 26, Russian Federation; Leading Researcher at the Research Institute of Building Physics of the Russian Academy of Architecture and Building Sciences (NIISF RAASN), 127238, Moscow, Lokomotivny Pr., 21, Russian Federation; Corresponding Member of the Russian Engineering Academy (RIA), 125009, Moscow, Gazetny Lane, 9, building 4, Russian Federation, lj211@yandex.ru, https://orcid.org/0000-0003-0593-3259

Andrey A. Medvedev – Cand. Sci. (Eng.), Associate Professor, Associate Professor of the Department of Higher Mathematics at the National Research Moscow State University of Civil Engineering, 129337, Moscow, Yaroslavskoe Highway, 26, Russian Federation; Associate Professor of the Department of Geophysics at Moscow Geological Exploration University (MGRI), 117485, Moscow, Miklukho-Maklaya Street, 23, Russian Federation, medvedev747@yandex.ru, https://orcid.org/0000-0002-2930-2606

Ekaterina Yu. Bobrova – Cand. Sci. (Econ.), Associate Professor at the Faculty of Urban and Regional Development at the National Research University Higher School of Economics (HSE), Associate Professor at the Department of Testing Structures at the National Research Moscow State University of Civil Engineering (MGSU), Corresponding Member of the Russian Academy of Engineering (RIA), 125009, Moscow, Gazetny Lane, 9, building 4, Russian Federation, mla-gasis@mail.ru, https://orcid.org/0000-0001-6541-4552

ISSN 2075-8545 (online)

Anton S. Pilipenko – Cand. Sci. (Eng.), Associate Professor, Department of Civil Engineering Materials Science at the National Research Moscow State University of Civil Engineering (NRU MGSU). 129337, Moscow, Yaroslavskoe Highway, 26, Russian Federation; pilipenko.ans@gmail.com, https://orcid.org/0000-0001-7525-0117

CONTRIBUTION OF THE AUTHORS

Savely O. Artemenko – development of methodology, conducting active experiment.

Alexey D. Zhukov – formation of the general concept of research, writing the original text.

Andrey A. Medvedev – development of the concept of research, development of methodology and its adaptation to the tasks of research.

Ekaterina Yu. Bobrova – development of research methodology and its adaptation to the objectives of the study, final conclusions.

Anton S. Pilipenko – adaptation of the methodology of analytical optimization final conclusions.

The authors declare no conflicts of interests.

The article was submitted 23.06.2026; approved after reviewing 28.09.2026; accepted for publication 02.10.2026.

ISSN 2075-8545 (online)

Nanotechnologies in construction
Нанотехнологии в строительстве

2026; 18 (5):
621–626

Nanobuild.ru

THE RESULTS OF THE SPECIALISTS' AND SCIENTISTS' RESEARCHES

CC BY 4.0

Original article
https://doi.org/10.15828/2075-8545-2026-18-5-621-626

Creating a technology to coat the insulating material on the "cold" section of a cartridge-style electric heater for operation in aggressive environments

Oleg R. Latypov[1]*, Karina V. Kim[1, 2], Vasily V. Lukyanov[1, 2], Dina R. Latypova[1], Rustem R. Daminev[1], Alisa F. Ahmadullina[1, 2]

[1] Ufa State Petroleum Technological University, Ufa, Kosmonavtov str 1, 450064, Russian Federation
[2] Scientific and Production Association "Technopark of Aviation Technologies", Tramvaynaya str. 5, building 1, 450112, Russian Federation

* Corresponding author: e-mail: o.r.latypov@mail.ru

ABSTRACT

Introduction. Currently, fluorine polymers have become quite widespread in various industries. One of the fields of application of fluoroplastic coatings in the oil industry is their use as protective coatings to prevent the deposition of paraffin plugs on the walls of tubing and field pipelines. Fluoroplastic parts find promising application in machines and units of oil refining and petrochemical industries, where high corrosion resistance, sufficient strength and high tribotechnical properties are required. The complexity of the ubiquity of fluoroplastic coatings is its low adhesion to the metal surface. In this regard, fluoroplastic coatings are typically complex systems comprising directly fluoroplastic polymer, binders and functional fillers. **Materials and methods.** The study used metal plates made of titanium alloy VT6 and carbon steel St3 coated with an aqueous fluoroplastic suspension. Fluoroplastic polymer coatings have poor adhesive strength to the metal surface on which they are applied. Therefore, in order to ensure a high level of adhesion of the coating to the metal substrate, it is necessary to use complex methods of preliminary surface preparation. The coating was applied to the pre-prepared surface of the metal plates by air spraying using a spray gun and compressed air. The key parameters for the formation of the fluoroplastic film were drying and sintering modes. Adhesion was evaluated by the methods of "X-shaped" notch (State Standard 32702.2-2014) and tearing in a tensile machine on cylinders (State Standard 32299-2025). **Results.** Proposed method comprises application of intermediate primer layer from suspension containing chromium (III) oxide, phosphoric acid, water and fluoroplastic. The intermediate adhesive primer layer was applied by air spraying under the same conditions as the base fluoroplastic coating. This ensured that the proposed drying and sintering conditions met the base layer. The use of a primer made it possible to realize a gradient transition from the metal substrate to the fluoroplastic layer and significantly increase the adhesion properties. **Conclusion.** The results show a significant improvement in adhesion compared to the control samples without primer: the tensile strength value by the tear method is 2.56 N/mm^2, and by the X-notch method - from 5 points to 1 point (traces of peeling or removal of the coating along the incisions). The method is easy to implement and promising for use in protective coatings.

KEYWORDS: fluoroplastic, adhesion, primer, chromium (III) oxide, phosphoric acid, "X-notching" method, tearing method

SOURCES OF FUNDING FOR THE SCIENTIFIC WORK THAT RESULTED IN THE PUBLICATION: This work was conducted as part of the Strategic Project "New technologies, technical, and intelligent systems in mechanical engineering" of the Ufa State Petroleum Technological University Development Program for 2021–2030 in accordance with the Priority 2030 Strategic Academic Leadership Program.

ACKNOWLEDGEMENTS: The authors are grateful for the financial support of this project.

FOR CITATION:
Latypov O.R., Kim K.V., Lukyanov V.V., Latypova D.R., Daminev R.R., Ahmadullina A.F. Creating a technology to coat the insulating material on the "cold" section of a cartridge-style electric heater for operation in aggressive environments. *Nanotechnologies in construction.* 2026;18(5):621–626. https://doi.org/10.15828/2075-8545-2026-18-5-621-626. – EDN: MYGYGS.

© Latypov O.R., Kim K.V., Lukyanov V.V., Latypova D.R., Daminev R.R., Ahmadullina A.F., 2026

ISSN 2075-8545 (online)

Nanotechnologies in construction
Нанотехнологии в строительстве

2026; 18 (5):
621–626

Nanobuild.ru

THE RESULTS OF THE SPECIALISTS' AND SCIENTISTS' RESEARCHES

Разработка технологии нанесения изолирующего материала на «холодную» часть патронного электрического нагревателя для эксплуатации в агрессивных средах

Олег Ренатович Латыпов[1]*, Карина Вадимовна Ким[1, 2], Василий Васильевич Лукьянов[1, 2], Дина Ринатовна Латыпова[1], Рустем Рифович Даминев[1], Алиса Фанировна Ахмадуллина[1, 2]

[1] Уфимский государственный нефтяной технический университет, 450064, Уфа, улица Космонавтов, 1, Российская Федерация

[2] Научно-производственная ассоциация «Технопарк Авиационных Технологий», 450112 г. Уфа, ул. Трамвайная 5, к. 1, Российская Федерация

* Автор, ответственный за переписку: e-mail: o.r.latypov@mail.ru

АННОТАЦИЯ

Введение. В настоящий момент фторполимеры получили достаточно широкое распространение в различных отраслях промышленности. Одной из областей применения фторопластовых покрытий в нефтяной промышленности является использование их в качестве защитных покрытий для предотвращения отложения парафиновых пробок на стенках насосно-компрессорных труб и промысловых трубопроводов. Детали из фторопластов находят перспективное применение в машинах и агрегатах нефтеперерабатывающих и нефтехимических производств, где необходимы высокая коррозионная стойкость, достаточная прочность и высокие триботехнические свойства. Сложностью повсеместного распространения покрытий на основе фторопласта является его низкая адгезия к металлической поверхности. В связи с этим покрытия на основе фторопластов обычно представляют сложные системы, включающие непосредственно фторопластовый полимер, связующие добавки и функциональные наполнители. **Материалы и методы.** В исследовании использовались металлические пластины из титанового сплава ВТ6 и углеродистой стали Ст3 с нанесенным покрытием из водной фторопластовой суспензии с наноразмерными частицами. Фторопластовые полимерные покрытия имеют слабую адгезионную прочность к металлической поверхности, на которую они наносятся. Поэтому для обеспечения высокого уровня адгезии покрытия к металлической подложке необходимо применение комплексных методов предварительной подготовки поверхности. Покрытие наносилось на предварительно подготовленную поверхность металлических пластин методом пневматического распыления с использованием краскопульта и сжатого воздуха. Ключевыми параметрами формирования фторопластовой пленки являлись режимы сушки и спекания. Адгезия оценивалась по методам «Х-образного» надреза (ГОСТ 32702.2-2014) и отрыва в разрывной машине на цилиндрах (ГОСТ 32299-2025). **Результаты.** В работе предложен метод повышения адгезии фторопластовой пленки толщиной 500 мкм к металлической пластине путем нанесения промежуточного грунтовочного слоя из суспензии, содержащей оксид хрома (III), фосфорную кислоту, воду и фторопласт. Промежуточный адгезионный грунтовочный слой наносили пневмораспылением с теми же режимами, что и основное фторопластовое покрытие. За счет этого обеспечивалось соответствие предложенных условий сушки и спекания к основному слою. Применение грунтовки позволяло реализовать градиентный переход от металлической подложки к фторопластовому слою и значительно повысить адгезионные свойства. **Заключение.** Полученные результаты демонстрируют значительное улучшение адгезии по сравнению с контрольными образцами без грунтовки: значение предела прочности по методу отрыва равно 2,56 Н/мм^2, а по методу Х-надреза – с 5 баллов до 1 балла (следы отслаивания или удаления покрытия вдоль надрезов). Метод прост в реализации и перспективен для применения в защитных покрытиях.

КЛЮЧЕВЫЕ СЛОВА: фторопласт, адгезия, грунтовка, оксид хрома (III), фосфорная кислота, метод «Х- образного» надреза, метод отрыва

ИСТОЧНИКИ ФИНАНСИРОВАНИЯ НАУЧНОЙ РАБОТЫ, РЕЗУЛЬТАТОМ КОТОРОЙ СТАЛА ПУБЛИКАЦИЯ: Работа проводилась в рамках реализации Стратегического проекта «Новые технологии, технические и интеллектуальные системы в машиностроении» программы развития ФГБОУ ВО «Уфимский государственный нефтяной технический университет» на 2021–2030 годы в соответствии с программой стратегического академического лидерства «Приоритет 2030».

БЛАГОДАРНОСТИ: Авторы выражают благодарность за финансовую поддержку проекта.

ДЛЯ ЦИТИРОВАНИЯ:

Латыпов О.Р., Ким К.В., Лукьянов В.В., Латыпова Д.Р., Даминев Р.Р., Ахмадуллина А.Ф. Разработка технологии нанесения изолирующего материала на «холодную» часть патронного электрического нагревателя для эксплуатации в агрессивных средах. *Нанотехнологии в строительстве.* 2026;18(5):621–626. https://doi.org/10.15828/2075-8545-2026-18-5-621-626. – EDN: MYGYGS.

ISSN 2075-8545 (online)

INTRODUCTION

Polytetrafluoroethylene (fluoroplastic) is one of the most promising fluoropolymers used as protective coatings for metal structures. Due to its high chemical resistance, low coefficient of friction, wide temperature range of operation and dielectric properties, fluoroplastic films are used in petrochemical equipment, aircraft engineering, mechanical engineering and a number of other industries. At the same time, low surface energy and high crystallinity of polytetrafluoroethylene lead to its low adhesion to most materials, which requires special surface preparation and the use of appropriate primers or copolymer bonds [1]. In particular, the literature describes in detail the properties and features of the use of an intermediate layer based on gossypol resin [2], which demonstrates high compatibility with various paint materials. Most studies are devoted to modified epoxy compositions [3], which, due to their high adhesion, often serve as the basis for primers. In addition, studies are being conducted on polyaniline primer as a functional component of anti-corrosion coatings that can affect electrochemical processes at the phase interface [4]. In general, the use of primers and adhesive layers helps to significantly increase the service life of the coating, including in a corrosive environment, where this sublayer acts as additional protection against corrosion. In some cases, a system of a primer and an additional intermediate coating between the soil and the finish coating is used to protect the metal from chemically aggressive media.

A number of studies have shown that modification of the surface of fluoroplastic using plasma treatment, in particular atmospheric nitrogen plasma, leads to an increase in wettability, partial surface defluorination and the introduction of oxygen and nitrogen-containing functional groups, which improves adhesion characteristics compared to non-modified polymer [5, 6]. Similar effects are observed during ion-beam treatment of fluoroplastic films, when ion irradiation causes a change in the chemical composition of the upper layers, an improvement in metal adhesion to the modified surface of the polymer [7]. However, such methods require vacuum or plasma equipment and often focus on thin films and specific material pairs, which limits their use in mass processes. Along with the modification of the polymer itself, the preparation of the metal substrate plays an important role. Phosphating treatments are traditionally used to increase the adhesion of paint and polymer coatings to steels and galvanized steel due to the formation of a thin layer of metal phosphates on the surface [8, 9]. Reviews of conversion coatings emphasize that phosphate and chromate films act as an intermediate layer that increases the adhesion of subsequent coatings [10].

Work on phosphating and the use of phosphate primers shows that such conversion layers can significantly increase the adhesion of organic and polymer coatings to metal substrates. A number of studies have found that during preliminary phosphating of steel and galvanized surfaces, subsequent paint and polymer systems form a stronger and more stable connection with the substrate compared to unmodified surfaces, while the most pronounced effect is achieved in systems with epoxy, polyester binders and polymer films applied to the phosphated layer [11, 12].

The purpose of this work is to experimentally evaluate the adhesion of a 500 μm thick fluoroplastic film to a metal substrate using a primer containing fluoroplastic, chromium oxide (III) (Cr_2O_3) in an aqueous medium and phosphoric acid (H_3PO_4). This primer is aimed at the "metal-primer-fluoroplastic (film)" system and uses fluoroplastic directly in the primer layer, forming a gradient transition to the main coating.

MATERIALS AND METHODS

The study used metal plates made of titanium alloy VT6 (analogous to Ti–6Al–4V) and carbon steel St3, which had dimensions of 120×60×1 mm. Before coating, the plates were cleaned of contaminants and degreased with acetone xh. in an ultrasonic bath "ODA-MH280" (China) with a power of 1100 W at a frequency of 40 kHz for 10 minutes at a temperature of 20–22 °C. This operation removed surface organic contaminants, which is an important condition for forming a uniform and stable adhesive bond.

An aqueous fluoroplastic suspension manufactured by HaloPolymer Perm JSC was used as the main coating material. The coating was applied to pre-prepared plates by a spray method using a spray gun and compressed air. The working pressure of compressed air was 0.2–0.3 MPa, the distance from the nozzle to the treated surface was in the range of 300-400 mm, which ensured uniform formation of a monolayer of suspension without splashing and draining.

The key parameters for the formation of the fluoroplastic film were drying and sintering modes. Drying was carried out at a temperature not exceeding 90 °C for 45 minutes to complete the removal of free and bound moisture from the aqueous suspension, while the absence of cracks and bubbles in the dried layer was monitored. Sintering was carried out at a temperature of 370 °C for 8–10 minutes, followed by cooling in an oven to room temperature. To achieve a given coating thickness (500 μm), the process was repeated repeatedly in sequence, ensuring the accumulation of layers with control of their thickness and continuity. All drying and sintering operations were carried out in the laboratory electric furnace "KS-18" (Russia), equipped with thermal control and uniform temperature distribution over the working volume.

The adhesion strength of the formed fluoroplastic films was evaluated using two standard methods: the

ISSN 2075-8545 (online)

X-cut method according to State Standard 32702.2-2014 and the normal tear method according to State Standard 32299-2025 on samples with dimensions of 50×50×1 mm. Due to the pronounced release properties and the difficulty of gluing the bursting cylinders to the surface of the fluoroplastic film, the use of classical methods for assessing tear strength has proven difficult. In this regard, a modified technique has been developed that allows measurements to be carried out without compromising the integrity of the coating. Films were formed on the end faces of the pair of plates, contacted and thermoplastic bonded at 330 °C (near the melting point of the fluoroplastic) for 5–7 minutes. As a result, a continuous layer of fluoroplastic serving as an adhesive seam was formed between the ends. Metal bursting cylinders fixed with epoxy rubber adhesive KDS-19 were mounted on the thus prepared glued plates. Adhesion tests by the tearing method were carried out on the universal test machine "REM-U-A" (Russia) at a fixed loading speed. The scheme of the proposed procedure is shown in Fig. 1.

A number of studies have shown that in order to improve the adhesive strength of fluoroplastic films, it is advisable for kmetallic substrates to pre-apply an intermediate adhesive layer. In this work, as such an intermediate layer, a suspension containing fluoroplast, chromium (III) oxide (Cr_2O_3) in an aqueous medium and phosphoric acid (H_3PO_4) was used. This intermediate coating formed a thin primer layer applied by air spraying under the same conditions as the base fluoroplastic coating, whereby the drying and sintering conditions of the base layer were satisfied. The use of a primer made it possible to realize a gradient transition from a metal substrate to a fluoroplastic layer and improve adhesion properties.

RESULTS AND DISCUSSION

When evaluating the adhesion of fluoroplastic films with a thickness of 500 μm using the "X-shaped" notch method [13], a significant difference was found in the behavior of coatings on samples with and without primer. For films formed without a preliminary primer layer, intense and continuous peeling of the coating around the perimeter of the notch was observed. In the visual assessment on a five-point scale, this corresponded to 5 points. Which indicates the complete absence of adhesion of fluoroplastic films to the metal substrate under direct contact conditions. For films applied with a primer layer, delamination along the perimeter of the notch was expressed to a minimal extent. In most cases, only local, fragmentary flaking was observed, with a visual score corresponding to 1 point. This indicates a significant improvement in adhesion strength and the formation of a sufficiently stable joint capable of withstanding the mechanical effects applied by the X-notch method.

When evaluating adhesion by the normal tearing method using the developed method, it was found that the absence of a primer layer leads to systematic defects in the formation of an adhesive seam. For films formed from a fluoroplastic slurry without primer and subsequent thermoplastic bonding of the plate end faces, spontaneous peeling of the coating from both ends was observed. The defect manifested itself in the form of separation of the fluoroplastic film at the border of contact with the ends of the metal plates, which led to the destruction of the integrity of the "metal-fluoroplastic (film)" system. As a result, such samples could not be used to quantify the peel adhesion strength because the

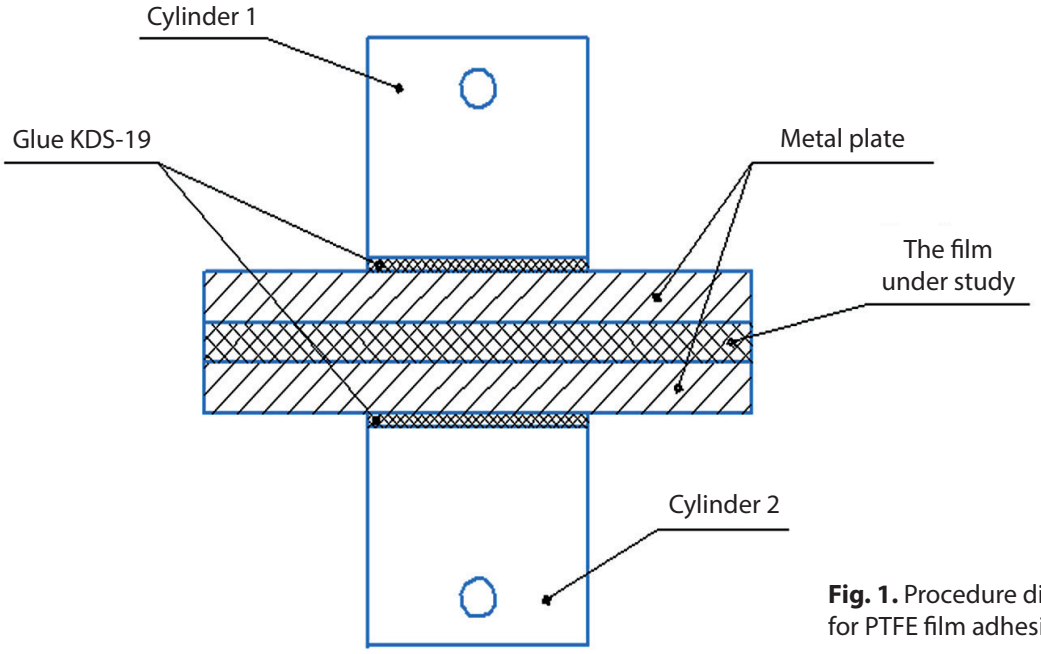


Fig. 1. Procedure diagram for PTFE film adhesion test

ISSN 2075-8545 (online)



Fig. 2. Appearance of coating with primer layer after normal tearing test (modified method)

failure occurred during the preparation stage and was not due to external loading.

For films formed using a primer layer, the adhesive seam at the ends of the plates retained integrity, and the destruction occurred under the influence of an external load on the test machine (Fig. 2).

A series of tests on the metal-soil-fluoroplastic (film) system resulted in the average values presented in Table 1.

These values indicate the formation of a physically correct and stable adhesive joint, in which the fracture occurs cohesively within the fluoroplastic matrix or adjacent zone, and not in the form of spontaneous detachment of the coating from the substrate.

Table 1. Peel adhesion test results

Maximum breaking load, N	Maximum deformation, mm	Tensile strength, N/mm²
1807.35	4.39	2.56

CONCLUSION

1. Application of a primer layer from a suspension containing fluoroplastic, chromium oxide (III) (Cr_2O_3) in aqueous medium and phosphoric acid (H_3PO_4), increases the adhesion strength of a fluoroplastic film with a thickness of 500 microns to metal substrates, which is confirmed by both visual assessment by the method of "X-shaped" notch and quantitative data by the method of normal separation. In a system with a primer layer, the degree of delamination is reduced to 1 point according to State Standard 32702.2-2014, and stable values are recorded during the test for the separation of registration under load: the average maximum load is 1807.35 N. The maximum deformation is 4.39 mm, the ultimate strength is 2.56 N/mm², which indicates the formation of a physically correct adhesive joint.

2. The mechanism of increasing adhesion is associated with the complex effect of the phosphate oxide layer and the gradient transition. Phosphoric acid, together with chromium oxide, forms a porous structure on the metal surface with a developed actual contact area, improving mechanical engagement with subsequent polymer and fluoroplastic coatings. The presence of fluoroplastic in the primer provides a gradient transition from the metal substrate through the intermediate layer to the main fluoroplastic film, which reduces the jump in physical and mechanical properties and reduces the concentration of stresses in the contact zone.

3. The results obtained demonstrate that the developed primer suspension can be recommended for use in technologies for applying fluoroplastic coatings to metal structures, where high chemical resistance, low coefficient of friction and sufficient adhesive strength are required at the same time.

REFERENCES

1. *Patent US7462667B2. Primer coating of PTFE for metal substrates /3M Innovative Properties Company*; applicant: Klaus Hintzer, Michael C. Dadalas, Tilman Zipplies, Gernot Loehr. Application numbers: 11/172345; declared. 30.06.2005; publ. 09.12.2008.

2. Nadirov K.S., Zhantasov M.K., Sakybayev B.A. The study of the gossypol resin impact on adhesive properties of the intermediate layer of the pipeline three-layer rust protection coating. *International Journal of Adhesion and Adhesives*. 2017;78:195-199. https://doi.org/10.1016/j.ijadhadh.2017.07.001

3. Baby M. Universal adhesion promoters for enhanced adhesion on metal and polymeric substrates. *International Journal of Adhesion and Adhesives*. 2025;140:104103. https://doi.org/10.1016/j.ijadhadh.2025.104013

4. Ali M.R.R., Tigno D., Honeyman Ja.S., Caldona E.B. Adhesion-Diffusional-Based Corrosion Protection Mechanisms of Polyaniline-Primed Fluoropolymer Coatings. *Applied Polymer Materials*. 2024;6(5):2719-2732. https://doi.org/10.1021/acsapm.3c02944

5. Caceres-Ferreira W.-M., Destrieux A., Profili J., Guay-Bégin A.-A., Ravichandran S., Laurent M., Nolan M., Smith A., Wang H., Laroche G. Alternative Surface Treatment for the Enhanced Adhesion of Polytetrafluoroethylene Films via Atmospheric Pressure Nitrogen Plasma.*ACS Applied Polymer Materials*. 2024;6(20):12585–12597. https://doi.org/10.1021/acsapm.4c02152

ISSN 2075-8545 (online)

6. Miyake E., Nishino M., Seto Y., Komatsu I., Endo K., Yamamura K., Ohkubo Y. Surface modification and adhesive-free adhesion of polytetrafluoroethylene (PTFE) and silicone gel containing oleophilicSiO_2 powder by plasma treatment.*RSC Advances*. 2023;13(3):1500–1510. https://doi.org/10.1039/D2RA05749B

7. LeeS.W., HongJ.W., WyeM.Y., KimJ.H., KangH.J., LeeY.S. Surface modification and adhesion improvement of PTFE film by ion beam irradiation. *Nuclear Instruments and Methods in Physics Research Section B: Beam Interactions with Materials and Atoms*. 2004;219–220:963-967. https://doi.org/10.1016/j.nimb.2004.01.197

8. Kubo Y., Sonohara Y., Uemura S., Saito Y. High-Energy Electron-Irradiated Fluorinated Ethylene Polypropylene Copolymer Coatings on Al Substrates for Enhanced Metal Adhesion and Protection.*ACS Applied Nano Materials*. 2022;5(5):6750–6758. https://doi.org/10.1021/acsanm.2c00766

9. Mequanint K., Sanderson R., Pasch H. Adhesion properties of phosphate- and siloxane-containing polyurethane dispersions to steel: An analysis of the metal-coating interface. *Journal of Applied Polymer Science*. 2003;88(4):900–907. https://doi.org/10.1002/app.11680

10. Saran D., Kumar A., Bathula S., Klaumünzer D., Sahu K. K. Review on the phosphate-based conversion coatings of magnesium and its alloys. International *Journal of Minerals, Metallurgy and Materials*. 2022;29(7):1435–1452.https://doi.org/10.1007/s12613-022-2419-2

11. Lukosiute I., Aniuniene J., Levinskas R. Effect of phosphate coatings on the performance of epoxy polyamide red oxide primer on galvanized steel.*Progress in Organic Coatings*. 2005;54(1):5–9. https://doi.org/10.1016/j.porgcoat.2004.03.012

12. Jayaganthan A., Surya P., Teja P. J. Performance and Characterization Study of Zinc Phosphate Coating over Steel for Automotive Application. *International Research Journal of Engineering and Technology (IRJET)*. 2022;9 (3):1014–1018.

ADDITIONAL INFORMATION

The authors declare that the preparation of the article did not use technologies of generative artificial intelligence and technologies based on artificial intelligence.

INFORMATION ABOUT THE AUTHORS

Oleg R. Latypov – Dr. Sci. (Eng.), Professor, head of the Materials science and corrosion protection department, Ufa state petroleum technological university, 450064, Ufa, Kosmonavtov, 1, Republic of Bashkortostan, Russian Federation, o.r.latypov@mail.ru, https://orcid.org/0000-0002-4487-1516

Karina V. Kim – Master's student, Materials science and corrosion protection department, Ufa State Petroleum Technological University, Ufa, Kosmonavtov str. 1, 450064, Republic of Bashkortostan, Russian Federation, vadimovnakk@gmail.com, https://orcid.org/0009-0004-9434-0408

Vasily V. Lukyanov – Cand. Sci. (Eng.), Associate Professor, Intelligent systems, technologies and equipment in mechanical engineering department, Ufa State Petroleum Technological University, Ufa, Kosmonavtov str. 1, 450064, Republic of Bashkortostan, Russian Federation; Senior Researcher at the Center for Intelligent Mechanical Engineering, Ufa State Petroleum Technological University; Head of the Department for the Management of Special Technology and Equipment Development, Technopark of Aviation Technologies, Ufa, Tramvaynaya str. 5, building 1, 450112, Republic of Bashkortostan, Russian Federation, lukianovv@bk.ru, https://orcid.org/0009-0006-3621-3966

Dina R. Latypova – Cand. Sci. (Eng.), Associate Professor, Materials science and corrosion protection department, Ufa State Petroleum Technological University, Ufa, Kosmonavtov str. 1, 450064, Republic of Bashkortostan, Russian Federation, d.r.latypova@mail.ru, https://orcid.org/0000-0002-0637-3313

Rustem R. Daminev – Dr. Sci. (Eng.), Professor, head of the of Oil and gas engineering and digital technologies institute, Ufa State Petroleum Technological University, Ufa, Kosmonavtov str. 1, 450064, Republic of Bashkortostan, Russian Federation, daminew@mail.ru, https://orcid.org/0000-0001-8673-5240

Alisa F. Ahmadullina – Research Engineer at the Center for Intelligent Mechanical Engineering, Ufa State Petroleum Technological University, Ufa, Kosmonavtov str. 1, 450064, Republic of Bashkortostan, Russian Federation; Lead Design Engineer, Technopark of Aviation Technologies, Ufa, Tramvaynaya str. 5, building 1, 450112, Republic of Bashkortostan, Russian Federation, alisa_fanirovna@mail.ru, https://orcid.org/0009-0007-0911-0731

CONTRIBUTION OF THE AUTHORS

Oleg R. Latypov – scientific supervision; analysis of the research results; writing the article; drawing up final conclusions.

Karina V. Kim – editing and data processing.

Vasily V. Lukyanov – scientific supervision; development of the concept and methodology of the research.

Dina R. Latypova – scientific supervision, scientific editing of the text, participation in scientific discussion.

Rustem R. Daminev – scientific supervision, scientific editing of the text, participation in scientific discussion.

Alisa F. Ahmadullina – editing and data processing.

The authors declare no conflict of interest.

The article was submitted 04.07.2026; approved after reviewing 02.10.2026; accepted for publication 08.10.2026.

ISSN 2075-8545 (online)

Nanotechnologies in construction
Нанотехнологии в строительстве

2026; 18 (5):
627–656

Nanobuild.ru

APPLICATION OF NANOMATERIALS AND NANOTECHNOLOGIES IN CONSTRUCTION

Original article
https://doi.org/10.15828/2075-8545-2026-18-5-627-656

CC BY 4.0

Experimental studies of reinforced concrete structures in the "HPP supporting piers – powerhouse headwall" system strengthened with prestressed basalt composite reinforcement. Part II[1)]

Oleg D. Rubin, Anton S. Antonov*, Amer Almasri

National Research Moscow State University of Civil Engineering, 26 Yaroslavskoye Shosse, Moscow, 129337, Russian Federation

* Corresponding author: e-mail: antonov.an.s@yandex.ru

ABSTRACT

Introduction. With long-term operation of head run-of-river powerhouses of hydroelectric power plants (HPP), technical changes occur that lead to a decrease in operational properties in reinforced concrete structures. To substantiate a new nanotechnology for strengthening long-term operated hydraulic structures based on the use of prestressed reinforcement from nanomaterials (basalt fiber reinforced polymer rebar, BFRP), a set of experimental studies with elements of computational studies was carried out, taking into account the characteristic features of reinforced concrete structures of HPPs. **Methods and materials.** Experimental studies were carried out on the basis of reinforced concrete models of hydraulic structures "HPP supporting piers – powerhouse headwall" (scale M 1:25), which were manufactured and tested for static impact; after which they were strengthened with external reinforcement made of prestressed BFRP nanomaterial, with rebars installed in two directions: along and across the flow. A 3D finite element model of a run-of-river HPP powerhouse was developed to analyze its stress-strain state (SSS), taking into account seismic actions of more than 8 points (MSK scale) within the framework of the dynamical theory. **Results.** As a result of experimental studies of reinforced concrete models of hydraulic structures "hydroelectric power plant piers – headwall of the HPP powerhouse", the nature of crack formation, the width of crack opening and inter-block construction joints were determined, which were recorded in magnitude higher in non-strengthened reinforced concrete experimental models than in models strengthened with prestressed basalt composite reinforcement. In experimental reinforced concrete models under the acting loads, tensile stresses in the steel reinforcement in the area of the interface of the piers and the headwall were determined, which almost reached the value corresponding to the yield strength. In the article, calculations of the run-of-river HPP powerhouse were performed using the dynamic theory of calculation under the action of seismic loads of more than 8 points (MSK scale). At the same time, deformations of the structure and stresses in its elements in different periods of time (in seconds) were obtained, counting from the beginning of the seismic action. **Discussion.** It was obtained that the new technology of strengthening using reinforcement made of BFRP nanomaterial across and along the river flow leads to a decrease in tensile stresses in steel horizontal reinforcement across the flow in the headwall and in piers by more than 1.5 times with redistribution to basalt composite reinforcement. In case of seismic actions, the operation of the above structures will be more complex and the parameters of this work must be determined by calculations, taking into account all factors that will allow to study and ensure long-term safe operation of HPP structures. To achieve this goal, it is necessary to develop a 3D mathematical model of experimental reinforced concrete structures and verify it using a set of experimental data obtained. Further, the verified mathematical model can be used to calculate the SSS of the HPP powerhouse under the action of a set of loads and influences: static, hydraulic, temperature, seismic. **Conclusion.** On the basis of a set of experimental and computational studies of experimental reinforced concrete models "HPP supporting piers – powerhouse headwall", strengthened with prestressed basalt composite reinforcement, nanotechnology for strengthening reinforced concrete structures of long-term operated hydraulic structures based on the use of prestressed reinforcement from nanomaterials (basalt fiber reinforced polymer rebar BFRP) was substantiated, including the load-bearing capacity, displacement, width of opening of inter-block construction joints and cracks, deformations of steel and basalt composite reinforcement depending on the method of strengthening of reinforced concrete structures by external reinforcement.

KEYWORDS: hydraulic structures, HPP supporting piers, HPP powerhouse headwall, inter-block construction joints, nanotechnology of reinforcement, prestress, basalt composite nanomaterial, width of opening of inter-block joints and cracks, displacements

[1)] Ending. Part I was published in "Nanotechnologies in construction". 2026; 18(4).

© Rubin O.D., Antonov A.S., Almasri A., 2026

ISSN 2075-8545 (online)

Nanotechnologies in construction
Нанотехнологии в строительстве

2026; 18 (5):
627–656

Nanobuild.ru

APPLICATION OF NANOMATERIALS AND NANOTECHNOLOGIES IN CONSTRUCTION

SOURCES OF FUNDING FOR THE SCIENTIFIC WORK THAT RESULTED IN THE PUBLICATION: The Study was carried out from the personal funds of the authors with the scientific and technical support of the branch of JSC "Institute of Hydroproject" – NIIES.

FOR CITATION:
Rubin O.D., Antonov A.S., Almasri A. Experimental studies of reinforced concrete structures in the "HPP supporting piers – powerhouse headwall" system strengthened with prestressed basalt composite reinforcement. Part II. *Nanotechnologies in Construction.* 2026;18(5):627–656. https://doi.org/10.15828/2075-8545-2026-18-5-627-656. – EDN: EHJVET.

Экспериментальные исследования железобетонных конструкций системы «бычки ГЭС – напорная стена здания ГЭС», усиленной предварительно напряженной базальтокомпозитной арматурой. Часть II[1)]

Олег Дмитриевич Рубин, Антон Сергеевич Антонов*, Амер Алмасри

Национальный исследовательский Московский государственный строительный университет, 129337, Москва, Ярославское шоссе, 26, Российская Федерация

* Автор, ответственный за переписку: e-mail: antonov.an.s@yandex.ru

АННОТАЦИЯ

Введение. При длительной эксплуатации напорных русловых зданий гидроэлектростанций возникают технические изменения, которые приводят к снижению эксплуатационных свойств в железобетонных конструкциях. Для обоснования новой технологии (нанотехнологии) усиления длительно эксплуатируемых гидротехнических сооружений на основе применения предварительно напряженной арматуры из наноматериалов (базальтокомпозитной арматуры) проведен комплекс экспериментальных исследований с элементами расчетных исследований, учитывающий характерные особенности железобетонных конструкций ГТС. **Методы и материалы.** Экспериментальные исследования проводились на основе железобетонных моделей гидротехнических сооружений «бычки ГЭС – напорная стена здания ГЭС» (масштаб М 1:25), которые были изготовлены и испытаны на статическое воздействие, после чего они были усилены внешним армированием из наноматериала – предварительно напряженной базальтокомпозитной арматуры, установленной в двух направлениях: вдоль и поперек потока. Была разработана пространственная конечно-элементная модель руслового здания ГЭС для расчетных исследований НДС с учетом сейсмических воздействий более 8 баллов в рамках динамической теории. **Результаты.** В результате экспериментальных исследований опытных железобетонных моделей гидротехнических сооружений «бычки ГЭС – напорная стена здания ГЭС» определен характер трещинообразования, ширина раскрытия трещин и межблочных строительных швов, зафиксированных по величине выше в неусиленных железобетонных опытных моделях, чем в усиленных предварительно напряженной базальтокомпозитной арматурой моделях. В опытных железобетонных моделях при действующих нагрузках определены растягивающие напряжения в стальной арматуре в зоне сопряжения бычков и напорной стены, которые практически достигли величины, соответствующей пределу текучести. В настоящей работе были выполнены расчеты руслового здания ГЭС с применением динамической теории расчета при действии сейсмических нагрузок более 8 баллов. При этом были получены деформации сооружения и напряжения в его элементах в различные периоды времени (в секундах), отсчитывая от начала сейсмического воздействия. **Обсуждение.** Было получено, что новая технология (нанотехнология) усиления с применением наноматериала – предварительно напряженной базальтокомпозитной арматуры поперек и вдоль потока – приводит к снижению растягивающих напряжений в стальной горизонтальной арматуре поперек потока в напорной стене и в бычках более чем в 1,5 раза с перераспределением на базальтокомпозитную арматуру. При сейсмических воздействиях работа вышеуказанных конструкций будет более сложной и параметры этой работы необходимо определять расчетами с учетом всех факторов, которые позволят изучить и обеспечить длительную безопасную эксплуатацию гидротехнических сооружений ГЭС. Для достижения этой цели необходимо разработать трехмерную математическую модель железобетонных экспериментальных конструкций и провести её верификацию с использованием комплекса полученных экспериментальных данных. Далее верифицированную расчетную математическую модель возможно применить для расчетов НДС здания ГЭС при действии комплекса нагрузок и воздействий: статических, гидравлических, температурных, сейсмических. **Заключение (выводы).** На основе проведенного комплекса экспериментальных и расчетных исследований опытных железобетонных моделей «бычки ГЭС – напорная стена здания ГЭС», усиленных предварительно напряженной базальтокомпозитной арматурой, была обоснована нанотехнология усиления железобетонных конструкций длительно эксплуатируемых гидротехнических

ISSN 2075-8545 (online)

Nanotechnologies in construction
Нанотехнологии в строительстве

2026; 18 (5):
627–656

Nanobuild.ru

APPLICATION OF NANOMATERIALS AND NANOTECHNOLOGIES IN CONSTRUCTION

сооружений на основе применения предварительно напряженной арматуры из наноматериалов (базальтокомпозитной арматуры), в том числе определялись несущая способность, перемещение, ширина раскрытия межблочных строительных швов и трещин, деформация стальной и базальтокомпозитной арматуры в зависимости от способа усиления железобетонных конструкций внешним армированием.

КЛЮЧЕВЫЕ СЛОВА: гидротехнические сооружения, бычки ГЭС, напорная стена здания ГЭС, межблочные строительные швы, нанотехнология усиления, предварительное напряжение, наноматериал – базальтокомпозитная арматура, ширина раскрытия межблочных швов и трещин, перемещения

ИСТОЧНИКИ ФИНАНСИРОВАНИЯ НАУЧНОЙ РАБОТЫ, РЕЗУЛЬТАТОМ КОТОРОЙ СТАЛА ПУБЛИКАЦИЯ: Работа выполнена инициативно из личных средств авторов при научно-технической поддержке филиала АО «Институт Гидропроект»–«НИИЭС».

ДЛЯ ЦИТИРОВАНИЯ:
Рубин О.Д., Антонов А.С., Алмасри А. Экспериментальные исследования железобетонных конструкций системы «бычки ГЭС – напорная стена здания ГЭС», усиленной предварительно напряженной базальтокомпозитной арматурой. Часть II. *Нанотехнологии в строительстве.* 2026;18(5):627–656. https://doi.org/10.15828/2075-8545-2026-18-5-627-656. – EDN: EHJVET.

RESULTS

During the experimental studies, the following main results were obtained:

1. In the experimental reinforced concrete models M 1-1 and M 2-1, under the load P = 20.0–30.0 kN, at the corners on the contact "supporting piers – headwall" (Fig. 1) the cracks were formed, with a maximum crack width of α_{cr} = 0.53 mm at P = 120 kN (M 1-1), that is higher than the standard value [24]. The diagram of the width of crack opening in the corners at the "piers – headwall" contact are presented in Fig. 2 and 3. It should be noted that the opening width α_{cr} of these cracks is significantly higher in the experimental models without reinforcement M1-1 and M 2-1 than in the experimental models reinforced with prestressed basalt composite reinforcement M 1-2, M 1-3, M 2-2 and M 2-3.

2. Under the action of a load P = 30.0–60.0 kN, the inclined cracks appeared on the inner and outer lateral surfaces of the piers of the experimental reinforced concrete models M 1-1 and M 2-1, reaching to the lower inter-block joint (Fig. 4), which are shown as diagrams in Fig. 5–8 with a maximum of $\alpha_{cr,1}$ = 0.46 mm in the M 2-1 model (Fig. 5), that is higher than the standard value [24].

It should be noted that the opening width of the inclined cracks is significantly higher in the experimental models without reinforcement M 1-1 and M 2-1 than in the experimental models M 1-2, M 1-3, M 2-2 and M 2-3 reinforced with prestressed basalt composite reinforcement.

3. In the experimental models M 1-1 and M 2-1, under the load P in the piers and in the headwall, the inter-block construction joints α^{j}_{cr} were opened (Fig. 9–13). In this case, the opening width of the upper inter-block joint



Fig. 1. Crack formation in the corners of the experimental reinforced concrete models M 1-1 and M 2-1 (top view)

ISSN 2075-8545 (online)

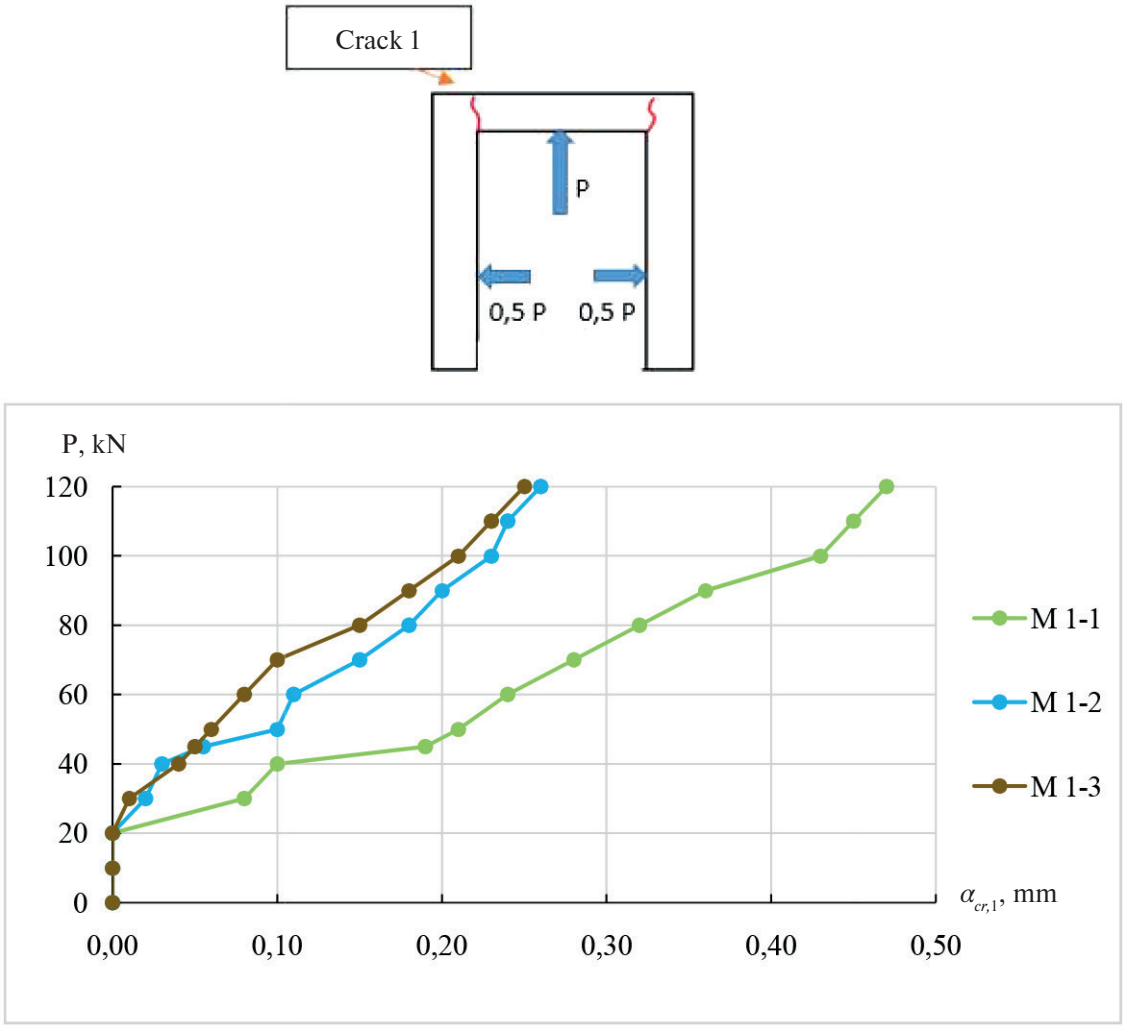


Fig. 2. Opening width of crack 1 at the contact "piers-headwall" ($P = f(\alpha_{cr,1})$)

ISSN 2075-8545 (online)

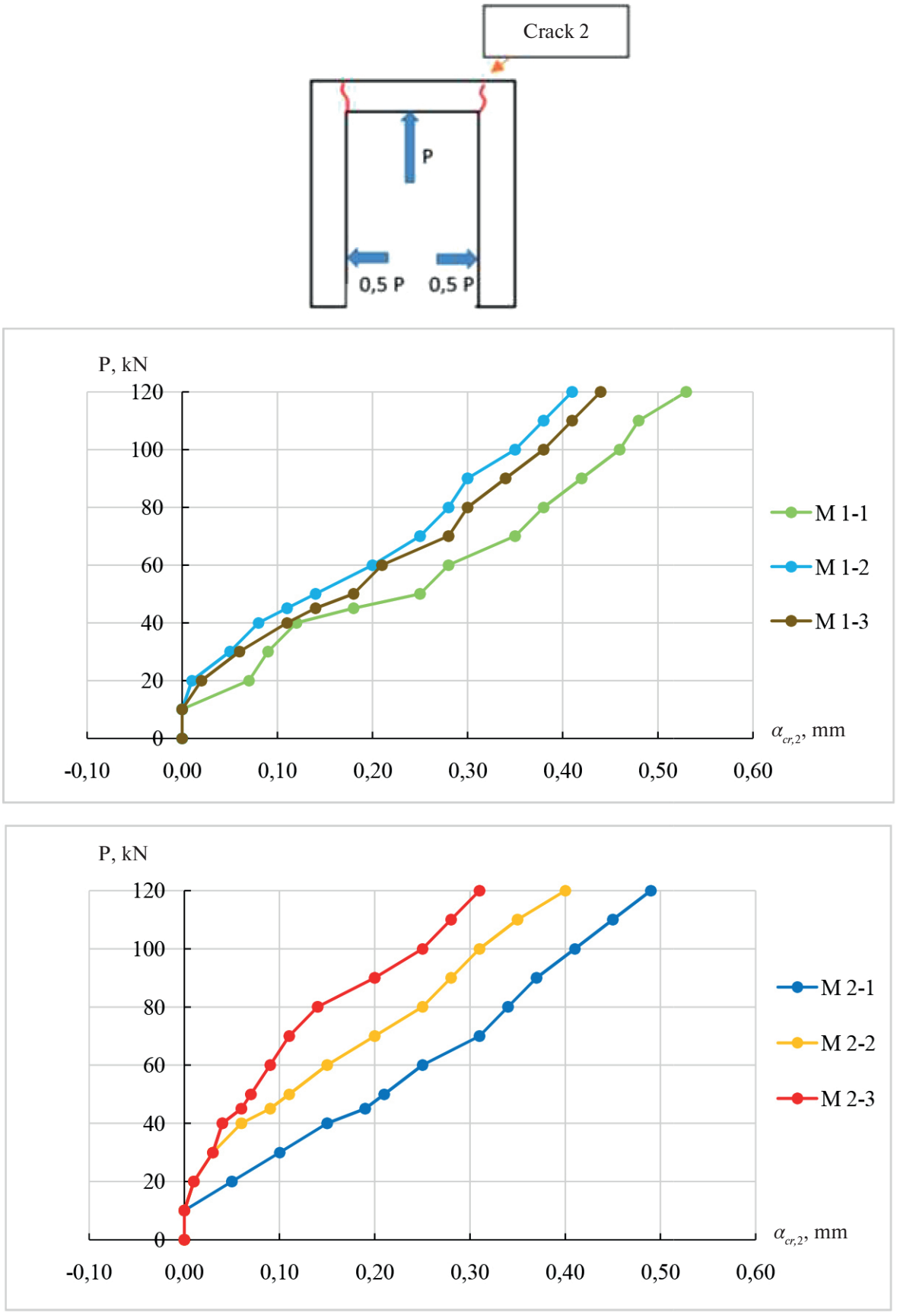


Fig. 3. Opening width of crack 2 at the contact "piers- headwall" ($P = f(\alpha_{cr,2})$)

ISSN 2075-8545 (online)

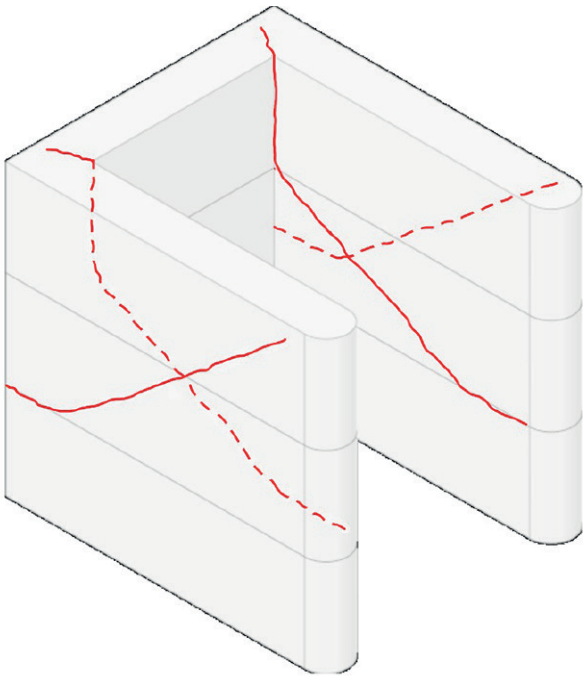


Fig. 4. Crack pattern in the reinforced concrete models: inclined cracks in the piers with a transition to the lower inter-block construction joint

$\alpha^{j}_{cr} \leqslant 0.05$ mm (Fig. 9, 11 and 13); the opening width of the lower inter-block joint $\alpha^{j}_{cr} \leqslant 0.16$ mm (Fig. 10 and 12).

It should be noted that the opening width of inter-block construction joints is higher in the experimental models without reinforcement M 1-1 and M 2-1than in the experimental models M 1-2, M 1-3, M 2-2 and M 2-3 reinforced with prestressed basalt composite reinforcement.

4. In the experimental reinforced concrete models M 1-1 and M 2-1, lateral divergence of the piers was recorded under the load P = 40,0 kN (Fig. 14) with a maximum total value of 9.2 mm at $P = 120\ kN$, which corresponds to 1/74 of the span $l = 680.0$ mm (Fig. 3, Part I). It should be noted that the total divergence width of the piers is higher in the unstrengthened models M 1-1 and M 2-1 than in the models M 1-2, M 1-3, M 2-2 and M 2-3 strengthened with prestressed basalt composite reinforcement.

5. In experimental reinforced concrete models (Fig. 5, Part I) under the load P, deformations (converted into tensile stresses) in the upper horizontal steel reinforcement in the area of the interface between the piers and the headwall were determined (Fig. 15-18). The stresses σ_s reach a value of 380 MPa at a load $P = 120\ kN$ (M 2-1, Fig. 16), which is close to the standard yield limit $R_{sn} = 390\ MPa$.

Stresses in the upper horizontal steel reinforcement in the interface between the piers and the headwall were recorded to be higher in unstrengthened models M 1-1 and M 2-1 than in models strengthened with prestressed basalt composite reinforcement M 1-2, M 1-3, M 2-2, and M 2-3.

It should be noted that the tensile stresses in the upper horizontal steel reinforcement in the span of the headwall $\sigma_{s,17}$ and $\sigma_{s,18}$ (Fig. 15–18) were relatively small (within up to 20 MPa) due to the formation and opening of corner cracks at the contact interface "piers – headwall" (Fig. 1) under static load P. Furthermore, tensile stresses σ_s in the horizontal steel reinforcement positioned lower down (in the cross-section of the upper inter-block construction joint; see Figs. 3 and 7, Part I) were approximately 30% lower than in the upper horizontal steel reinforcement.

6. In the experimental reinforced concrete models (Fig. 5, Part I) under the load P, strains (converted to tensile stresses) were determined in the vertical steel reinforcement located at the edge of the piers in the zone of the lower inter-block construction joint (Figs. 19–22). Tensile stresses reach 52.0 MPa (M 2-1, Fig. 19), which constitutes 13.3% of the tensile strength of the steel reinforcement $R_s = 390\ MPa$ at $P = 120\ kN$.

7. In the experimental reinforced concrete models (Fig. 5: M 1-2, M 1-3, M 2-2, and M 2-3) under the load P, strain increments (converted to tensile stress increments $\Delta\sigma\ \sigma_f$)) in the basalt composite reinforcement prestressed to 280 MPa were determined (Figs. 23–26). At the load $P = 120\ kN$, the maximum value was $\Delta of\ \sigma\ \sigma_f = 32.5$ MPa (M 1-3, Fig. 24), which corresponds to 32.5/280*100% = 11.6% of the tensile strength of the basalt composite reinforcement $R_{f\mu} = 800\ MPa$.

8. It should be noted that the load P applied to the experimental reinforced concrete models was brought up to $P = 120 \div 140\ kN$, with no signs of brittle failure recorded.

9. It also should be noted that the experimental reinforced concrete models, equipped with monitoring and measuring instrumentation, fully enabled the determination of the crack pattern and the experimental stress-strain state under stepwise application of static loads.

CONCLUSION

1. During many years of operation of head run-of-river HPP powerhouses, deviations from design assumptions arise, caused by non-design displacements and settlements, opening of inter-block construction joints and cracks, and a variety of other factors (as detailed in the introduction). In this regard, experimental investigations were required to substantiate the nanotechnology for strengthening reinforced concrete structures of head run-of-river HPP powerhouses using nanomaterial – prestressed basalt composite reinforcement, aimed at restoring load-bearing capacity to ensure long-term safe operation of hydraulic structures.

ISSN 2075-8545 (online)

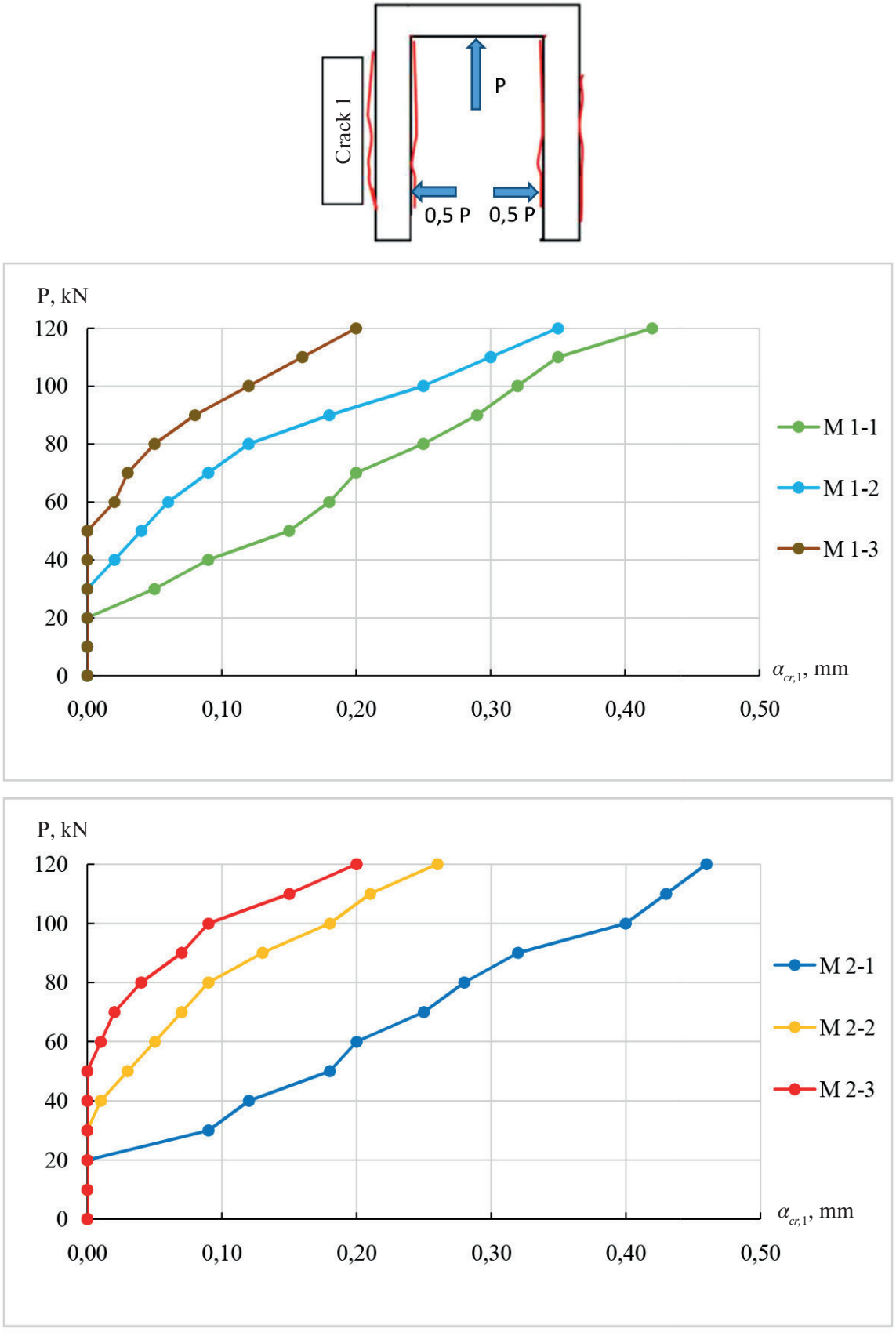


Fig. 5. Opening width of inclined crack 1 on the outer side surface of the pier ($P = f(\alpha_{cr,1})$)

ISSN 2075-8545 (online)

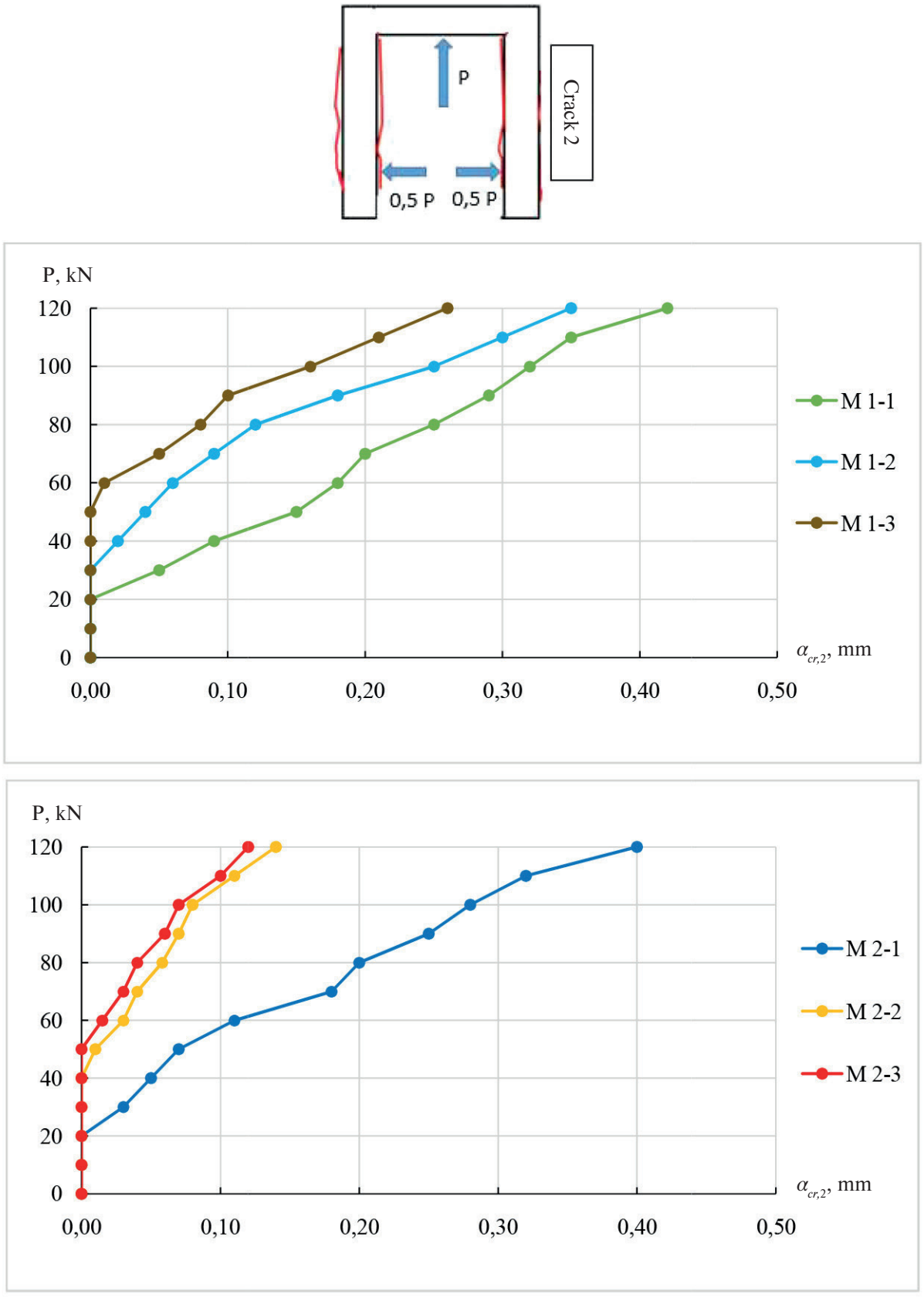


Fig. 6. Opening width of inclined crack 2 on the outer side surface of the pier ($P = f(\alpha_{cr,2})$)

ISSN 2075-8545 (online)

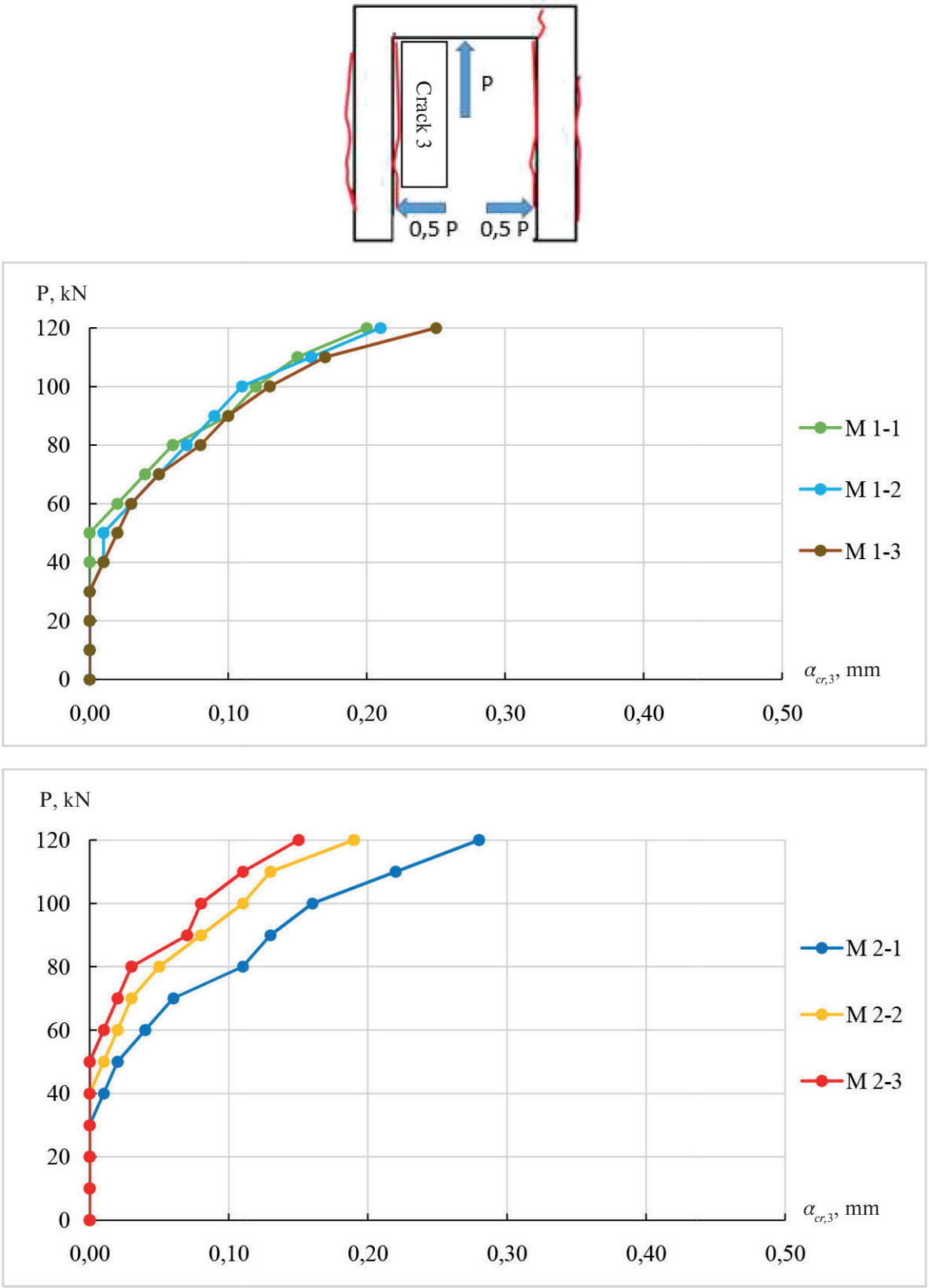


Fig. 7. Opening width of inclined crack 3 on the inner side surface of the pier ($P = f(\alpha_{cr,3})$)

ISSN 2075-8545 (online)

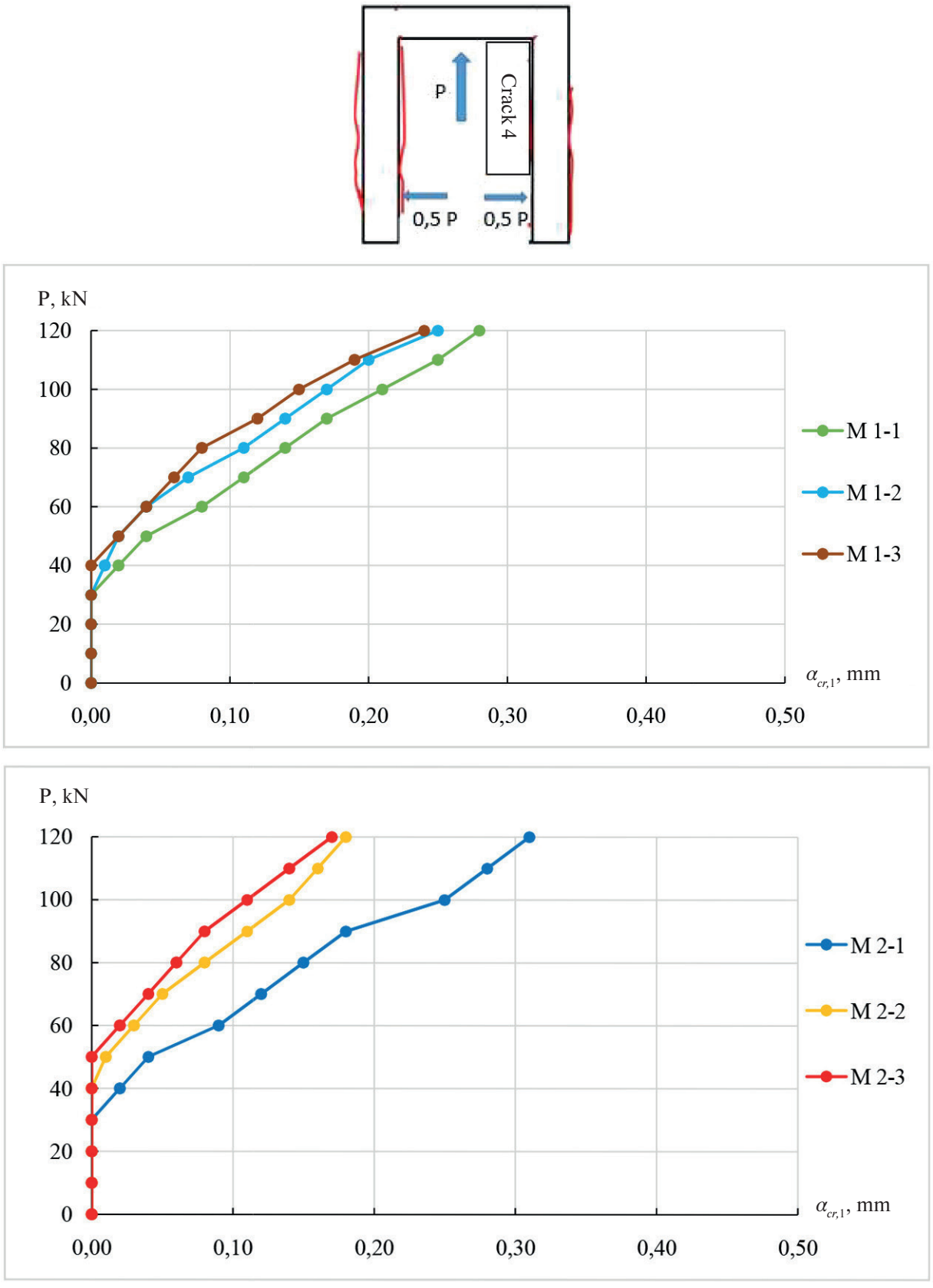


Fig. 8. Opening width of inclined crack 4 on the inner side surface of the pier ($P = f(\alpha_{cr,4})$)

ISSN 2075-8545 (online)

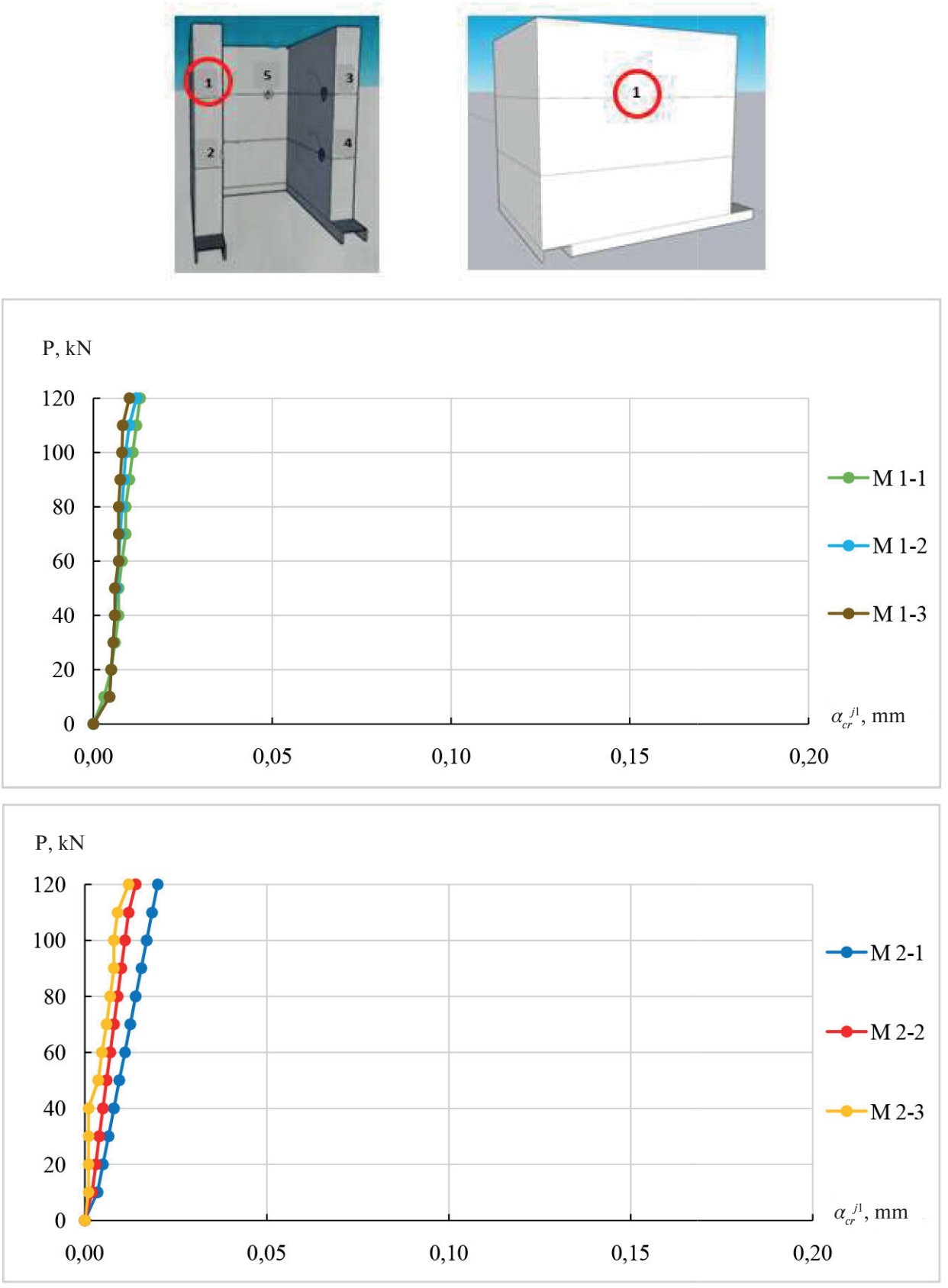


Fig. 9. Opening width of inter-block construction joint 1 in the pier ($P = f(\alpha^{j1}_{cr})$)

ISSN 2075-8545 (online)
Nanotechnologies in construction
Нанотехнологии в строительстве
2026; 18 (5): 627–656

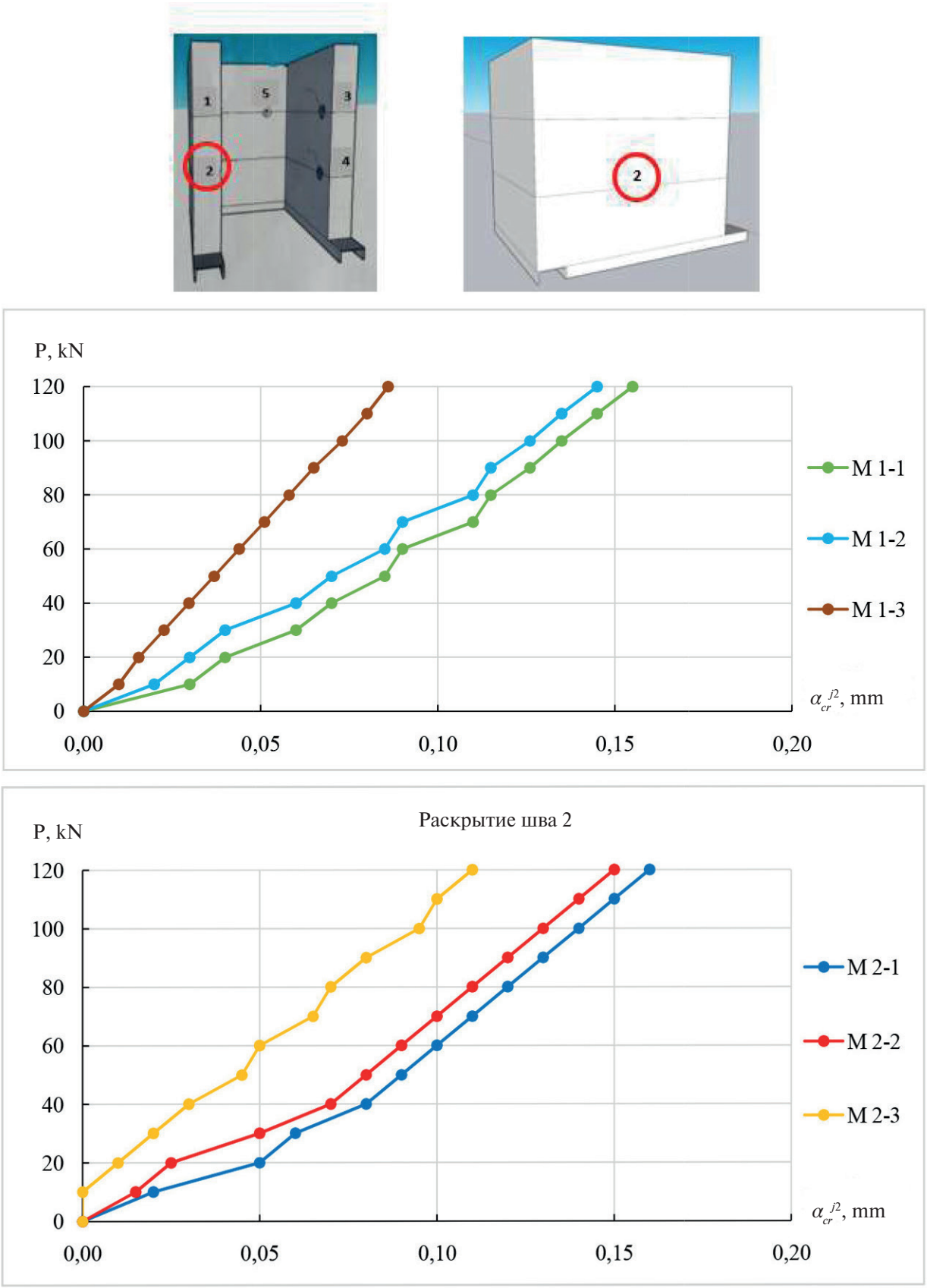


Fig. 10. Opening width of inter-block construction joint 2 in the pier ($P = f(\alpha^{j2}_{cr})$)

ISSN 2075-8545 (online)

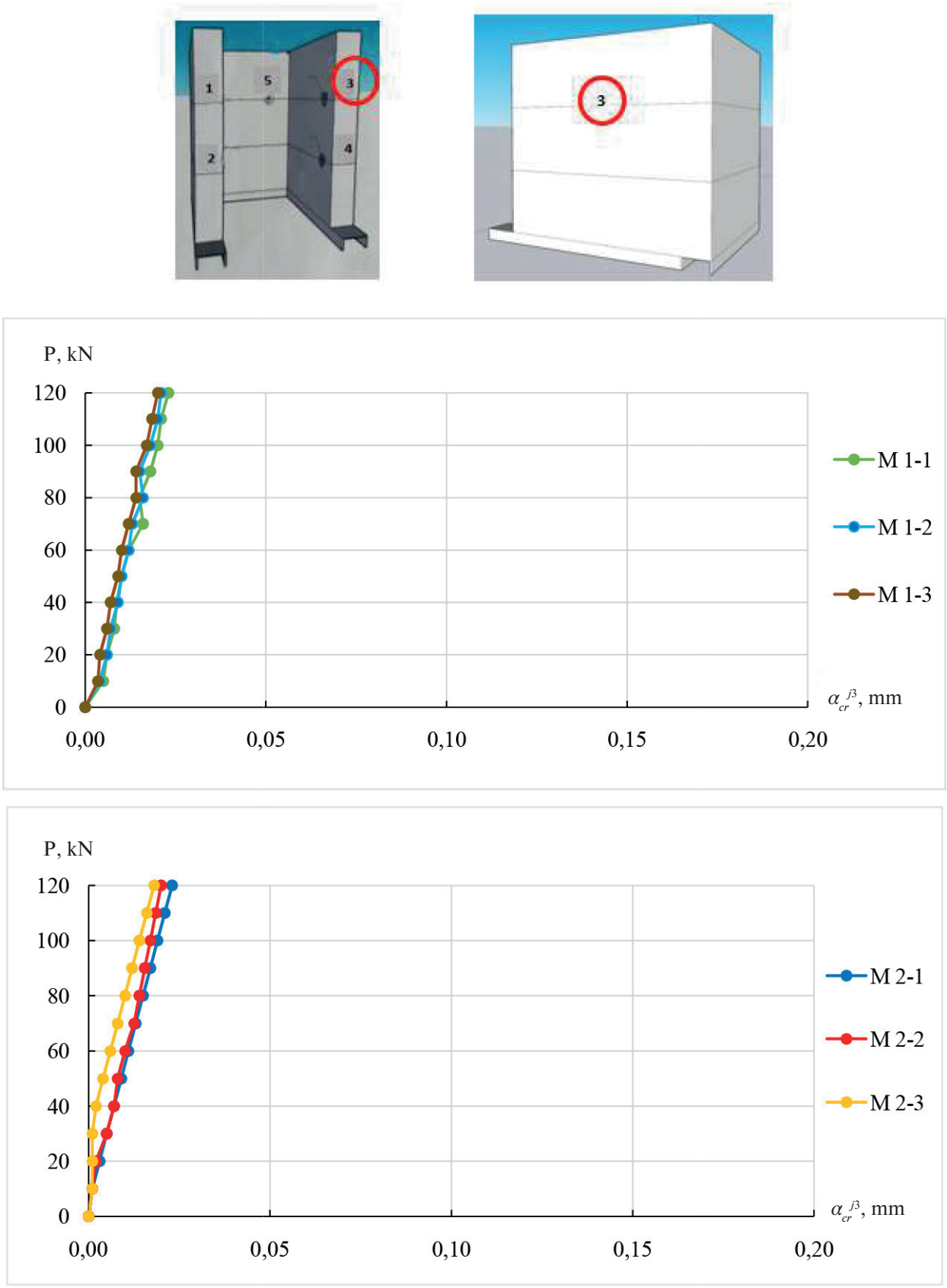


Fig. 11. Opening width of inter-block construction joint 3 in the pier ($P = f(\alpha^{j3}_{cr})$)

ISSN 2075-8545 (online)

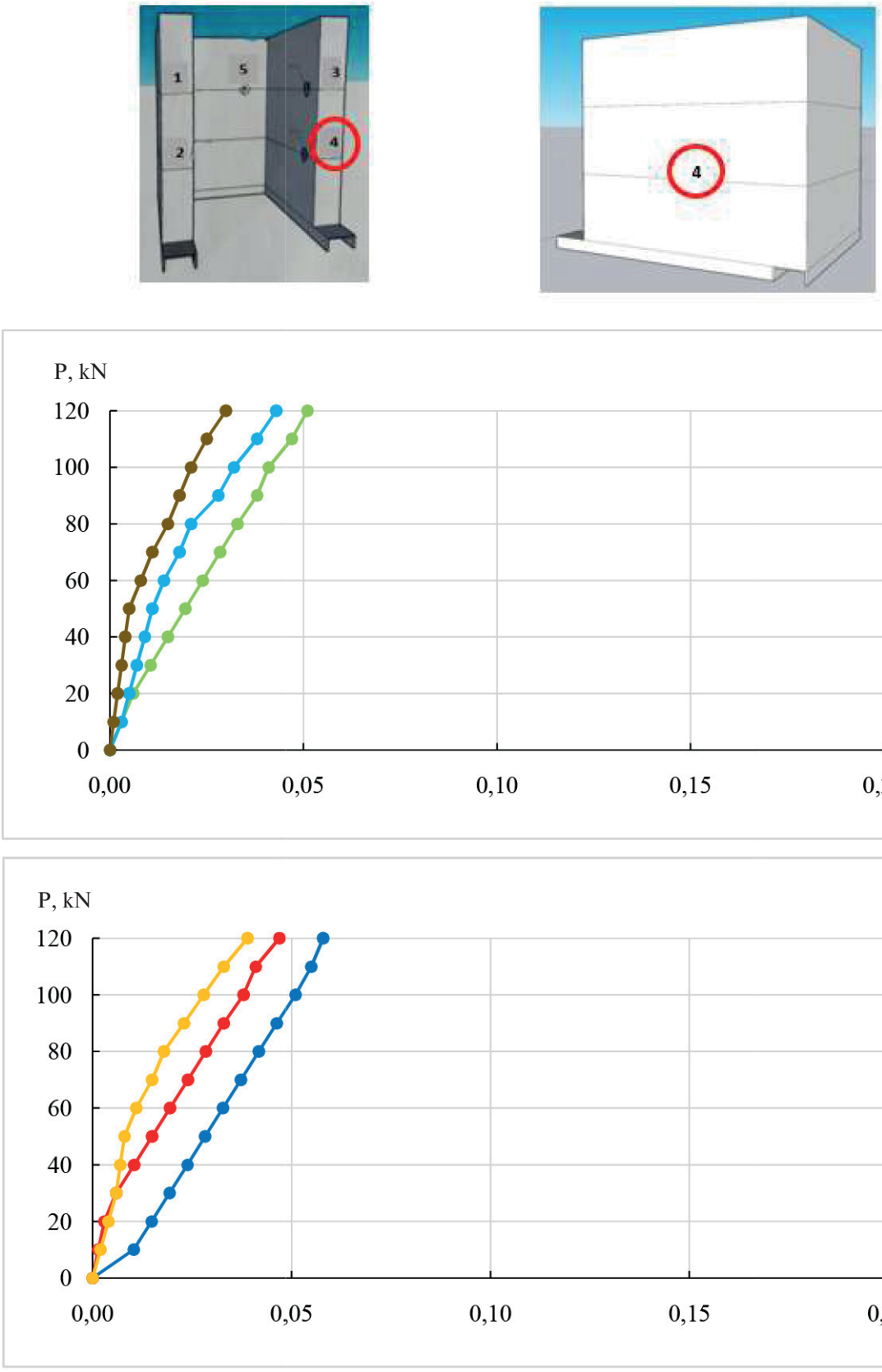


Fig. 12. Opening width of inter-block construction joint 4 in the pier ($P = f(\alpha^{j4}_{cr})$)

ISSN 2075-8545 (online)

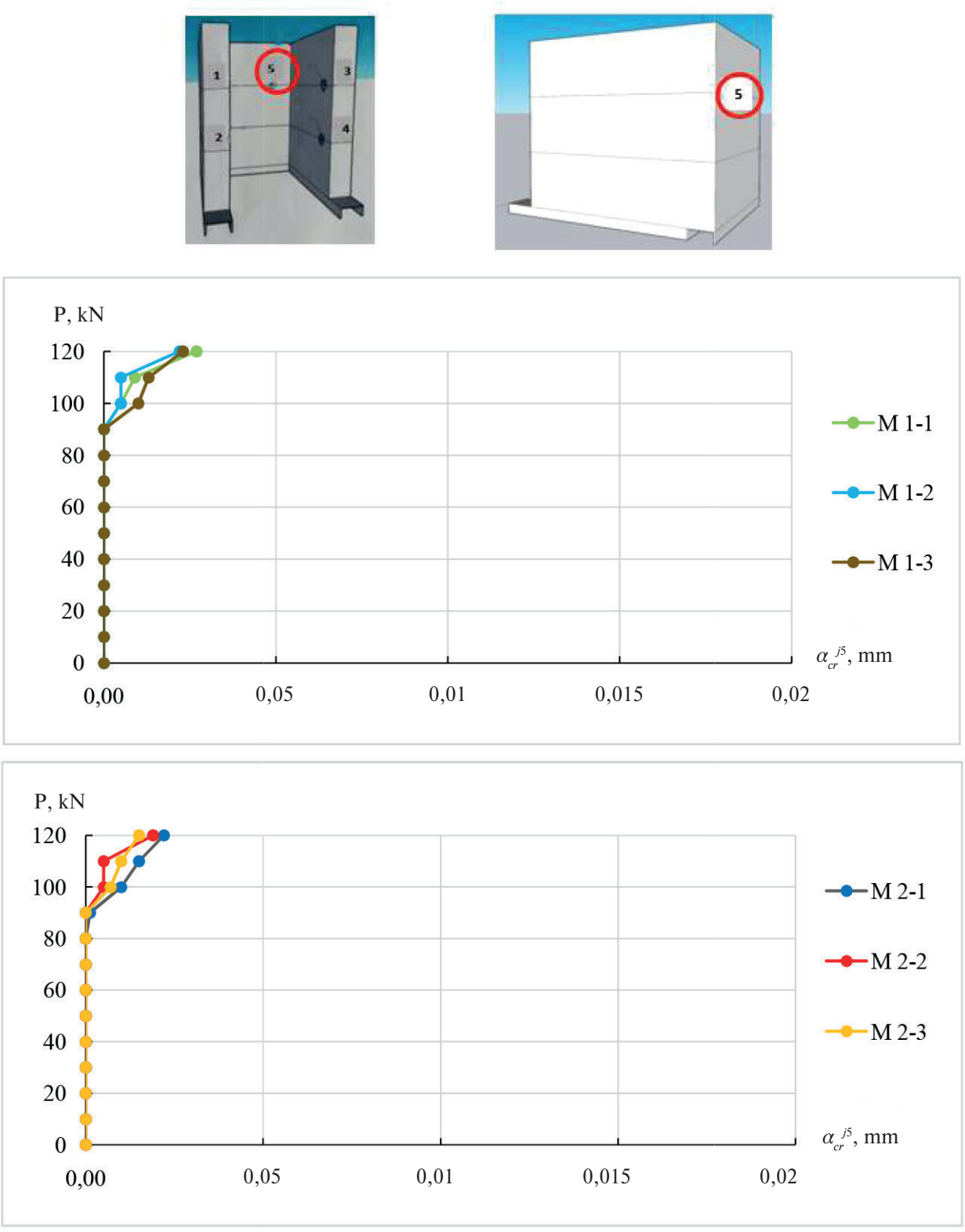


Fig. 13. Opening width of inter-block construction joint 5 in the headwall ($P = f(\alpha^{j5}_{cr})$)

ISSN 2075-8545 (online)

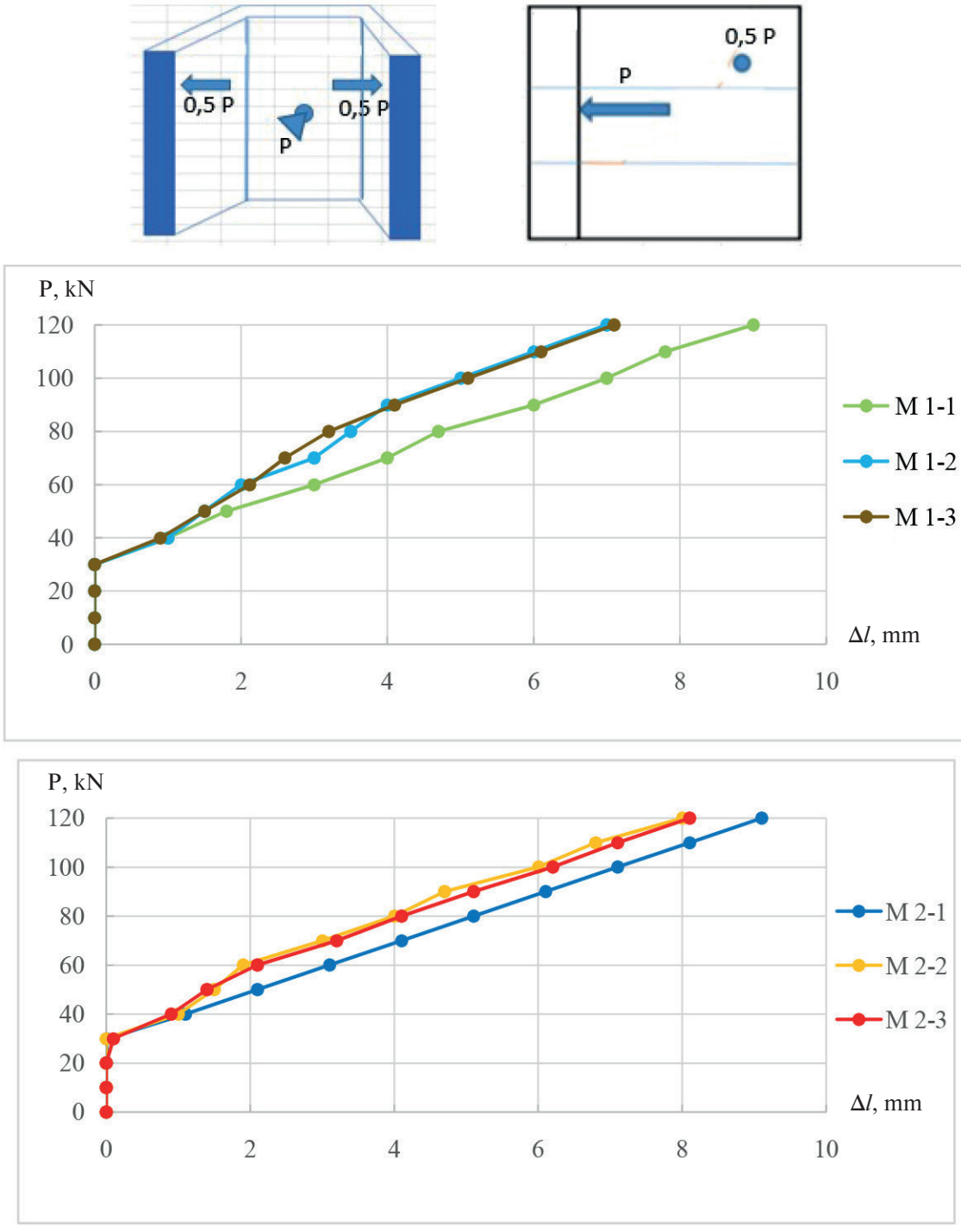


Fig. 14. Total divergence width of the piers ($P = f(\Delta l)$)

ISSN 2075-8545 (online)

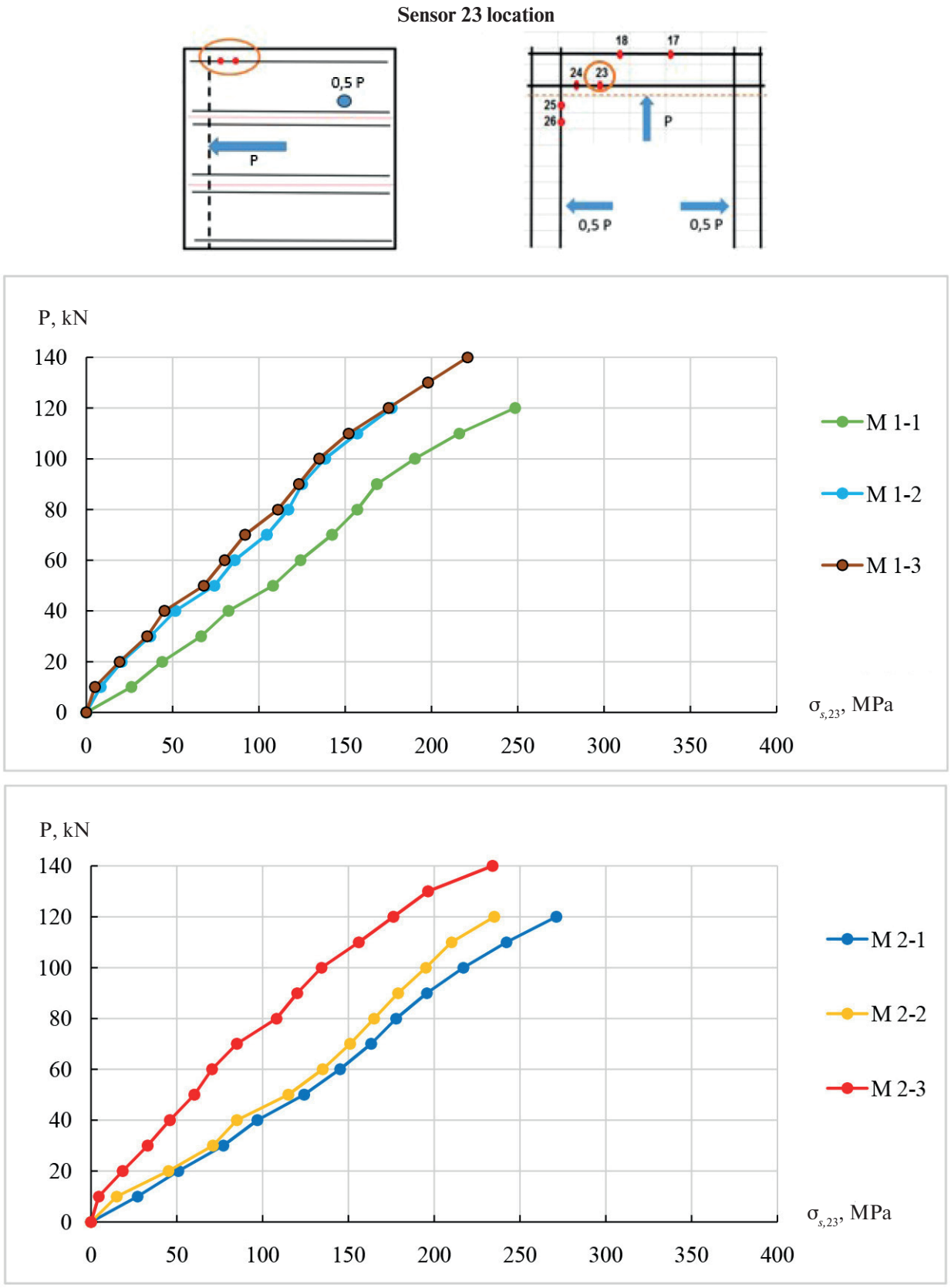


Fig. 15. Tensile stresses in the upper horizontal steel reinforcement of the headwall in the interface zone with the piers ($P = f(\sigma_{s,23})$)

ISSN 2075-8545 (online)

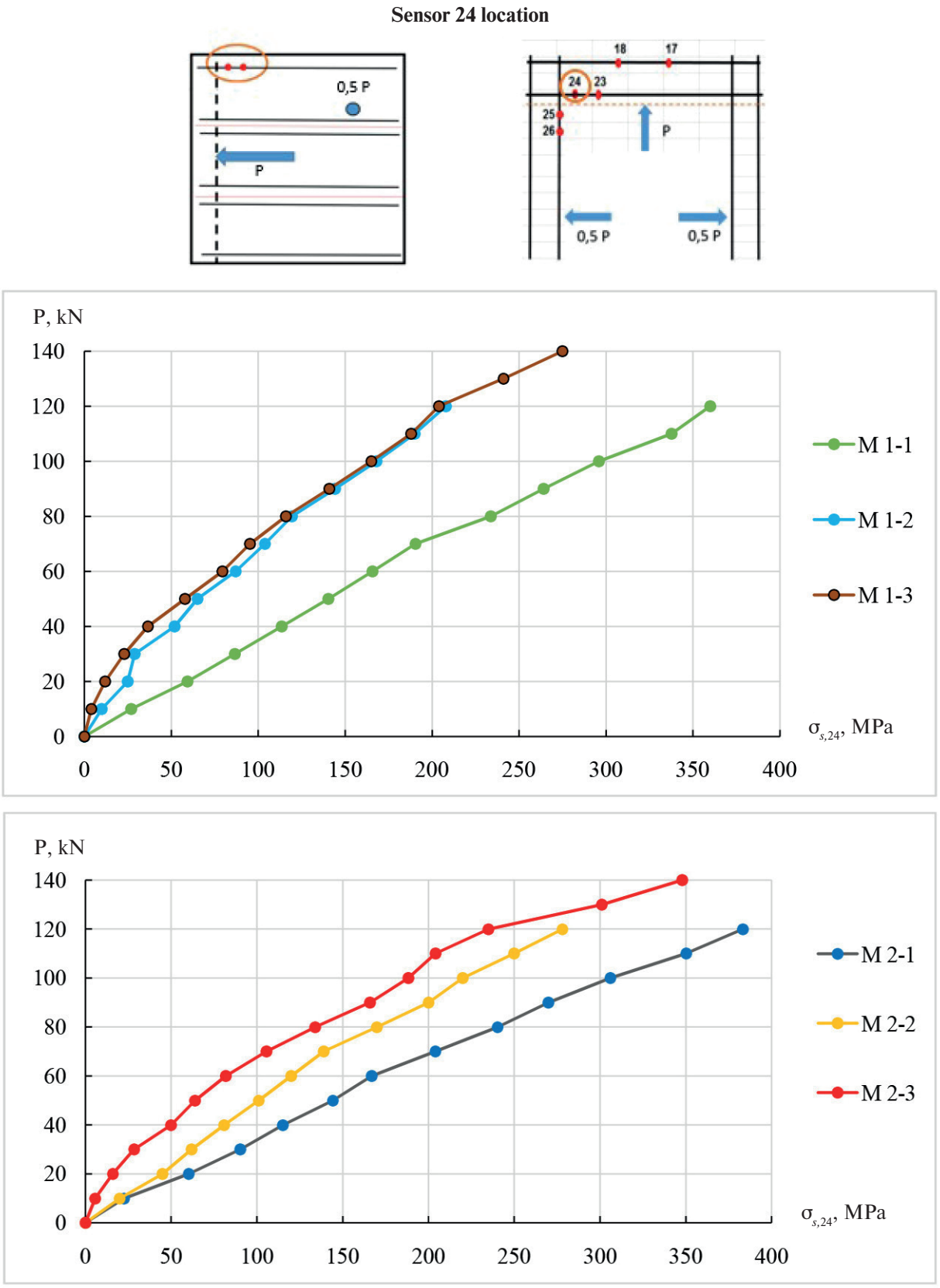


Fig. 16. Tensile stresses in the upper horizontal steel reinforcement of the headwall in the interface zone with the HPP piers ($P = f(\sigma_{s,24})$)

ISSN 2075-8545 (online)

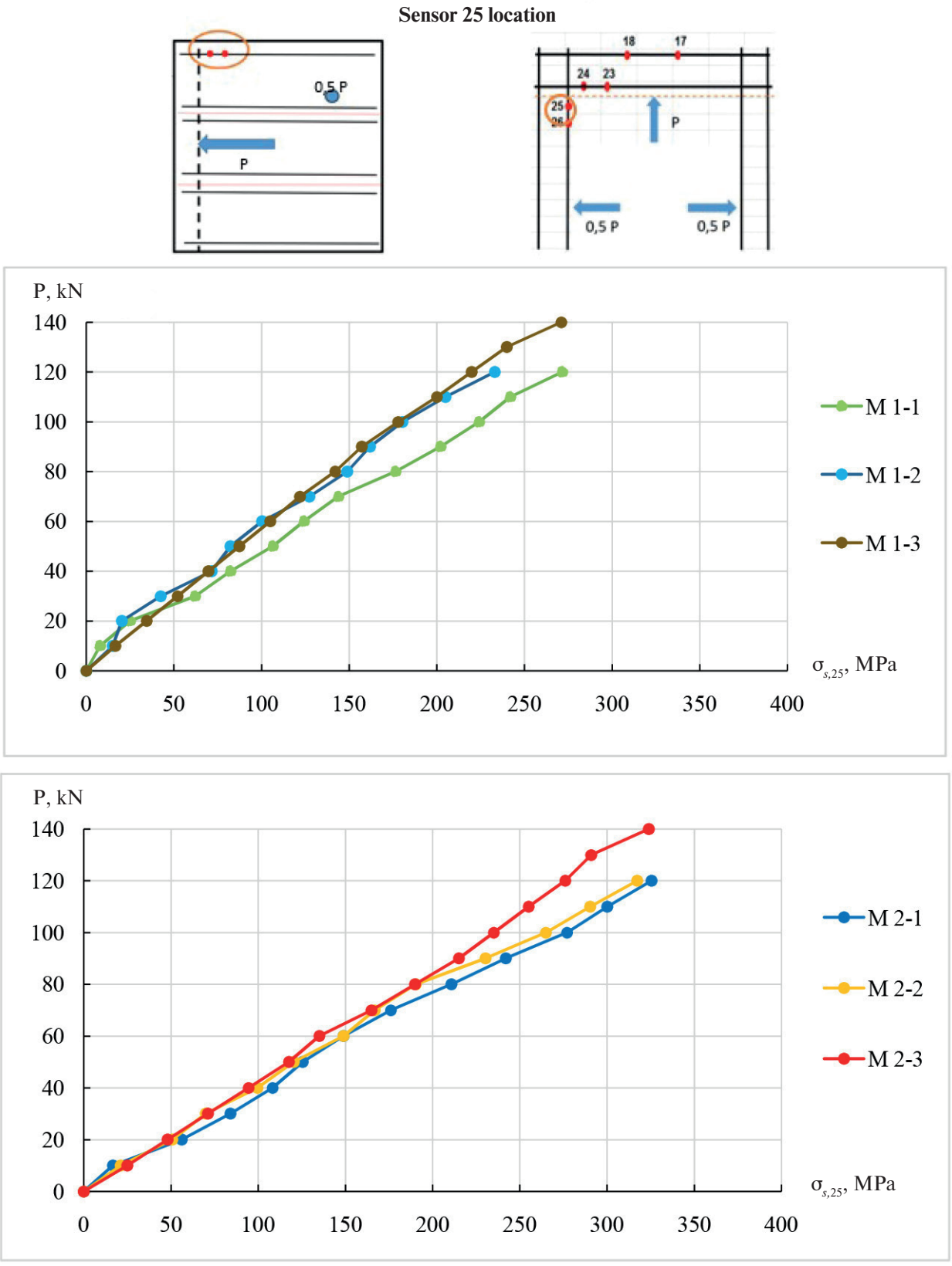


Fig. 17. Tensile stresses in the upper horizontal steel reinforcement of the piers in the interface zone with the headwall ($P = f(\sigma_{s,24})$)

ISSN 2075-8545 (online)

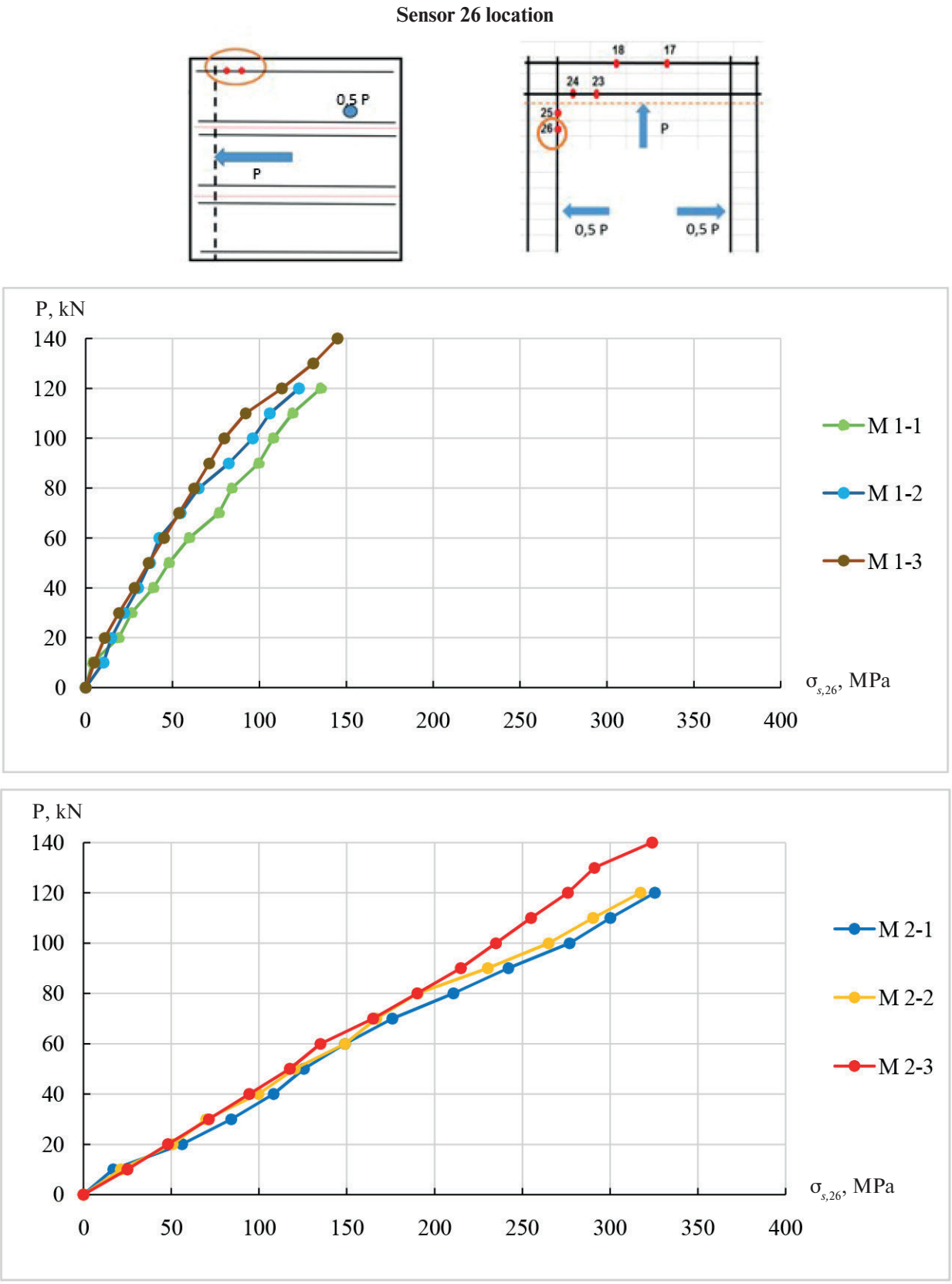


Fig. 18. Tensile stresses in the upper horizontal steel reinforcement of the piers in the interface zone with the headwall ($P = f(\sigma_{s,26})$)

ISSN 2075-8545 (online)

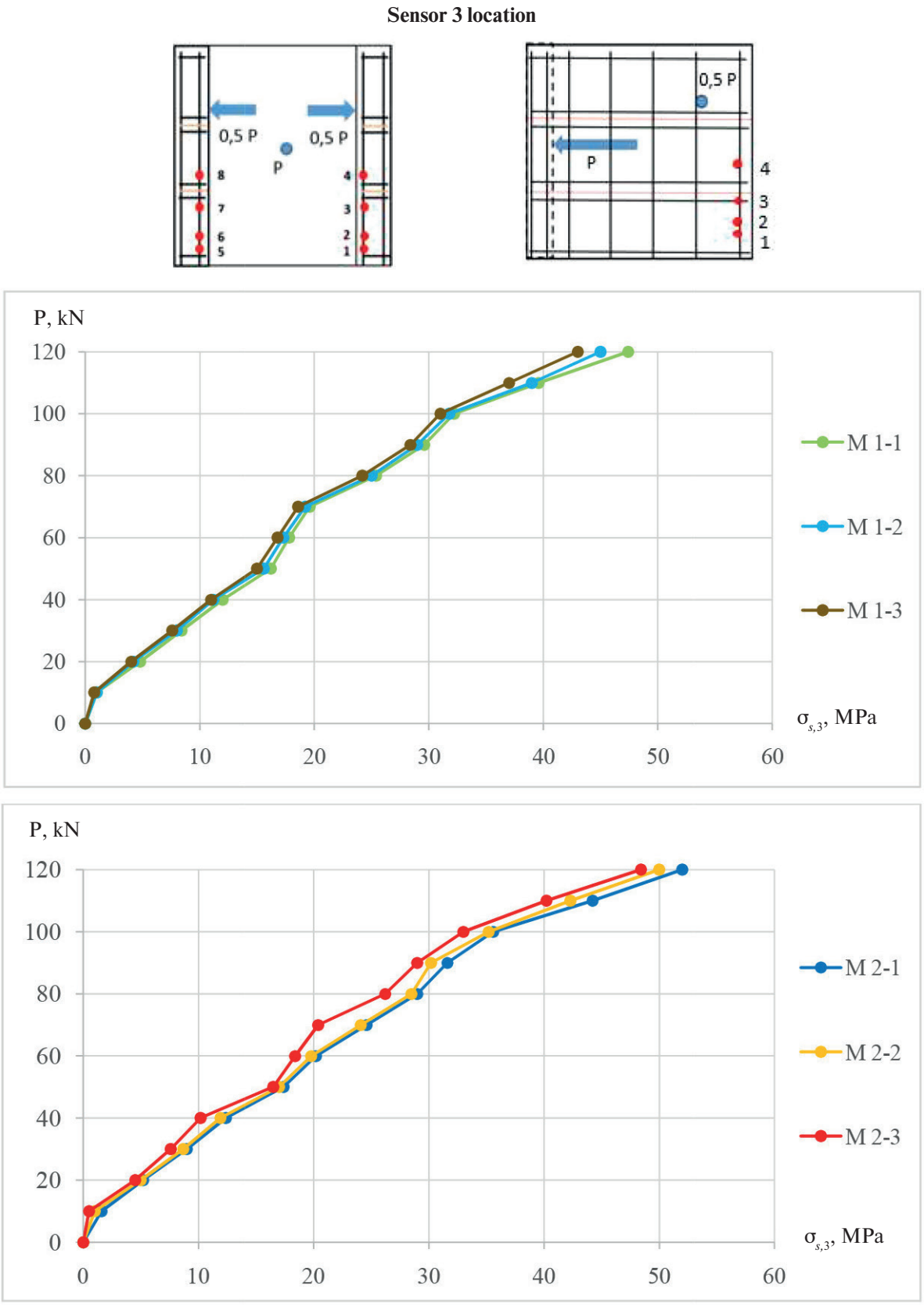


Fig. 19. Tensile stresses in the vertical steel reinforcement of the piers in the zone of the lower inter-block construction joint ($P = f(\sigma s_{s,3})$)

ISSN 2075-8545 (online)

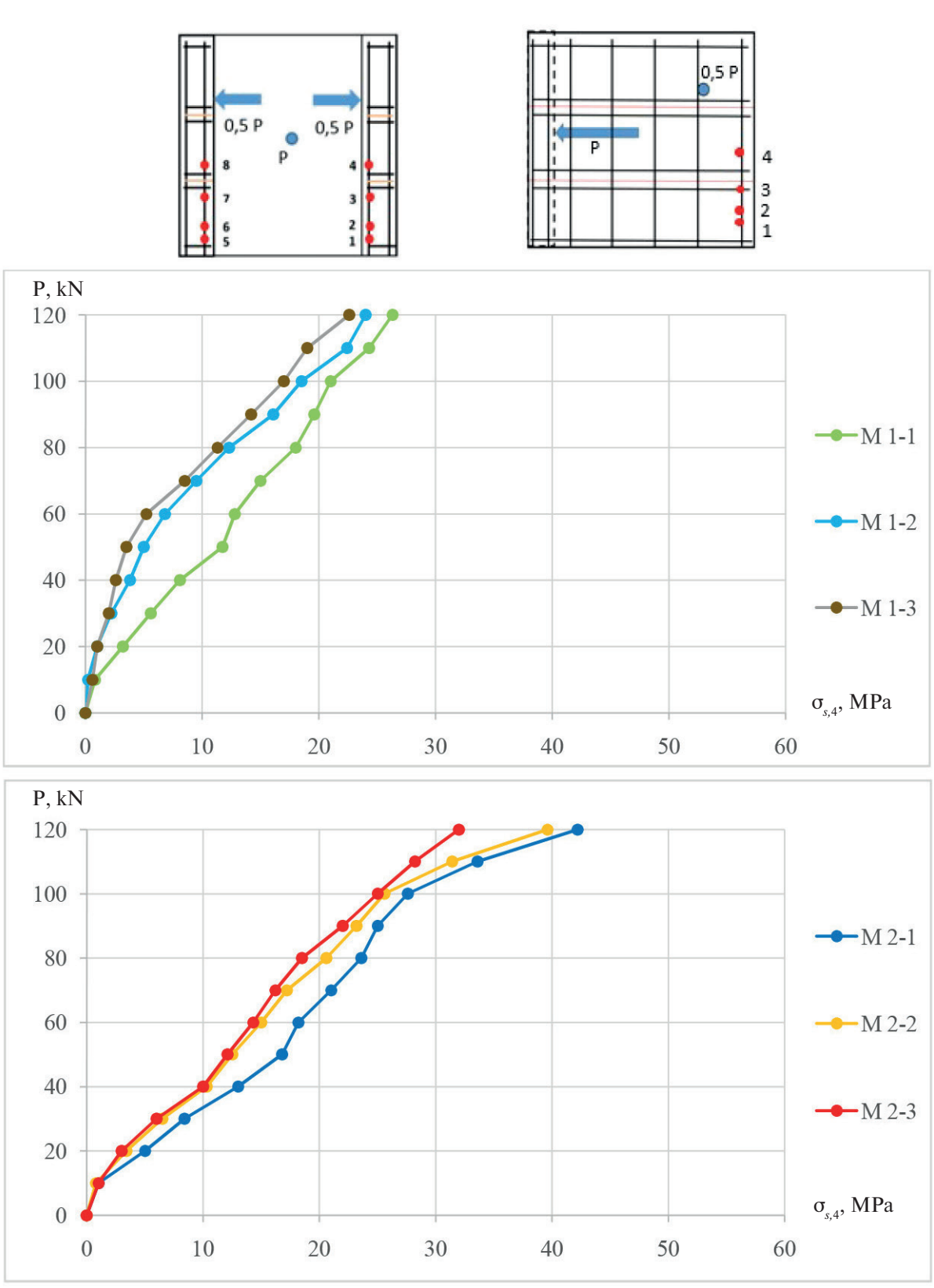


Fig. 20. Tensile stresses in the vertical steel reinforcement of the piers in the zone of the lower inter-block construction joint ($P = f(\sigma_{s,4})$)

ISSN 2075-8545 (online)

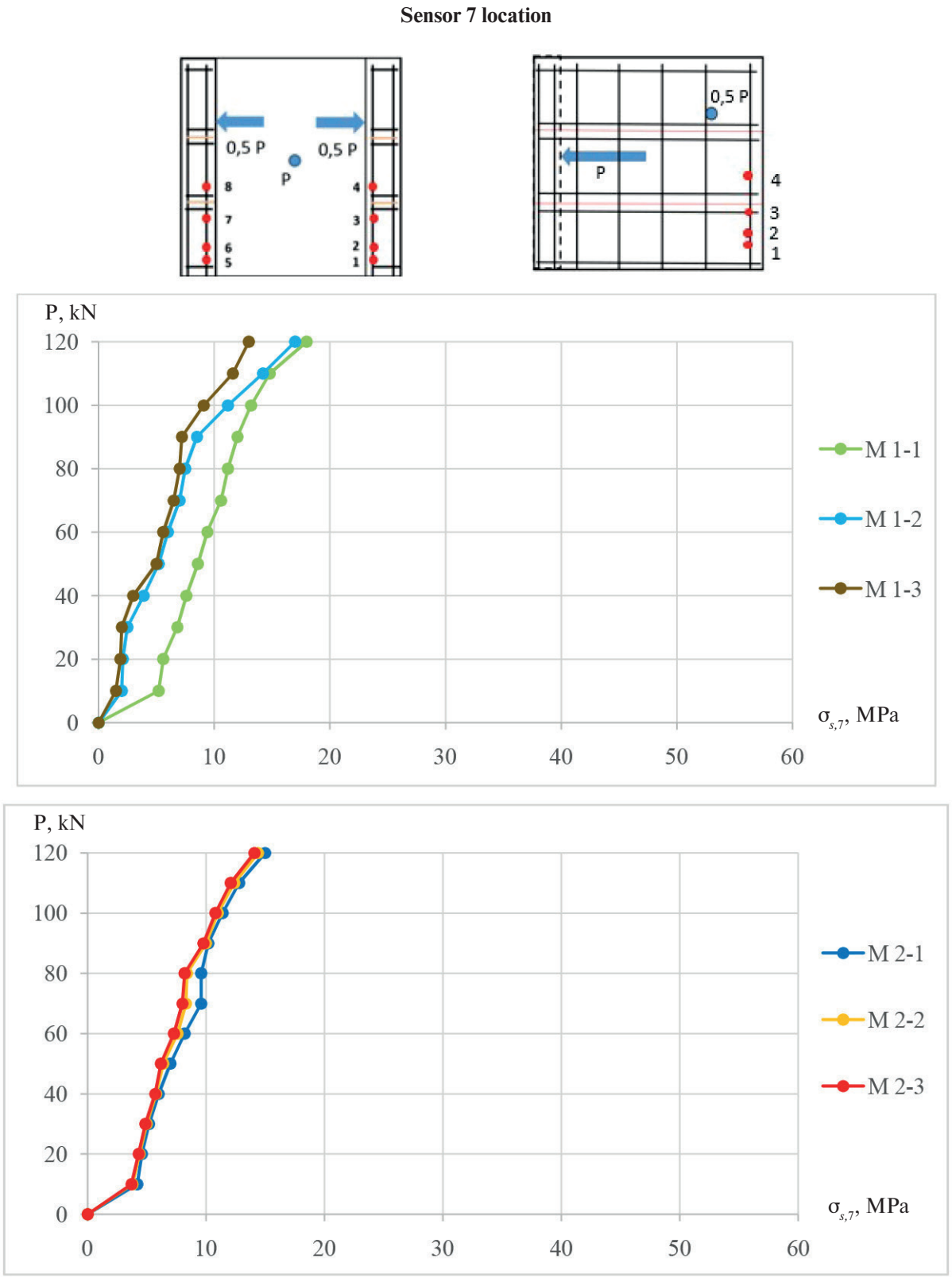


Fig. 21. Tensile stresses in the vertical steel reinforcement of the piers in the zone of the lower inter-block construction joint ($P = f(\sigma_{s,7})$)

ISSN 2075-8545 (online)

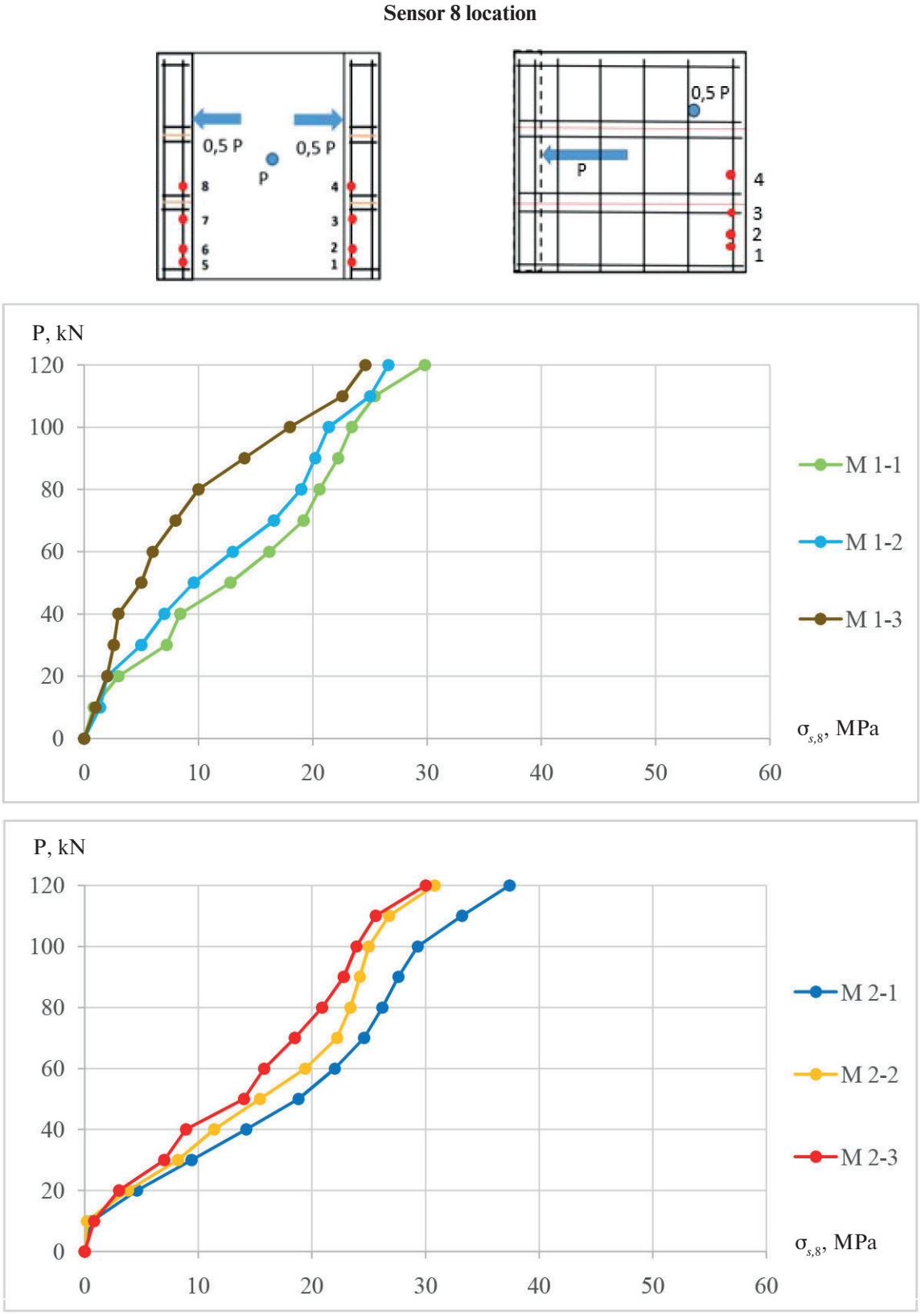
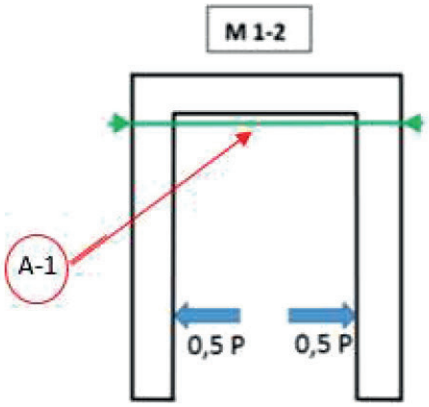


Fig. 22. Tensile stresses in the vertical steel reinforcement of the piers in the zone of the lower inter-block construction joint ($P = f(\sigma_{s,8})$)

ISSN 2075-8545 (online)



A-1 – prestressed reinforcement installed across the flow (Fig. 5, Part I)

prestress	**280**	**MPa**

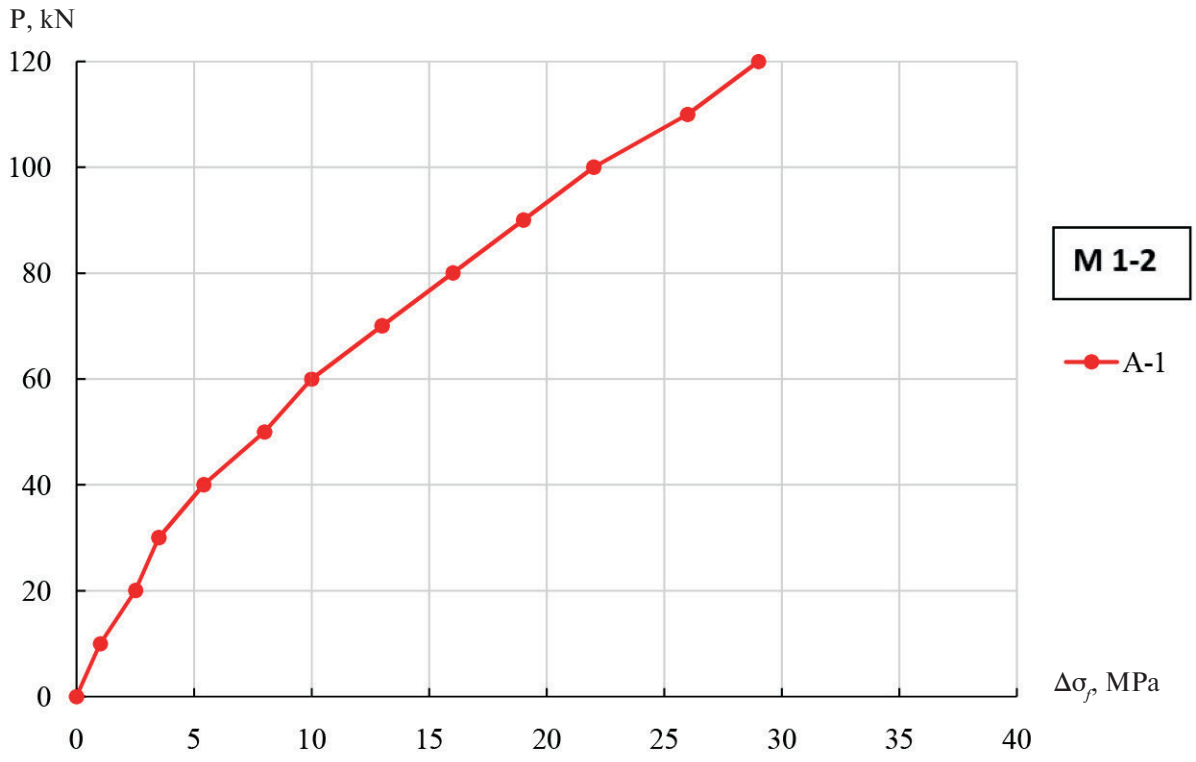
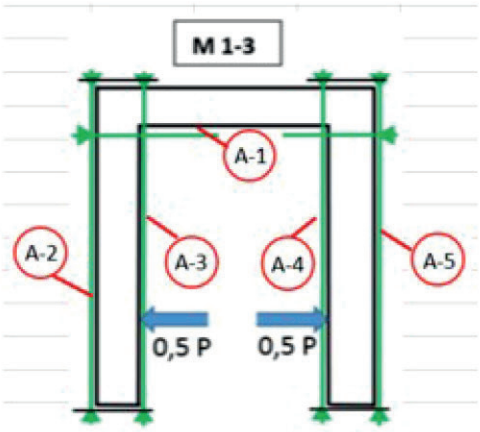


Fig. 23. Increment of tensile stresses in prestressed basalt composite strengthening reinforcement installed across the flow (M 1-2, Fig. 5, Part I; $P = f(\Delta\sigma_f)$)

ISSN 2075-8545 (online)



A-1 – prestressed reinforcement installed across the flow (Fig. 5, Part I)
A-2, A-3, A-4, A-5 – prestressed reinforcement installed along the flow (Fig. 5, Part I)

prestress	**280**	**MPa**

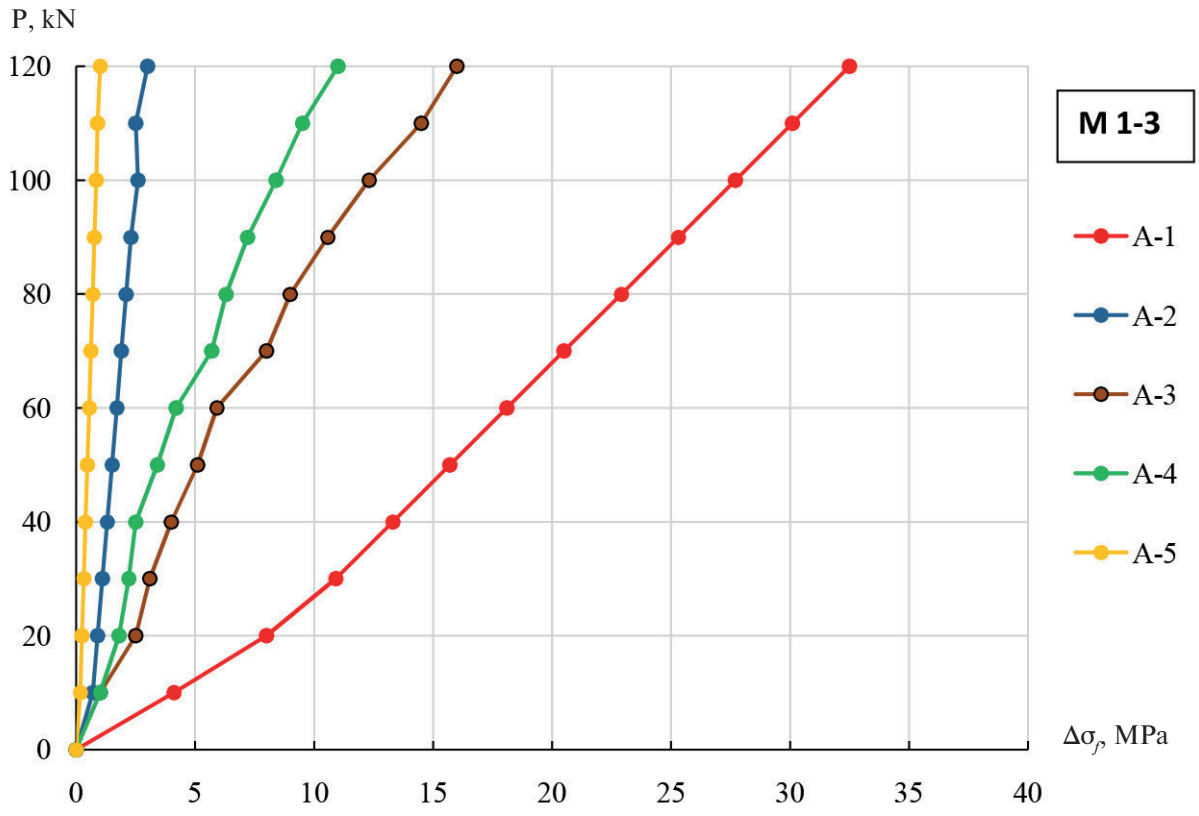
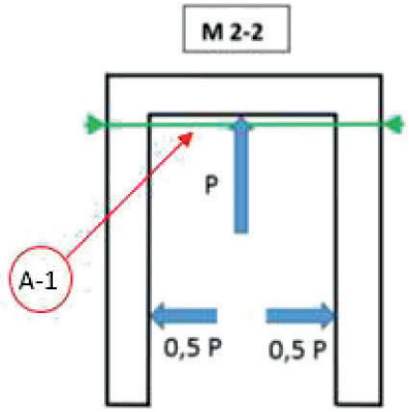


Fig. 24. Stress variation in prestressed basalt composite reinforcement oriented across and along the flow (M 1-3, Fig. 5, Part I; $P = f(\Delta\sigma_f)$)

ISSN 2075-8545 (online)



A-1 – prestressed reinforcement installed across the flow (Fig. 5, Part I)

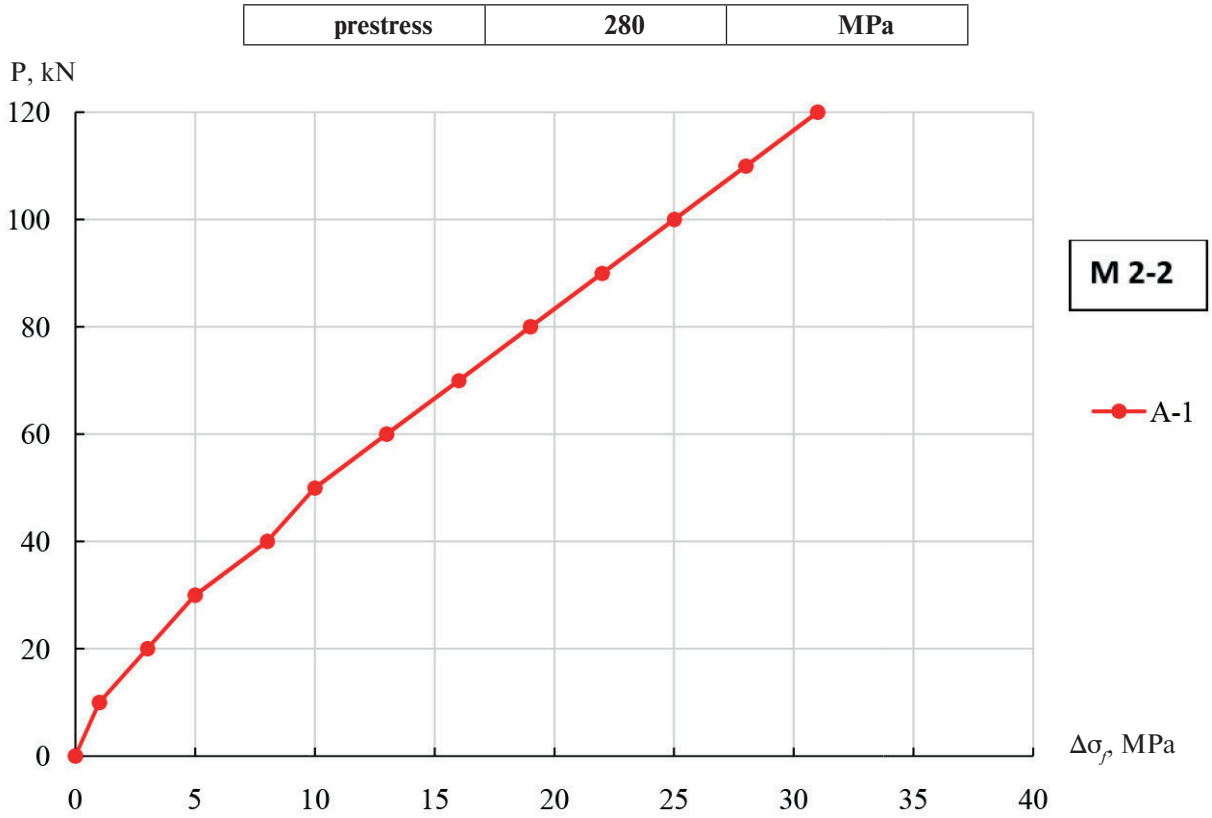


Fig. 25. Stress variation in prestressed basalt composite reinforcement oriented across the flow (M 2-2, Fig. 5 Part I; $P = f(\Delta\sigma_f)$)

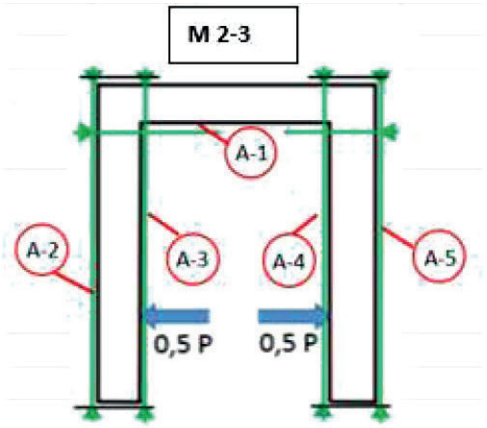
2. Experimental models of pressure front fragments of hydraulic structures ("HPP piers – headwall of the HPP powerhouse") were fabricated at a scale of M 1:25 and tested under static loads; they were subsequently strengthened with external reinforcement made of nanomaterial – prestressed basalt composite reinforcement, installed in two directions: along and across the flow.

3. In the course of experimental investigations, the crack formation pattern was established:

a) cracks at the contact interface "piers – headwall" (Fig. 1);

b) inclined multi-directional cracks transitioning to the lower inter-block construction joint (Fig. 4). It should be noted that the opening width of cracks and inter-block construction joints was recorded higher in unstrengthened reinforced concrete models than in those strengthened with prestressed basalt composite reinforcement (Fig. 2, 3, Fig. 5–13).

ISSN 2075-8545 (online)



A-1 – prestressed reinforcement installed across the flow (Fig. 5, Part I)
A-2, A-3, A-4, A-5 – prestressed reinforcement installed along the flow (Fig. 5, Part I)

prestress	**280**	**MPa**

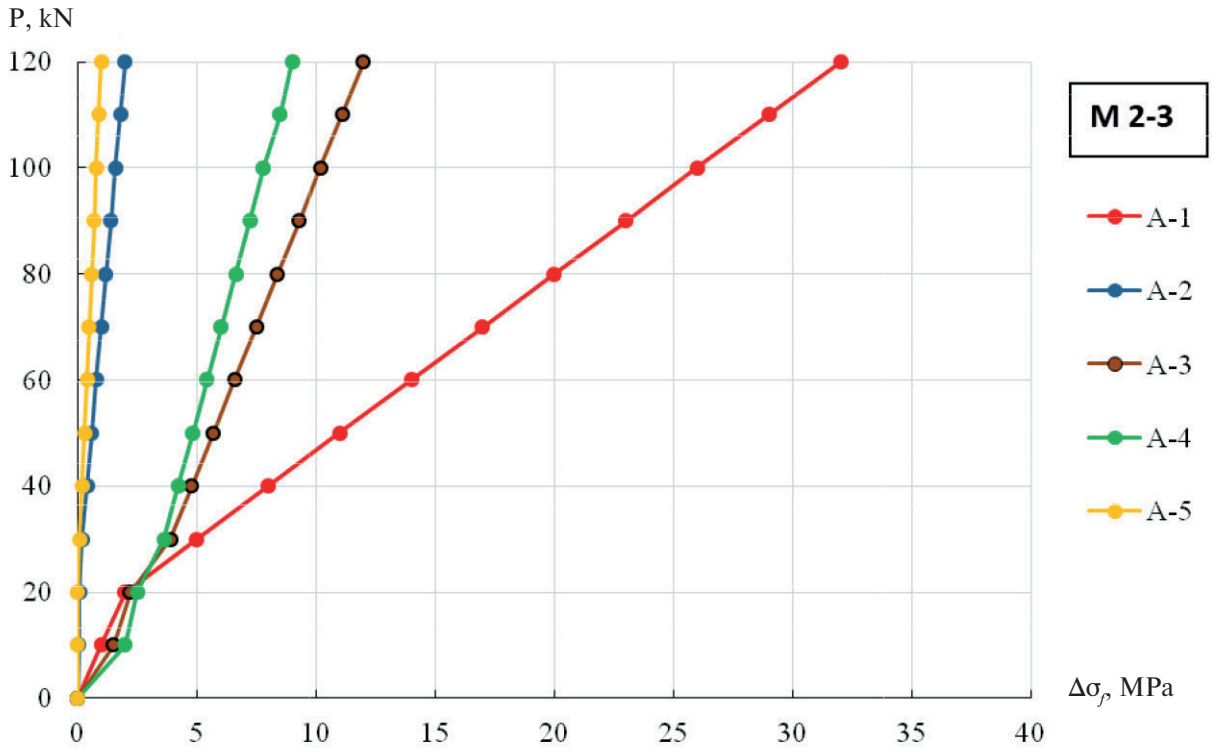


Fig. 26. Stress variation in prestressed basalt composite reinforcement oriented across and along the flow (M 2-3, Fig. 5; Part I;$P = f(\Delta\sigma_f)$)

4. In the experimental reinforced concrete models, divergence of the piers under the acting load $P = 120\ kN$ by a value of 9.2 mm (1/74 of the span) was recorded. At the same time, the total divergence width of the piers was higher in unstrengthened reinforced concrete models than in models strengthened with prestressed basalt composite reinforcement (Fig. 14).

5. In the experimental reinforced concrete models (Fig. 5, Part I) under loads P, tensile stresses were determined in the metal reinforcement in the interface zone of

ISSN 2075-8545 (online)

Nanotechnologies in construction
Нанотехнологии в строительстве

2026; 18 (5):
627–656

Nanobuild.ru

the piers and the headwall (Fig. 15–18), which practically reached the value corresponding to the tensile yield limit R_{sn}. It should be noted that strengthening with basalt composite reinforcement across and along the flow (Fig. 5, Part I) leads to a reduction of tensile stresses in the metal horizontal reinforcement across the flow in the headwall and in the piers by more than 1.5 times.

6. In the course of experimental investigations, it was established that strengthening reinforced concrete structures of complex geometric shape of the "HPP piers – headwall of the HPP powerhouse" type using nanomaterial – prestressed basalt composite reinforcement directed across and along the flow significantly affects the stress-strain state, including the level of stresses in the steel reinforcement, causing their reduction and partial transfer to the prestressed basalt composite reinforcement.

7. Under seismic actions, the structural performance of the above structures will be more complex and the parameters of this performance must be determined by calculations taking into account all factors that will allow studying and ensuring long-term safe operation of HPP hydraulic structures. To achieve this goal, it is necessary to develop a three-dimensional mathematical model of experimental reinforced concrete structures and perform its verification using the set of obtained experimental data. Further, the verified computational mathematical model can be applied to calculate the SSS of the HPP powerhouse under a combination of loads and impacts: static, hydraulic, temperature, and seismic.

REFERENCES

1. Arshenevsky N.N., Gubin M.F., Mityurev E.L., Mikhailov I.E., Orlov V.A., Popov A.I. *Hydroelectric Power Plants*. M.: Energoatomizdat. 1987;464. – EDN: SNSPBJ (in Russian).

2. Raja A.K., Srivastava A.P., Dwivedi M. *Power Plant Engineering*. New Delhi: New Age International. 2006;354. ISBN 81-224-1831-7. Available at: https://www.academia.edu/attachments/63581667/download_file (accessed: 06.07.2026).

3. Lenkov A. Yu., Fisenko V. F. Experience gained from operation of the hydraulic structures of the Votkinsk hydroelectric power plant. *Power Technology and Engineering*. 2017;51(1):33-39. https://doi.org/10.1007/s10749-017-0779-y. – EDN: XNDQPU.

4. Vasilevskaya L. S., Anufrenkova, P. S., Gracheva D. A. Evaluation of Concrete Structure Condition of the Volzhskaya Hydroelectric Power Plant. *Power Technology and Engineering*. 2018; 52(2):181-184. https://doi.org/10.1007/s10749-018-0929-x. – EDN: YBPZOH.

5. Rodrigues R. V. Structural Design of a Surface Hydropower Plant. *Technical University of Lisbon*. 2014; 1-9, Available at: https://fenix.tecnico.ulisboa.pt/downloadFile/563345090413168/resumo.pdf (accessed: 06.07.2026).

6. Rubin O.D., Lisichkin, S.E., Baklykov I.V., Almasri A. Objectives of the Computational Studies of the Long-term Operational Run-of-River Buildings of Tishrin and Baath HPPs Located in Seismic Areas of Syria. *VI International Scientific Conference Construction Mechanics, Hydraulics & Water Resources Engineering (CONMECHYDRO 2024)*. Karshi, Uzbekistan. https://doi.org/10.1063/5.0279432

7. SNiP A-II. 12-62 *Construction in seismic areas. Design norms*. Moscow. 1963; 54 (in Russian).

8. SNiP 11-7-81* *Construction in seismic areas. Design norms*. Moscow. 2006; 44 (in Russian).

9. SP 14.13330.2018 *Construction in seismic areas. Updated edition of SNiP 11-7-81**. Moscow. 2018; 115 (in Russian).

10. Zaki M., Tobaa A., Shehata A. Potential advantages of basalt FRP bars compared to carbon FRP bars & conventional steel. *Australian Journal of Civil Engineering*. 2020;19(1):1-16. https://doi.org/10.1080/14488353.2020.1816638. – EDN: NENRWF.

11. Subramanian N. Sustainability of RCC Structures using Basalt Composite Rebars. *The Master builder*. 2010; (9):156-164. https://www.academia.edu/4328510/Sustainability_of_RCC_using_Basalt_composite_Rebars_Master_Builder_Sept2010

12. Mohamed-Akram Khanfour, Ahmed El Refai. Effect of freeze-thaw cycles on concrete reinforced with basalt fiber-reinforced polymers (BFRP) bars. *Construction and Building Materials*. 2017;(145):135-146. https://doi.org/10.1016/j.conbuildmat.2017.03.237

13. Elamathi E., Priyanka R., Sangeetha V. Flexural Study on Basalt Rebar Reinforced Concrete Beams. *Journal of Engineering*. 2018;8(1):01-05. https://www.iosrjen.org/pages/volume8-issue1(part-3).html

14. Fareed Elgabbas, Ehab A. Ahmed, M.ASCE, Brahim Benmokrane. Flexural Behavior of Concrete Beams Reinforced with Ribbed Basalt-FRP Bars under Static Loads. *Journal of Composites for Construction*. 2016;21(3). https://doi.org/10.1061/(ASCE)CC.1943-5614.0000752

15. Thilan Ovitigala, Mustapha A. Ibrahim, Mohsen A. Issa. Serviceability and Ultimate Load Behavior of Concrete Beams Reinforced with Basalt Fiber-Reinforced Polymer Bars. *ACI Structural Journal*. 2016;113(4):757-768. https://doi.org/10.14359/51688752

ISSN 2075-8545 (online)

16. Pavlovic A., Donchev T. Pretensioned BFRP reinforced concrete beams: Flexural behaviour and estimation of initial prestress losses. *MATEC Web of Conferences*. 2019;289. https://doi.org/10.1051/matecconf/201928909001

17. Sokairge H., Elgabbas F., Elshafie H. Structural behavior of RC beams strengthened with prestressed near surface mounted technique using basalt FRP bars. *Engineering Structures*. 2022;250(9):113489. https://doi.org/10.1016/j.engstruct.2021.113489. – EDN: VQHDNK.

18. Thorhallsson E., Zhelyazov T., Gunnarsson A., Snaebjornsson J.T. Concrete beams reinforced with prestressed basalt bars. *Concrete – Innovation and Design, fib Symposium*. Copenhagen; 2015. https://iris.hi.is/en/publications/concrete-beams-reinforced-with-prestressed-basalt-bars/

19. Andri Gunnarsson, Eythor Rafn Thorhallson, Jonas Thor Snaebjornsson. Simulation of Experimental Research of Concrete Beams Prestressed with BFRP Tendons. *Nordic Concrete Research Symposium. Reykjavik, Iceland*; 2014. https://www.researchgate.net/publication/265467614_SIMULATION_OF_EXPERIMENTAL_RESEARCH_OF_CONCRETE_BEAMS_PRESTRESSED_WITH_BFRP_TENDONS

20. Eythor Thorhallsson, Sindri Hlifar Gudmundsson. Test of prestressed basalt FRP concrete beams with and without external stirrups. *Proceedings of Fib symposium Engineering a Concrete future: Technology, modelling & Construction. At: Tel Aviv*. Israel. 2013. https://www.researchgate.net/publication/265467715_Test_of_prestressed_basalt_FRP_concrete_beams_with_and_without_external_stirrups

21. Bellendir E.N., Rubin O.D., Lisichkin S.E., Zyuzina O.V. Experimental Study into Prestress Losses of Basalt Composite Reinforcement Used in the Composition of Concrete Elements. *Power Technology and Engineering*. 2021;54(5):605–608. https://doi.org/10.1007/s10749-020-01259-y. – EDN: VLSBAJ.

22. Pearson M., Donchev T., Salazar J. Long-Term Behaviour of Prestressed Basalt Fibre Reinforced Polymer Bars. *The 2nd International Conference on Rehabilitation and Maintenance in Civil Engineering. Procedia Engineering*. 2013;54:261 – 269. https://doi.org/10.1016/j.proeng.2013.03.024

23. Rubin O.D., Lisichkin S.E., Zyuzina O.V. Strength of low-reinforced concrete structures with the inter-block construction joints reinforced by prestressed basalt-composite bars. *Prirodoobustrojstvo*. 2021;5(1):53–62. https://doi.org/10.26897/1997-6011-2021-1-53-62. – EDN: ZHAYMH (in Russian).

24. SP 295.1325800.2017. *Concrete structures reinforced with polymer composite reinforcement. Design rules*. M: Standardinform. 2017; 55. (in Russian).

ADDITIONAL INFORMATION

The authors state that generative artificial intelligence technologies and technologies based on artificial intelligence were not used in the preparation of the article.

INFORMATION ABOUT THE AUTHORS

Oleg D. Rubin – Dr. Sci. (Eng.), Professor, Department of Hydraulics and Hydraulic Engineering, National Research Moscow State University of Civil Engineering, 129337, Moscow, Yaroslavskoye shosse, 26, Russian Federation, rubinod@niies.ru, https://orcid.org/0000-0002-0630-3251

Anton S. Antonov – Cand. Sci. (Eng.), Associate Professor, Department of Hydraulics and Hydraulic Engineering, National Research Moscow State University of Civil Engineering, 129337, Moscow, Yaroslavskoye shosse, 26, Russian Federation, antonov.an.s@yandex.ru, https://orcid.org/0000-0002-8310-9604

Amer Almasri – Postgraduate Student, Department of Hydraulics and Hydraulic Engineering, National Research Moscow State University of Civil Engineering, 129337, Moscow, Yaroslavskoye shosse, 26, Russian Federation, ameralmasri3522@gmail.com, https://orcid.org/0009-0007-4090-4353

CONTRIBUTION OF THE AUTHORS

Oleg D. Rubin – scientific supervision, development of the concept and development of research methodology, analysis of research results, writing the text of the article, drawing up final conclusions.

Anton S. Antonov – conducting experimental work, processing and analysis of experimental data using machine learning methods, writing the text of the article, drawing up final conclusions.

Amer Almasri – literature review, collection and systematization of experimental data, writing the text of the article.

The authors declare no conflict of interest.

The article was submitted 19.05.2026; approved after reviewing 28.09.2026; accepted for publication 01.10.2026.

ISSN 2075-8545 (online)

Nanotechnologies in construction
Нанотехнологии в строительстве

2026; 18 (5):
657–672

Nanobuild.ru

SYSTEM SOLUTIONS FOR TECHNOLOGICAL PROBLEMS

CC BY 4.0

Original article
https://doi.org/10.15828/2075-8545-2026-18-5-657-672

Study of the effect of part geometry on the pressure rise law of the forming gas using computer simulation

Nikolay Yu. Stepanenko, Sergey V. Chertovskikh*, Irek V. Kandarov, Alexey V. Rubtsov
Ufa state petroleum technological university, 450064, Ufa, Kosmonavtov St., 1, Russian Federation
* Corresponding author: e-mail: chertovskikh@mail.ru

ABSTRACT

Introduction. Currently, in the industry, the method of superplastic molding (SPM) is used to manufacture complex-profile thin-walled parts, as well as elements of a hollow structure. To increase the efficiency of the SPM process, it is advisable to pre-form a nanostructured state in materials. The accuracy of the part geometry, the quality of the final product and the duration of the production process are significantly affected by the supply of forming gas using a gas distribution system (GDS). One of the key aspects of GDS operation is the identification of optimal gas supply modes for parts with different geometries. Computer modeling of the SPM process allows you to analyze molding modes without the need for expensive and lengthy real experiments. The study is aimed at identifying the relationship between the pressure increase of the forming gas and the geometry of the part. **Methods and materials.** Modeling and finite element analysis (FE analysis) of SPM parts of the "dome" type made of titanium alloy VT-6 with different thickness of workpieces and geometry was carried out using the MSC Marc software package. The results and discussion are given. The results of the FE analysis of the SPM process are given. In the course of research, it was found that when the thickness of the billet changes, the graphs of the forming gas supply do not change their behavior, but their scale changes. That is, while maintaining the running time of the main forming steps, the pressure of the forming gas is significantly increased, resulting in an increase in the supply rate of the forming gas. Three steps can be distinguished in the molding gas supply plots, and the gas pressure rise between the steps is non-linear. Depending on the shape of the part, these steps may vary. **Conclusion.** The obtained gas supply dependencies make it possible to form experience in working with the technological process of molding various parts, as well as to identify requirements for the development of promising gas distribution systems.

KEYWORDS: nanostructured materials, part, geometry, thickness, superplas-tic molding, molding gas pressure and feed rate, finite element analysis

SOURCES OF FUNDING FOR THE SCIENTIFIC WORK THAT RE-SULTED IN THE PUBLICATION: The study was carried out within the frame-work of the program of the Ministry of Science and Higher Education of the Russian Federation "PRIORITET 2030."

ACKNOWLEDGEMENTS: The authors are grateful for the financial support of the project.

FOR CITATION:
Stepanenko N.Yu., Chertovskikh S.V., Kandarov I.V., Rubtsov A.V. Study of the effect of part geometry on the pressure rise law of the forming gas using computer simulation. *Nanotechnologies in Construction.* 2026;18(5):657–672. https://doi.org/10.15828/2075-8545-2026-18-5-657-672. – EDN: EOTVES.

© Stepanenko N.Yu., Chertovskikh S.V., Kandarov I.V., Rubtsov A.V., 2026

ISSN 2075-8545 (online)

Nanotechnologies in construction
Нанотехнологии в строительстве

2026; 18 (5):
657–672

Nanobuild.ru

SYSTEM SOLUTIONS FOR TECHNOLOGICAL PROBLEMS

Исследование влияния геометрии детали на закон повышения давления формующего газа с применением компьютерного моделирования

Николай Юрьевич Степаненко, Сергей Владимирович Чертовских*, Ирек Вилевич Кандаров, Алексей Вячеславович Рубцов

Уфимский государственный нефтяной технический университет, 450064, Уфа, ул. Космонавтов, 1, Российская Федерация

* Автор, ответственный за переписку: e-mail: chertovskikh@mail.ru

АННОТАЦИЯ

Введение. В настоящее время в промышленности для изготовления сложнопрофильных тонкостенных деталей, а также элементов полой конструкции используется метод сверхпластической формовки (СПФ). Для повышения эффективности процесса СПФ целесообразным является предварительное формирование в материалах наноструктурного состояния. Значительное влияние на точность геометрии детали, качество конечного изделия и продолжительность производственного процесса оказывает подача формующего газа, реализуемая с использованием газораспределительной системы (ГРС). Одним из ключевых аспектов работы ГРС является выявление оптимальных режимов подачи газа для деталей с различной геометрией. Компьютерное моделирование процесса СПФ позволяет анализировать режимы формовки без необходимости проведения дорогостоящих и длительных реальных экспериментов. Исследование направлено на выявление зависимости между повышением давления формующего газа и геометрией детали. **Методы и материалы.** Моделирование и конечно-элементный анализ (КЭ анализ) СПФ деталей типа «купол» из титанового сплава ВТ-6 с различной толщиной заготовок и геометрией проводилось с помощью программного комплекса MSC Marc. **Результаты и обсуждение.** Приводятся результаты КЭ анализа процесса СПФ. В ходе проведения исследований установлено, что при изменении толщины заготовки графики подачи формующего газа не изменяют своего характера поведения, но при этом изменяется их масштаб. То есть при сохранении времени протекания основных этапов формовки значительно увеличивается давление формовочного газа, что приводит к повышению скорости подачи формовочного газа. На графиках подачи формовочного газа можно выделить три этапа, и рост давления газа между этапами происходит нелинейно. В зависимости от формы детали данные этапы могут отличаться. **Заключение.** Полученные зависимости подачи газа позволяют сформировать опыт работы с технологическим процессом формовки различных деталей, а также выявить требования для разработки перспективных систем газораспределения.

КЛЮЧЕВЫЕ СЛОВА: наноструктурные материалы, деталь, геометрия, толщина, сверхпластическая формовка, давление и скорость подачи формовочного газа, конечно-элементный анализ

ИСТОЧНИКИ ФИНАНСИРОВАНИЯ НАУЧНОЙ РАБОТЫ, РЕЗУЛЬТАТОМ КОТОРОЙ СТАЛА ПУБЛИКАЦИЯ: Исследование выполнено в рамках программы Министерства науки и высшего образования Российской Федерации «ПРИОРИТЕТ 2030».

БЛАГОДАРНОСТИ: Авторы выражают благодарность за финансовую поддержку проекта.

ДЛЯ ЦИТИРОВАНИЯ:

Степаненко Н.Ю., Чертовских С.В., Кандаров И.В., Рубцов А.В. Исследование влияния геометрии детали на закон повышения давления формующего газа с применением компьютерного моделирования. *Нанотехнологии в строительстве.* 2026;18(5):657–672. https://doi.org/10.15828/2075-8545-2026-18-5-657-672. – EDN: EOTVES.

INTRODUCTION

In modern high-tech industries, such as aircraft and mechanical engineering, complex-profile thin-walled parts, as well as elements of a hollow structure, are widespread. These parts can significantly reduce the mass of products, and complex geometry is often used to improve the performance of parts, which makes products competitive. For example, aircraft engine blades with complex geometry and hollow structure provide high thrust characteristics of gas turbine engines [1].

Traditional methods of manufacturing such parts are labor intensive and time consuming. In some cases, the use of such production methods is generally impossible. Therefore, the introduction of innovative technologies, such as the SPF method, becomes an urgent task [1–6]. This method makes it possible to manufacture parts of complex geometry and hollow structure with high efficiency, which is especially important for advanced industries.

The structure of the material is extremely important for the manifestation of superplasticity of parts. Thus, the formation of a nanostructured state of the material makes

ISSN 2075-8545 (online)

it possible to more efficiently mold more geometrically complex parts, which makes the SPF process more energy efficient.

One of the key aspects of SPF technology is the injection of blowing gas, which has a significant impact on the accuracy of the part geometry, the quality of the final product and the duration of the production process. Gas distribution stations [7–9] are used to supply gas to the process complexes of the SPF.

To create and justify the requirements for GDS, it is necessary to conduct a comparative analysis of gas supply modes for parts of different geometries. Computer modeling of the SPF process allows analyzing molding modes without the need for expensive and lengthy real experiments [10–18]. This analysis allows you to determine the optimal parameters for the production of parts of various geometries, ensuring high quality and accuracy of products. This significantly reduces time and financial costs, and also accelerates the introduction of SPF technology into production processes.

In addition, the analysis of gas supply modes in various parts helps to optimize the production of parts by the SPF method, which in turn affects the increase in the productivity of production lines, reducing the cost of materials and energy resources.

Thus, comparative analysis of forming gas supply modes is an important step in the development and optimization of the SPF technology.

The purpose of this work is to simulate (with FE analysis) the process of SPF of parts of the "dome" type with different thickness of blanks and geometry using the MSCMarc software package [19].

METHODS AND MATERIALS.

During the FE analysis, two types of part geometry were analyzed. For each type of geometry, three workpiece thicknesses are considered: 1, 2, and 3 mm. The considered material of the parts is titanium alloy VT-6 [20, 21].

The dome part is selected for investigation due to the fact that its optimal geometry allows to demonstrate the basic SPF processes. Geometry of this part is taken as a basis for scientific research and experiments in the direction of superplasty. Finite element computations were performed in the MSC Marc software package [19, 22–26].

Cross-sections of molds 1 and 2 into which the initial billet was formed are shown in Figure 1. The workpiece is a circle with a diameter of 200 mm of various thicknesses (1, 2 and 3 mm).

The finite element model of the workpiece surface is shown in Figure 2 and contains 14400 elements.

Fastening the workpiece simulates its clamping at the edges in a die fixture that fixes along all axes of freedom. Maximum forming gas pressure limit is 10 MPa.

The workpiece surface and shapes are shown in Figure 3.

RESULTS AND DISCUSSION

The results of the Form 1 stock calculation are shown below.

The results of the calculation of the workpiece with a thickness of 1 mm are shown in Figures 4–5. The maximum equivalent stresses in the workpiece are 38.9 MPa. Maximum pressure of forming gas is p = 0.32 MPa, time of forming process is t = 3061 s.

The results of the calculation of the workpiece with a thickness of 2 mm are shown in Figures 6–7. The maximum equivalent stresses in the workpiece are 38.7 MPa, the maximum pressure of the molding gas is 0.60 MPa, and the molding process time is 3061 s.

The results of the calculation of the workpiece with a thickness of 3 mm are shown in Figures 8–9. The maximum equivalent stresses in the billet are 38.6 MPa, the

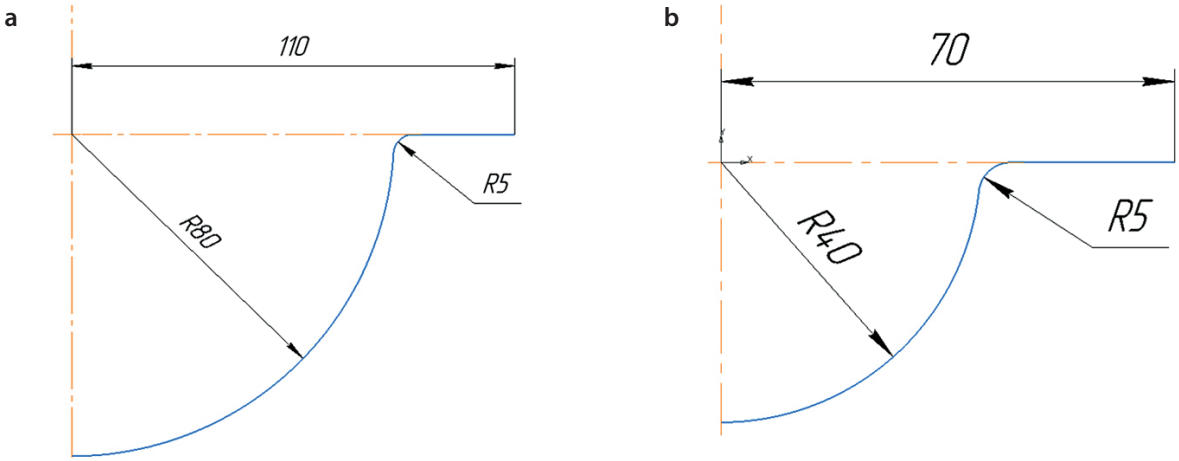


Fig. 1. Shape sections: a – form 1; b – form 2

ISSN 2075-8545 (online)

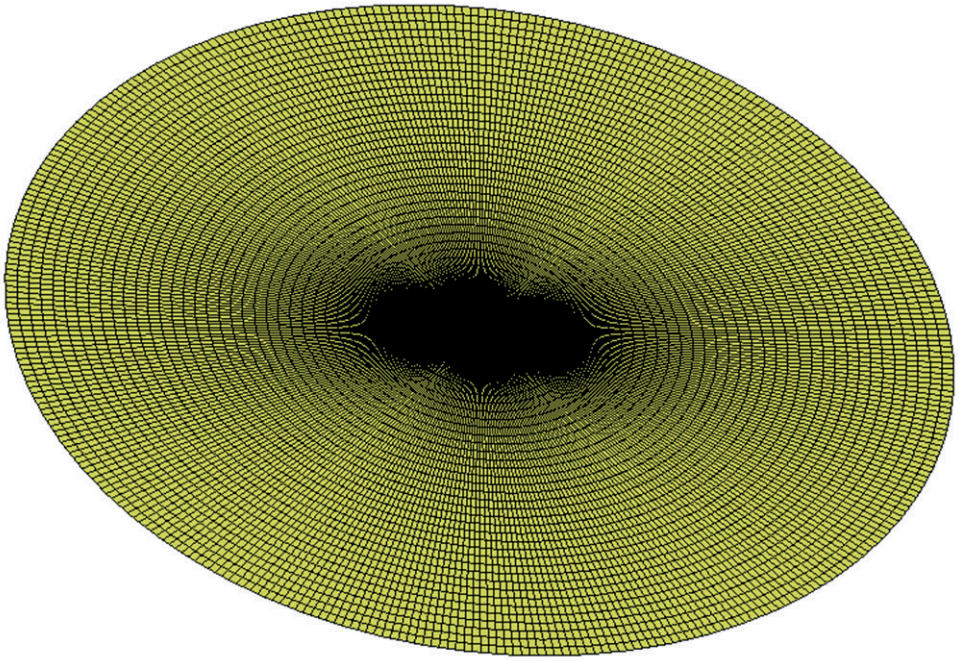


Fig. 2. FEM workpiece surface model

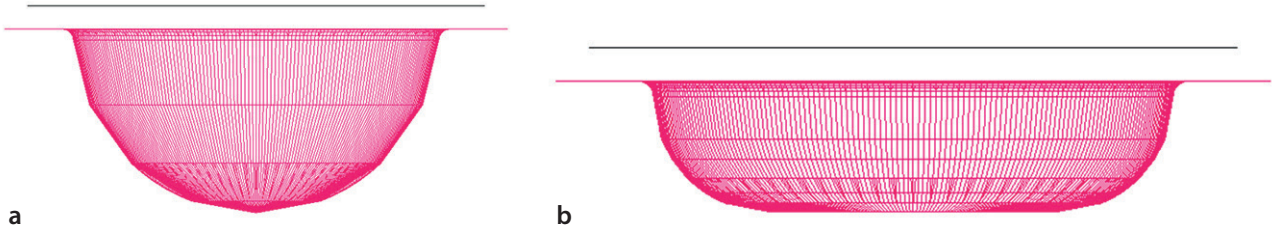


Fig. 3. Workpiece surface and shapes: a – blank with form 1; b – blank with form 2

maximum pressure of the molding gas is 0.91 MPa, and the molding process time is 3131 s.

It can be seen that as the thickness of the billet increases, the equivalent stresses in it practically do not change during the molding process. But this significantly increases the area of exposure to maximum equivalent stresses in the part. This should be taken into account when designing complex-profile products with "thin" places in geometry.

Equivalent plastic deformations with an increase in the thickness of the workpiece are also practically unchanged.

The law of gas supply does not change its behavior when the thickness of the part increases. However, it should be noted that with an increase in thickness by 1 mm, the process time remains practically unchanged (an increase of not more than 3%), and the maximum pressure of the forming gas increases significantly (when switching from 1 mm to 2 mm, an increase of 100%, when switching from 2 mm to 3 mm, an increase of 50%). If the behavior of the gas supply law is unchanged, this means that the gas supply speed in the main sections of the graph also increases significantly.

Divide the graph shown in Figure 8 into 3 main area (Fig. 10):

– area 1 – "opening" of the workpiece – at this stage the gas pressure overcomes the forces of resistance of the material to the flow;
– area 2 – the main stage of molding – plastic deformation of the workpiece occurs with increasing pressure;
– area 3 – "holding" – residual flow of material with slight pressure release.

We estimate the rate of gas supply (discharge) for each of the sections. Table 1 shows the gas feed rates for each section on different thickness blanks.

Analyzing the obtained results, it can be seen that the pressure increase (decrease) occurs non-linearly, both

ISSN 2075-8545 (online)

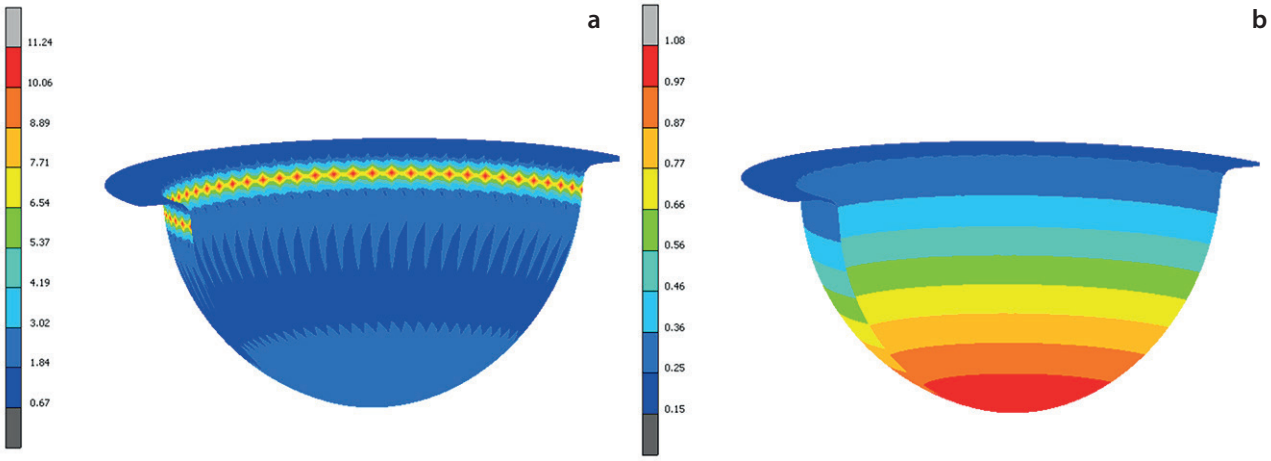


Fig. 4. Distribution of equivalent stresses in the workpiece with thickness 1 mm equivalent plastic deformations: a – equivalent stresses in the part at the end of the molding process; b – equivalent plastic deformations of the part

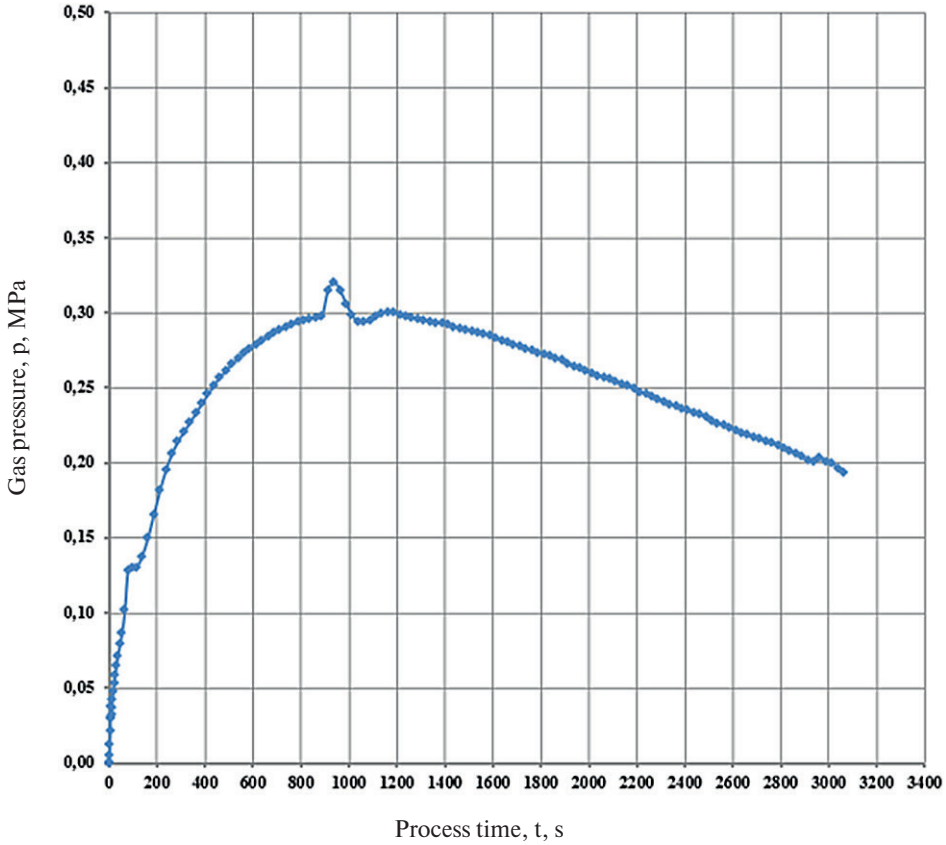


Fig. 5. Diagram of forming gas supply to the billet with thickness of 1 mm

ISSN 2075-8545 (online)

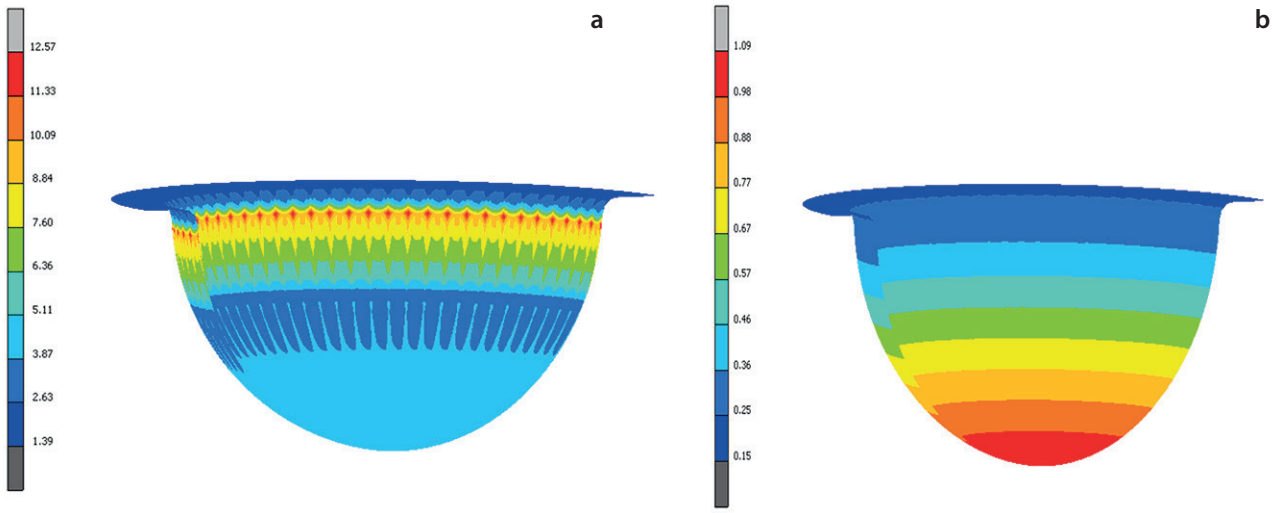


Fig. 6. Distribution of equivalent stresses in the workpiece with thickness 2 mm and equivalent plastic deformations: a – equivalent stresses in the part at the end of the molding process; b – equivalent plastic deformations of the part

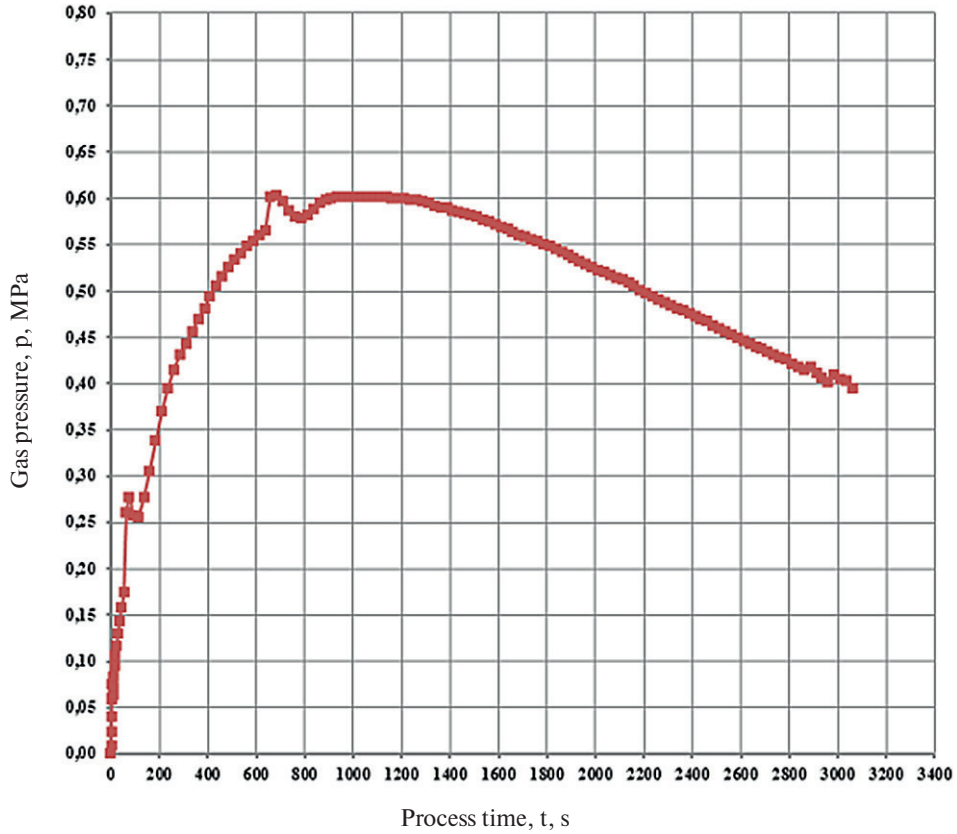


Fig. 7. Diagram of forming gas supply to the billet 2 mm thick, MPa/s

ISSN 2075-8545 (online)

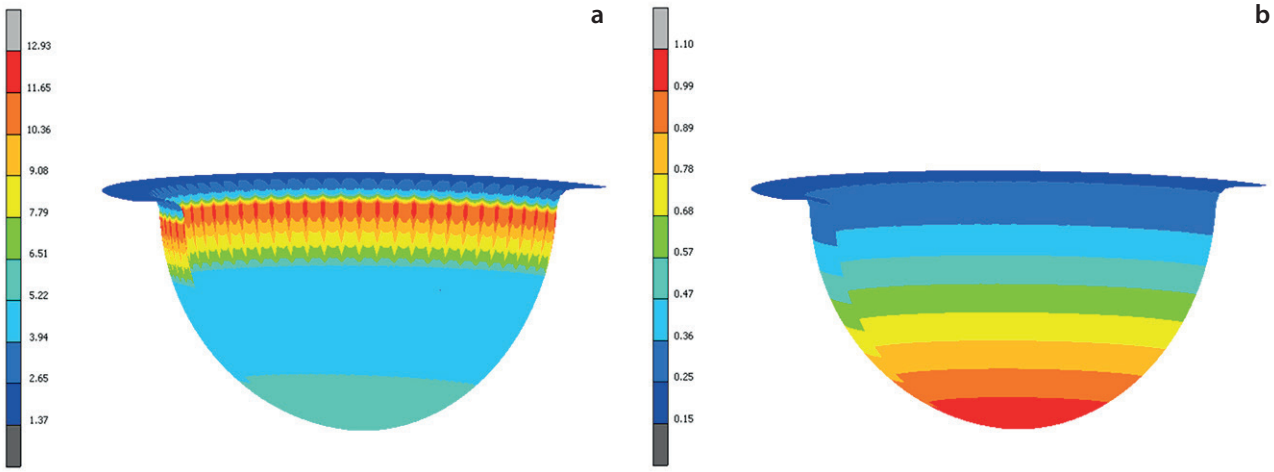


Fig. 8. Distribution of equivalent stresses in the workpiece with thickness 3 mm and equivalent plastic deformations: a – equivalent stresses in the part at the end of the molding process; b – equivalent plastic deformations of the part

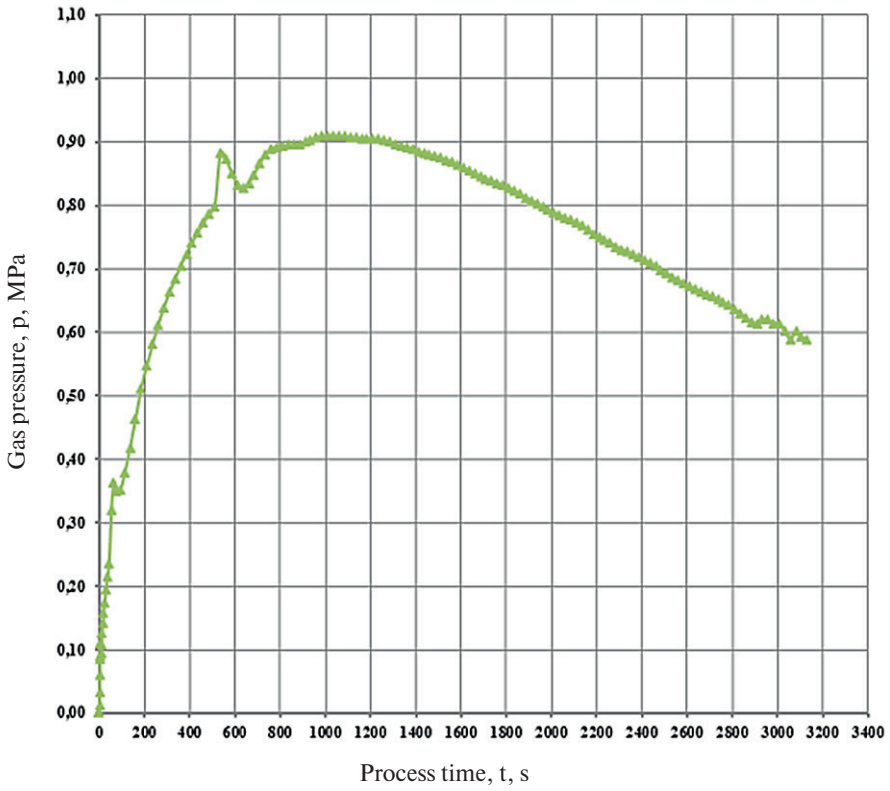


Fig. 9. Graph of forming gas supply to 3 mm thick preform

ISSN 2075-8545 (online)

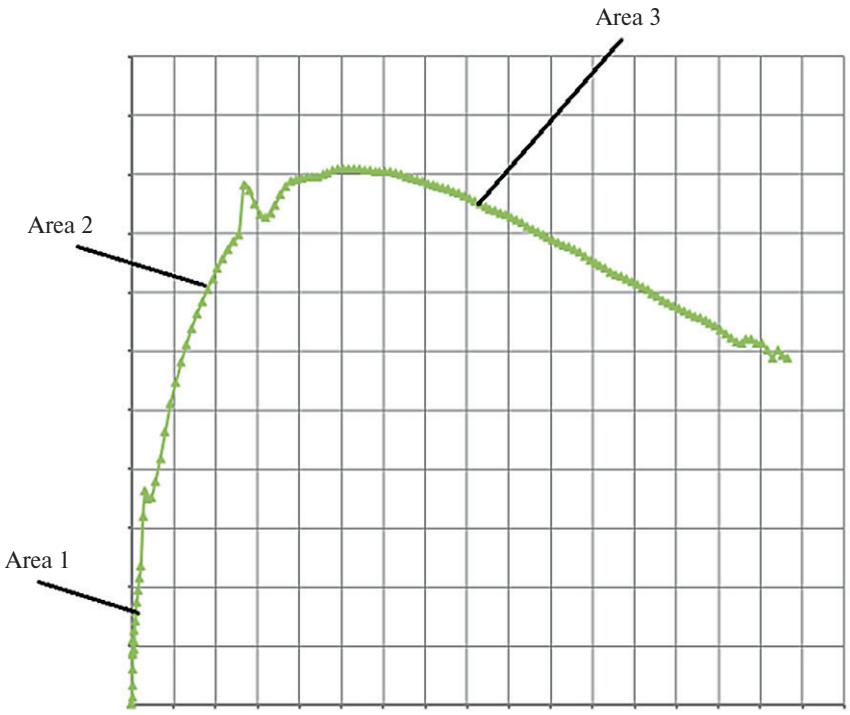


Fig. 10. Main sections of the gas supply schedule: area 1 – "opening" of the workpiece; area 2 – main forming step; area 3 – "exposure"

Table 1. Gas feed rates to Form 1 blanks of different thicknesses

Workpiece thickness, mm	Gas feed rate, MPa/s		
	Area 1	Area 2	Area 3
1	0.001700	0.000180	0.000051
2	0.002200	0.000410	0.000100
3	0.005700	0.000590	0.000150

between stages in a workpiece of the same thickness, and between the same stages in workpieces of different thickness.

The following are the results of the Form 2 billet calculation.

The results of the calculation of the workpiece with a thickness of 1 mm are shown in Figures 11–12. The maximum equivalent stresses in the workpiece are 38.9 MPa, the maximum pressure of the molding gas is 0.57 MPa, and the molding process time is 1564 s.

The results of the calculation of the workpiece with a thickness of 2 mm are shown in Figures 13–14. The maximum equivalent stresses in the billet are 38.7 MPa, the maximum pressure of the forming gas is 1.14 MPa, the molding process time is 1581 s.

The results of the calculation of the workpiece with a thickness of 3 mm are shown in Figures 15–16. The maximum equivalent stresses in the workpiece are 38.6 MPa, the maximum pressure of the molding gas is 1.68 MPa, and the molding process time is 1590 s.

From the obtained results, it can be seen that with an increase in the thickness of the workpiece, the equivalent stresses in it during the molding process practically do not change, as well as the zone of their influence.

Equivalent plastic deformations with an increase in the thickness of the workpiece are also practically unchanged.

The law of gas supply does not change its behavior when the thickness of the part increases. However, it should be noted that with an increase in thickness by 1 mm, the process time remains practically unchanged (an increase of not more than 1%), and the maximum pressure of the forming gas increases significantly (when switching from 1 mm to 2 mm, an increase of 100%, when switching from 2 mm to 3 mm, an increase of 47%). If the behavior of the gas supply law is unchanged, this means that the gas supply speed in the main sections of the graph also increases significantly.

ISSN 2075-8545 (online)

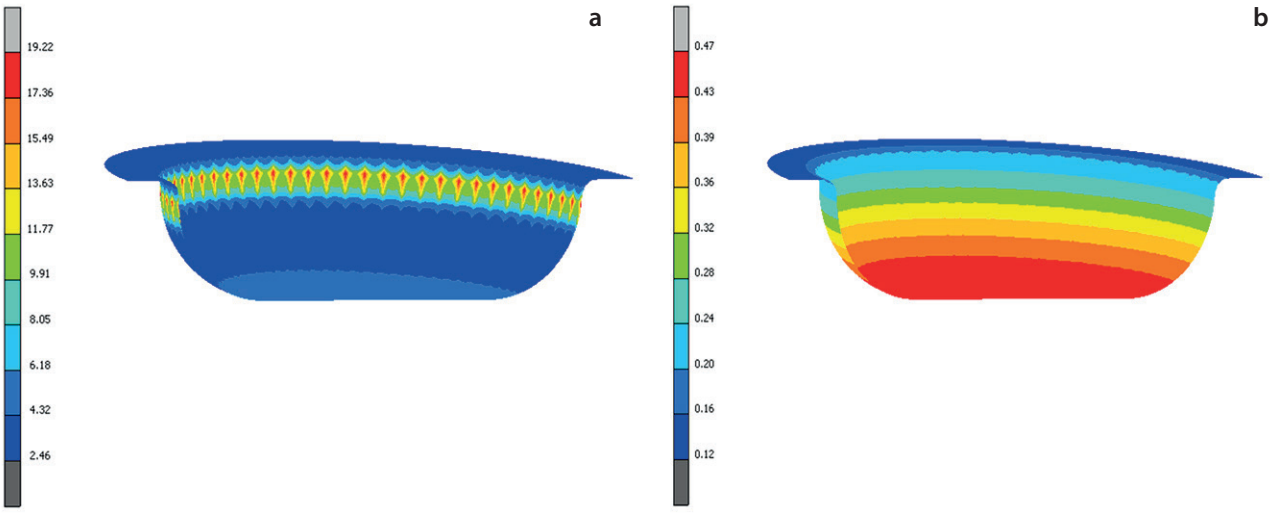


Fig. 11. Distribution of equivalent stresses in the workpiece with thickness 1 mm and equivalent plastic deformations: a – equivalent stresses in the part at the end of the molding process; b – equivalent plastic deformations of the part

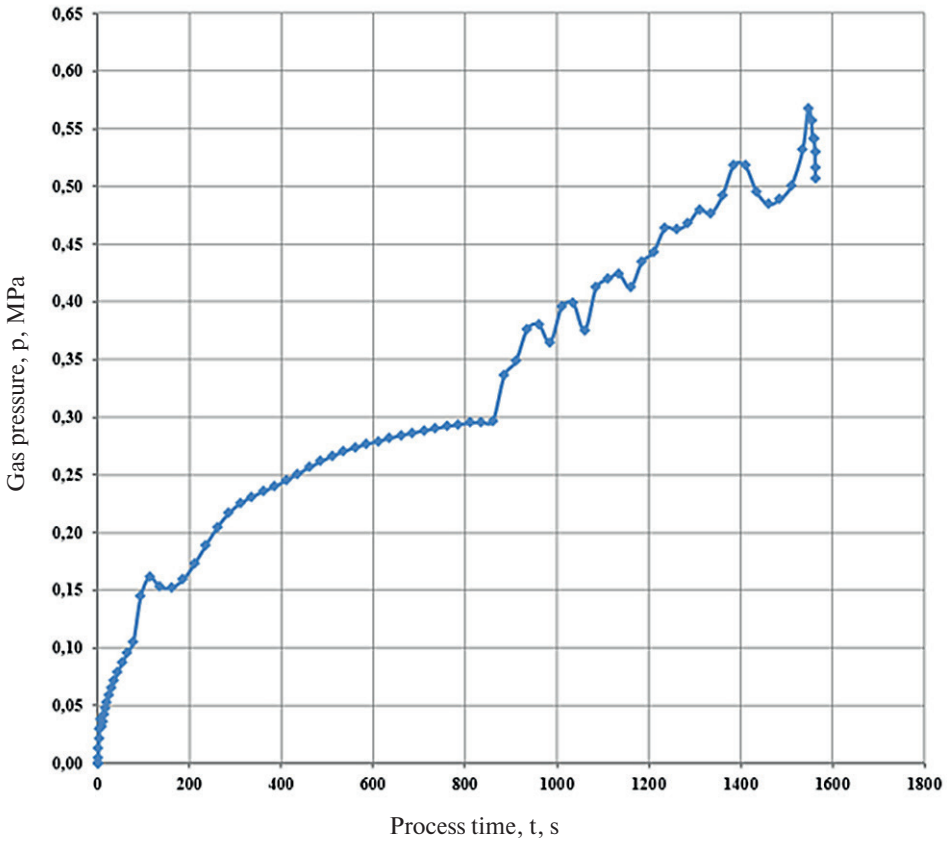


Fig. 12. Graph of forming gas supply to 1 mm thick preform

ISSN 2075-8545 (online)

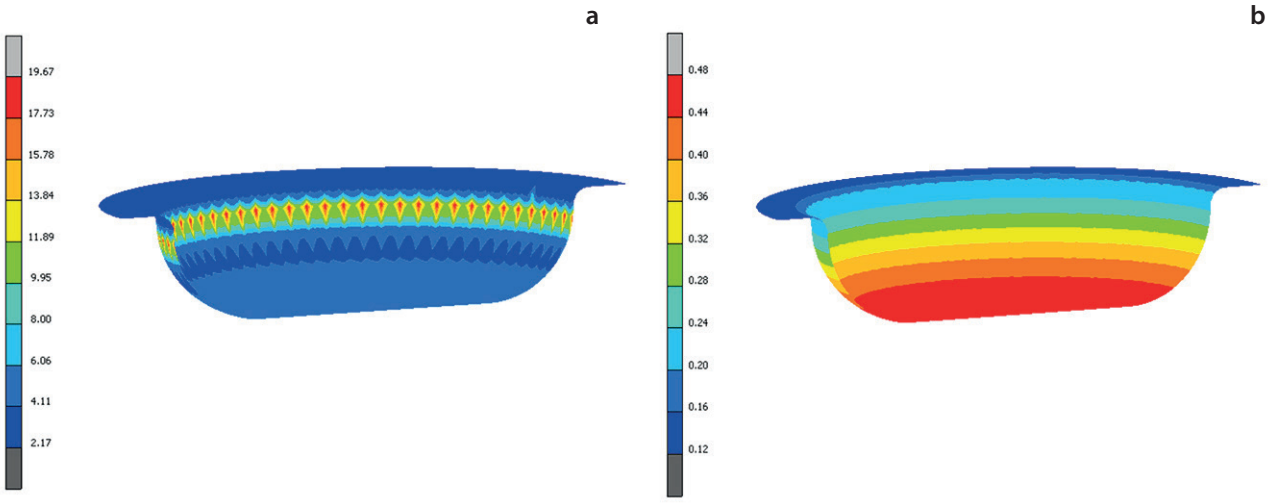


Fig. 13. Distribution of equivalent stresses in the workpiece with thickness 2 mm and equivalent plastic deformations: a – equivalent stresses in the part at the end of the molding process; b – equivalent plastic deformations of the part

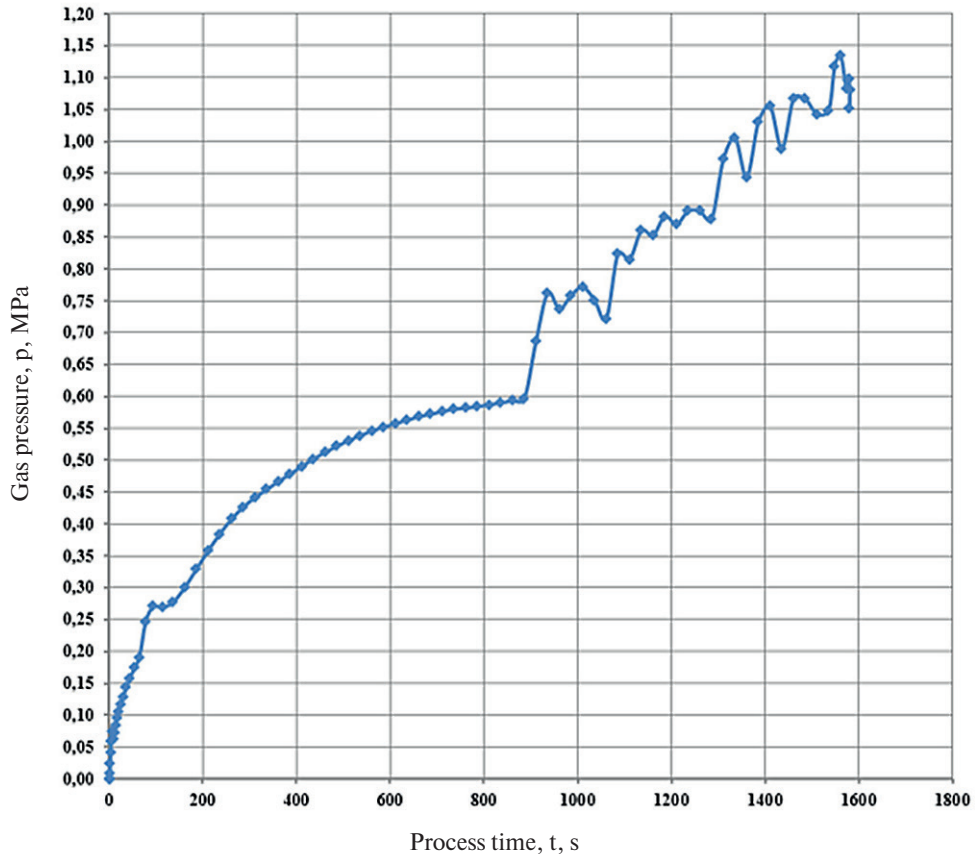


Fig. 14. Graph of forming gas supply to 2 mm thick preform

ISSN 2075-8545 (online)

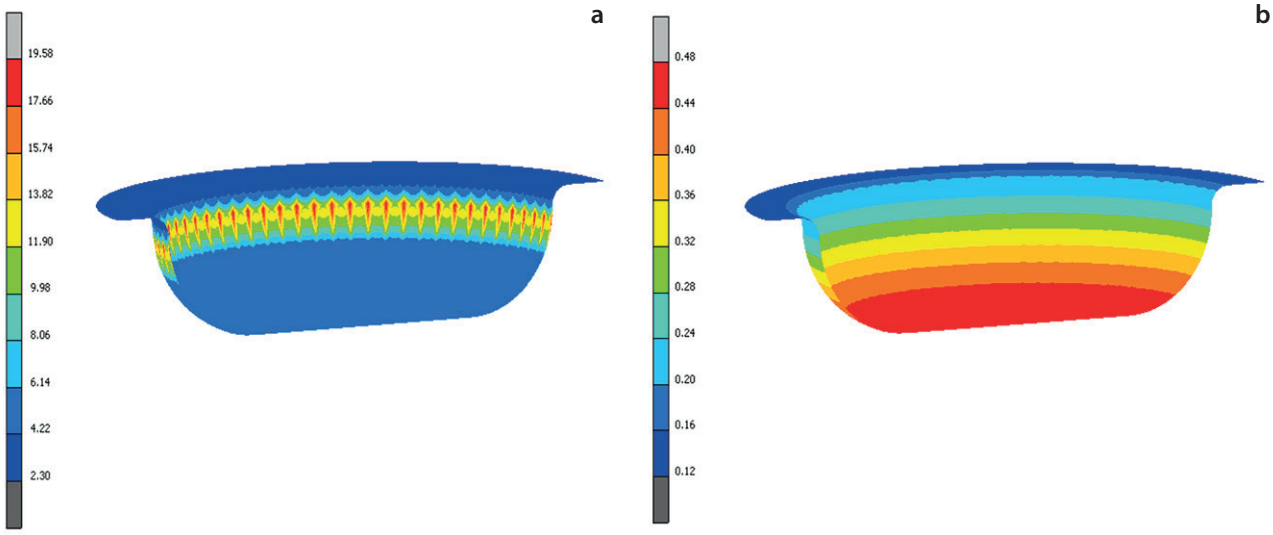


Fig. 15. Distribution of equivalent stresses in the workpiece with thickness 3 mm and equivalent plastic deformations: a – equivalent stresses in the part at the end of the molding process; b – equivalent plastic deformations of the part

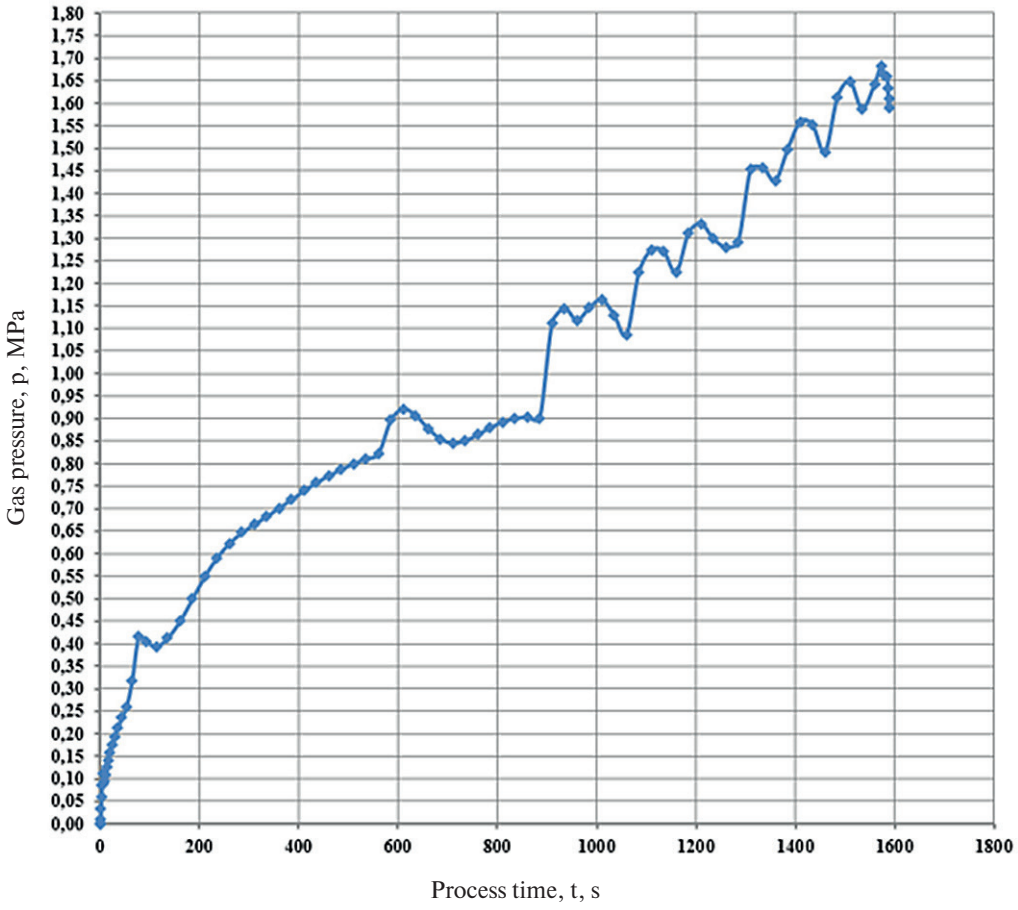


Fig. 16. Graph of forming gas supply to 3 mm thick preform

ISSN 2075-8545 (online)

Let's divide the graph shown in Figure 16 into 3 main area (Fig. 17):

- area 1 – "opening" of the workpiece - at this stage the gas pressure overcomes the forces of resistance of the material to the flow;
- area 2 – the main stage of molding - plastic deformation of the workpiece occurs with increasing pressure;
- area 3 – "preforming" - residual geometry forming.

Let's estimate the gas supply rate for each of the sections. Table 2 shows the gas feed rates for each section on different thickness blanks (in section 3 the rate is estimated from the averaged curve).

It can be seen that the pressure increase occurs nonlinearly, both between stages in a workpiece of the same thickness, and between the same stages in workpieces of different thickness.

Let us compare the moulding gas supply schedules of mould parts 1 and 2 with each other. As mentioned above, depending on the thickness of the workpiece, the behavior of the graphs does not change, only their scale changes, which entails a significant change in gas supply rates.

For comparison purposes, the superimposed plots are shown in Figure 18. It can be seen that step 1 and step 2 are approximately the same for both workpiece geometries. But stage 3 is radically different. For comparison, we give the thickness of the parts during the transition to the 3rd stage of molding in Figure 19a, b.

For analysis, geometry parts 1 and 2 with a stock thickness of 2 mm (parts with a stock thickness of 1 and 3 mm behave similarly). Figure 19a shows mold 1 with a preform thickness of 2 mm at 1111 seconds of the molding process at a gas pressure of 0.6 MPa. Figure 19b shows mold 2 with a preform thickness of 2 mm at 885 seconds of molding at a gas pressure of 0.62 MPa.

It can be seen that mold 1 has a depth significantly greater than mold 2. Because of this, at the beginning of the third stage of the molding process, the mold part 2 has already touched the bottom. But the part of the

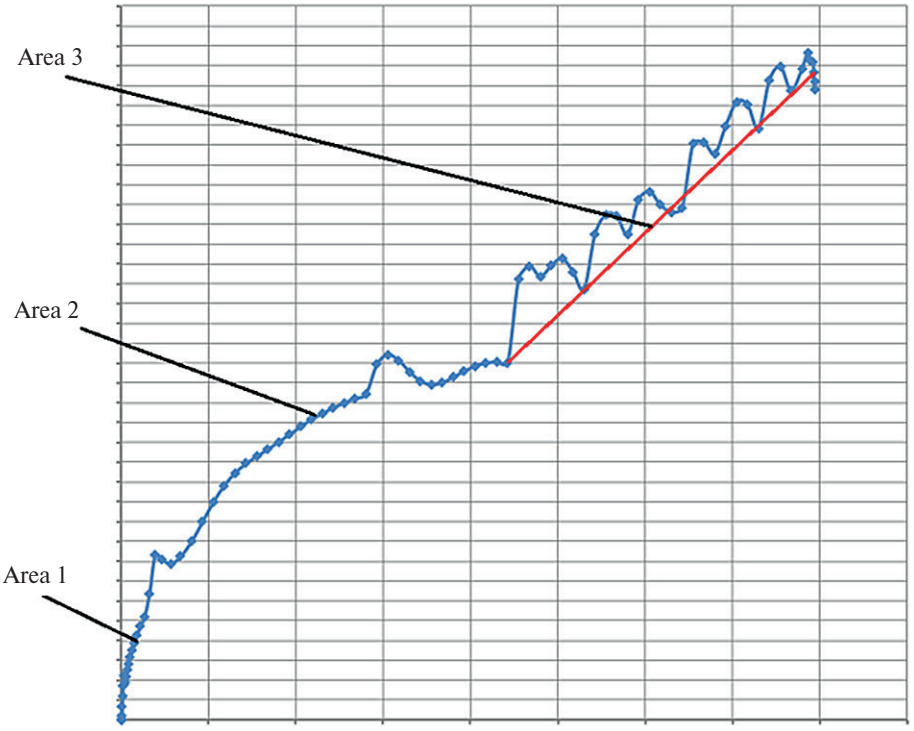


Fig. 17. Main sections of the gas supply schedule: area 1 – "opening" of the workpiece; area 2 – main forming step; area 3 – "preforming"

Table 2. Gas feed rates to mold 2 blanks of different thicknesses

Workpiece thickness, mm	Gas feed rate, MPa/s		
	Area 1	Area 2	Area 3
1	0.00140	0.00018	0.00030
2	0.00240	0.00043	0.00065
3	0.00540	0.00066	0.00098

ISSN 2075-8545 (online)

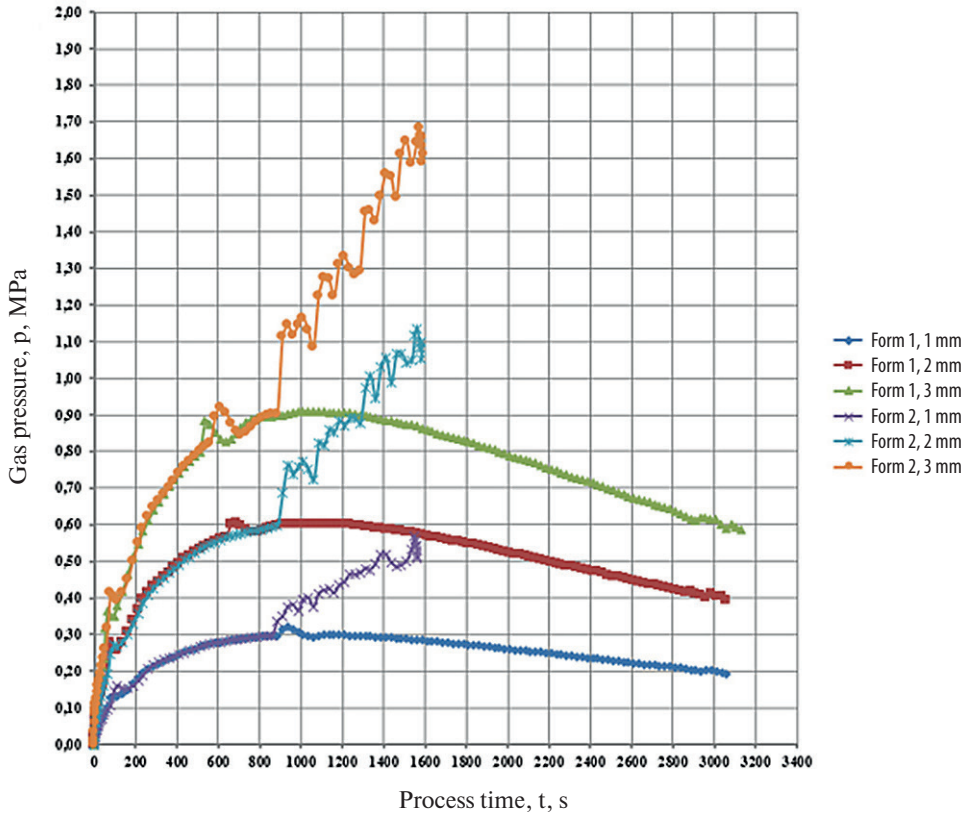


Fig. 18. Molding Gas Schedule Comparison

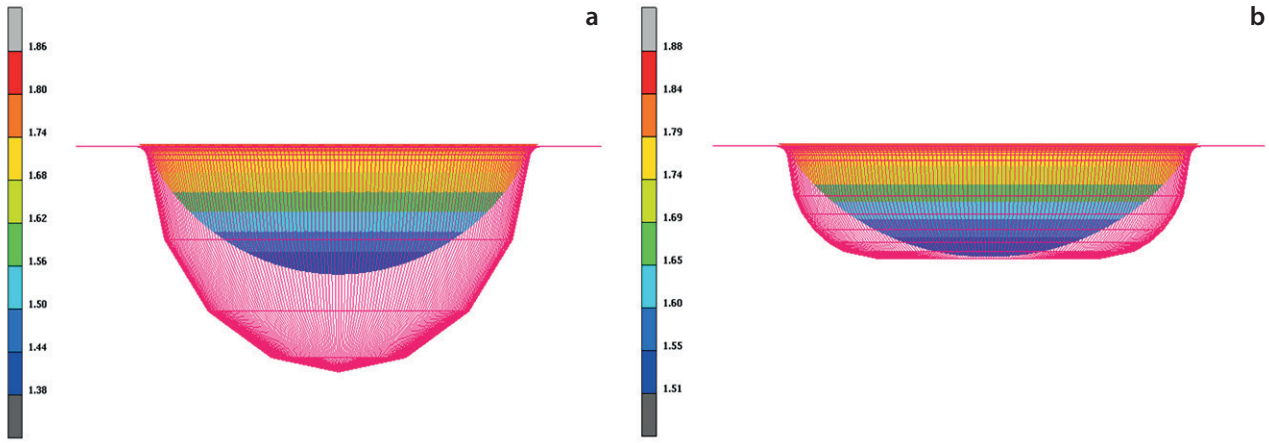


Fig. 19. Thickness of the part during the transition to the 3rd stage of molding: a – mold 1, workpiece 2 mm thick; b – mold 2, billet 2 mm thick

ISSN 2075-8545 (online)

mold 1 still has a significant margin in terms of distance to the bottom. Because of this, there is a risk of excessive thinning of the material during further stretching of the mould 1 until the bottom is touched, which may lead to tearing of the blank. In order to prevent this phenomenon, the molding step 3 of the mold 1 is carried out by releasing the pressure. At the same time, the formation of the workpiece continues, since the material is already able to deform with minimal forces.

At the same time, there is no danger of such a phenomenon in form 2. At this time, the plastic deformation degree of the material in the mold 2 is lower than that in the mold 1, therefore, it is necessary to increase the pressure growth rate of the forming gas as compared with step 2 to obtain the desired geometry. At this point, a new phase of material drawing begins, when the side zones of the elongated "dome" begin to form in a new way.

In conclusion, it is worth noting that during the study, the graphs of the supply of forming gas into a part of the "dome" type with different geometry and thickness of the workpieces were studied.

FE analysis of the SMA operations showed that when the thickness of the preform changes, the molding gas supply schedules do not change their behavior, but their scale changes. That is, while maintaining the running time of the main forming steps, the pressure of the forming gas is significantly increased, resulting in an increase in the supply rate of the forming gas.

Three steps are identified on the molding gas delivery schedules. The increase in gas pressure between stages occurs non-linearly. Depending on the shape of the part, these steps may vary. Thus, for mold 1, the third step is a "hold," in which the gas pressure is smoothly released, and in mold 2, in the third step, an "overmolding" occurs, in which the gas feed rate is increased compared to the second step. This is due to the fact that the shallower depth of the mold 2 reduces the plastic deformation of the workpiece, and as a result, a new phase of part molding appears. In mold 1, because of the greater depth, there is a risk of excessive thinning and breakage of the preform when the forming gas is supplied at this stage.

Thus, the analysis of gas supply schedules allows you to form experience with the technological process of molding various parts, as well as identify the requirements for the development of promising gas distribution systems.

REFERENCES

1. Temis Yu.M., Khudyakov A.P. Mathematical modeling of isothermal stamping and superplastic forming operations for manufacturing a hollow fan blade. *USATU Bulletin*. 2015;19(3):50–60.

2. Stroganov G.B. Novikov I.I., Boytsov V.V., Pshirkov V.F. *Use of superplasticity in metal forming*. Moscow: Mechanical Engineering; 1989.

3. Kaibyshev O.A. *Superplasticity of industrial alloys*. Moscow: Metallurgy; 1984.

4. Arabale V. Super-Plastic Forming of High Specific Strength Aluminum Al-loys. In: *International Conference on Automotive Materials & Manufacturing*. Pune, India; 2014.

5. Arabale V. Super-Plastic Forming of High Specific Strength Aluminum Alloys. *SAE Technical Papers*. 2014;4. https://doi.org/10.4271/2014-28-0040

6. Zhihao Du, Xinhua Gao, Xiangxiang Dai, Guofeng Wang, Shuobing Chen, Congzheng Zhang, et al. Structural optimization and direct reverse superplastic forming process for aluminum alloy multi cavities pallet. *Scientific Reports*. 2025;15:15508. https://doi.org/10.1038/s41598-025-00250-9

7. Isothermal stamping. Available at: URL: https://pressmash.ru/product/izotermicheskaya-shtampovka/ (access date 27.05.2026).

8. Akhunova A.Kh., Mulyukov R.R., Safiullin R.V. Finite element modeling of superplastic forming processes. *Chebyshevsky collection*. 2017;3(63):55–71.

9. Hot Forming & Superplastic Forming Press. Available at: URL: https://formingequip-en.com/1-1-hot-forming-superplastic-forming-presses.html (access date 27.05.2026).

10. Kruglov A.A., Karimova A.F., Enikeev F.U. Finite element modeling of folding during the superplastic forming of corrugated core panels. *Letters on Materials*. 2018;8(2):174–177.

11. Kruglov A.A., Musina R.Sh., Enikeev F.U. Computer modeling of the process of superplastic molding of hollow three-layer structures. *Mechanical engineering technology*. 2015;2:57–62.

12. Murzina G.R., Ganieva V.R., Kruglov A.A., Enikeev F.U. Modeling of the process of superplastic forming of hemispherical shells from blanks of different profiles. *Letters on Materials*. 2021;11(4):548–552.

13. Panchenko E.V., Alekseev P.A. Modeling of three-dimensional problems of superplastic formation of thin-walled shells. Forging and stamping. *Pressure treatment of materials*. 2012;3:28–32.

ISSN 2075-8545 (online)

14. Giuliano G., Polini W. FEM Analysis of Superplastic-Forming Process to Manu-facture a Hemispherical Shell. *Applied Sciences*. 2025;15(14):8080. https://doi.org/10.3390/app15148080

15. Michael J. O'Brien, Hubertus F. von Bremen, Minoru Furukawa, Zenji Horita, Terence G. Langdon. A finite element analysis of the superplastic forming of an aluminum alloy processed by ECAP. *Materials Science and Engineering*. 2007;456(1–2):236–242. https://doi.org/10.1016/j.msea.2006.11.116

16. Kandasamy J. FE Analysis of Superplastic Forming Complex Shapes in Aluminum-Coated Magnesium Alloys. In: *Recent Trends in Mechanical Engineering*. Singapore: Springer (Lecture Notes in Mechanical Engineering); 2021:247–259. https://doi.org/10.1007/978-981-15-7557-0_23

17. Murzina G.R., Zharmukhametova A.R., Ganieva V.R., Enikeev F.U. Method for calculating the parameters of superplasticity of titanium alloys based on the results of test forming into a rectangular matrix at constant pressure. *Bulletin of SUSU. Series: Mathematical modeling and programming*. 2023;16(1):96–107.

18. Kukhar V.D., Yakovlev S.S. Evaluation of stress-strain state in the manufacture of shells with external ribs. *News of Tula State University. Technical sciences*. 2023;2:530–536.

19. *Mentat User's Guide, Version 3.3*. Palo Alto: MARC Analysis Research Corporation; 1999.

20. Alabort E., Putman D., Reed R.C. Superplasticity in Ti–6Al–4V: Characterisation, modelling and applications. *Acta Materialia*. 2015;95:428–442. http://dx.doi.org/10.1016/j.actamat.2015.04.056

21. Shao-song Jiang, Zhen Lu, Xiao-dong He, Guo-feng Wang, Kai-feng Zhang. Superplastic forming Ti–6Al–4V titanium alloy cylinder with near uniform thickness distribution. *Transactions of Nonferrous Metals Society of China*. 2012;22(2):472–478. https://doi.org/10.1016/S1003-6326(12)61748-8

22. Kolesnikov A.V. Analysis of the possibility of pneumatic thermal forming of multilayer structures by virtual modeling. In: *Reshetnevsky readings*: *checkpoints of the XVI International. scientific. conf., dedicated to the memory of the gene. designer rocket space. systems acad. M.F. Reshetneva*. Under the general. ed. Yu.Yu. Loginova. Krasnoyarsk: Sib. state. aerospace. un-t; 2012. PART 2.

23. Rollin M., Penazzi L., Velay V., Dupuy A., Gallet S.A new numerical strategy for SPF pressure profile computing based on statistical strain rate controlling. *International Journal of Mechanical Sciences*. 2018;141:479–490. https://doi.org/10.1016/j.ijmecsci.2018.04.021

24. Stepanenko N.Yu., Chertovskikh S.V., Lukyanov V.V. The study of the formation of a hollow cellular structure with a given geometry. *Nanotechnologies in construction*. 2025;17(4):455–465. https://doi.org/10.15828/2075-8545-2025-17-4-455-465

25. Stepanenko N.Yu., Chertovskikh S.V., Lukyanov V.V. Optimization of the geometry of the characteristic section of a complex-profile thin-walled workpiece of the original geometry by modeling and finite element analysis. *Materials. Technologies. Design*. 2025;7(3):5–20. https://doi.org/10.54708/26587572_2025_73225

26. Stepanenko N.Yu., Chertovskikh S.V., Lukyanov V.V., Astanin V.V. Manufacturing technology of protective edge for polymer composite products. *News of Tula State University. Technical sciences*. 2024; 8:197–203.

ADDITIONAL INFORMATION

The authors declare that the preparation of the article did not use technologies of generative artificial intelligence and technologies based on artificial intelligence.

INFORMATION ABOUT THE AUTHORS

Nikolai Yu. Stepanenko – Postgraduate student, Department of Technological Machines and Equipment, Ufa State Petroleum Technological University, 450064, Ufa, Kosmonavtov St., 1, Republic of Bashkortostan, Russian Federation, koly.stepanenko@yandex.ru, https://orcid.org/0009-0002-0843-480X

Sergey V. Chertovskikh – Cand. Sci. (Eng.), Head of the Department of Technological Machines and Equipment, Ufa State Petroleum Technological University, 450064, Ufa, Kosmonavtov St., 1, Republic of Bashkortostan, Russian Federation, chertovskikh@mail.ru, https://orcid.org/0000-0001-9758-7677

Irek V. Kandarov – Cand. Sci. (Eng.), Associate Professor, Department of Intelligent Systems, Technologies and Equipment in Mechanical Engineering, Ufa State Petroleum Technological University, 450064, Republic of Bashkortostan, Ufa, Kosmonavtov St., 1, Russian Federation; General Director, Scientific and Production Association "Technopark of Aviation Technologies", 450027, Republic of Bashkortostan, Ufa, Tramvaynaya St. 5, room 1, tpat@tp-at.ru, https://orcid.org/0009-0009-6330-8524

Aleksey V. Rubtsov – Cand. Sci. (Eng.), Associate Professor, Department of Technological Machines and Equipment, Ufa State Petroleum Technological University, 450064, Ufa, Kosmonavtov St., 1, Republic of Bashkortostan, Russian Federation, sunset202@mail.ru, https://orcid.org/0000-0001-6087-5579

ISSN 2075-8545 (online)

CONTRIBUTION OF THE AUTHORS

N.Yu. Stepanenko – modeling and finite element analysis, work with the MSCMarc software package. Interpretation of the obtained data.

S.V. Chertovskikh – scientific management of the project, development of the general structure of the article, quality control of all stages of the study, scientific editing and revision of the text, formation of conclusions and recommendations for practical use. Participation in the formulation of the purpose and objectives of the study, writing the introduction and conclusion, justification of the practical significance of the work.

I.V. Kandarov – methodological support of the study, control over the correctness of the experimental design, participation in writing and editing the text of the article.

A.V. Rubtsov – participation in writing and editing the text of the article.

The authors declare no conflict of interest.

The article was submitted 18.06.2026; approved after reviewing 01.10.2026; accepted for publication 05.10.2026.

ISSN 2075-8545 (online)

Nanotechnologies in construction
Нанотехнологии в строительстве

2026; 18 (5):
673–680

Nanobuild.ru

SYSTEM SOLUTIONS FOR TECHNOLOGICAL PROBLEMS

Original article
https://doi.org/10.15828/2075-8545-2026-18-5-673-680

CC BY 4.0

Analysis of the OWLv2 model usage for real-time object detection

Konstantin Y. Ustyuzhanin, Fairuza T. Ziganshina*, Regina R. Sadykova
Ufa State Petroleum Technological University, Ufa, Kosmonavtov str. 1, 450064, Russian Federation
* Corresponding author: e-mail: fairusa85@mail.ru

ABSTRACT

The implementation of an AI-enabled video processing system for industry often faces a trade-off between accuracy, speed, cost, and safety. The authors present a plan and scheme of operation of an industrial AI system for searching objects in images in real time using only local budget solutions from the user segment. **Introduction.** This research describes the structure of an industrial scalable multi-camera system for detecting objects in a production environment based on text descriptors. The system is based on the OWLv2 (Open-World Localization Vision Transformer) model: a visual transformer for localizing objects in open space. **Methods and materials.** A video stream with various objects is used as objects, which must then be recognized and identified. The use of the open OWLv2 model and Nvidia's user-level GPU together with the microservices architecture allows you to create flexible software that can be scaled as the needs of the enterprise using a single local service that is completely isolated from the outside world. Such a service, among other things, will allow you to further implement advanced versions of models that solve complex problems, such as quality control of composites, without the need to significantly rebuild the service, while maintaining a single API. The system is designed to process real-time video streams and single images from multiple cameras in real time using graphics processing unit (GPU) acceleration, distributed task processing on Celery and RabbitMQ, centralized observability with Prometheus, Grafana and Loki. **Results and discussion.** The architecture prioritizes operational resilience, cost efficiency, and the ability to scale from two to a hundred cameras without a fundamental redesign. By adopting a decentralized, microservices approach from the outset, the project avoids the technical debt and refactoring burden that would arise from building a monolithic system and trying to distribute it later. Using MinIO, RabbitMQ, Prometheus, Loki, and Celery is a good choice for an industrial solution.

KEYWORDS: Artificial intelligence, OWLv2 model, object detection, system architecture, system requirements, Kubernetes system

SOURCES OF FUNDING FOR THE SCIENTIFIC WORK THAT RESULTED IN THE PUBLICATION: The study was carried out within the framework of the program of the Ministry of Science and Higher Education of the Russian Federation "PRIORITY 2030".

ACKNOWLEDGEMENTS: The authors express their gratitude for the financial support of the project.

FOR CITATION:
Ustyuzhanin K.Yu., Ziganshina F.T., Sadykova R.R. Analysis of the OWLv2 model usage for real-time object detection. *Nanotechnologies in Construction.* 2026;18(5):673–680. https://doi.org/10.15828/2075-8545-2026-18-5-673-680. – EDN: AXXVVG.

© Ustyuzhanin K.Yu., Ziganshina F.T., Sadykova R.R., 2026

ISSN 2075-8545 (online)

Nanotechnologies in construction
Нанотехнологии в строительстве

2026; 18 (5):
673–680

Nanobuild.ru

SYSTEM SOLUTIONS FOR TECHNOLOGICAL PROBLEMS

Анализ использования модели OWLv2 для обнаружения объектов в режиме реального времени

Константин Юрьевич Устюжанин, Файруза Тахваловна Зиганшина*, Регина Римовна Садыкова

Уфимский государственный нефтяной технический университет, 450064, Уфа, улица Космонавтов, 1, Российская Федерация

* Автор, ответственный за переписку: e-mail: fairusa85@mail.ru

АННОТАЦИЯ

Внедрение системы обработки видеоинформации с помощью ИИ для промышленности часто сталкивается с компромиссом между точностью, скоростью, дороговизной и безопасностью. Авторы представляют план и схему работы промышленной ИИ-системы поиска объектов на изображениях в реальном времени с использованием только локальных бюджетных решений из пользовательского сегмента. **Введение.** Работа описывает структуру промышленной масштабируемой многокамерной системы детектирования объектов в производственном окружении на основе текстовых дескрипторов. В основе системы лежит модель OWLv2 (англ. Open-World Localization Vision Transformer): визуальный трансформер локализации объектов в открытом пространстве. **Методы и материалы.** В качестве объектов используется видеопоток с различными объектами, которые в дальнейшем должны быть распознаны и определены. Использование открытой модели OWLv2 и ГП Nvidia пользовательского уровня вместе с архитектурой микросервисов позволяет создать гибкое ПО, которое можно масштабировать по мере нужд предприятия, используя единый локальный сервис, полностью изолированный от внешнего мира. Такой сервис, в том числе, позволит в дальнейшем внедрять продвинутые версии моделей, решающих сложные задачи, такие как контроль за качеством композитов без необходимости существенной перестройки сервиса, при этом сохраняя единый API. Система разработана для обработки видеопотока и единичных изображений в реальном времени со множества камер в реальном времени с использованием ускорения на графическом процессоре (ГП), распределенной обработкой задач на Celery и RabbitMQ, централизованной наблюдаемостью с Prometheus, Grafana и Loki. **Результаты и обсуждения.** Архитектура ставит приоритетом операционную устойчивость, эффективность по стоимости и возможность масштабирования с двух до сотни камер без фундаментального редизайна. Применяя с самого начала децентрализованный, микросервисный подход, проект избегает технического долга и бремени рефакторинга, которые возникли бы при создании монолитной системы и попытке ее последующего распределения. Гибкая облачная система на базе Kubernetes, где каждый компонент независим, масштабируется по потребности и легко поддерживается. Использование MinIO, RabbitMQ, Prometheus, Loki и Celery – хороший выбор для промышленного решения.

КЛЮЧЕВЫЕ СЛОВА: Искусственный интеллект, модель OWLv2, детектирование объектов, архитектура системы, системные требования, система Kubernetes

ИСТОЧНИКИ ФИНАНСИРОВАНИЯ НАУЧНОЙ РАБОТЫ, РЕЗУЛЬТАТОМ КОТОРОЙ СТАЛА ПУБЛИКАЦИЯ: Исследование выполнено в рамках программы Министерства науки и высшего образования Российской Федерации «ПРИОРИТЕТ 2030».

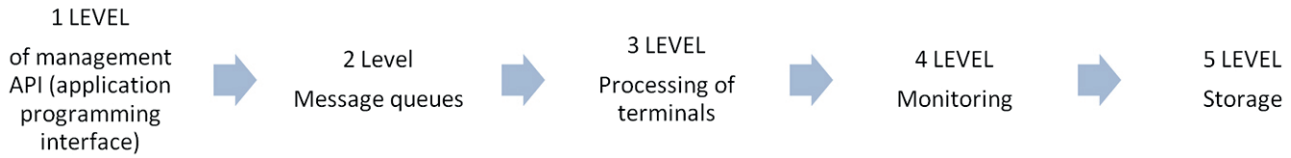
БЛАГОДАРНОСТИ: Авторы выражают благодарность за финансовую поддержку проекта.

ДЛЯ ЦИТИРОВАНИЯ:

Устюжанин К.Ю., Зиганшина Ф.Т., Садыкова Р.Р. Анализ использования модели OWLv2 для обнаружения объектов в режиме реального времени. *Нанотехнологии в строительстве.* 2026;18(5):673–680. https://doi.org/10.15828/2075-8545-2026-18-5-673-680. – EDN: AXXVVG.

INTRODUCTION

This paper offers an overview of the system and the justification of design solutions for the creation of a machine vision module [1]. The proposed system operates on the principle of separation of duties, where each component performs a separate task within the output pipeline. The architecture consists of five main layers:



ISSN 2075-8545 (online)

This approach reduces latency and does not lead to system-wide errors.

When implementing artificial intelligence (AI) in production, two related problems arise: the cost of implementing a unit of the system in a separate production area and the limitation of horizontal scaling, which in turn requires the implementation of an expensive AI system in each area separately. The increased cost is primarily due to the limited software licenses and the high cost of graphics accelerators when implementing isolated AI. In many industries, security standards do not allow the movement of company data outside its network, which makes it impossible to use third-party computing services and rented facilities. Production AI should be located inside the network and be isolated from the outside world, especially when its work is related to the management and support of production robots and monitoring the state of production areas. In this paper, the authors propose an architecture for a scalable computer vision system based on microservices and Kubernetes orchestration, the cost of which will grow linearly, not exponentially, and which will allow for the implementation of updates and improvements without stopping work.

METHODS AND MATERIALS

This paper describes the integration of several technologies and tools for processing video streams from multiple cameras. Such technologies are: Kubernetes, Docker, RabbitMQ, Redis, Prometheus, Grafana, Loki, FastAPI, and ONNX Runtime [2–6].

As a basis, the principle of dividing the task into subtasks is used, which create their environment for the convenience of storing and transferring data, that is, the principle of microservices architecture. This technology is achieved using Kubernetes and Docker. To control the operation of the system, collect and analyze, the following tools are used: Prometheus, Grafana and Loki, and for message transfer and data storage in RAM, RabbitMQ and Redis are used. This principle of operation can be presented in the form of a diagram shown in Figure 1.

In this case, the AI is launched as a Celery job service based on the created job in RabbitMQ with access to data via links to saved objects in Redis. The data itself is stored in MinIO. FastAPI serves as a layer for managing system flows, creating and managing work status, and providing access to information for external enterprise services. The video stream from the cameras goes directly to MinIO, the AI works independently, on demand of the task, and consumes resources only during inference directly, when the AI was created for image processing. The AI itself can be any model that can be run on the selected hardware, but the authors suggest using OWLv2 as the basis for solving most computer vision production problems based on a text prompt. At the same time, OWLv2 with an accuracy of FP16 takes up only 0.35–0.4 Gb along with weights, activations, and overhead (360 MB of scales, 155 million parameters).

RESULTS AND DISCUSSION

Below are the justifications for choosing a particular system and technology.

CPU and GPU Acceleration: Performance and Cost Analysis. The inclusion of the NVIDIA RTX 5060 Ti graphics card is a critical decision in system design.

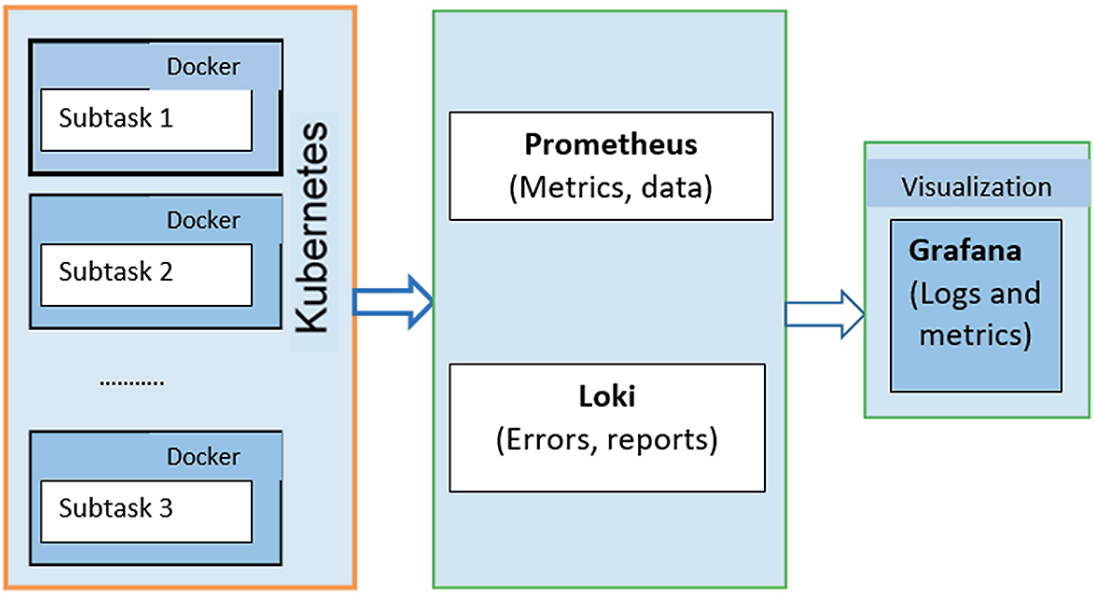


Fig. 1. Approximate scheme of video stream processing

ISSN 2075-8545 (online)

OWLv2 is a graphics data conversion program with approximately 1.5 billion parameters [9]. Table 1 below shows the characteristics of a single stage of data processing using the CPU and the RTX 5060 Ti [10].

The analysis points to the advantage of GPU acceleration [11, 12]. A CPU-only system would require eight to ten high-performance cores to achieve comparable throughput, which means a larger, more power-hungry server at a significantly higher cost [12].

Thus, the use of a GPU, despite the cost, allows you to reduce operating and capital costs. At the same time, it becomes possible to move to real-time data processing with high resolution, which will increase the accuracy of detection [13]. The main limitation of the RTX 5060 Ti is 4Ti is 8 gigabytes of video memory, which limits the packet size, image resolution, and the number of streams from cameras that can be processed simultaneously.

To solve this problem, you can delegate control of Kubernetes resources [14], allocating them explicitly to the pods responsible for running the model. If you restrict access to the GPU only to inference pods, and run APIs, databases, and support services pods strictly on CPU resources, then the limited GPU resources will be spent strictly on the most difficult and costly task of the system.

If a monolithic Docker container [15] with a single FastAPI application and ONNX Runtime [16] were used, then when moving from 1 camera to 2–3, it would be necessary to scale the entire instance, which would require a separate video processor for each additional instance, each camera [17]. The microservice architecture allows you to move all resource-intensive tasks into a separate container, which will run the model and take up GPU resources alone, but which will be able, firstly, to process many camera streams simultaneously, and secondly, will be connected to the rest of the system only through the API. The advantages of this approach are emphasized in Newman's book "Creating Microservices". The use of message queues will allow you to receive video streams from many cameras and process them using limited resources. Table 2 shows a comparison of the two main tools for organizing queues: RabbitMQ and Redis.

If you need to provide horizontal scaling as in the described system, then RabbitMQ is the best choice. It will allow, among other things, to create queues with different priorities and tasks for different cameras, which can be important for large production with many sites. It will work as a StatefulSet [26] to ensure a constant state during reboots. In the future, this choice will allow you to expand the system to several models running on separate GPUs performing different tasks within a single service. This approach allows you to provide resource management at the nanotechnology level and solve priority problems and flexibly redistribute the load.

At the same time, it would be rational to provide centralized storage of camera frames, work results, and system artifacts in the MinIO object storage [18], which is compatible with S3 [19]. Direct transfer of large objects through the internal network will introduce undue delay and increase the load on limited system resources. MinIO can work locally even in Docker Compose [20] and provide a compatible S3 API [21], which makes it possible to unify the protocols for storing and retrieving information in the system, linking all services to a single local storage of large objects. It is very popular in the

Table 1. Characteristics of the data processing stage using a CPU and an RTX 5060 Ti

Characteristics	CPU Processing Stage (720p)	RTX 5060 Ti (c 8GB VRAM)
Frame rate (frames per second)	5–10 frames	20–30 frames
Impact on system requirements	Real-time limitation	Real-time application support
Example of human tracking (at 5 frames per second)	Difficult to track at 5 frames	125 Frames – Smooth Motion and Analysis

Table 2. A comparison of two tools: RabbitMQ and Redis

Criterion	RabbitMQ	Redis
Ease of Use	More difficult to set up and operate	Easy to use, minimal setup
Performance	Suitable for complex scenarios, high throughput	Very high, especially for basic operations
Message routing support	Advanced Routing, Priority Queues	Limited routing options
Handling dead-letter messages	There are mechanisms for handling errors and retries	No built-in error handling mechanisms
Priority queue support	Yes	No
Suitable for multidimensional systems	Better, thanks to complex processing and prioritization	Fewer opportunities for complex scenarios

ISSN 2075-8545 (online)

Nanotechnologies in construction
Нанотехнологии в строительстве

2026; 18 (5):
673–680

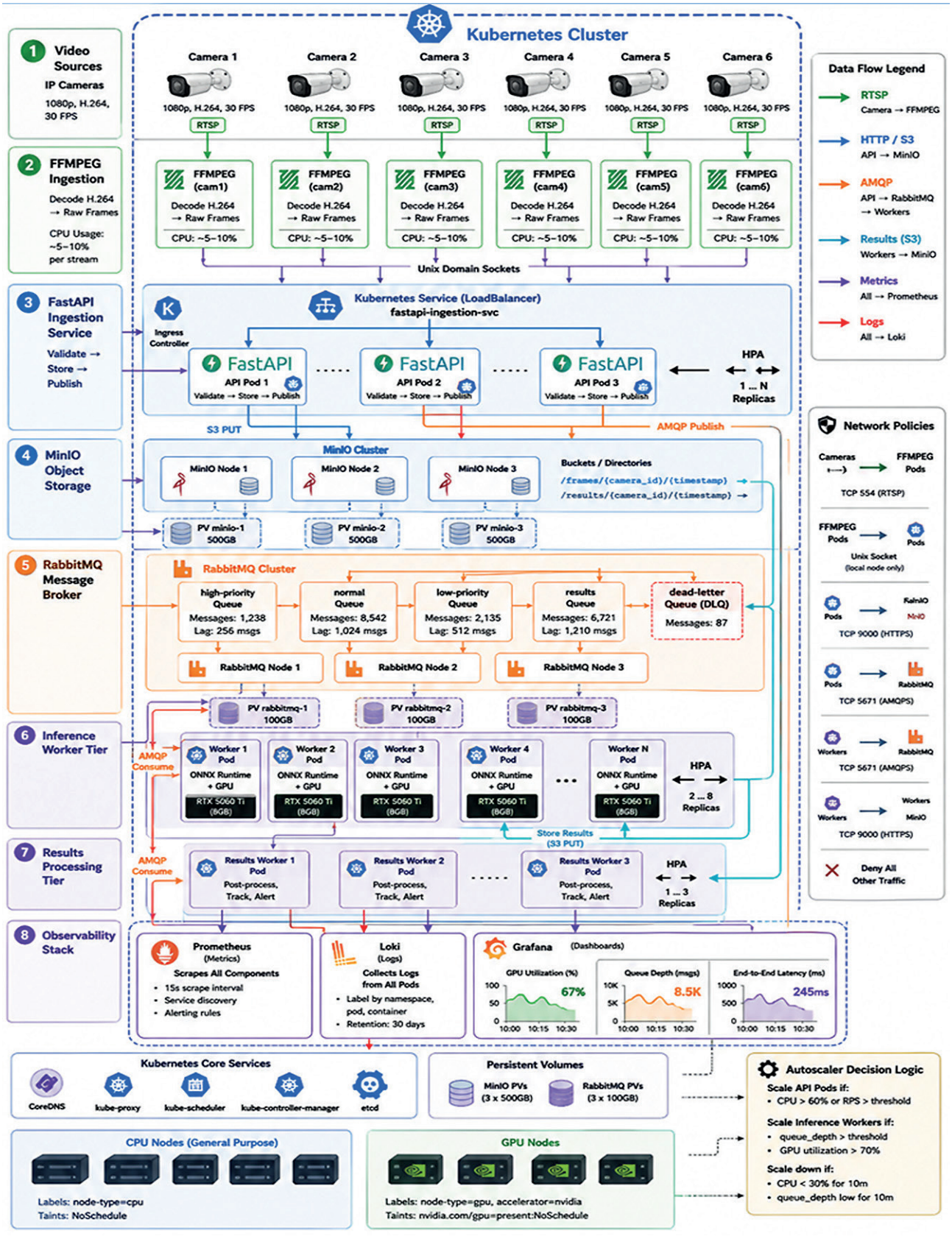


Fig. 2. Architecture of the industrial computer vision system

ISSN 2075-8545 (online)

DevOps community [22] due to its ease of operation. In this scheme, the stream from cameras will be directly stored in MinIO, and access to them will be strictly via the frame URI in RabbitMQ [23]. Similarly, the results will go directly to the storage without being transferred between other components of the system. Even in the event of a storage failure, the system will be able to keep messages in the queue until access to MinIO is restored. It is advantageous to run MinIO itself as a StatefulSet with persistent volumes to preserve data in the event of a crash [27].

To ensure control over everything that happens in the system, it is also necessary to add centralized services for collecting statistics, monitoring and collecting logs. Prometheus [28] can centrally collect metrics from the entire system at regular intervals, and Loki will take care of centralized log collection. Their display can be given to the Grafana dashboard. In the future, Jaeger traces can be added [24]. Unlike traditional logging systems [25], with Loki you can index only median characteristics and access all other data through filtering and queries.

The system architecture is shown in Figure 2. The cameras transmit RTSP video in H.264 format to the FFMPEG decoder, after which they are stored in the MinIO repository. FastAPI automatically publishes messages to RabbitMQ for the model with a hint that corresponds to the current task or the objects being searched for for each of the cameras. Under the inference, it loads images and hints into the OWLv2 model and stores the result in MinIO. It runs on Celery with sessions on NVIDIA Multi-Process Service. The results are post-processed in a separate pod independent of the model, after which they are ready to be displayed in the system's GUI or transferred.

This architecture is capable of scaling linearly from two cameras to a hundred with minimal investment. When adding a new camera, you only need to update the camera configuration in the API, after which the stream will be automatically added to the data pipeline without further involvement of the API itself. Additional workflows will be created automatically if the current ones are not enough. If the GPU itself becomes a bottleneck, then it is enough to add another GPU to the cluster without changing the configurations of existing threads or reconfiguring the system.

The OWLv2 model can find any objects in the image with a high level of confidence from a text prompt, making it the best choice for the implementation of the computing core of an industrial vision system, where the final object of interest is unknown, can change, or has a complex, variable structure, poor lighting, and complex, volatile backgrounds. When the model is exported to ONNX format using standard pytorch, with optimum optimizing for FP16 floating-point accuracy, the use becomes cost-effective even in the absence of a message queue and a direct video stream over the Docker network.

NVIDIA GTX 4060 8Gb VRAM Laptop GPU, 32GB RAM, Intel Core i9-13900H graphics card used in the test. Figures 3–7 show the results of testing the model on a set of objects.

Search for "tool", "hose", "glasses" (Figs. 3–5) individually at a confidence level of at least 0.2, frame-by-frame script, stationary objects are shown in Figures 3–5.

Figure 6 shows the search result for "powerbank" at a confidence level of at least 0.2 for a frame-by-frame script, an example of a classification error, this is clearly not "powerbank", a static batch. Figure 7 shows the search result for "metal dish, tool, hose, glasses" at a confidence level of at least 0.2 for a thread-based ensemble script, dynamic batch. You can see that the model is basically able to adapt to the recognition of very different objects in noise conditions. Even on miniature and low-power hardware, the OWLv2 model showed an FPS of 5–30 frames with direct continuous image streaming. With the use of OpenCV trackers and periodic updates, the simplified version of the service consistently produces 60 FPS on a single camera.

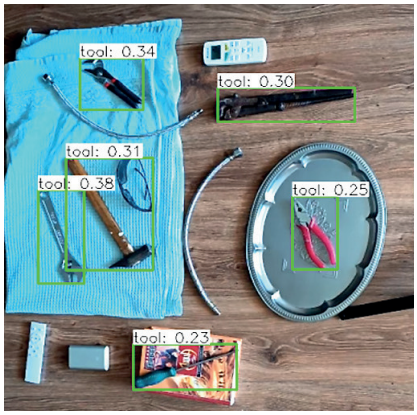


Fig. 3. Search for "tool"

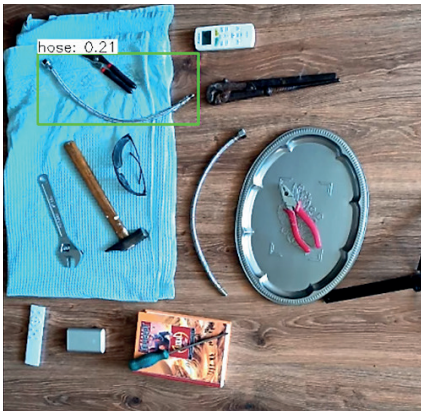


Fig. 4. Search for "hose"



Fig. 5. Search for "glasses"

ISSN 2075-8545 (online)



Fig. 6. Search for "powerbank" (classification error)

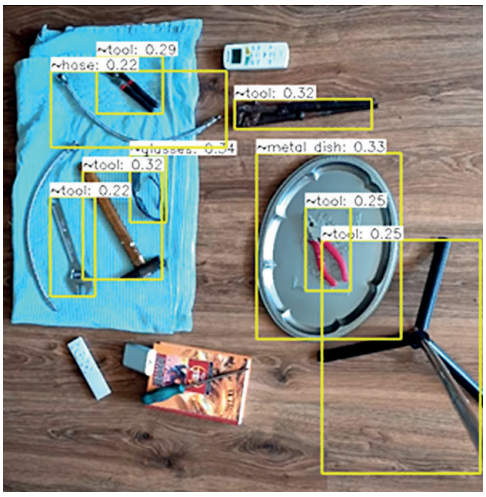


Fig. 7. Search for «metal dish, tool, hose, glasses»

CONCLUSION

Finding a sustainable and scalable solution for computer vision comes down to the task of moving from the exponential growth of the cost of horizontal scaling to linear scaling. The use of modern AI requires the use of graphics accelerators and the division of the task between loosely coupled services within a single architecture.

Moving on to the real applications of the described AI system, its application is not field-specific and is not limited to one type of work. If necessary, the system can monitor the movement of personnel, foreign objects and the position of workpieces in the working area of the manipulator, or even detect defects in composite materials, including those reinforced with nanofills, where it is necessary to quickly detect defects or foreign objects to supplement the standard OWLv2 model with an extended context, or implement a satellite model to solve this specific task without significant changes in the system and linear cost increase.

REFERENCES

1. *Amazon Simple Storage Service Documentation*. Amazon S3; 2026. URL: https://docs.aws.amazon.com/s3/ (accessed: 04.05.2026).
2. Burns K., Beda K. *Kubernetes Up and Running: Dive into the Future of Infrastructure*. 2nd ed. O'Reilly Media; 2019
3. *Celery – Distributed Task Queue*; 2023. URL: https://docs.celeryq.dev/ (accessed: 04.05.2026).
4. DevOps. Humble J., Farley D. *Continuous Delivery: Reliable Software Releases through Build, Test, and Deployment Automation*. Boston: Addison-Wesley Professional; 2010.
5. Docker Compose. *Docker Compose Documentation*; 2026. (Accessed: 04.05.2026). URL: https://docs.docker.com/compose/ (accessed: 04.05.2026)
6. *Docker Documentation*; 2026. URL: https://docs.docker.com/ (accessed: 04.05.2026)
7. *FastAPI Documentation*; 2026. URL: https://fastapi.tiangolo.com/ (accessed: 04.05.2026)
8. FFmpeg Documentation; 2024. *FFmpeg Protocols*. URL: https://ffmpeg.org/ffmpeg-protocols.html (accessed: 04.05.2026)
9. Grafana Labs. *Grafana Documentation*; 2026. URL: https://grafana.com/docs/ (accessed: 04.05.2026)
10. *Grafana Loki Documentation*; 2026. URL: https://grafana.com/docs/loki/latest/ (accessed: 04.05.2026)
11. Hänsel M. Real-Time Streaming Protocol (RTSP): Architecture and Design Considerations. *IEEE Communications Surveys & Tutorials*. 2020. Vol. 22, no. 3. P. 1234–1256. https://doi.org/10.1109/COMST.2020.2987258
12. Jaeger: open source, end-to-end distributed tracing; 2026. URL: https://www.jaegertracing.io/docs/ (accessed: 04.05.2026)
13. Kubernetes Documentation; 2026. URL: https://kubernetes.io/docs/home/ (accessed: 04.05.2026)Load balancer. Kubernetes. *Service – Type LoadBalancer*; 2026. URL: https://kubernetes.io/docs/concepts/servicesnetworking/service/#loadbalancer (accessed: 04.05.2026)
14. MinIO Documentation; 2026. URL: https://min.io/docs/minio/kubernetes/upstream/index.html (accessed: 04.05.2026)
15. Newman S. *Building Microservices: Designing Fine-Grained Systems*. O'Reilly Media; 2015.

ISSN 2075-8545 (online)

16. NVIDIA Corporation; 2023. *CUDA C++ Programming Guide*. URL: https://docs.nvidia.com/cuda/cuda-c-programming-guide/ (accessed: 04.05.2026)
17. *ONNX Runtime Documentation*; 2026. URL: https://onnxruntime.ai/docs/ (accessed: 04.05.2026)
18. OWLv2 (Open-World Localization Vision Transformer). Minderer M., Gritsenko A., Stone A. et al. Scaling Open-Vocabulary Object Detection. *Advances in Neural Information Processing Systems (NeurIPS 2023)*. 2023;36:72983–73007. URL: https://arxiv.org (accessed: 04.05.2026). https://doi.org/10.5555/3666122.3669313
19. *Prometheus – Monitoring system & time series database*; 2026. URL: https://prometheus.io/docs/ (accessed: 04.05.2026)
20. *RabbitMQ Documentation;* 2026. URL: https://www.rabbitmq.com/docs (accessed: 04.05.2026)
21. RabbitMQ StatefulSet. Kubernetes. *StatefulSets*; 2026. URL: https://kubernetes.io/docs/concepts/workloads/controllers/statefulset/ (accessed: 04.05.2026)
22. *RabbitMQ Documentation: Message Queues and Priority Queues*; 2024. URL: https://www.rabbitmq.com/priority.html (accessed: 04.05.2026)
23. Tannenbaum A. S., Van Steen M. *Distributed Systems: Principles and Paradigms*. 2nd ed. Prentice Hall; 2006.
24. WebRTC W3C Working Group; 2023. *WebRTC 1.0: Real-time Communication Between Browsers*. W3C Recommendation. URL: https://www.w3.org/TR/webrtc/ (accessed: 04.05.2026)
25. Architectural storage pattern. Kleppmann M. *Designing Data-Intensive Applications: The Big Ideas Behind Reliable, Scalable, and Maintainable Systems*. Boston: O'Reilly Media; 2017.
26. Horizontal autoscaling by metrics Prometheus. Kubernetes. *Horizontal Pod Autoscaler*. URL: https://kubernetes.io/docs/tasks/run-application/horizontal-pod-autoscale/ (accessed: 04.05.2026).
27. *Prometheus Adapter for Kubernetes Metrics*. URL: https://github.com/kubernetes-sigs/prometheus-adapter (accessed: 04.05.2026)
28. Power consumption: 150 W; NVIDIA Corporation. *GeForce RTX 5060 Ti Graphics Card – Specifications*; 2026. URL: https://www.nvidia.com/en-us/geforce/graphics-cards/rtx-5060-ti/ (accessed: 04.05.2026).
29. 20–30 FPS performance on the RTX 5060 Ti. *ONNX Runtime Performance Tuning*. Microsoft. URL: https://onnxruntime.ai/docs/performance/ (accessed on 04.05.2026). Note: Exact measurements for this map are not available in open sources; the link is to the optimization documentation to extrapolate the expected performance.
30. Traditional log aggregation systems (ELK). *Elastic Stack Documentation*; 2026. URL: https://www.elastic.co/guide/index.html (accessed 04.05.2026).

ADDITIONAL INFORMATION

The authors state that generative artificial intelligence technologies and technologies based on artificial intelligence were not used in the preparation of the article.

INFORMATION ABOUT THE AUTHORS

Konstantin Yu. Ustyuzhanin – Senior Lecturer, Department of Gas Chemistry and Modeling of Chemical and Technological Processes, Ufa State Petroleum Technological University, Ufa, Kosmonavtov str. 1, 450064, Republic of Bashkortostan, Russian Federation, ustyuzhanin.ky@gmail.com, https://orcid.org/0000-0003-0256-155X

Fairuza T. Ziganshina – Cand. Sci. (Phys.-Math.), Associate Professor, Department of Integrated Engineering and Computer Graphics, Ufa State Petroleum Technological University, Ufa, Kosmonavtov str. 1, 450064, Republic of Bashkortostan, Russian Federation, fairusa85@mail.ru, https://orcid.org/0009-0004-8627-5714

Regina R. Sadykova – Lecturer, Department of Integrated Engineering and Computer Graphics, Ufa State Petroleum Technological University, Ufa, Kosmonavtov str. 1, 450064, Republic of Bashkortostan, Russian Federation, umbaru@mail.ru, https://orcid.org/0000-0003-2967-882X

CONTRIBUTION OF THE AUTHORS

Konstantin Yu. Ustyuzhanin – scientific supervision; development of the concept and methodology of the research, analysis of the research results, writing the initial text of the article, drawing up the final conclusions.

Fayruza T. Ziganshina – processing and analysis of experimental data using machine learning methods, graphical and tabular presentation of the research results, writing the initial text of the article, drawing up the final conclusions.

Regina R. Sadykova – literature review, conducting experimental work, collecting and systematizing experimental data.

The authors declare no conflicts of interest.

The article was submitted 23.06.2026; approved after reviewing 01.10.2026; accepted for publication 06.10.2026.

ISSN 2075-8545 (online)

Nanotechnologies in construction
Нанотехнологии в строительстве

2026; 18 (5):
681–690

Nanobuild.ru

SYSTEM SOLUTIONS FOR TECHNOLOGICAL PROBLEMS

CC BY 4.0

Original article
https://doi.org/10.15828/2075-8545-2026-18-5-681-690

Inverse kinematics algorithm for trajectories with specified tool orientation

Petr A. Kulakov*, **Vitaly G. Afanasenko**
Ufa State Petroleum Technological University, Ufa, Kosmonavtov str. 1, 450064, Russian Federation
* Corresponding author: e-mail: kulakov.p.a@mail.ru

ABSTRACT

Introduction. During welding, coating application, and assembly or installation operations, the tool's position is specified in conjunction with its orientation. A single specified pose may correspond to various sets of manipulator joint angles, and the solutions obtained for individual points do not always form a continuous trajectory. In such cases, the transition from one point to another involves a sudden change in joint angles, a factor that must be taken into account when setting movement speeds. The trajectory is defined either by joint angles or by an array of Cartesian tool poses. In the latter case, the input data consists of coordinates and orientations derived from a CAD model, teach points, or an external planner. Calculating the trajectory from this data requires reconciling inverse kinematics solutions at adjacent points; in the algorithm under consideration, this is achieved by passing the calculated angles to the computation for the next point. **Methods and Materials.** The object of study is a six-link manipulator with six degrees of freedom. Joint angles were determined based on specified Tool Center Point (TCP) positions and orientations using the pseudoinverse of the numerical Jacobian matrix, while the orientation error component was calculated using ZYX Euler angles. The solution obtained for a given point served as the initial approximation for the subsequent point. Verification was performed using trajectories comprising varying numbers of points. **Results and Discussion.** The procedure for formulating the six-dimensional error, the Jacobian calculation, and the iteration termination criteria are presented. Position and orientation errors, iteration counts, and computation times were determined for trajectories consisting of 5, 10, and 20 points; trajectories with up to 50 points were also examined. Calculation results for an identical geometric trajectory showed average iteration counts per point of 28, 18, and 12, respectively. Utilizing the previous solution reduced the number of iterations and, in the tests conducted, enabled the maintenance of the selected solution branch. **Conclusion.** The developed algorithm enables the derivation of a sequence of manipulator joint angles from a set of tool positions and orientations. In the calculations performed, the transfer of the solution between adjacent points ensured smooth angular variation; however, this mechanism alone does not guarantee the avoidance of a solution branch switch for every possible trajectory. The algorithm's applicability is constrained by the convergence conditions of the numerical computation. When approaching a singular configuration or using sparse point spacing, it is necessary to additionally check the condition number of the Jacobian. Enhancing computational stability may require finer trajectory discretization and regularized pseudo-inversion.

KEYWORDS: six-link manipulator, inverse kinematics, trajectory tracking, Euler angles, numerical Jacobian, positioning error

SOURCES OF FUNDING FOR THE SCIENTIFIC WORK THAT RESULTED IN THE PUBLICATION: This work was conducted as part of the Strategic Project "New technologies, technical, and intelligent systems in mechanical engineering" of the Ufa State Petroleum Technological University Development Program for 2021–2030 in accordance with the Priority 2030 Strategic Academic Leadership Program.

ACKNOWLEDGEMENTS: The authors are grateful for the financial support of this project.

FOR CITATION:
Kulakov P.A., Afanasenko V.G. Inverse kinematics algorithm for trajectories with specified tool orientation. *Nanotechnologies in Construction.* 2026;18(5):681–690. https://doi.org/10.15828/2075-8545-2026-18-5-681-690. – EDN: BDBXER.

© Kulakov P.A., Afanasenko V.G., 2026

ISSN 2075-8545 (online)

Nanotechnologies in construction
Нанотехнологии в строительстве

2026; 18 (5):
681–690

Nanobuild.ru

SYSTEM SOLUTIONS FOR TECHNOLOGICAL PROBLEMS

Алгоритм обратной кинематики для траекторий с заданной ориентацией инструмента

Петр Алексеевич Кулаков*, Виталий Геннадьевич Афанасенко

Уфимский государственный нефтяной технический университет, 450064, Уфа, улица Космонавтов, 1, Российская Федерация

* Автор, ответственный за переписку: e-mail: kulakov.p.a@mail.ru

АННОТАЦИЯ

Введение. При сварке, нанесении покрытий и выполнении сборочных и монтажных операций положение инструмента задается совместно с его ориентацией. Одной заданной позе могут соответствовать различные наборы углов в суставах манипулятора, причем решения, полученные для отдельных точек, не всегда образуют непрерывную траекторию. В таком случае переход от одной точки к другой сопровождается скачком углов, что необходимо учитывать при задании скоростей движения. Траекторию задают углами в суставах либо массивом декартовых поз инструмента. Во втором случае исходными данными служат координаты и ориентации, полученные по CAD-модели, точкам обучения или от внешнего планировщика. Для расчета по этим данным требуется согласовать решения обратной кинематики в соседних точках; в рассматриваемом алгоритме это выполняется за счет передачи найденных углов в расчет следующей точки. **Материалы и методы.** Объектом исследования является шестизвенный манипулятор с шестью степенями свободы. По заданным положениям и ориентациям TCP определялись углы в суставах с использованием псевдообратной матрицы численного якобиана, а ориентационная часть ошибки рассчитывалась по углам Эйлера ZYX. Начальным приближением для каждой последующей точки служило решение, полученное на предыдущей. Проверка проведена для траекторий с различным числом точек. **Результаты и обсуждение.** Приведены порядок формирования шестимерной ошибки, расчет якобиана и условия завершения итераций. Для траекторий из 5, 10 и 20 точек определены ошибки положения и ориентации, число итераций и время расчета; дополнительно рассмотрены траектории до 50 точек. По данным расчетов для одинаковой геометрической траектории среднее число итераций на точку составило 28, 18 и 12 соответственно. Использование предыдущего решения уменьшало число итераций, а в рассмотренных тестах позволяло сохранять выбранную ветвь решения. **Выводы.** Разработанный алгоритм позволяет по массиву положений и ориентаций инструмента получить последовательность углов в суставах манипулятора. В проведенных расчетах передача решения между соседними точками обеспечивала плавное изменение углов, однако сама по себе не исключает смену ветви решения при любой траектории. Область применения алгоритма ограничивается условиями сходимости численного расчета. При приближении к сингулярной конфигурации или при редком задании точек необходима дополнительная проверка числа обусловленности якобиана. Для повышения устойчивости расчета могут потребоваться более плотная дискретизация траектории и регуляризованное псевдообращение.

КЛЮЧЕВЫЕ СЛОВА: шестизвенный манипулятор, обратная кинематика, движение по траектории, углы Эйлера, численный якобиан, ошибка позиционирования

ИСТОЧНИКИ ФИНАНСИРОВАНИЯ НАУЧНОЙ РАБОТЫ, РЕЗУЛЬТАТОМ КОТОРОЙ СТАЛА ПУБЛИКАЦИЯ: Работа проводилась в рамках реализации Стратегического проекта «Новые технологии, технические и интеллектуальные системы в машиностроении» программы развития ФГБОУ ВО «Уфимский государственный нефтяной технический университет» на 2021–2030 годы в соответствии с программой стратегического академического лидерства «Приоритет 2030».

БЛАГОДАРНОСТИ: Авторы выражают благодарность за финансовую поддержку проекта.

ДЛЯ ЦИТИРОВАНИЯ:
Кулаков П.А., Афанасенко В.Г. Алгоритм обратной кинематики для траекторий с заданной ориентацией инструмента. *Нанотехнологии в строительстве.* 2026;18(5):681–690. https://doi.org/10.15828/2075-8545-2026-18-5-681-690. – EDN: BDBXER.

INTRODUCTION

Controlling a manipulator along a trajectory requires specifying the tool's position and orientation at each point. This approach is used in seam welding, coating application, assembly, and gripper positioning. For a single target pose, inverse kinematics yields one or more sets of joint angles. During continuous motion, it is necessary to select solutions that avoid configuration jumps and exceedance of permissible joint speeds [2–5].

Trajectory problems are solved in either joint space or cartesian space [2–4]. In the former case, joint angles are specified as functions of time, while the TCP position and orientation are determined via forward kinematics. In the latter case, a sequence of target poses is defined, and the inverse kinematics problem is solved for each pose.

ISSN 2075-8545 (online)

Nanotechnologies in construction
Нанотехнологии в строительстве

2026; 18 (5):
681–690

This approach is advantageous when the trajectory is derived from a CAD model, teach points, or data from an external planner. However, using an arbitrary initial guess can cause the algorithm to switch to a different solution branch. This results in discontinuities in the joint angle sequence, complicating time-based interpolation [3, 4, 11, 12]. In this study, the solution obtained for the previous point is used for the next point; with a sufficiently small step size, this technique preserves the selected solution branch [2–4].

For a given pose, inverse kinematics can be calculated using the Jacobian pseudoinverse, the Jacobian transpose, or the regularized least-squares method [5–9, 16]. Positional error is defined by the difference in Cartesian coordinates. Euler angles, axis-angle representation, quaternions, or a rotation vector can be used for orientation [7–10]. The algorithm's convergence and behavior near singular configurations depend on the chosen representation. In the algorithm under consideration, orientation error is defined using ZYX Euler angles, and the numerical Jacobian is calculated via the finite difference method.

The influence of the sampling step on the continuity of joint coordinates is discussed in [3, 4, 11–15]. When poses are specified at sparse intervals, the solution for a given point may not be sufficiently close to the solution for the subsequent point, causing the difference $q_{i+1} - q_i$ to increase. This constraint is particularly significant near singularities, during a switch between solution branches, and when there is a substantial change in tool orientation. Therefore, the step size between points is selected based on changes in position and orientation, rather than solely on the number of trajectory nodes. The initial trajectory is represented as an array of target poses obtained from teaching points or an external planner [3, 4, 11, 12].

The study utilized the kinematic model of the STP3 project [17], for which the forward kinematics, a numerical Jacobian, and an inverse kinematics algorithm for a single pose had previously been derived. The objective was to develop and validate a trajectory calculation algorithm based on specified TCP positions and orientations. The algorithm takes an array of target poses as input and generates a sequence of joint angles as output. To achieve this goal, continuity conditions were formulated, a method for specifying orientation was selected, convergence criteria were defined, and calculations were performed for 5, 10, 20, and 50 points.

A six-link manipulator is considered, the kinematics of which are defined by Denavit-Hartenberg parameters. The model corresponds to an anthropomorphic manipulator with revolute shoulder, elbow, and wrist joints. Parameter values are provided in [17]. Forward kinematics defines the mapping $q \to T_0^6(q)$, where $T_0^6(q)$ is a 4×4 homogeneous matrix of the form $[R(q)\ p(q);\ 0\ 1]$, $q \in \mathbb{R}^6$ is the vector of joint angles, $p(q) \in \mathbb{R}^3$ is the TCP position, and $R(q) \in SO(3)$ is the tool orientation matrix [1–5, 17]. For a given pose $T_d = (R_d, p_d)$, it is necessary to determine a vector q^* satisfying the conditions $\| p(q^*) - p_d \| \leqslant \varepsilon_p$ and $\rho(R(q^*), R_d) \leqslant \varepsilon_R$. The quantity $\rho(\cdot,\cdot)$ characterizes the orientation mismatch.

An array of positions $p_i \in \mathbb{R}^3$ and an array of orientations $R_i \in SO(3)$, $i = 1, \ldots, N$ are given. The objective is to determine a sequence of joint angles $q_i \in \mathbb{R}^6$, $i = 1, \ldots, N$, such that, for each i, the matrix $T_0^6(q_i)$ corresponds to the specified pose $T_i = (R_i | p_i)$ within a prescribed tolerance. The differences $\| q_{i+1} - q_i \|$ between consecutive points must not result in exceeding permissible joint velocities and accelerations during time-based interpolation [2–4, 11, 12]. The initial guess for point $i + 1$ is set to the solution obtained for the previous point: $q_0^{(i+1)} = q_i$.

The orientation is defined by Euler angles in the ZYX convention, which are subsequently used to construct a six-dimensional error vector:

$$R = R_z(\psi) R_y(\theta) R_x(\phi),\ \eta = (\phi, \theta, \psi)^T.$$

Taking into account the positional and orientational components, an error vector is obtained

$$e = \begin{pmatrix} p_d - p(q) \\ \eta_d - \eta(q) \end{pmatrix}.$$

The first three components characterize the position error, while the last three characterize the orientation error [7–10]. This representation is used when constructing the numerical Jacobian. Special handling of the angles is required in the vicinity of gimbal lock.

It is assumed that the target poses are reachable and not located in the immediate vicinity of singular configurations. If this condition is violated, the Jacobian becomes ill-conditioned, the number of iterations increases, and a small change in the target pose can cause a significant change in the angles [5–9, 16]. Therefore, alongside solving the inverse problem, it is necessary to monitor the stability of the calculation and select an appropriate trajectory step size.

METHODS

The calculation is performed sequentially for points $i = 1, \ldots, N$, with an internal iterative calculation carried out for each point. For $i = 1$, the initial approximation $q_0^{(1)}$ is set as either the zero configuration or a known configuration close to the first target pose. For the remaining points – that is, for $i \geqslant 2$ the previously obtained solution is used:

$$q_0^{(i)} = q^*_{i-1},$$

where the initial approximation is set equal to the result from the previous point. At iteration k, we first deter-

ISSN 2075-8545 (online)

Nanotechnologies in construction
Нанотехнологии в строительстве

2026; 18 (5):
681–690

mine the current pose $T_0^6(q_k)$ and the error e_k, then find the numerical Jacobian $J(q_k)$ and the increment

$$\Delta q = J^+(q_k)e_k.$$

After determining the increment, the angles are refined using the formula

$$q_{k+1} = q_k + \lambda \Delta q.$$

The iterative calculation terminates when $\| e_k \| < \varepsilon$ or after the specified number of iterations N_{max} is reached [5–9, 16].

The ZYX Euler angles (ϕ, θ, ψ) required to calculate the orientation error are determined from the rotation matrix $R \in SO(3)$. When writing

$$R = R_z(\psi)R_y(\theta)R_x(\phi)$$

the inverse transformation can be performed using the formulas

$$\theta = \text{atan2}\left(-r_{31}, \sqrt{r_{11}^2 + r_{21}^2}\right);$$

$$\phi = \text{atan2}\left(\frac{r_{32}}{\cos\theta}, \frac{r_{33}}{\cos\theta}\right);$$

$$\psi = \text{atan2}\left(\frac{r_{21}}{\cos\theta}, \frac{r_{11}}{\cos\theta}\right)$$

provided that $\cos\theta \neq 0$ [9, 10]. Special handling is applied in the vicinity of gimbal lock, and the resulting angles are mapped to the interval $[-\pi, \pi]$. These same angles are used in the six-dimensional error vector and in the calculation of the numerical Jacobian.

The Jacobian $J(q) \in \mathbb{R}^{6\times6}$ relates the increment in angles Δq to the increment of the "position + orientation" state vector:

$$\Delta x \approx J(q)\Delta q.$$

The i-th column of the matrix is calculated using the finite difference.

$$J_{:,i}(q) \approx \frac{f(q + \delta e_i) - f(q)}{\delta},$$

where $f(q)$ contains the three TCP coordinates and three Euler angles, e_i is a unit vector, and $\delta = 10^{-6}$ rad [5, 6]. Next, we compute the pseudoinverse matrix J^+ using scipy.linalg.pinv or an equivalent SVD procedure. Using this matrix, we determine the increment $\Delta q = J^+e$ that minimizes the residual norm $\| J\Delta q - e \|_2$.

In the implementation used, the condition number cond(J) is not automatically monitored. When cond(J) $> 10^5$, standard pseudoinversion should be replaced by a regularized damped least squares scheme.

$$J_\mu^+ = (J^T J + \mu I)^{-1} J^T,$$

where $\mu > 0$ is the regularization parameter [7–9, 16]. Regularization limits the increment Δq when the singular values of the Jacobian decrease.

Convergence is determined based on the error norm $\| e \|$. The threshold ε combines the positional component (in meters) and the orientational component (in radians). If the required accuracy is not achieved after N_{max} iterations, the calculation can be repeated using a different initial guess or a regularized pseudoinverse [5–9]. In the developed script, the parameter λ remains constant. For a point where convergence is not achieved, a warning is issued, and the value q_i is set equal to the previous solution q_{i-1}. This prevents a large increment from propagating to subsequent points, although it increases the error at the node in question.

At each step, forward kinematics, error generation, Jacobian calculation, increment determination, and stopping criterion check are performed. In Figure 1 shows the sequence of operations and shows the transfer of the result of the previous point as an initial approximation.

The step size determines what fraction of the calculated increment is used to refine the angles. If the matrix J is well-conditioned, the increment is fully utilized when $\lambda = 1$; however, in the presence of a large initial mismatch, such a step may lead to oscillations in the solution. To limit the step size, values of $\lambda \in [0.5, 1]$ are considered, or the coefficient is made dependent on the current error:

$$\lambda = \min\left(1, \frac{\lambda_0}{\| e \|}\right),$$

where λ_0 is the base coefficient for step-size selection [5–9]. A different approach was adopted for the calculations: a value of $\lambda = 0.7$ was selected based on preliminary

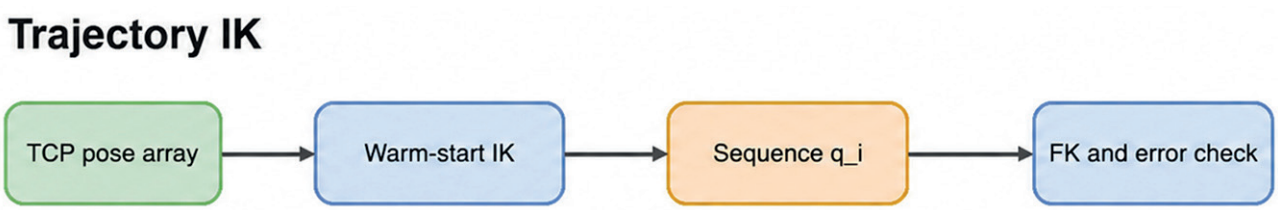


Fig. 1. Block diagram of the IK algorithm for the trajectory

ISSN 2075-8545 (online)

tests and used for all iterations. The relationship shown illustrates a possible method for varying λ; however, adaptive step-size selection was not implemented in the version tested.

When formulating the error vector $e \in \mathbb{R}^6$, there are three positional components (expressed in meters) and three orientation components (expressed in radians). In the calculation model, these are included in the combined vector without additional weighting coefficients:

$$e = \begin{pmatrix} e_p \\ e_\eta \end{pmatrix}.$$

With this calculation, the overall norm depends on the chosen units for position and orientation. If the permissible orientation mismatch differs from the positional requirement, the influence of the angular component can be adjusted by introducing a weighting factor:

$$e = \begin{pmatrix} e_p \\ w_\eta e_\eta \end{pmatrix},$$

where $w_\eta \approx 0.1 \ldots 0.2$ [7–10]. Separate tolerances can also be specified: ε_p for position and $\varepsilon_\eta \approx 10^{-4}$ rad for orientation, with $w_\eta = 1$. In this case, the convergence condition is expressed as $\| e \| \leq \sqrt{\varepsilon_p^2 + \varepsilon_\eta^2}$. The error on the order of 10^{-8} rad observed in experiments allows for the use of separate criteria without imposing stricter requirements on the solver.

Several iterations are performed for a single point. In each iteration, forward kinematics, a numerical Jacobian, and a 6×6 pseudoinverse matrix are calculated. The greatest computational cost is associated with the numerical Jacobian, as its construction requires six additional forward kinematics calculations. The total time can be estimated by the expression

$$T_{\text{total}} \sim N_{\text{точек}} \cdot \overline{N}_{\text{iter}} \cdot T_{\text{iter}},$$

where $\overline{N}_{\text{iter}}$ is the average number of iterations per point, and T_{iter} is the time for a single iteration [3–6, 14, 15]. To reduce computation time, an analytical Jacobian, the storage of intermediate matrices, and compiled linear algebra libraries can be employed. In the algorithm under consideration, the initial approximation obtained at the previous point reduces computational cost by decreasing the number of iterations.

Figure 1 shows the data flow from the array of TCP poses to the array of joint angles. This scheme corresponds to the sequence of operations in the algorithm's software implementation.

Calculations were performed in a Python 3 environment using the kinematic model described in [17]. The script `ik_trajectory.py` utilized functions for forward kinematics, the numerical Jacobian, and the inverse kinematics solution for a single pose. Coordinates were specified in meters, and angles in radians.

Three scenarios were considered. In the first case, the trajectory consisted of five points located along a straight line segment within the workspace; the tool orientation remained constant. In the second case, ten points were defined along an arc in the x–y plane at a constant height, with the orientation either remaining constant or changing to align with the direction of motion. The third scenario involved twenty points with a uniform change in position and a rotation of the orientation around the vertical axis.

For each scenario, the following parameters were determined: the number of iterations, the position error $\| p(q_i) - p_i \|$, the orientation error based on the difference in Euler angles, and the total computation time for the sequence $q_1, \ldots, q_N$ [3–9, 11, 12]. Trajectory smoothness was evaluated based on the change in angles between adjacent points.

The calculations utilized a convergence threshold of $\varepsilon = 10^{-6}$, a maximum iteration count of $N_{\max} = 100$, and a step coefficient of $\lambda = 0.7$. The value $\lambda = 0.7$ was selected based on preliminary tests; λ remained constant thereafter – meaning no adaptive step-size adjustment was applied. For the first point, the initial approximation was set to the zero configuration $q_0 = (0,0,0,0,0,0)$, while the solution from the previous point was used for each subsequent point. No additional weighting factors for orientation error were introduced.

Calculations were performed on Windows 10 using Python 3.8 and the NumPy, SciPy, and Matplotlib libraries. The total trajectory computation time (excluding visualization) was measured using the time.perf_counter function. Based on the results, the TCP trajectory and plots showing position error and joint angle changes were generated.

Additionally, points at the boundary of the workspace and small pose variations relative to a previously obtained solution were tested. With small pose variations, the number of iterations decreased. Calculations were performed for a single geometric trajectory using $N = 5, 10, 20, 50$. As the number of nodes increased, the average number of iterations per point decreased. At $N = 50$, the total time was 1–2 seconds, making the algorithm suitable for offline planning.

For a trajectory consisting of 15 points, a 30° orientation rotation around the z-axis was specified. The resulting sequence q_i was continuous, and the error did not exceed the established threshold. When the same extended segment was defined by only three points, a solution branch switch occurred in one of the calculations, resulting in a jump in joint angles. For trajectories of 10 and 20 points, the condition number cond(J) remained within the range of 8–12. At certain nodes of the 5-point trajectory, however, it reached higher values. Consequently, the density of pose specification significantly influences the algorithm's performance [2–4, 11, 12].

ISSN 2075-8545 (online)

RESULTS

The convergence condition was met for five points. The highest number of iterations was required for the first point, for which the zero configuration was used. According to Table 1, the average number of iterations for this trajectory was also the highest. The position error did not exceed 10^{-7} m or 10^{-4} mm (Fig. 2). The resulting TCP trajectory matches the target trajectory within the specified accuracy, and the joint angles vary smoothly [5–10] (Fig. 3).

As the number of points increased, the average number of iterations decreased from 28 at $N = 5$ to 18 at $N = 10$ and to 12 at $N = 20$ (Table 1). Position and orientation errors did not exceed the specified threshold. The computation time for 20 points allows the algorithm to be used for offline planning (Fig. 4). Operation at a frequency of 100–500 Hz would require an analytical Jacobian or

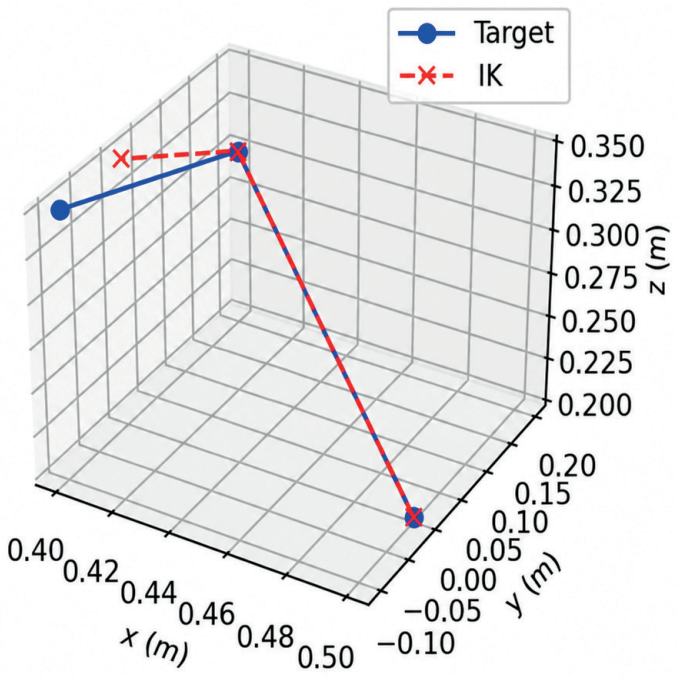


Fig. 2. Target and actual TCP trajectory in 3D (5 points)

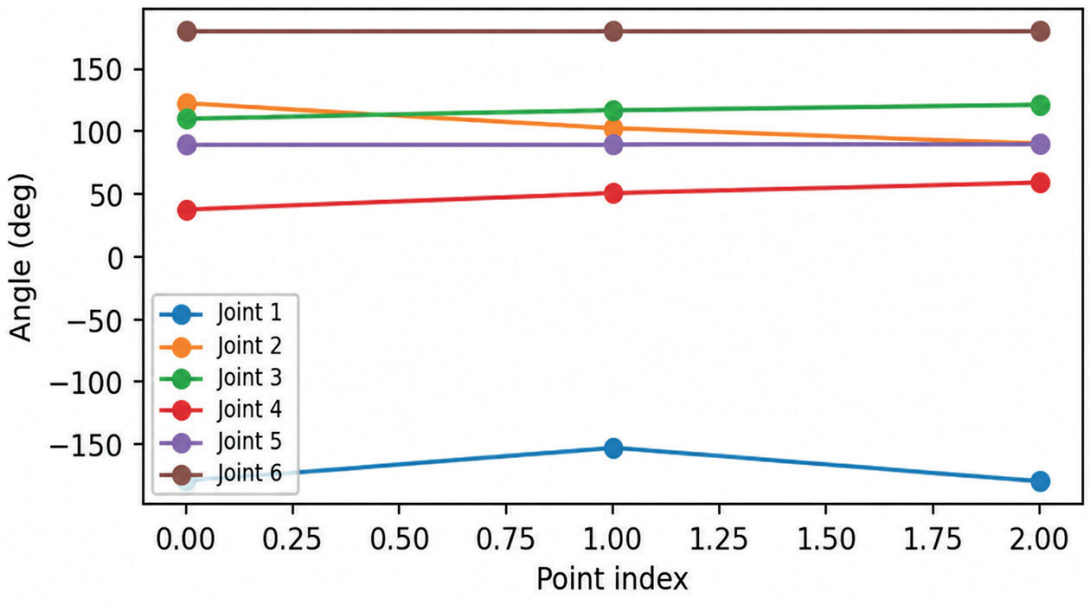


Fig. 3. Joint angles based on trajectory points

ISSN 2075-8545 (online)

Table 1. Number of iterations and inverse kinematics computation time for the trajectory

N points	Average number of iterations per point	Max. iterations per point	Total time (ms)
5	28	45	180
10	18	35	220
20	12	28	320

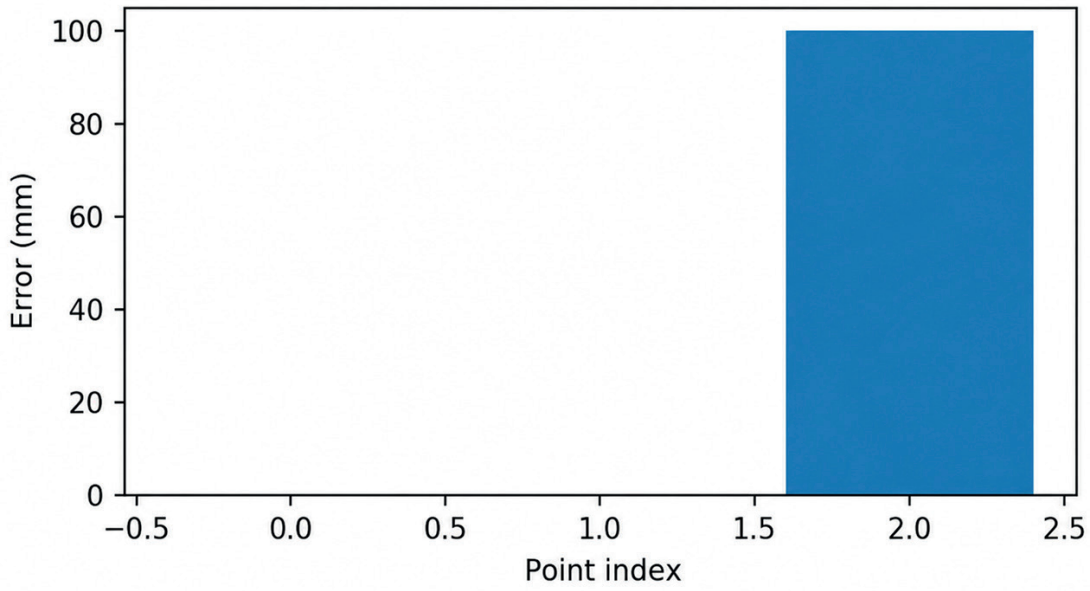


Fig. 4. Positioning error along trajectory points (mm)

a faster implementation of the computational operations [3–8, 14–16].

For a trajectory consisting of 10 points, the position error did not exceed 10^{-7} m or 10^{-4} mm. This value is smaller than the relevant manufacturing tolerances; therefore, in practical application, accuracy will be determined by the kinematic model, calibration, and specified tolerances.

A comparison was made with a calculation in which a zero initial guess was specified for each point (Fig. 5). In that case, the number of iterations increased, and a switch to a different solution branch could occur. Using the previous result reduced the average number of iterations by a factor of 2–3 and eliminated discontinuities in the trajectories under consideration (Table 1). Thus, the initial guess affects both the computation time and the continuity of joint coordinates [2–4, 7–9].

The number of iterations and the computation time for a single geometric trajectory were compared across different discretization levels (Table 1). As N increases, adjacent target poses become closer to one another; consequently, the previously found solution requires fewer refinements when transitioning to the next point.

Table 1 shows that the average time per point decreases from 36 ms for a 5-point trajectory to 16 ms for a 20-point trajectory. At the same time, the total computation time increases from 180 to 320 ms: the reduction in the number of iterations per point does not compensate for the increase in the number of points themselves.

Based on the calculation results, the discretization step should be selected by taking into account the changes in position and orientation between adjacent poses. When approaching a singularity, the condition number should be monitored, and a switch made to regularized pseudoinversion. For trajectories consisting of 10 and 20 points, cond(J) remained moderate, whereas poor conditioning was observed at specific nodes of the 5-point trajectory. If orientation requirements are less stringent than position requirements, one can maintain $w_\eta = 1$, set a tolerance of $\varepsilon_\eta \approx 10^{-4}$ rad, and use the criterion $\| e \| \leq \sqrt{\varepsilon_p^2 + \varepsilon_\eta^2}$. The algorithm is designed for offline trajectory generation and can be implemented as part of a planning module [3, 4, 7–9, 11–16].

The algorithm was developed using engineering control of solution continuity, orientation representation via Euler angles, monitoring of singular configurations, and regularized pseudoinversion. The combination of these methods aligns with the Russian and international approaches discussed previously [2–9, 16].

ISSN 2075-8545 (online)

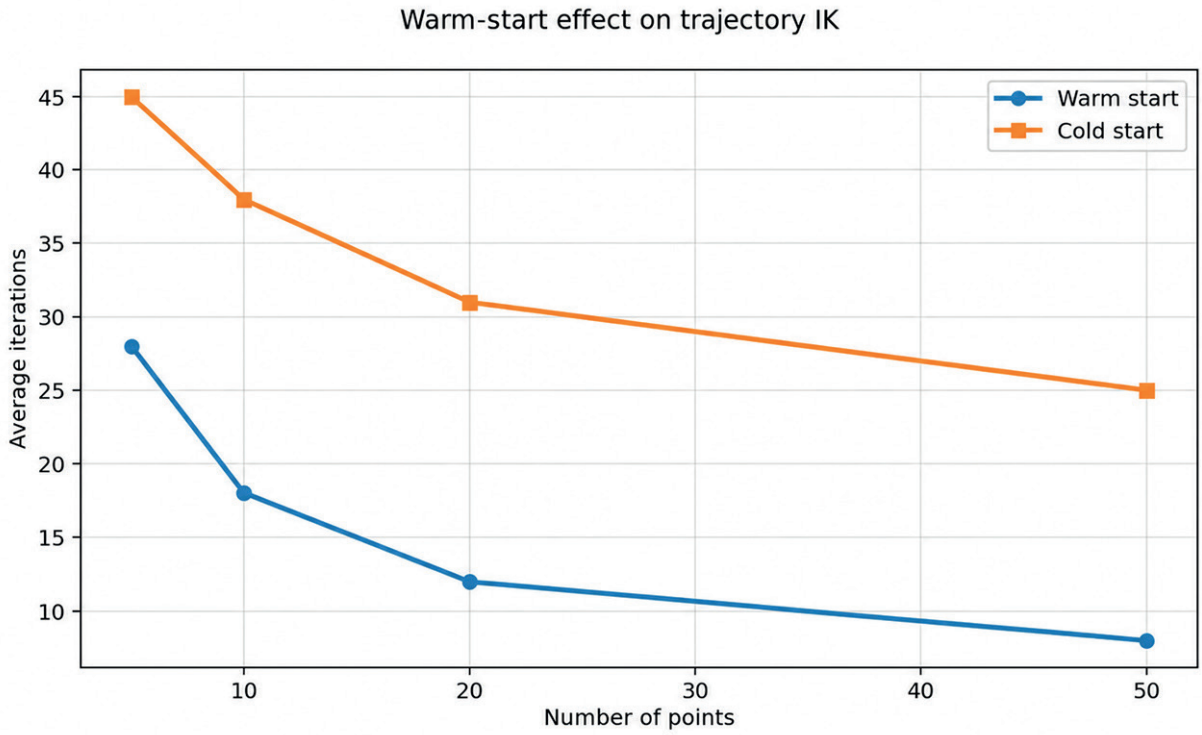


Fig. 5. Comparison of warm start and zero-order approximation

Table 2. Russian and foreign views on trajectory inverse kinematics

Criterion	Russian practice	International practice
Primary focus	Solution continuity and engineering resilience	Warm start, branch consistency, task-space pipelines
Representation of orientation	More often Euler angles and matrix description	Euler, quaternion, axis-angle
Primary risk	Switch solution branch	Loss of continuity near singularity
Typical sources	Robotics training courses and engineering manuals	Craig, Siciliano, Buss, Wampler

CONCLUSION

An inverse kinematics algorithm is proposed for trajectories with specified tool orientation, utilizing the solution from the preceding point as the initial approximation. For the trajectories analyzed, this computational approach ensured continuity of joint coordinates and reduced the number of iterations. By employing the pseudoinverse of the numerical Jacobian and ZYX Euler angles, a positional error on the order of 10^{-7} m was achieved with a threshold of $\varepsilon = 10^{-6}$ [5–10].

Convergence conditions deteriorate as the system approaches a singular configuration; furthermore, if poses are defined sparsely, a switch in the solution branch may occur even when using the previous result. For trajectories consisting of 10 and 20 points, the condition number remained moderate, whereas an increase was observed at specific nodes of a 5-point trajectory. These results highlight the need to monitor cond(J), refine the discretization step, and apply regularization when signs of instability arise [7–9, 16].

The algorithm enables the determination of joint coordinates based on Cartesian poses specified by an operator or a CAD system, thereby reducing the manual effort required for trajectory definition. Future research could focus on incorporating joint constraints, avoiding singular configurations, utilizing an analytical Jacobian, and validating the algorithm on a physical manipulator [3, 4, 11–17].

ISSN 2075-8545 (online)

REFERENCES

1. Denavit J., Hartenberg R. S. A kinematic notation for lower-pair mechanisms based on matrices. *Journal of Applied Mechanics*. 1955;22:215–221. https://doi.org/10.1115/1.4011045

2. Craig J. J. *Introduction to Robotics: Mechanics and Control*. 3rd ed. Boston: Pearson; 2005.

3. Siciliano B., Sciavicco L., Villani L., Oriolo G. Robotics: *Modelling, Planning and Control*. London: Springer; 2009. https://doi.org/10.1007/978-1-84628-642-1

4. Lynch K. M., Park F. C. *Modern Robotics: Mechanics, Planning, and Contro*l. Cambridge: Cambridge University Press; 2017. https://doi.org/10.1017/9781316661239

5. Spong M. W., Hutchinson S., Vidyasagar M. *Robot Modeling and Control*. New York: Wiley; 2006.

6. Murray R. M., Li Z., Sastry S. S. *A Mathematical Introduction to Robotic Manipulation*. Boca Raton: CRC Press; 1994. https://doi.org/10.1201/9781315136370

7. Wampler C. W. Manipulator inverse kinematic solutions based on vector formulations and damped least-squares methods. *IEEE Transactions on Systems, Man, and Cybernetics*. 1986;SMC-16(1):93–101. https://doi.org/10.1109/TSMC.1986.289285

8. Chiaverini S. Singularity-robust task-priority redundancy resolution for real-time kinematic control of robot manipulators. *IEEE Transactions on Robotics and Automation*. 1997;13(3)398–410. https://doi.org/10.1109/70.585902

9. Buss S. R. *Introduction to Inverse Kinematics with Jacobian Transpose, Pseudoinverse and Damped Least Squares Methods*. 2004. URL: http://www.math.ucsd.edu/~sbuss/ResearchWeb/ikmethods/ikmethods.pdf (accessed: 21.04.2026).

10. Kuipers J. B. *Quaternions and Rotation Sequences*. Princeton: Princeton University Press; 1999. https://doi.org/10.1515/9780691211701

11. LaValle S. M. *Planning Algorithms*. Cambridge: Cambridge University Press; 2006. https://doi.org/10.1017/CBO9780511546877

12. Latombe J.-C. *Robot Motion Planning*. Boston: Kluwer Academic Publishers; 1991. https://doi.org/10.1007/978-1-4615-4022-9

13. Khatib O. Real-time obstacle avoidance for manipulators and mobile robots. *The International Journal of Robotics Research*. 1986;5(2):90–98. https://doi.org/10.1177/027836498600500106

14. Yoshikawa T. Dynamic and kinematic redundancy of robot manipulators. *Journal of Robotic Systems*. 1985;2(1):83–93. https://doi.org/10.1177/027836498500400201

15. Slotine J.-J. E., Li W. *Applied Nonlinear Control*. Englewood Cliffs: Prentice Hall; 1991.

16. Siciliano B. Handling robot inverse kinematics with redundancy and singularity robustness. *Advanced Robotics*. 2010;24(7-8):1021–1038. https://doi.org/10.1163/016918610X493592

17. Kinematic model of a 6-DOF manipulator based on Denavit-Hartenberg parameters: forward and inverse kinematics. *STP3 project internal preprint (paper St1)*. 2026.

ADDITIONAL INFORMATION

Automated language editing tools were used in the preparation of the manuscript. The scientific formulation, calculations, analysis of results, and final review of the text were performed by the authors.

INFORMATION ABOUT THE AUTHORS

Petr A. Kulakov – Cand. Sci. (Eng.), Associate Professor, Department of Machine Design and Mechanics, Ufa State Petroleum Technological University, Ufa, Kosmonavtov str. 1, 450064, Republic of Bashkortostan, Russian Federation, kulakov.p.a@mail.ru; https://orcid.org/0000-0003-1402-1366

Afanasenko Vitaly Gennadyevich – Cand. Sci. (Eng.), Head of the Department of Machine Design and Mechanics, Ufa State Petroleum Technological University, Ufa, Kosmonavtov str. 1, 450064, Republic of Bashkortostan, Russian Federation, afanasenko.v.g@yandex.ru; https://orcid.org/0000-0002-4349-1925

ISSN 2075-8545 (online)

CONTRIBUTION OF THE AUTHORS

P.A. Kulakov – scientific supervision, development of research concept and methodology, analysis of research results, writing the article, formulation of final conclusions.

V.G. Afanasenko – data editing and processing, preparation and drafting of the article's conclusions.

The authors declare no conflicts of interest.

The article was submitted 30.06.2026; approved after reviewing 02.10.2026; accepted for publication 07.10.2026.

ISSN 2075-8545 (online)

Nanotechnologies in construction
Нанотехнологии в строительстве

2026; 18 (5):
691–700

Nanobuild.ru

SYSTEM SOLUTIONS FOR TECHNOLOGICAL PROBLEMS

Review article
https://doi.org/10.15828/2075-8545-2026-18-5-691-700

CC BY 4.0

Choice of a method for assessing the depth of the tempered layer in a martensitic steel welded joint

Airat M. Fayrushin, Elena Yu. Tumanova, Alexander S. Sobachkin, Marcel F. Imayev, Andrey S. Tokarev*, Diana R. Musina

Ufa State Petroleum Technological University, Ufa, Kosmonavtov str. 1, 450064, Russian Federation

* Corresponding author: e-mail: andrewtok07@gmail.com

ABSTRACT

Introduction. This review considers the choice of a nondestructive testing method for estimating the depth of the tempered martensitic layer in welded joints of martensitic steel pipes after high-temperature tempering. During heat treatment of welded joints, martensite does not always decompose through the entire weld thickness, especially in the root zone of thick-walled pipes, and averaged characteristics may conceal local areas of increased hardness and brittleness. **Methods and Materials.** Four groups of methods were compared: eddy current testing, magnetic Barkhausen noise analysis, ultrasonic methods and magnetic coercimetry. For each group, the depth from which the signal carries information about the structural-phase state and nanoscale features of the weld metal was assessed. **Results.** Eddy current and Barkhausen methods mainly characterize the surface and near-surface layer. Ultrasonic methods can probe deeper layers, but when the acoustic contrast between structures is weak, the tempered-layer boundary is difficult to identify from the backscattered signal, and the results are difficult to interpret. Coercimetry was chosen for field conditions. Interchangeable attached U-shaped electromagnets of different sizes magnetize the metal to different depths, which makes it possible to construct a conditional layer-by-layer magnetic profile. **Discussion.** It is proposed to select transducers, construct calibration curves on welded specimens, and check the transformed-layer thickness estimate by metallography, microhardness testing and, if necessary, X-ray diffraction. **Conclusion.** The resulting layer-by-layer profile is conditional. Depth estimation requires calibration for the specific steel grade and welding technology, with allowance for residual stresses and transducer orientation. Pipe inspection also requires allowance for lift-off, surface curvature and weld reinforcement.

KEYWORDS: nondestructive testing, martensitic steel, welded joint, high-temperature tempering, coercimetry, coercive force, magnetic testing, nanoscale structural state

SOURCES OF FUNDING FOR THE SCIENTIFIC WORK THAT RESULTED IN THE PUBLICATION: This research was funded by the Ministry of Science and Higher Education of the Russian Federation "PRIORITY 2030" (National Project "Science and University").

FOR CITATION:
Fayrushin A.M., Tumanova E.Yu., Sobachkin A.S., Imayev M.F., Tokarev A.S., Musina D.R. Choice of a method for assessing the depth of the tempered layer in a martensitic steel welded joint. *Nanotechnologies in Construction*. 2026;18(5):691–700. https://doi.org/10.15828/2075-8545-2026-18-5-691-700. – EDN: CQGODM.

Выбор методики оценки глубины отпущенного слоя сварного шва мартенситной стали

Айрат Миннуллович Файрушин, Елена Юрьевна Туманова, Александр Сергеевич Собачкин, Марсель Фаниревич Имаев, Андрей Сергеевич Токарев*, Диана Рафаилевна Мусина

Уфимский государственный нефтяной технический университет, 450064, Уфа, ул. Космонавтов, 1, Российская Федерация

* Автор, ответственный за переписку: e-mail: andrewtok07@gmail.com

© Fayrushin A.M., Tumanova E.Yu., Sobachkin A.S., Imayev M.F., Tokarev A.S., Musina D.R., 2026

ISSN 2075-8545 (online)

Nanotechnologies in construction
Нанотехнологии в строительстве

2026; 18 (5):
691–700

Nanobuild.ru

SYSTEM SOLUTIONS FOR TECHNOLOGICAL PROBLEMS

АННОТАЦИЯ

Введение. В обзоре рассмотрен выбор методики неразрушающего контроля глубины отпущенного мартенситного слоя в сварных швах труб из сталей мартенситного класса после высокого отпуска. При термической обработке сварных соединений распад мартенсита не всегда проходит по всей толщине шва, особенно в корневой зоне толстостенных труб, а усредненные характеристики могут скрывать локальные участки с повышенной твердостью и хрупкостью. **Методы и материалы.** Сравнивали четыре группы методов: вихретоковый контроль, анализ магнитного шума Баркгаузена, ультразвуковые методы и магнитную коэрцитиметрию. Для каждой оценивали, с какой глубины сигнал несет информацию о структурно-фазовом состоянии и наносостоянии металла шва. **Результаты.** Вихретоковый и баркгаузеновский методы дают сведения в основном о поверхности и приповерхностном слое. Ультразвуковые методы позволяют исследовать более глубокие слои, однако при слабом акустическом контрасте структур выделить границу отпущенного слоя по обратнорассеянному сигналу сложно, а интерпретация результатов затруднена. Для полевых условий выбрана коэрцитиметрия. Сменные приставные П-образные электромагниты разного размера промагничивают металл на разную глубину, что позволяет построить условный послойный магнитный профиль. **Обсуждение.** Предложено подбирать преобразователи, строить градуировочные зависимости на сварных образцах, а оценку толщины превращенного слоя проверять металлографией и по микротвердости, при необходимости рентгеноструктурным анализом. **Заключение.** Получаемый послойный профиль условен. Для оценки глубины нужна градуировка под конкретную сталь и технологию сварки с учетом остаточных напряжений и ориентации преобразователя. При контроле труб учитывают также зазор, кривизну поверхности и усиление шва.

КЛЮЧЕВЫЕ СЛОВА: неразрушающий контроль, мартенситная сталь, сварной шов, высокий отпуск, коэрцитиметрия, коэрцитивная сила, магнитный контроль, наноструктурное состояние

ИСТОЧНИКИ ФИНАНСИРОВАНИЯ НАУЧНОЙ РАБОТЫ, РЕЗУЛЬТАТОМ КОТОРОЙ СТАЛА ПУБЛИКАЦИЯ: Работа выполнена при финансовой поддержке Министерства науки и высшего образования Российской Федерации в рамках программы «Приоритет-2030» (национальный проект «Наука и университеты»).

ДЛЯ ЦИТИРОВАНИЯ:
Файрушин А.М., Туманова Е.Ю., Собачкин А.С., Имаев М.Ф., Токарев А.С., Мусина Д.Р. Выбор методики оценки глубины отпущенного слоя сварного шва мартенситной стали. *Нанотехнологии в строительстве.* 2026;18(5):691–700. https://doi.org/10.15828/2075-8545-2026-18-5-691-700. – EDN: CQGODM.

INTRODUCTION

Martensitic-grade steel pipes are widely used in the oil and gas industry. Domestically produced pipes range from 11 to 550 mm in diameter, while wall thicknesses range from 1.5 to 40 mm depending on the forming process (cold or hot) and the applicable standard [1]. Pipes of this class – most commonly grades 15Kh5M, 20Kh13, 15Kh11MF, and 12Kh11V2MF – are manufactured by a seamless process and used under severe service conditions in petroleum refining (cracking furnace tubes), the chemical industry, and well construction involving highly corrosive fluids [1, 2, 3]. During cooling after fusion welding, a martensitic structure forms in the weld metal. Because martensite is brittle, high-temperature tempering is required to decompose it into ferrite and cementite. Tempering is generally performed using surface-mounted electric heaters. However, martensite does not always decompose through the full weld depth; it often remains in the weld root, especially in thick-walled pipes. Selecting a nondestructive testing (NDT) method for assessing the extent of martensite decomposition is therefore important. A characteristic averaged over the weld depth is insufficient because the transformation depth must also be estimated. An averaged characteristic does not reveal the distribution of tempering through the depth and may conceal local areas of untempered martensite. A thin layer of untempered or insufficiently tempered martensite may contribute little to the average value, so a welded joint may meet the acceptance criterion based on the average value even though a locally harder and more brittle zone remains at the surface, the fusion line, the weld root, or in the heat-affected zone (HAZ), where it acts as a stress concentrator. Tempering changes martensite lattice tetragonality, the dislocation structure, and carbide dispersion. These changes affect the coercive force [17–19], so magnetic measurements provide indirect information about the structural state of the metal. Their individual contributions cannot be separated using a single magnetic parameter.

The aim of this work is to select an NDT method suitable for field assessment of the heat-treatment quality of martensitic-grade steel pipe welds, including evaluation of the completeness of martensite decomposition through the wall thickness of the welded joint.

METHODS AND MATERIALS

The NDT methods applicable to this task are considered below (Table 1). Eddy current testing is sensitive to changes in electrical conductivity and magnetic permeability and can therefore respond to structural heterogene-

ISSN 2075-8545 (online)

Table 1. Effectiveness of NDT methods for assessing the completeness of tempering through the welded-joint cross-section

NDT method	Measured quantities	Potential for estimating the depth of the tempered zone	Main limitation
Eddy current testing	Probe impedance, electrical conductivity, magnetic permeability	High for assessing tempering quality in near-surface metal layers. At depths of 1–3 mm and low frequencies, quantitative accuracy is limited because sensitivity to property gradients decreases	Skin effect (limited penetration depth); effect of sensor-to-metal lift-off; geometric heterogeneity of the weld
Magnetic Barkhausen noise	Root-mean-square (RMS) voltage and amplitude of the noise electromotive-force (EMF) envelope	High sensitivity for mapping structural changes in the near-surface layer	Limited information depth because of the skin effect
Ultrasonic testing	Propagation velocity, attenuation coefficient, and backscattered-wave parameters	Applicable to millimeter-scale regions when a pronounced structural gradient is present	Requires a pronounced acoustic boundary or a calibration model
Coercive-force magnetic testing (coercimetry)	Demagnetizing current and coercive force (H_c) of the magnetized region	Allows the layer thickness to be estimated under field conditions from readings of transducers with different geometries, after calibration	Requires transducers with different geometries and the construction of calibration curves

ities caused by martensite decomposition [4]. Its principal limitation in ferromagnetic steels is the skin effect [5]. The standard depth of eddy current penetration is given by:

$$\delta = \frac{1}{\sqrt{\pi f \mu \mu_0 \sigma}}, \quad (1)$$

where δ is the penetration depth (skin depth); f is the alternating-current frequency; μ_0 is the permeability of free space; μ is the magnetic permeability of the medium; σ is electrical conductivity.

In ferromagnetic steel, high μ sharply reduces δ; at megahertz frequencies, the penetration depth is therefore a fraction of a millimeter [5]. Millimeter-scale depths require low frequencies, multifrequency or pulsed configurations, control of sensor-to-metal lift-off, and calibration using specimens of the same steel and geometry [4]. Eddy current testing is consequently suitable as a surface and near-surface indicator [6]. Estimating the tempered-zone depth in a weld quantitatively with this method is difficult, because the instrument must be precisely calibrated for the specific microstructure and lift-off variations on the uneven weld bead must be taken into account [7].

The magnetic Barkhausen noise method is based on detecting jumps of domain walls pinned by dislocations, secondary-phase particles, grain boundaries, and residual stresses. It is used for mapping near-surface tempering, residual stresses, and structural heterogeneity [8]. The signal formation depth is small and, in hard, fine-grained structures, including martensitic ones, amounts to tens or hundreds of micrometers [9]. The thickness of hardened layers in the millimeter range was estimated indirectly, using models built on specimens that relate near-surface signal parameters to hardening depth [10, 11]. In the present task, the method is suitable for preliminary testing of the weld surface but does not measure the tempered-layer depth directly.

Ultrasonic methods can probe metal to a depth of several millimeters. In [12, 13], the depth of hardened and carburized layers was determined from the backscattered signal of shear waves introduced at an angle to the surface. For welded joints of martensitic chromium steels after heat treatment, tomograms (maps of elastic-wave velocity) have also been constructed [14]. Boundary detection from the backscattered signal has been described for induction-hardened parts, where the structure changes sharply at the edge of the hardened layer [15]. In a tempered weld, the transition between the martensitic and partially tempered (sorbitic) structures may be gradual, and if the weld metal and HAZ are nearly homogeneous through the wall thickness, the boundary is difficult to identify from this signal. Instead, the phase or group velocity of the waves and their attenuation or scattering are mapped [16], and the resulting maps are compared with metallography and microhardness measurements.

Magnetic coercimetry, based on measurement of the coercive force (H_c), was selected for further analysis because the depth of the tested zone can be changed by selecting the dimensions of the attached electromagnetic transducer. The method is applicable to ferromagnetic steels and allows the magnetic properties of individual regions of a welded joint to be assessed. The Barkhausen noise signal is formed by weak high-frequency electromagnetic pulses that attenuate in the metal at depths of

ISSN 2075-8545 (online)

fractions of a millimeter. Under quasistatic magnetization reversal in coercimetry, the testing depth is governed mainly by transducer geometry and magnetic circuit reluctance.

RESULTS

Coercive force is a structure-sensitive parameter of ferromagnetic steels. It increases with the density of fine structural defects and dislocations, the total extent of grain boundaries, and internal stresses that act as effective obstacles to domain-wall motion. During high-temperature tempering, the supersaturated solid solution decomposes, martensite lattice tetragonality decreases, carbon redistributes, nanoscale carbides precipitate and coarsen, and microstresses relax. In most cases, these processes reduce magnetic hardness relative to the freshly quenched or undertempered condition. H_c measurements have therefore long been used to monitor the quality of thermal and thermochemical treatment of steel products [17, 18, 19].

The basic principle for measuring H_c in extended products is local magnetization to saturation using an attached U-shaped electromagnet [17, 20] (Fig. 1). An attached electromagnet made of a soft-magnetic material magnetizes a local region, rather than the entire object, to a specified depth below the surface. From the depth distribution of magnetic induction in a massive plate, Mikheev [17] concluded that when the pole width b_p equals the width of the magnetized plate, the magnetization depth z_p of a U-shaped electromagnet with a pole thickness-to-width ratio $a_p:b_p = 1:3$ is approximately equal to the pole thickness. As the plate surface area increases, z_p may decrease to $0.5a_p$ because of lateral magnetic-flux leakage.

Reference [21] summarizes H_c measurements of massive products using attached two-pole electromagnets of different geometries. It shows that the minimum thickness h_m of a homogeneous massive body, above which a further increase in thickness has almost no effect on the coercimeter reading, is approximately proportional to the square root of the pole area:

$$h_m = 2\sqrt{S_e}. \quad (2)$$

This means that the magnetic properties of layers located deeper than h_m have almost no effect on the measured demagnetizing current. The value h_m can therefore be regarded as the maximum depth from which a given attached electromagnet can obtain information about material structure.

For a surface-hardened layer, a maximum measurable thickness h_k was also introduced. Up to h_k, the coercimeter reading depends appreciably on layer thickness, which allows this range to be used for quantitative estimation of hardened-layer depth:

$$h_k \approx 0.6\sqrt{S_e}. \quad (3)$$

When the layer thickness exceeds h_k, the increase in the reading slows, and the instrument increasingly characterizes the layer's own coercive force rather than its thickness. For an electromagnet with a pole width-to-thickness ratio $b/a \approx 3$, h_k is close to the pole thickness a, consistent with earlier recommendations for selecting the geometry of attached electromagnets [17].

An initial thickness h_n was also defined; a thinner layer has almost no effect on the coercimeter reading [21]:

$$h_n \approx 0.03\sqrt{S_e}. \quad (4)$$

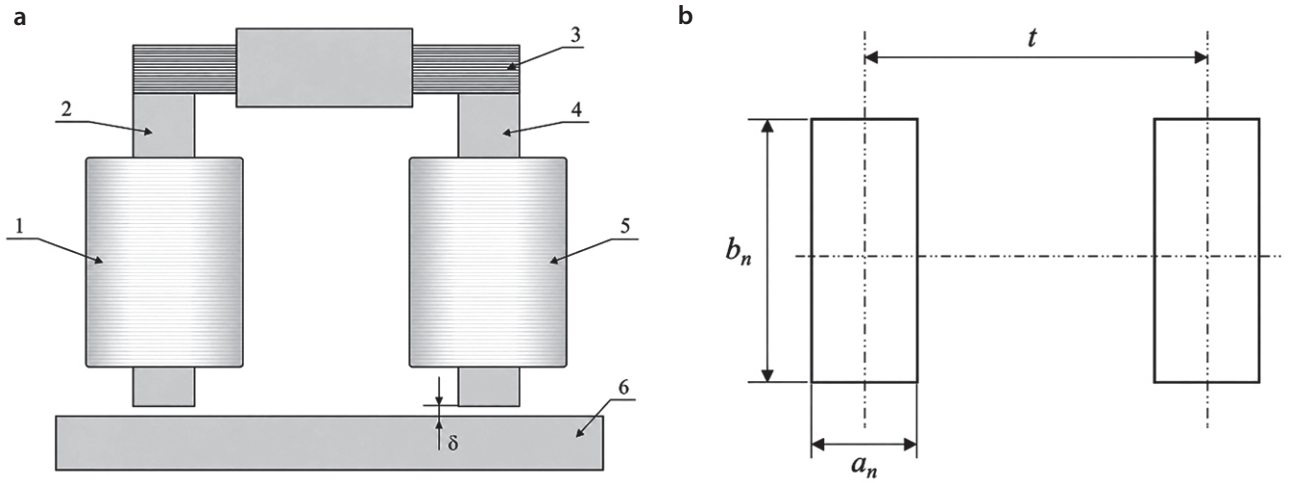


Fig. 1. (a) Schematic of an attached U-shaped electromagnet on the test object: 1, 5 – magnetizing (demagnetizing) coils; 2, 4 – core elements; 3 – magnetic-field sensor (ferroprobe); 6 – test object; δ – lift-off gap. (b) Diagram of a rectangular electromagnet, where a_p, b_p, and t are pole thickness, pole width, and interpole distance, respectively [19, 20]

ISSN 2075-8545 (online)

Nanotechnologies in construction
Нанотехнологии в строительстве

2026; 18 (5):
691–700

The given electromagnet does not reliably measure the thickness of such a layer, and the reading depends mainly on the properties of the substrate or core.

The three boundaries h_n, h_k, and h_m divide the generalized curve reported in [21] into four regions (Fig. 2). Thickness is measured in region II between h_n and h_k, where the readings depend simultaneously on the coercive force of the magnetically hard layer, its thickness, and the properties of the core. In region I ($h < h_n$), the readings are determined mainly by the core. In region III ($h_k < h < h_m$), the effect of layer thickness weakens, and in region IV ($h > h_m$) the readings correspond to a homogeneous massive product. Knowing these boundaries, one can select the pole area for the expected layer thickness or, conversely, evaluate the capabilities of an existing electromagnet with a known S_e.

For a correct H_c measurement, the object must be magnetized to a level close to technical saturation. Modeling has shown that preliminary magnetization of the test region to near technical saturation is achieved when the cross-sectional area of the test region is smaller than or comparable to the cross-sectional area of the electromagnet poles and any lift-off gaps between the transducer and the object are sufficiently small. When magnetizing massive objects, the interpole distance should be reduced by using converging pole pieces to obtain the required magnetic-flux density [22].

An attached electromagnet does not measure H_c directly. The instrument measures a demagnetizing current I_c that is related to H_c. For a U-shaped attached transducer with a built-in zero magnetic-flux indicator, reference [23] expresses the relationship between the demagnetizing current I_c and the coercive force H_c of a homogeneous magnetized volume as:

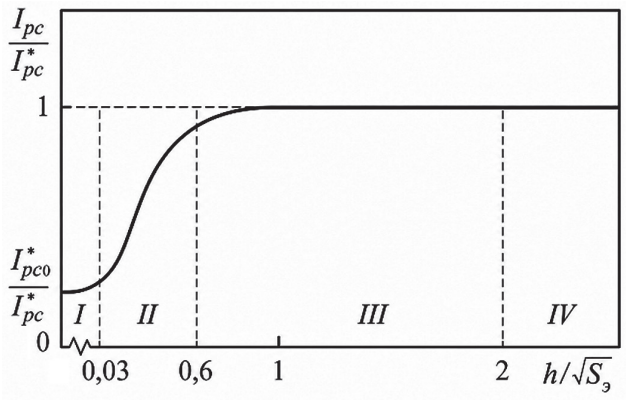


Fig. 2. Generalized coercimeter response curve in relative units. Ordinate notation: I_{pc} – demagnetizing current; I^*_{pc} – demagnetizing current of a structurally homogeneous massive product with thickness $h \geq h_m$; I^*_{pc0} – demagnetizing current of the soft-magnetic core [21]

$$I_c = \frac{1}{W}\left[\frac{R_{F1}U_{cu}}{R_{F1}+R_\delta+R_u} + U_{ce}\right], \quad (5)$$

where W is the total number of turns in the electromagnet winding; U_{cu} is the magnetic-potential drop across the test object; U_{ce} is the magnetic-potential drop across the electromagnet; R_{F1} is the reluctance of the flux path through air between the poles; R_δ is the reluctance of the lift-off gaps between the poles and the object; and R_u is the reluctance of the test object.

Because U_{cu} is related to H_c and to the length of the magnetic field line in the object, the expression shows that the demagnetizing current depends not only on metal properties but also on object geometry, lift-off, and circuit reluctance. For a welded joint, the instrument reading therefore requires calibration and characterizes the magnetized volume as a whole rather than the intrinsic H_c of an individual microregion.

Approximate H_c values for the steels of interest in different structural states are useful when selecting measurement equipment and planning experiments. For the widely used 15Kh5M steel, these data were not found together in a single publication. Reference [24] reports H_c = 6–7 A/cm for 15Kh5M furnace coils after long-term service. T91/P91 steel, an analogue of 15Kh5M, has H_c = 19.65–20.47 A/cm in the as-welded condition, whereas after prolonged tempering it does not exceed 10.75 A/cm [25]. Published H_c values can be used only as reference points, and acceptance testing of a welded joint requires a dedicated calibration.

Basic Methodological Framework

In surface-hardened products, the hardened layer follows the product surface. A weld is oriented differently: its plane runs across the product surface. The welded joint is also structurally heterogeneous. Moving outward from the weld metal, the weld (solidification) zone, the fusion zone (the boundary between weld metal and base metal), and the HAZ occur in sequence. The model of a surface layer over a substrate therefore applies only partially to a welded joint. In thick-walled products, it is difficult to measure the coercive force of the weld metal separately from the contributions of the HAZ and base metal, even when the electromagnet pole width is comparable to the weld width. In practice, an attached electromagnet averages the response of the weld, the HAZ, and part of the base metal. If the weld is sufficiently wide and the wall is thin, however, the attached electromagnet can be oriented along the weld. This orientation reduces the influence of the fusion zones and HAZ, allowing the depth profile of the weld metal itself to be estimated [26, 27].

After high-temperature tempering of a martensitic steel weld, the surface layer of the joint consists of tempered or decomposed martensite and has a lower H_c than

ISSN 2075-8545 (online)

Nanotechnologies in construction
Нанотехнологии в строительстве

2026; 18 (5):
691–700

the martensitic core. The initial values of the generalized curve will therefore exceed unity (Fig. 3), where I^*_{pc} is the demagnetizing current of a structurally homogeneous massive product with a soft-magnetic structure and thickness $h \geqslant h_m$, and I^*_{pc0} is the demagnetizing current of the magnetically hard core. In region I (0 to $h_n \approx 0.03\sqrt{S_e}$), corresponding to electromagnets with large pole cross-sections, coercimeter readings are almost constant and depend mainly on the coercive force of the martensitic core. In region II (h_n to $h_k \approx 0.6\sqrt{S_e}$), corresponding to a medium-sized electromagnet, the readings depend on the coercive force and thickness of the tempered layer and on the coercive force of the martensitic core. In region III (h_k to $h_m = 2\sqrt{S_e}$), corresponding to an electromagnet with a still smaller cross-section, the readings are governed mainly by the coercive force of the tempered layer and depend only weakly on changes in its thickness and the properties of the martensitic core. In region IV ($h \geqslant h_m$), corresponding to electromagnets with the smallest cross-sections, the readings depend only on the coercive force of the tempered layer.

Procedure for Measuring Transformed-Layer Thickness

1. Prepare the test area: remove scale and contaminants, ensure repeatable pole contact, specify the permissible lift-off, use radius-matched tooling for the pipe, and define the orientation of the U-shaped electromagnet relative to the weld.

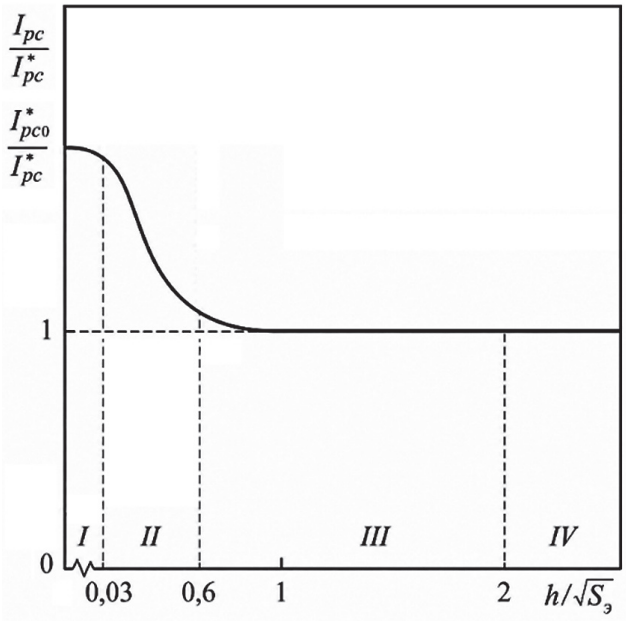


Fig. 3. Expected generalized coercimeter response curve in relative units for a product with a soft-magnetic surface layer and a magnetically hard core

2. For each interchangeable electromagnet, determine $S_e = a \times b$ and calculate $h_n \approx 0.03\sqrt{S_e}$, $h_k \approx 0.6\sqrt{S_e}$, and $h_m \approx 2\sqrt{S_e}$. Select a set of transducers such that the expected transformed-layer thickness lies within the working interval $h_n < h < h_k$ for at least one transducer.

3. Prepare calibration specimens made from the same steel and welded joint: specimens in the as-welded condition without tempering, after the standard high-temperature tempering cycle, and after cycles that produce different depths of transformed or undertempered material.

4. Select the criterion that defines the transformed-layer boundary and measure its depth on metallographic sections. Examine the micro- and nanostructure and the microhardness distribution through the weld depth and, if necessary, assess the degree of martensite decomposition by X-ray diffraction.

5. For each selected electromagnet, use the calibration specimens to construct an $I_{pc}(h)$ or $H_c(h)$ relationship, preferably in normalized form as a function of $h/\sqrt{S_e}$. Because the tempered layer is magnetically softer than undertempered martensite, the calibration curve will have the reverse trend (Fig. 3), but the working boundaries h_n, h_k, and h_m retain their meaning.

6. On the test object, perform a series of measurements at the same weld locations. First demagnetize the region or stabilize its magnetic state, install the transducer, magnetize to near technical saturation, and record the demagnetizing current I_{pc} or the calculated H_c. Make at least three repeated measurements at each point and discard readings associated with an evident loss of contact.

7. Use the calibration curve to find the normalized thickness $x = h/\sqrt{S_e}$ and calculate $h = x\sqrt{S_e}$. An estimate obtained within $h_n < h < h_k$ is considered quantitative. Values below h_n indicate a layer thinner than the lower sensitivity limit of that electromagnet; values above h_k provide only a lower bound for thickness or indicate that a larger transducer is required.

8. Reconcile the results obtained with several electromagnets. If the readings of the small transducer have already reached the plateau of the calibration curve ($h > h_k$) while the medium transducer remains within its working interval, determine the depth from the medium transducer. If the readings of all transducers are on the plateau, report $h \geqslant h_k$ for the largest working transducer and, if necessary, use an electromagnet with a larger S_e. If only the small transducer detects a deviation, classify the layer as surface or near-surface.

9. In the test report, state not only the estimated thickness h but also the pole dimensions and orientation, lift-off, surface curvature, weld-reinforcement height, number of repeats, scatter of the readings, and the criterion used to correlate the magnetic boundary with the transformation boundary determined by metallography or microhardness.

ISSN 2075-8545 (online)

Instruments for Method Implementation

A single fixed attached electromagnet cannot cover the full practically significant range of pipe wall thicknesses. An instrument system is therefore used, comprising a magnetic structure analyzer or coercimeter with a set of interchangeable U-shaped transducers and pole pieces. Traditionally, such tasks were addressed using KIFM-1 and KF-1 coercimeters and their modifications [18, 19, 28, 29]. Multiparameter systems are also used that are capable of measuring not only coercive force but also residual flux, maximum magnetic flux, or the tangential field within a single cycle. Reference [30] demonstrates the capabilities of the SM-401 magnetic structure analyzer with an attached electromagnet for monitoring quenching and tempering. Reference [23] shows the advantages of measuring H_c by the internal field, and in [31] H_c was used together with magnetic flux to selectively estimate layer thickness and degree of hardening.

Interchangeable pole pieces are required in three cases. First, when pipes of different diameters are tested, flat poles produce variable lift-off on a curved surface; quantitative measurements therefore require pole pieces matched to the outside radius. Second, narrow pole pieces are used for testing a narrow weld or fusion line to reduce the influence of the HAZ and base metal. Third, thick welds require poles with a larger cross-section, because the contribution of the deep region to the reading of a small transducer is small and the testing depth increases with the pole cross-sectional area (Eqs. 2–4). Calibration is valid only for the pole-piece configuration with which it was performed. Pole geometry changes circuit reluctance and flux distribution and, with them, the depth of the region contributing to the reading.

DISCUSSION

Calibration, Errors and Limitations

The tempered-layer thickness can be estimated quantitatively only after calibration on welded specimens of the same steel, with a similar thickness and made using the same welding procedure. Criteria obtained for P91, 30KhGSA, or carburized layers can be used only as a physical reference for 15Kh5M steel. We propose including specimens in the as-welded condition without tempering, after the standard high-temperature tempering cycle, and after undertempering. Tempering time, temperature, or heating power is varied to obtain specimens with different structural distributions through the depth. Each specimen is first measured with all transducers and then sectioned for metallography and microhardness measurements. Changing the tempering cycle affects both the layer depth and the degree of tempering within the layer. To establish the relationship between instrument readings and layer thickness, specimens with similar layer and core structures and microhardness values are therefore compared. If this similarity has not been confirmed, a relationship based on thickness alone is insufficient: the calibration model must account for differences in structural state. The tempered-layer boundary is defined by the chosen metallographic or microhardness criterion. The magnetically altered zone is compared with this boundary on the calibration specimens; their depths are not assumed to coincide.

The magnetic measurements are compared with the results of macrosection and microsection examination. The HAZ width and structure are determined on these sections. Microhardness is measured along profiles from the surface and from the weld axis. X-ray diffraction is used to refine the phase composition. The tetragonality of martensite is estimated from the splitting of diffraction peaks. At the low tetragonality typical of low-carbon and tempered martensite, the peak splitting may not be resolved. The following relation is used:

$$\frac{1}{d_{hkl}^2} = \frac{h^2+k^2}{a^2} + \frac{l^2}{c^2},$$

where d_{hkl} is the interplanar spacing for the reflection with indices hkl and a and c are the tetragonal lattice parameters of martensite. A decrease in the *c/a* ratio during tempering is one indicator of martensite decomposition, but for a welded joint this criterion must be compared with microhardness and microstructural analysis.

A significant error is introduced by the lift-off gap between the poles and the product. It increases circuit reluctance and lowers the coercimeter reading [22]. A 1 mm lift-off reduced KIFM-1 readings by more than 33%, whereas the readings of MMT-3, which operates using the internal field, decreased by less than 9% [23]. Lift-off effects can be reduced by accounting for additional magnetic parameters and measuring the tangential field component [32, 33]. The symmetry of the measured field also depends on the positions of the field and flux sensors in the transducer [34]. On a pipe, surface curvature and weld reinforcement add to the lift-off. The procedure specifies the permissible lift-off and reinforcement height in advance. It defines surface preparation, magnet orientation, and the demagnetization sequence. The number of repeated measurements and the outlier-rejection rule are fixed before testing. Residual stresses and residual magnetization affect the readings as well. The stress and structural contributions cannot be separated from a single H_c measurement. Because high-temperature tempering both relieves stresses and changes the structure, it is validated on a calibration series whose stress state is close to that of the actual product. Without such validation, the detected magnetic heterogeneity cannot be unambiguously related to the depth of the tempered layer.

ISSN 2075-8545 (online)

Method Limitations

The instrument averages the response over the entire volume through which the magnetic flux closes. For this reason, the layer-by-layer profile obtained with a set of electromagnets is conditional. It does not resolve adjacent layers in a narrow HAZ. Different transducers sample non-coincident volumes of metal. Magnetic anisotropy due to directional solidification of the weld and precipitation of dispersed carbides during tempering influence the readings as well. Calibration is performed on welded specimens for each steel grade. A calibration relationship from another grade may be used if testing on specimens of the steel under examination confirms that the thickness estimates meet the error limit specified in the procedure. Otherwise, a new calibration relationship is established.

CONCLUSION

Of the NDT methods considered, magnetic coercimetry with a set of interchangeable attached transducers was selected for estimating the depth of the tempered layer in welds of martensitic steels. After calibration, a single attached electromagnet gives an integral estimate of H_c over the magnetized volume. A set of electromagnets with different cross-sections provides a conditional layer-by-layer profile. A small electromagnet characterizes the surface layer, the reading of a medium one also includes the transition region, and a large one covers a deeper volume of the joint. The diagnostic feature is the change in H_c with increasing magnetization depth, since the absolute H_c value also depends on the degree of tempering and the properties of the core. The result is verified by metallography, microhardness testing, and, if necessary, X-ray diffraction analysis of martensite tetragonality and its nanoscale features. Further verification of the procedure should assess how much the simultaneous measurement of H_c, residual and maximum magnetic flux in the transducer-object circuit [32], and the tangential field between the poles reduces the ambiguity in separating the effects of layer depth and degree of tempering.

REFERENCES

1. GOST 550-2020. *Seamless steel pipes for petroleum refining and petrochemical industries. Specifications*. (In Russ.).
2. TU 14-3R-124-2017 / TU 14-3R-124-2012. *Seamless steel pipes with increased corrosion resistance and cold resistance for oil and gas field pipelines*. (In Russ.).
3. Trutnev N.V., Krasikov A.V., Ulyanov A.G., et al. Development of the technology for rolling 13Cr martensitic stainless-steel pipes on the TPA 159-426 unit at JSC VTZ. *Ferrous Metallurgy. Bulletin of Scientific, Technical and Economic Information*. 2018;(12):68-71. (In Russ.).
4. Cuffe J., Sun H., Plotnikov Y., Nath S., Sheila-Vadde A. Eddy current measurement of case-hardened depth of steel components. In: *Proceedings of the 17th World Conference on Nondestructive Testing*; 2008 Oct 25-28; Shanghai, China.
5. TO 33B-1-1 / NAVAIR 01-1A-16 / TM 1-1500-335-23. *Nondestructive Inspection Methods, Basic Theory*. Chapter 4: Eddy Current Inspection Method.
6. Cook K.H., Munyak J.J., Pember W.H. *Electromagnetic test for microstructure anomalies such as alpha-case, and for carbide precipitates and untempered and overtempered martensite*. US Patent US5811970A. 1998 Sep 22.
7. Wolter B., Gabi Y., Conrad C. Nondestructive testing with 3MA — an overview of principles and applications. *Applied Sciences*. 2019;9(6):1068. https://doi.org/10.3390/app9061068
8. Yelbay H.İ., Gür C.H. Non-destructive determination of surface residual stresses in electron beam welded AISI 410 martensitic stainless steel using the magnetic Barkhausen noise technique. *Metals*. 2025;15(3):305. https://doi.org/10.3390/met15030305
9. Stupakova A., Perevertova A., Neslušan M. Reading depth of the magnetic Barkhausen noise. II. Two-phase surface-treated steels. *Journal of Magnetism and Magnetic Materials*. 2020;513:167239. https://doi.org/10.1016/j.jmmm.2020.167239
10. Santa-aho S., Vippola M., Sorsa A., Leiviskä K., Lindgren M., Lepistö T. Utilization of Barkhausen noise magnetizing sweeps for case-depth detection from hardened steel. *NDT & E International*. 2012;52:95-102. https://doi.org/10.1016/j.ndteint.2012.05.005
11. Holmberg J., Hammersberg P., Lundin P., Olavison J. Predictive modeling of induction-hardened depth based on the Barkhausen noise signal. *Micromachines*. 2023;14(1):97. https://doi.org/10.3390/mi14010097
12. Willems H. Nondestructive determination of hardening depth in induction hardened components by ultrasonic backscattering. In: Thompson D.O., Chimenti D.E., editors. *Review of Progress in Quantitative Nondestructive Evaluation*. Boston: Springer; 1991. p. 1707-1713. https://doi.org/10.1007/978-1-4615-3742-7_74

13. Baqeri R., Honarvar F., Mehdizad R. Case depth profile measurement of hardened components by ultrasonic backscattering technique. *e-Journal of Nondestructive Testing*. 2012;17(7). Available at: https://www.ndt.net/?id=12444 (accessed: 06.07.2026).

14. Onwuama O., Na J., Aryan A., Bourgeois D., Zhang W. Assessment of weld microstructure through sound velocity measurements for power plant applications. *Materials Evaluation*. 2024;82(9):43. https://doi.org/10.32548/2024.me-04435

15. Fraunhofer IZFP. *Surface Hardening Depth (SHD): Nondestructive Inspection of Inductively Hardened Parts and Components Using Ultrasonic Backscattering*. Brochure No.180-2-2; 2022. Available at: https://shop.vision.fraunhofer.de/artikel/surface-hardening-depth (accessed: 06.07.2026).

16. Haderer W., Scherleitner E., Gseller J., Heise B., Mitter T., Ryzy M., Reitinger B., Hettich M. Spatial imaging of stratified heterogeneous microstructures: determination of the hardness penetration depth in thermally treated steel parts by laser ultrasound. *NDT & E International*. 2023;138:102868. https://doi.org/10.1016/j.ndteint.2023.102868

17. Mikheev M.N. Selection of optimum geometrical dimensions of attached coercimeter electromagnets for monitoring the quality of thermal and thermochemical treatment of steel and cast-iron products. *Physics of Metals and Metallography*. 1957;5(1):44-52. (In Russ.).

18. Gorkunov E.S., Zakharov V.A. Coercimeters with attached magnetic devices: a review. *Russian Journal of Nondestructive Testing*. 1995;(8):69-88. (In Russ.).

19. Bida G.V. Magnetic testing of the depth and hardness of surface-hardened layers in products: a review. *Russian Journal of Nondestructive Testing*. 2006;(5):10-28. (In Russ.).

20. Bida G.V. Effect of lift-off between the poles of an attached electromagnet and the test object on coercimeter readings and methods for reducing it: a review. *Russian Journal of Nondestructive Testing*. 2010;(11):62-81. (In Russ.).

21. Mikheev M.N., Fridman L.A., Morozova V.M., Tabachnik V.P., Bida G.V., Gorkunov E.S., Chernova G.S. Application of coercimeters with attached electromagnets to testing massive steel products. *Russian Journal of Nondestructive Testing*. 1978;(8):47-51. (In Russ.).

22. Kostin V.N., Lukinykh O.N., Smorodinsky Ya.G., Kostin K.V. Modeling the spatial distribution of field and induction in locally magnetized massive objects and optimization of U-shaped transducer design. *Russian Journal of Nondestructive Testing*. 2010;(6):13-21. (In Russ.).

23. Kostin V.N., Vasilenko O.N., Mikhailov A.V., Lukinykh N.P., Ksenofontov D.G. Advantages of local measurement of the coercive force of ferromagnetic objects by the internal field. *Russian Journal of Nondestructive Testing*. 2020;(7):21-27. https://doi.org/10.31857/S0130308220070039 (In Russ.).

24. Shkatulyak N.M., Dragomeretskaya E.A., Usov V.V., Rabkina M.D., Palienko A.L. Texture and coercive force of the metal of furnace tube coils. *Diagnostics, Resource and Mechanics of Materials and Structures*. 2016;(1):29-37. https://doi.org/10.17804/2410-9908.2016.1.029-037

25. Mondal A., Das A.K., Chand S., Kumar S., Kesari C.B. Coercivity measurement as a tool for assessing the quality of post weld heat treatment of T91 boiler tubes. In: *NTPC Transactions on Energy Research*. Singapore: Springer Nature; 2025. p. 61-78. https://doi.org/10.2991/978-94-6463-849-3_6

26. Kulikov V.P., Belyagov A.M., Bolotov S.V. Detection of welding thermal-cycle deviations in heat-resistant steels using magnetic characteristics of the metal in the heat-affected zone. *Bulletin of Mogilev State Technical University*. 2006;1(10). (In Russ.).

27. Bolotov S.V., Belyagov A.M., Vorobyov A.O. Weld quality control using magnetic characteristics of the metal in the joint region. *Bulletin of Mogilev State Technical University*. 2006;1(10). (In Russ.).

28. Mikheev M.N., Gorkunov E.S., Vostrotina T.I. Quality control of heat treatment of products hardened by high-frequency currents. *Russian Journal of Nondestructive Testing*. 1976;(1):66-70. (In Russ.).

29. Mikheev M.N., Bida G.V., Rigmant M.B., Kubachek V.V., Tikhonova L.A. Magnetic quality control of surface hardening of large gear teeth. *Russian Journal of Nondestructive Testing*. 1982;(2):16-19. (In Russ.).

30. Nichipuruk A.P., Bida G.V., Shanaurin A.M., Stashkov A.N. Functional capabilities of the SM-401 magnetic structure analyzer. *Russian Journal of Nondestructive Testing*. 2003;(1):3-12. (In Russ.).

31. Byzov A.V., Ksenofontov D.G., Kostin V.N., Vasilenko O.N. Selective magnetic testing of the thickness and degree of hardening of surface layers on steel objects. *Russian Journal of Nondestructive Testing*. 2021;(12):39-45. https://doi.org/10.31857/S0130308221120046 (In Russ.).

32. Kostin V.N., Vasilenko O.N. New possibilities for local measurement of the coercive force of ferromagnetic objects. *Russian Journal of Nondestructive Testing*. 2012;(7):15-26. (In Russ.).

33. Gobov Yu.L., Zhakov S.V., Mikhailov A.V., Reutov Yu.Ya. Coercimetry under magnetization by a U-shaped electromagnet. *Russian Journal of Nondestructive Testing*. 2019;(12):42-48. (In Russ.).

34. Batueva A.V., Vasilenko O.N., Kostin V.N. Optimization of field and flux sensor locations in attached transducers of magnetic structure analyzers. *Russian Journal of Nondestructive Testing*. 2024;(6):69-73. (In Russ.).

ISSN 2075-8545 (online)

ADDITIONAL INFORMATION

During the final preparation of the manuscript, artificial intelligence was used for technical editing and for structuring the metadata in accordance with the journal requirements. After use of this tool, the content was reviewed and edited by the authors; the authors assume full responsibility for the content of the published article.

INFORMATION ABOUT THE AUTHORS

Airat M. Fayrushin – Associate Professor, Head of the Department of Equipment and Technology of Welding and Testing, Institute of Oil and Gas Engineering and Digital Technologies, Ufa State Petroleum Technological University, Ufa, Russian Federation, tna_ugntu@mail.ru, https://orcid.org/0009-0004-5591-1036

Elena Yu. Tumanova – Cand. Sci. (Eng.), Associate Professor, Department of Equipment and Technology of Welding and Testing, Institute of Oil and Gas Engineering and Digital Technologies, Ufa State Petroleum Technological University, Ufa, Russian Federation, tumanova-elena@mail.ru, https://orcid.org/0009-0007-8120-0790

Alexander S. Sobachkin – Cand. Sci. (Eng.), Associate Professor, Department of Equipment and Technology of Welding and Testing, Institute of Oil and Gas Engineering and Digital Technologies, Ufa State Petroleum Technological University, Ufa, Russian Federation, acc1955@mail.ru, https://orcid.org/0009-0001-5494-9081

Marcel F. Imayev – Dr. Sci. (Phys.-Math.), Professor, Department of Equipment and Technology of Welding and Testing, Institute of Oil and Gas Engineering and Digital Technologies, Ufa State Petroleum Technological University, Ufa, Russian Federation, marcel_imayev@mail.ru, https://orcid.org/0000-0001-9386-7313

Andrey S. Tokarev – Senior Lecturer, Department of Equipment and Technology of Welding and Testing, Institute of Oil and Gas Engineering and Digital Technologies, Ufa State Petroleum Technological University, Ufa, Russian Federation, andrewtok07@gmail.com, https://orcid.org/0009-0000-5926-4658

Diana R. Musina – Senior Lecturer, Department of Equipment and Technology of Welding and Testing, Institute of Oil and Gas Engineering and Digital Technologies, Ufa State Petroleum Technological University, Ufa, Russian Federation, musidiana@yandex.ru, https://orcid.org/0009-0003-7117-9845

CONTRIBUTION OF THE AUTHORS

Airat M. Fayrushin – research concept; scientific supervision; critical revision of the text; final conclusions.

Elena Yu. Tumanova – literature analysis; research methodology; text editing; final conclusions.

Alexander S. Sobachkin – analysis of nondestructive testing methods; preparation of sections on welded joints; text editing.

Marcel F. Imayev – scientific consulting on physical and mathematical aspects; interpretation of magnetic and structural parameters; critical revision of the text.

Andrey S. Tokarev – problem statement; collection and analysis of sources; preparation of the original draft; manuscript formatting.

Diana R. Musina – systematization of sources; preparation of illustrative material; formatting of the reference list.

The authors declare no conflicts of interests.

The article was submitted 07.07.2026; approved after reviewing 06.10.2026; accepted for publication 10.10.2026.

ISSN 2075-8545 (online)

Nanotechnologies in construction
Нанотехнологии в строительстве

2026; 18 (5):
701–712

Nanobuild.ru

SYSTEM SOLUTIONS FOR TECHNOLOGICAL PROBLEMS

CC BY 4.0

Original article
https://doi.org/10.15828/2075-8545-2026-18-5-701-712

Study of the flow characteristics of a shut-off and control device for forming a controlled gas flow

Nikolay Yu. Stepanenko, Sergey V. Chertovskikh*, Alexey V. Rubtsov, Nikita E. Ivanov

Ufa State Petroleum Technological University, 450064, Republic of Bashkortostan, Ufa, Kosmonavtov St., 1, Russian Federation

* Corresponding author: e-mail: chertovskikh@mail.ru

ABSTRACT

Introduction. Industrial pipeline valves are among the most important elements of energy metering, both within common gas distribution systems and as a precision control element directly acting on an actuator or mechanism. The most specific requirements apply to shut-off and control devices (SCDs) used in high-risk industries, as well as in precision high-tech critical manufacturing. The ability to change and regulate the flow characteristic, as well as the response time of the element separating the two parts of the communicating system, play a significant role. The use of SCDs to shape an inert gas flow, according to the established law, is a key requirement for actuators in systems for manufacturing parts (the material of which is, as a rule, in a nanostructured state) using superplastic forming (SPF). The requirements for the actuator of a gas distribution system to perform the SPF operation are determined by a graph based on the part geometry. A bellows shut-off needle valve is adopted as the actuator unit, as it is optimal in design due to the seal used, as well as a metering needle that allows changing the flow cross-section of the channel. **Methods and Materials.** Modeling and finite element (FE) analysis to determine the flow characteristics of a bellows shut-off needle valve in a gas distribution system were performed using a specialized software package for scenarios of control rod handle rotation at 10°, 45°, and 90°, taking into account the required boundary conditions. Full-scale tests to verify the finite element method (FEM) calculations were carried out on a test bench using a bellows shut-off needle valve with the required parameters of the test bench elements. **Results and Discussion.** The article presents the results of finite element analysis (FE) and full-scale bench tests to verify the modeling results. The research revealed that the dependence of the working fluid flow rate on the angle of rotation of the control rod handle is not linear. In the range of handle rotation angles from 0° to 40°, a stable increase in flow rate is observed. With a further increase in the handle opening angle from 40° to 60°, the nature of the change in the working fluid flow rate changes. Abrupt changes are observed, which can be explained by a relatively large opening of the housing seat. This leads to phenomena (stalls, flow swirls, etc.), causing flow rate fluctuations. After reaching a rotation angle of 60°, the flow rate graph becomes oscillatory. In this section, the flow is constantly exposed to significant turbulent phenomena and becomes unstable, which complicates the accurate determination of the working fluid flow rate. **Conclusion.** A combination of finite element modeling and a full-scale experiment allowed us to verify the flow characteristic obtained through FEM calculations in a specialized software package with data from full-scale bench tests of a bellows-sealed shut-off needle valve. The discrepancy between the FE analysis results and those obtained during full-scale tests is within 5%, allowing the method described in this article to be used to obtain sufficiently accurate and reliable results.

KEYWORDS: blowdown, superplastic forming, bellows-sealed needle valve, flow characteristic, finite element analysis, nanostructured materials

SOURCES OF FUNDING FOR THE SCIENTIFIC WORK THAT RESULTED IN THE PUBLICATION: This research was conducted within the framework of the PRIORITY 2030 program of the Ministry of Science and Higher Education of the Russian Federation.

ACKNOWLEDGEMENTS: The authors express their gratitude for the financial support of this project.

FOR CITATION:
Stepanenko N.Yu., Chertovskikh S.V., Rubtsov A.V., Ivanov N.E. Study of the flow characteristics of a shut-off and control device for generating a controlled gas flow. *Nanotechnologies in Construction.* 2026;18(5):701–712. https://doi.org/10.15828/2075-8545-2026-18-5-701-712. – EDN: EPTGEW.

© Stepanenko N.Yu., Chertovskikh S.V., Rubtsov A.V., Ivanov N.E., 2026

ISSN 2075-8545 (online)

Nanotechnologies in construction
Нанотехнологии в строительстве

2026; 18 (5):
701–712

Nanobuild.ru

SYSTEM SOLUTIONS FOR TECHNOLOGICAL PROBLEMS

Исследование расходной характеристики запорно-регулирующего устройства для формирования управляемого потока газа

Николай Юрьевич Степаненко, Сергей Владимирович Чертовских*, Алексей Вячеславович Рубцов, Никита Евгеньевич Иванов

Уфимский государственный нефтяной технический университет, 450064, Уфа, ул. Космонавтов, 1, Российская Федерация

* Автор, ответственный за переписку: e-mail: chertovskikh@mail.ru

АННОТАЦИЯ

Введение. Промышленная трубопроводная арматура является одним из важнейших элементов дозирования передаваемой энергии как внутри распространенных газораспределительных систем, так и органом прецизионного воздействия непосредственно на исполнительное устройство или механизм. Наиболее конкретизированными являются требования к запорно-регулирующим устройствам (ЗРУ), применяемым в отраслях промышленности, имеющих повышенную опасность, а также на прецизионных высокотехнологичных ответственных производствах. Значительную роль играет возможность изменения и диапазон регулирования расходной характеристики, а также быстродействие элемента, разделяющего две части сообщающейся системы. Применение ЗРУ для формирования потока инертного газа, согласно сформированному закону, является ключевым требованием к исполнительным элементам системы для изготовления деталей (материал которых находится, как правило, в наноструктурном состоянии) методом сверхпластической формовки (СПФ). Формирование требований к исполнительному узлу газораспределительной системы для осуществления операции СПФ определяется графиком, основанным на геометрии детали. В качестве исполнительного узла принят сильфонный запорный игольчатый клапан как оптимальный по конструкции ввиду используемого уплотнения, а также дозирующей иглы, позволяющей изменять проходное сечение канала. **Методы и материалы.** Моделирование и конечно-элементный (КЭ) анализ с целью определения расходных характеристик сильфонного запорного игольчатого клапана газораспределительной системы проводились с применением специализированного программного комплекса для сценариев поворота рукоятки управляющего штока на: 10°, 45° и 90° с учетом необходимых граничных условий, а проведение натурных испытаний с целью верификации расчетов методом конечных элементов (МКЭ) осуществлялось на стенде с использованием сильфонного запорного игольчатого клапана при требуемых параметрах элементов стенда. **Результаты и обсуждение.** Приводятся результаты конечно-элементного (КЭ) анализа и натурных стендовых испытаний для верификации результатов моделирования. В ходе проведения исследований установлено, что зависимость расхода рабочей среды от угла поворота рукоятки управляющего штока не является линейной. В диапазоне углов поворота рукоятки от 0° до 40° наблюдается стабильное увеличение расхода. При дальнейшем увеличении угла открытия рукоятки от 40° до 60° характер изменения расхода рабочей среды меняется. Наблюдаются скачкообразные перепады, которые можно объяснить относительно большим открытием седла корпуса. Это приводит к явлениям (срывы, завихрения потока и т.д.), вызывающим колебания расхода. После достижения угла поворота в 60° график расхода приобретает колебательный характер. На данном участке поток испытывает постоянное значительное воздействие турбулентных явлений и становится нестабильным, что затрудняет точное определение расхода рабочей среды.

Заключение. Совместное проведение конечно-элементного моделирования и натурного эксперимента позволило провести верификацию расходной характеристики, полученной в ходе расчета МКЭ в специализированном программном комплексе с данными натурных стендовых испытаний сильфонного запорного игольчатого клапана. Расхождение результатов КЭ анализа с результатами, полученными в ходе натурных испытаний, находится в пределах 5 %, что позволяет использовать методику, приведенную в статье, для получения достаточно точных и достоверных результатов.

КЛЮЧЕВЫЕ СЛОВА: продувка, сверхпластическая формовка, сильфонный запорный игольчатый клапан, расходная характеристика, конечно-элементный анализ, наноструктурные материалы.

ИСТОЧНИКИ ФИНАНСИРОВАНИЯ НАУЧНОЙ РАБОТЫ, РЕЗУЛЬТАТОМ КОТОРОЙ СТАЛА ПУБЛИКАЦИЯ: Исследование выполнено в рамках программы Министерства науки и высшего образования Российской Федерации «ПРИОРИТЕТ 2030».

БЛАГОДАРНОСТИ: Авторы выражают благодарность за финансовую поддержку проекта.

ДЛЯ ЦИТИРОВАНИЯ:
Степаненко Н.Ю., Чертовских С.В., Рубцов А.В., Иванов Н.Е. Исследование расходной характеристики запорно-регулирующего устройства для формирования управляемого потока газа. *Нанотехнологии в строительстве.* 2026;18(5):701–712. https://doi.org/10.15828/2075-8545-2026-18-5-701-712. – EDN: EPTGEW.

ISSN 2075-8545 (online)

INTRODUCTION

Shut-off and control valves (SCVs) play a vital role in many industrial processes. The safety and quality of the processes in which they are used depend on the characteristics and precision of their operation. Commonly used in industry are dampers, gate valves, ball valves, and other types of shut-off valves. These valves have a relatively simple design, but they have a short service life under continuous, high-cycle conditions and lack the ability to smoothly regulate flow. Various types of pressure valves and regulators are among the most suitable for smooth control. Compared to shut-off valves, these devices have a more complex design and are less suitable for complete flow shut-off due to their poorer sealing properties due to their specific design.

One type of shut-off switchgear is the bellows-type shut-off needle valve (Fig. 1). It is a high-tech device designed for precise regulation and hermetically sealed shut-off of the flow of the working medium in various engineering systems [1–3].

Thanks to its special design, this valve can operate under high pressure and temperature conditions, which can be harsh on common industrial materials. These advantages allow these valves to be used in various gas distribution systems, including as part of the SPF process complex for the process of forming parts, the material of which, as a rule, is in a nanostructured state.

The valve consists of a handle 1, which is connected to a control stem 2, at the end of which is a metering needle 6, a stainless steel body 3, gas line connections 4, and a metal bellows 5.

When the handle 1 is rotated, the control rod 2 moves along the thread of the body 3. When the valve is closed, the control rod 2 moves downwards and thereby inserts the metering needle 6 into the seat located in the body 3. This seals the channels connecting the connection points of the gas main. When the valve is opened, the control rod 2 rises, removing the metering needle 6 from the seat. In this case, the metering needle 6 and the seat of the body 3 are designed in such a way that when the metering needle 6 is raised, the flow between the channels occurs along a variable cross-section, adjusted depending on the height of the metering needle 6. Bellows 5, connected to the body 3 and the control rod 2, is necessary to ensure the tightness of the valve body and protect the control rod 2 from the effects of the working medium on it [4–5].

In many technological processes, the control of bellows valves is automated using various devices (e.g., servo drives), which allows for increased speed and accuracy of process control. The initial parameter for writing a control program for valve operation corresponding to the technological process is the flow characteristic (the dependence of its flow area on the angle of rotation of the control rod). The flow characteristic is also necessary to ensure the quality of a large number of technological processes

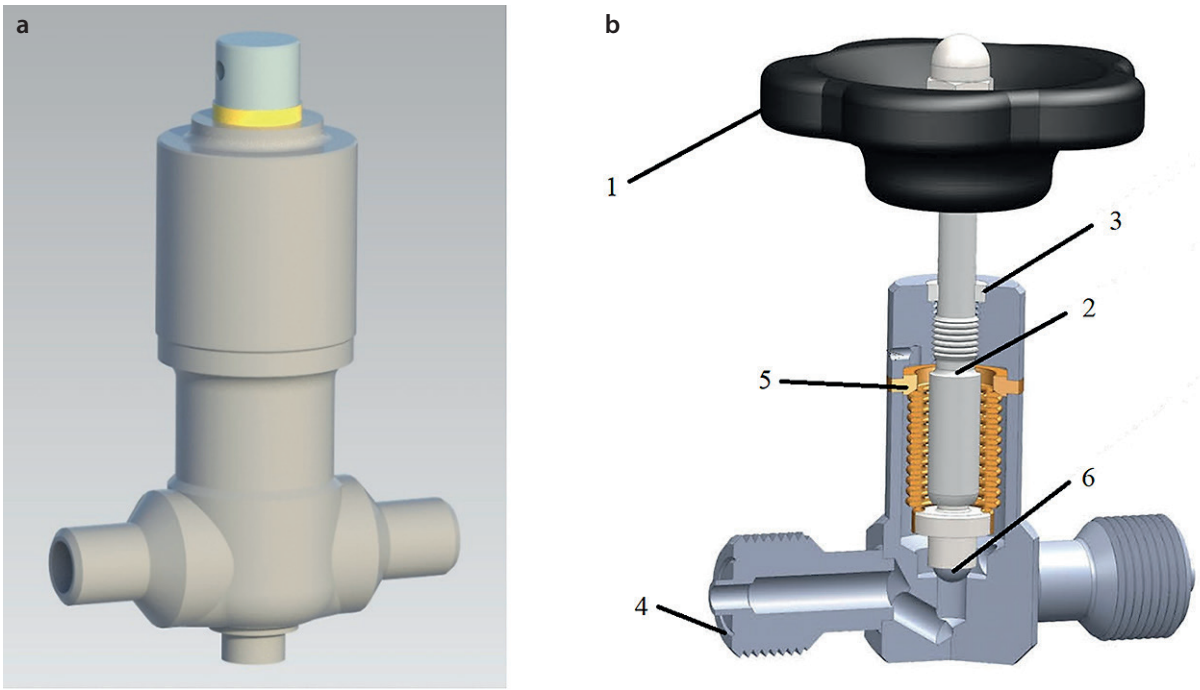


Fig. 1. Bellows shut-off needle valve: 1 – handle; 2 – control stem; 3 – body; 4 – gas line connections; 5 – bellows; 6 – metering needle; a) – 3D model; b) – design

ISSN 2075-8545 (online)

[1–3, 6]. Thus, in the SPF operation, the quality of the manufactured part directly depends on the accuracy of the forming gas supply.

A current method for obtaining the flow characteristics of bellows valves is mathematical modeling of the working fluid flow in valves under various operating conditions. The study of mathematical modeling of bellows valve operation is driven by the need to improve the efficiency and accuracy of technological processes (e.g., SPF), as well as to reduce the costs of experimental research. Modeling allows for the prediction of valve flow characteristics, which subsequently makes it possible to optimize process parameters [7–8].

Thus, the aim of this work is to model (with the implementation of FE analysis) the flow characteristics of a bellows valve in various operating modes with verification of calculations using bench tests.

METHODS AND MATERIALS

The FE analysis portion of the study was conducted using a specialized software package.

To calculate the flow characteristics, a model of a bellows-sealed needle valve section was used, consisting of:
- the working fluid inlet section;
- the metering needle and body seat, which regulate the valve flow area;
- the working fluid outlet section.

The position of the metering needle relative to the body seat (i.e., the height of the metering needle's lift from the seat) corresponds to the n-th angle of rotation of the valve handle. This lift is determined by converting the pitch of the body thread along which the control stem moves and the angle of rotation of the stem handle. The calculated air flow model is shown in Fig. 2.

The simulation was performed using the finite element method (FEM) using a specialized software package [2, 9–17]. To confirm the accuracy of the FEM analysis results, several calculations were performed using points obtained during the blowdown, specifically, rotating the control rod handle by 10°, 45°, and 90°.

The valve flow area between the metering needle and the body seat for various calculation options is shown in Fig. 3.

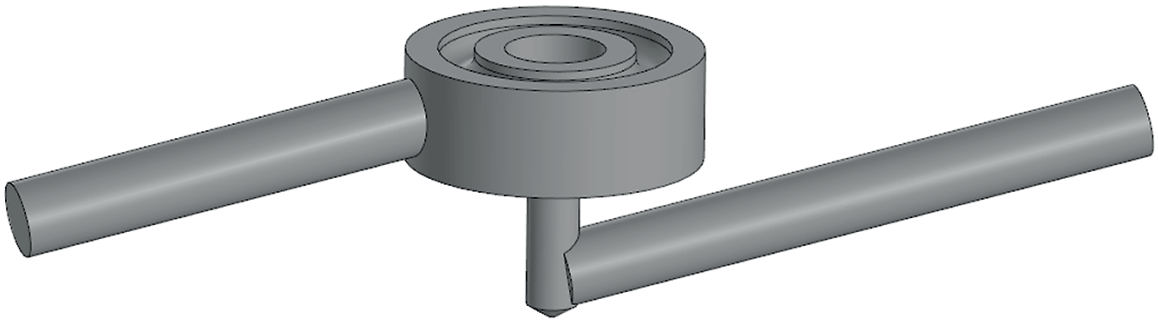


Fig. 2. Calculation model of air flow in a section of a bellows-type shut-off needle valve

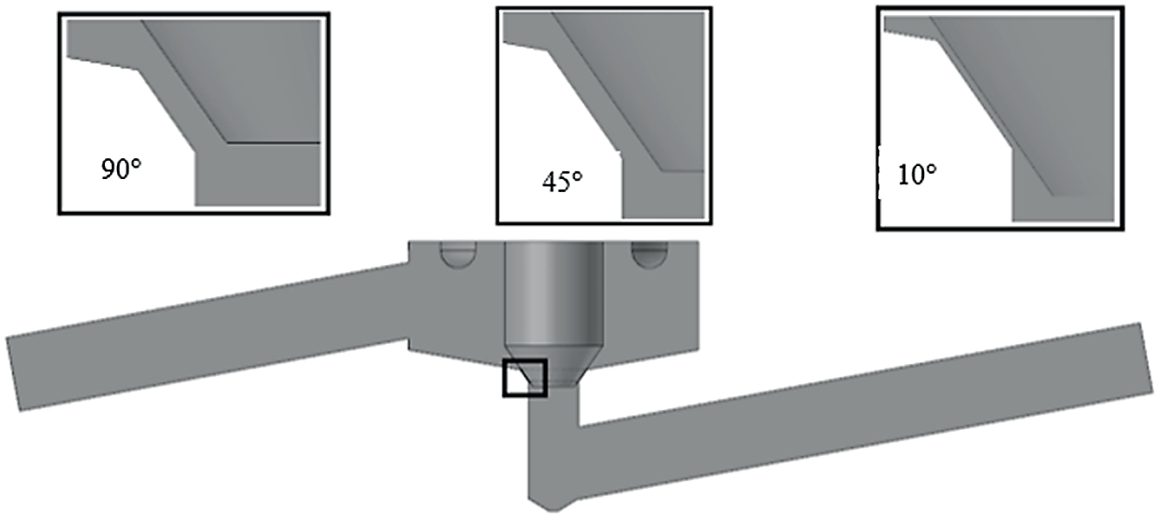


Fig. 3. Cross-section of the air flow model in a bellows shut-off valve when the handle is opened by 10°, 45° and 90°

ISSN 2075-8545 (online)
Nanotechnologies in construction
Нанотехнологии в строительстве
2026; 18 (5): 701–712

The mesh model in all calculation variants has a finer mesh at the point where the working fluid passes between the metering needle and the body seat, as well as prismatic layers near the walls on long straight sections of the working fluid's entry and exit from the valve. The mesh model for calculating air flow in a bellows shut-off needle valve, using the example of a variant with the handle opened by 10°, is shown in Fig. 4.

The boundary conditions for the calculation were:
- total pressure at the valve inlet – 1.42 MPa;
- free flow to the atmosphere – p_{atm} = 101325 Pa, T_{atm} = 15 °C;
- working fluid – air;
- turbulence model – k–ε.

The k–ε turbulence model was chosen because, in this problem, we are concerned not with losses in the wall air flow, but with the parameters of the main flow. This turbulence model has also been successfully applied in numerous studies of hydraulic flow characteristics [9, 18]. The computational model with boundary conditions is shown in Fig. 5.

Full-scale tests to verify the FEM calculations were conducted on a test bench using a bellows-sealed shut-off needle valve, the design of which is shown in Figure 1b. The technical characteristics of the test valve are presented in Table 1.

The stand for determining the flow characteristics of the valve is an installation, the diagram of which is shown in Fig. 6 [2, 12].

In this case, the device supplying the working fluid (air) is a compressor with a large-volume receiver. Using a preset pattern, the operator rotates the flow regulator

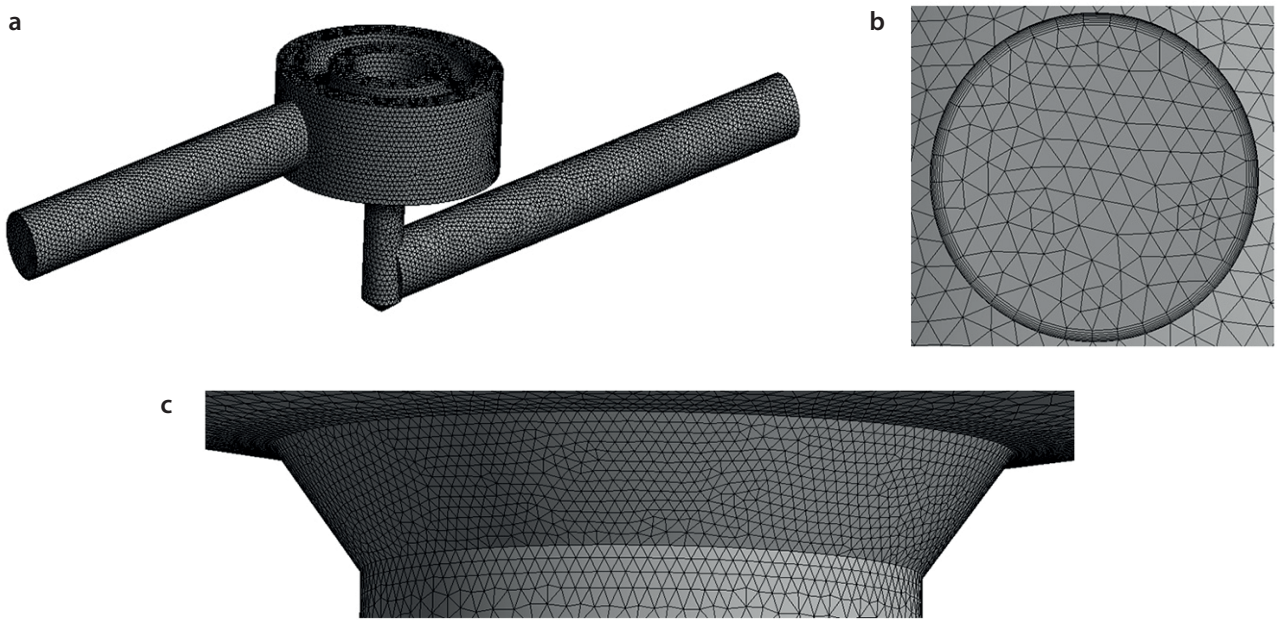


Fig. 4. A grid model for calculating air flow in a bellows-type shut-off needle valve, using the example of a handle opening of 10°: a) – mesh model of air flow in a bellows shut-off needle valve; b) – prismatic layers in the section of the inlet/outlet of the working medium in the mesh model; c) – the result of mesh refinement in the place where the working medium passes between the metering needle and the body seat

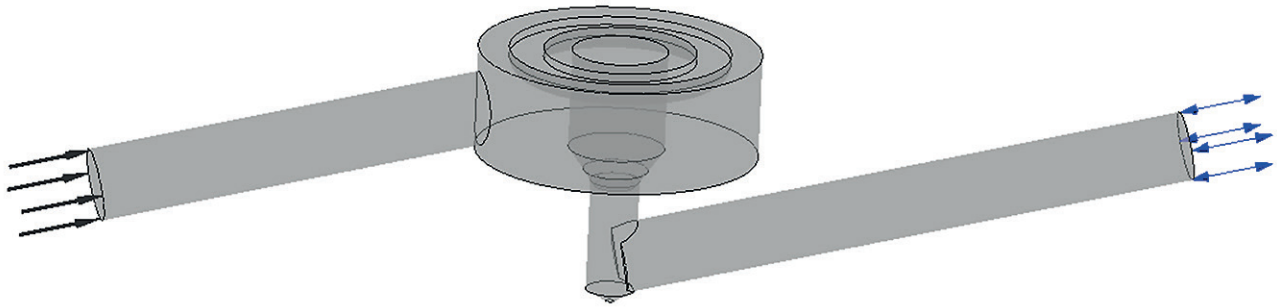


Fig. 5. Calculation model with boundary conditions

ISSN 2075-8545 (online)

Table 1. Technical characteristics of the tested valve

Parameter	Value
Nominal diameter, DN, mm	10
Working fluid temperature, °C, max	350
Working fluid pressure, MPa, max	20

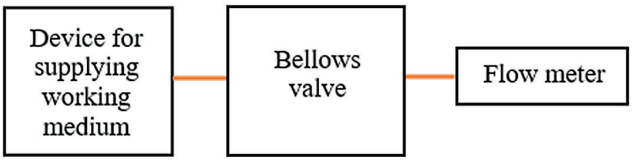


Fig. 6. Diagram of the stand for determining flow characteristics

of the bellows-type shut-off needle valve to the required angle. A flow meter measures the flow of the working fluid at the valve outlet. The air is released into the atmosphere.

Parameters of the test bench components:

– the compressor supplies compressed air at a pressure of $p_{вх}$ = 1.42 MPa;
– the position template of the bellows shut-off needle valve flow regulator allows for precise setting of the angular position of the regulator handle in 5° incrementsl;
– the flow meter measures the flow rate of the working medium at the valve outlet with an accuracy of ±1%.

Blowing on the stand was carried out according to the following law: turning the handle of the control rod in 5° increments and holding for one minute to equalize the flow indicators.

The error calculation was carried out using the relative error method, according to the following formula:

$$\delta = \Delta / x_{ист.} \cdot 100\%, \quad (1)$$

where Δ – limits of permissible absolute error;

x – the value of the measured quantity at the input (output) of the measuring instrument.

RESULTS AND DISCUSSION

The results of determining the flow velocity vectors in the valve, as well as the results of the total pressure distribution in the valve cross-section (Pa) when the control rod handle is opened by 10°, 45°, and 90° during the FE analysis are presented in Fig. 7–12.

The obtained results show that, with a sufficiently large valve opening (45° and 90°), turbulent phenomena (swirl, flow mixing, etc.) arise and continue to grow, the impact of which on the flow significantly exceeds the impact of similar phenomena when the valve is opened by 10°. Subsequently, it is these phenomena that play a key role in the occurrence of pulsations in the flow rate of the working medium, shown in Fig. 13.

Table 2 shows the experimental data obtained as a result of bench tests of a bellows shut-off needle valve.

Based on the results obtained during the FE analysis, as well as the results of bench tests, the dependence of air flow on the angle of rotation of the handle of the control rod of the bellows shut-off needle valve was established, which is presented in the form of a graph in Fig. 13.

Analysis of the results obtained during the blowdown test shows that the flow rate of the working fluid is not linearly related to the valve handle angle. A steady increase in flow rate is observed over a range of handle angles from 0° to 40°. This indicates that, with a relatively small valve opening, the working fluid flows through the valve without significant disturbances.

As the handle opening angle increases further from 40° to 60°, the flow rate pattern changes. The graph shows abrupt changes, which can be explained by the relatively large opening of the valve seat. This leads to phenomena (flow stalls, turbulence, etc.), causing flow rate fluctuations on the graph [9].

After reaching a 60° rotation angle, the flow rate curve becomes oscillatory. In this section, the flow is constantly and significantly affected by turbulence and becomes unstable, making it difficult to accurately determine the air flow rate.

Table 3 provides a comparative analysis of the air flow rates obtained from the finite element analysis and from the results of full-scale rig tests.

Having analyzed the results presented in Table 3, we can conclude that the discrepancy between the air flow values obtained during the FEM calculation and during bench tests, depending on the value of the valve handle rotation angle, is no more than 5%, which confirms the required accuracy and correctness of the FEM analysis.

CONCLUSION

Based on the data obtained from the research conducted, the following main conclusions were formulated:

1. It has been shown that the design of the bellows shut-off needle valve allows it to be used as a high-quality shut-off switchgear in critical industries with high operating environment parameters (pressure, temperature and flow).

2. A rig test of the bellows valve was conducted, which resulted in its flow characteristic being determined. The test results revealed that, due to the geometry of the working channel, flow stalls and turbulence occur at large opening angles, leading to an oscillatory

ISSN 2075-8545 (online)

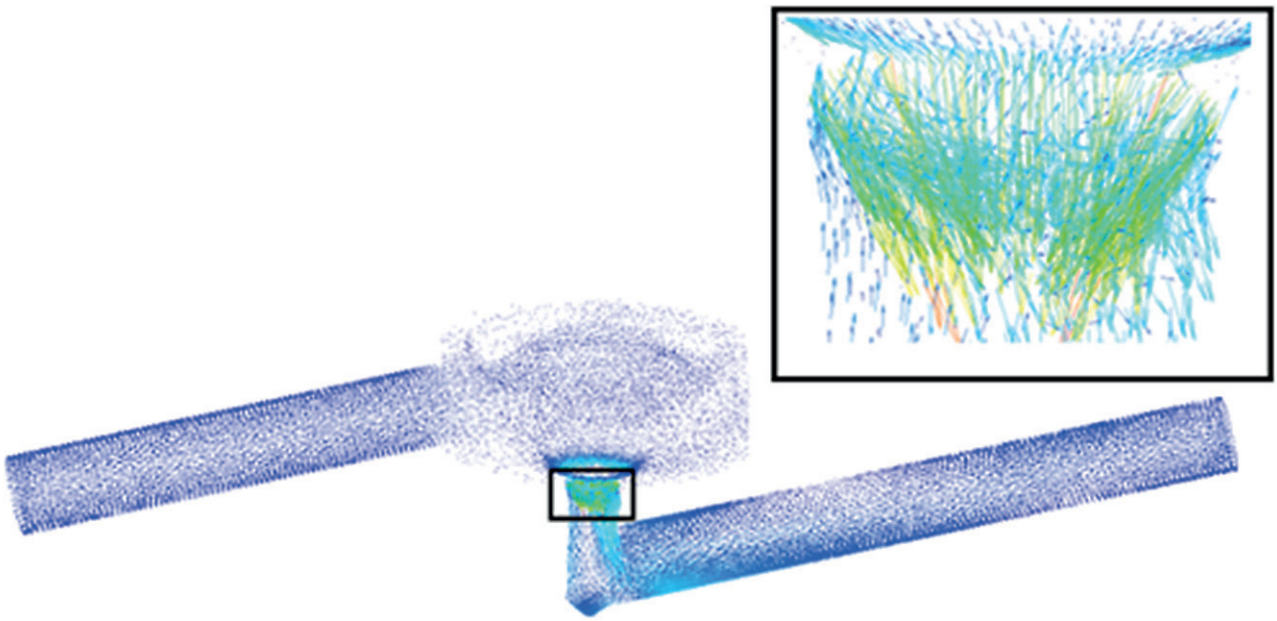


Fig. 7. Flow velocity vectors of the medium flowing through the valve when the control rod handle is opened by 10°

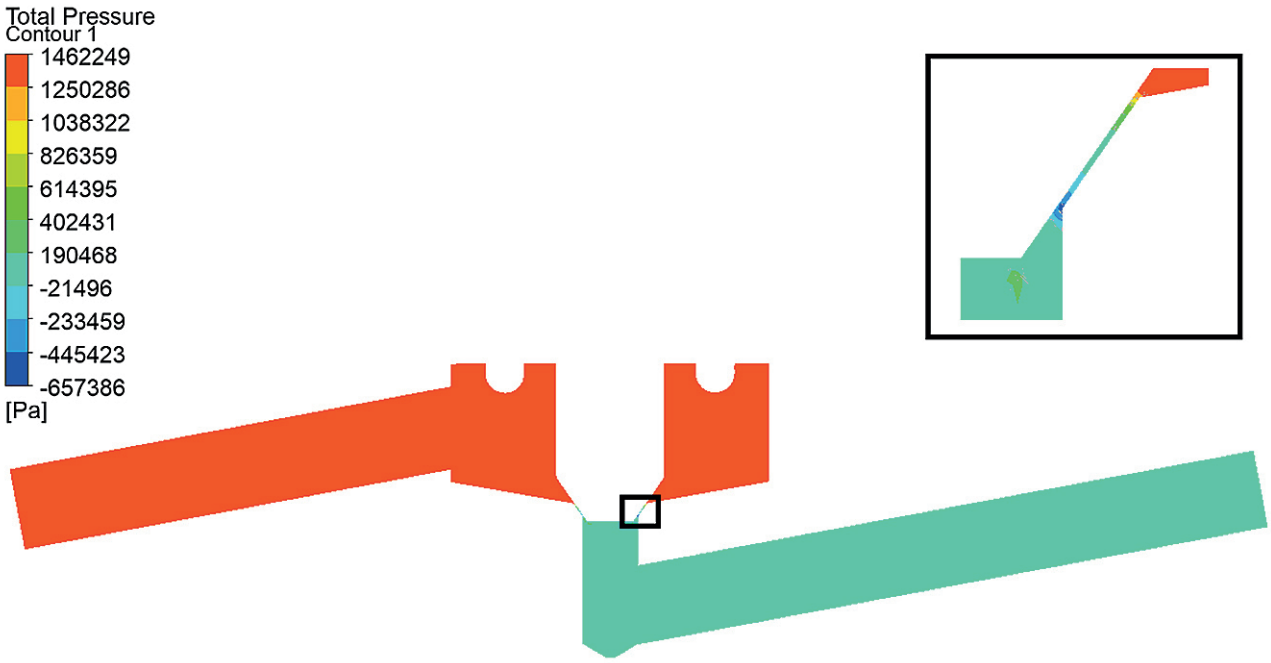


Fig. 8. Distribution of total pressure in the cross-section of the valve (Pa) when the control rod handle is opened by 10°

ISSN 2075-8545 (online)

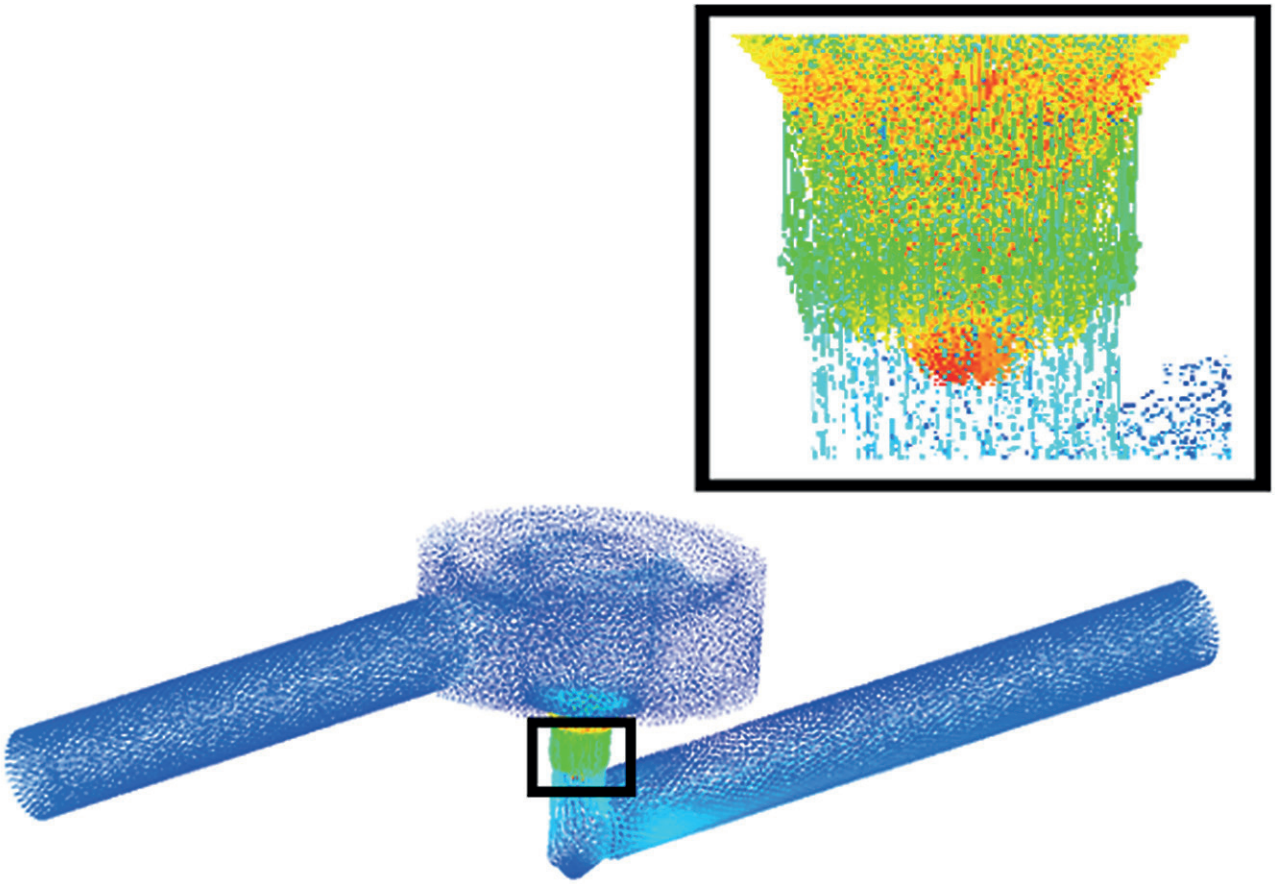


Fig. 9. Low velocity vectors of the medium flowing through the valve when the control rod handle is opened to 45°

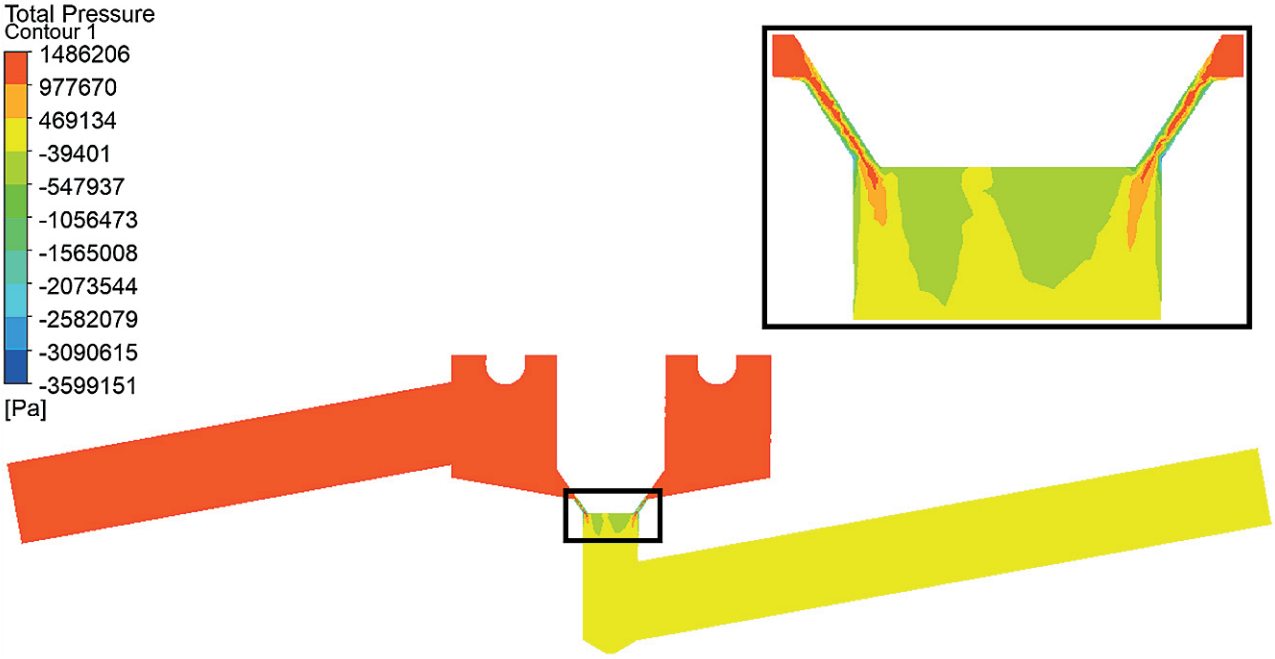


Fig. 10. Distribution of total pressure in the cross-section of the valve (Pa) when the control rod handle is opened by 45°

ISSN 2075-8545 (online)

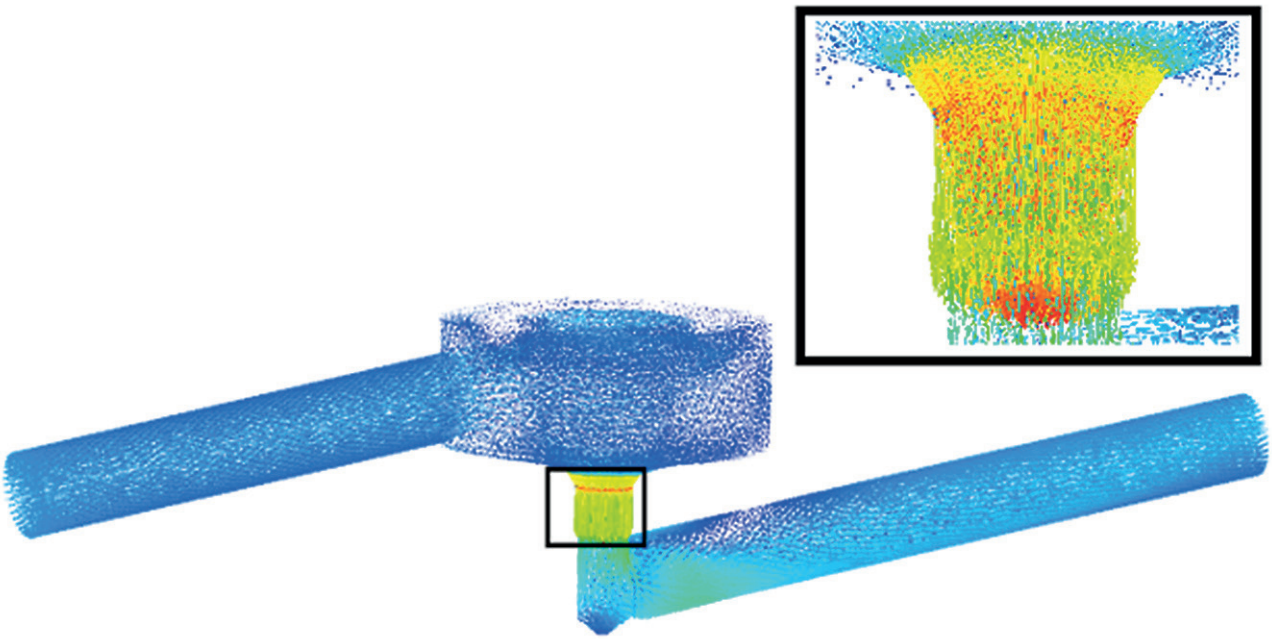


Fig. 11. Flow velocity vectors of the medium flowing through the valve when the control rod handle is opened to 90°

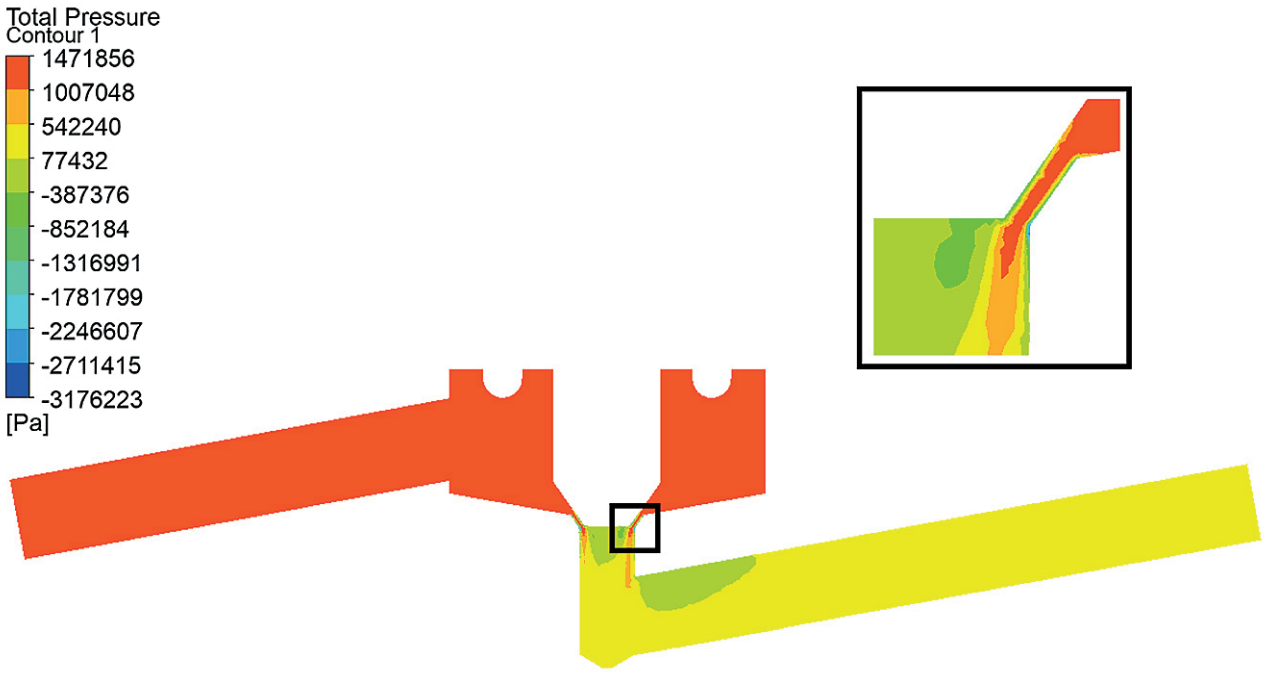


Fig. 12. Distribution of total pressure in the cross-section of the valve (Pa) when the control rod handle is opened by 90°

ISSN 2075-8545 (online)

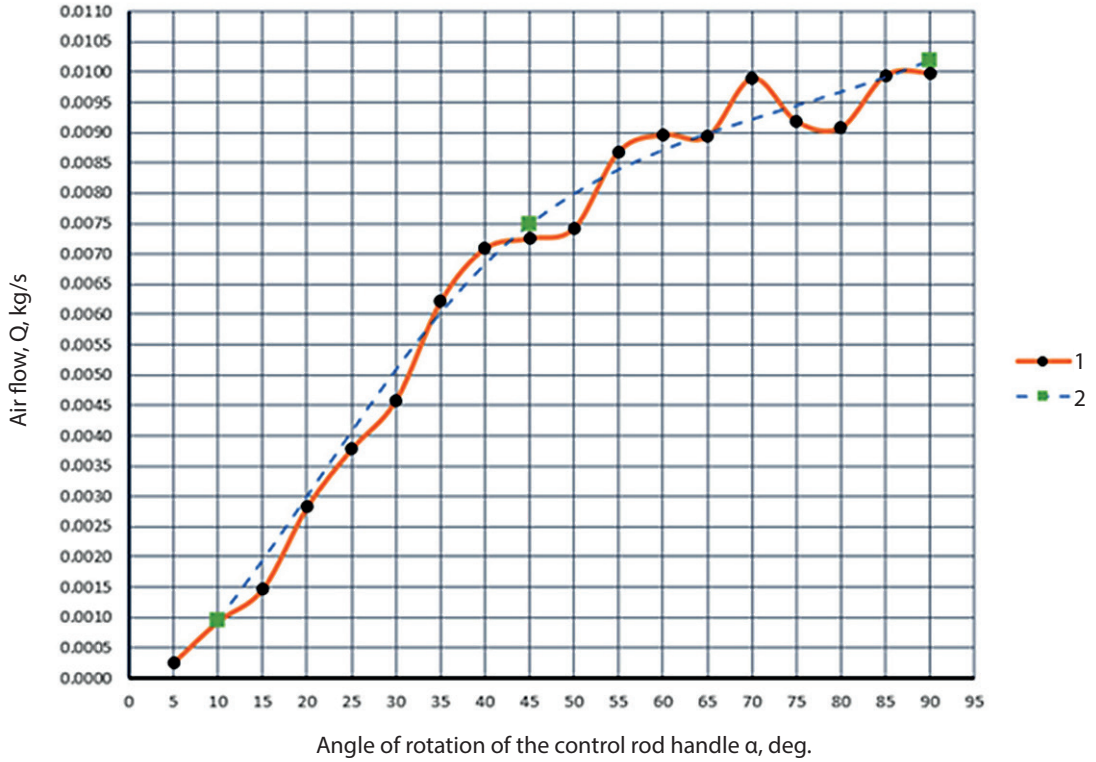


Fig. 13. Graph of air flow versus handle rotation angle of a bellows-sealed needle valve: 1 – experimental results; 2 – simulation results

Table 2. Experimental data obtained from bench tests of a bellows shut-off needle valve

Angle of rotation of the control rod handle α. deg.	Air flow. Q. kg/s
5	0.000255
10	0.000934
15	0.001468
20	0.002823
25	0.003778
30	0.004588
35	0.006216
40	0.007087
45	0.007250
50	0.007424
55	0.008687
60	0.008962
65	0.008936
70	0.009894
75	0.009180
80	0.009084
85	0.009949
90	0.009978

ISSN 2075-8545 (online)

Table 3. Comparative analysis of air flow values obtained from the results of the FE analysis, as well as from the results of full-scale tests on the stand

Calculation/ Parameter	Airflow obtained as a result of FE analysis, Q, kg/s	Airflow obtained as a result of full-scale tests, Q, kg/s	Discrepancy between results obtained by FE analysis and full-scale tests, %
Opening the valve handle by 10°	$0{,}96 \cdot 10^{-3}$	$0{,}93 \cdot 10^{-3}$	3,2
Opening the valve handle by 45°	$7{,}49 \cdot 10^{-3}$	$7{,}25 \cdot 10^{-3}$	3,3
Opening the valve handle by 90°	$10{,}2 \cdot 10^{-3}$	$9{,}98 \cdot 10^{-3}$	2,2

flow characteristic after the valve's control stem handle is opened more than 60°.

3. The FE method for analyzing the flow of the working medium in the valve allows us to determine the air flow through the valve at a certain opening angle of the control rod handle with an error of no more than 5% compared to full-scale tests on a bench.

Thus, data on the flow characteristics of bellows valves, obtained using mathematical modeling using the FE analysis method, will allow the creation of control programs for these valves for the required technological process, improving the quality of manufactured products and process safety, as well as minimizing the time of pilot testing of technological systems in which these valves are used.

REFERENCES

1. Telepneva A.V., Dymochkin D.D., Telepnev M.V. *Shut-off and control valves.* Available at: URL: https://cyberleninka.ru/article/n/zaporno-reguliruyuschaya-armatura (date of access: 04/28/2026).

2. Qingye Li, Chaoyong Zong, Fuwen Liu, Ao Zhang, Tianhang Xue, Xinhai Yu, et al. Numerical and experimental analysis of fluid force for nuclear valve. *International Journal of Mechanical Sciences*. 2022;241:107939. https://doi.org/10.1016/j.ijmecsci.2022.107939

3. Tamburrano P., Plummer A. R., Distaso E., Amirante R. A review of direct drive proportional electrohydraulic spool valves: Industrial state-of-the-art and research advancements. *Journal of Dynamic Systems, Measurement, and Control*. 2018;141(3). https://doi.org/10.1115/1.4041063

4. Churikov I.G., Arkhipov L.N., Lyscev A.F. *Bellows valve.* Patent RF No. 28904U1. 2003.

5. Onokhov Yu.A. *Bellows valve.* Patent RF No. 2250404C1. 2005.

6. Marco Simic, Niko Herakovic. Reduction of the flow forces in a small hydraulic seat valve as alternative approach to improve the valve characteristics. *Energy Conversion and Management*. 2015;89:708–718. https://doi.org/10.1016/j.enconman.2014.10.037

7. Xolani Prince Hadebe, Bernard Xavier Tchomeni Kouejou, Alfayo Anyika Alugongo, Desejo Filipeson Sozinando. Finite Element Analysis and Computational Fluid Dynamics for the Flow Control of a Non-Return Multi-Door Reflux Valve. *Fluids*. 2024;9(10):238. https://doi.org/10.3390/fluids9100238

8. Zhihui Zhao, Zhe Wu, Weiqiang Wang, Xingyu Wang, Shengnan Du, Xianlei Chen, et al. CFD-DPM Model of Gas–Solid Two-Phase Flow Erosion of Needle Throttle Valve. *Coatings*. 2025;15(2):248. https://doi.org/10.3390/coatings15020248

9. Xie Haibo, Li Tan, Jianbin Liu, Hanben Chen, Huayong Yang. Numerical and experimental investigation on opening direction steady axial flow force compensation of converged flow cartridge proportional valve. *Flow Measurement and Instrumentation*. 2018;62:123–134. https://doi.org/10.1016/j.flowmeasinst.2018.05.013

10. Lei Chen, Ce Zhang, Bo Jin, Yuan Tangbo. Simulation and experimental research on steady flow force compensation for a servo proportional valve. *Flow Measurement and Instrumentation*. 2023;94:102457. https://doi.org/10.1016/j.flowmeasinst.2023.102457

11. Jilu Liu, Ruichuan Li, Xinkai Ding, Qi Liu. Flow force research and structure improvement of cartridge valve core based on CFD method. *Heliyon*. 2022;8(11):e11700. https://doi.org/10.1016/j.heliyon.2022.e11700

ISSN 2075-8545 (online)

12. GOST 34437-2018. *Pipeline fittings. Methodology for experimental determination of hydraulic and cavitation characteristics*. Moscow: Standartinform, 2018.

13. Suyao Gui, Shishuang Zhang, Bo Fu, Mingxiang Ling. Fluid-dynamic analysis and multi-objective design optimization of piezoelectric servo valves. *Flow Measurement and Instrumentation*. 2022;85:102157. https://doi.org/10.1016/j.flowmeasinst.2022.102157

14. Niko Herakovic, Jozef Duhovnik, Marco Simic. CFD simulation of flow force reduction in hydraulic valves. *Tehnicki vjesnik*. 2015;22(2):453–463. https://doi.org/10.17559/TV-20141128090939

15. Stepanenko N.Y., Chertovskikh S.V., Lukyanov V.V. The study of the formation of a hollow cellular structure with a given geometry. *Nanotechnologies in construction*. 2025;17(4):455–465. https://doi.org/10.15828/2075-8545-2025-17-4-455-465

16. Stepanenko N.Yu., Chertovskikh S.V., Lukyanov V.V., Astanin V.V. Manufacturing technology of protective edges for polymer composite products. *Bulletin of Tula State University. Technical sciences*. 2024;8:197–203.

17. Stepanenko N.Yu., Chertovskikh S.V., Lukyanov V.V. Optimization of the geometry of the characteristic section of a complex-profile thin-walled workpiece of the original geometry using modeling and finite element analysis methods. *Materials. Technologies. Design*. 2025;7(3):5–20. https://doi.org/10.54708/26587572_2025_73225

18. Xinkai Ding, Ruichuan Li, Jikang Xu, Qi Liu, Yi Cheng, Jilu Liu. Study on flow force compensation characteristics and optimization design of jet guiding groove. *Flow Measurement and Instrumentation*. 2022;86:102194. https://doi.org/10.1016/j.flowmeasinst.2022.102194

ADDITIONAL INFORMATION

The authors declare that generative artificial intelligence (AI) and AI-based technologies were not used in the preparation of this article.

INFORMATION ABOUT THE AUTHORS

Nikolai Yu. Stepanenko – Postgraduate student, Department of Technological Machines and Equipment, Ufa State Petroleum Technological University, 450064, Ufa, Kosmonavtov St., 1, Republic of Bashkortostan, Russian Federation, koly.stepanenko@yandex.ru, https://orcid.org/0009-0002-0843-480X

Sergey V. Chertovskikh – Cand. Sci. (Eng.), Head of the Department of Technological Machines and Equipment, Ufa State Petroleum Technological University, 450064, Ufa, Kosmonavtov St., 1, Republic of Bashkortostan, Russian Federation, chertovskikh@mail.ru, https://orcid.org/0000-0001-9758-7677

Aleksey V. Rubtsov – Cand. Sci. (Eng.), Associate Professor, Department of Technological Machines and Equipment, Ufa State Petroleum Technological University, 450064, Republic of Bashkortostan, Ufa, Kosmonavtov St., 1, Russian Federation, sunset202@mail.ru, https://orcid.org/0000-0001-6087-5579

Nikita E. Ivanov – Research engineer at the Center for Intelligent Engineering, Ufa State Petroleum Technological University, 450064, Ufa, Kosmonavtov St., 1, Republic of Bashkortostan, Russian Federation; electronics engineer, Scientific and Production Association «Technopark of Aviation Technologies», 450027, Ufa, Tramvaynaya St., 5, bldg. 1, Republic of Bashkortostan, Russian Federation, nikita.ivan2001@yandex.ru, https://orcid.org/0009-0006-6184-3011

CONTRIBUTION OF THE AUTHORS

N.Yu. Stepanenko – modeling and finite element analysis, working with Ansys CFX software. Performed bench tests and interpreted the obtained data.

S.V. Chertovskikh – scientific supervision of the project, development of the overall structure of the article, quality control of all stages of the research, scientific editing and revision of the text, formation of conclusions and recommendations for practical application. Participation in formulating the goal and objectives of the study, writing the introduction and conclusion, and substantiating the practical significance of the work.

A.V. Rubtsov – contributed to the writing and editing of the article.

N.E. Ivanov – performing modeling and finite element analysis, working with the MSC Marc software package.

The authors declare no conflicts of interest.

The article was submitted 10.07.2026; approved after reviewing 07.10.2026; accepted for publication 10.10.2026.

ISSN 2075-8545 (online)

Nanotechnologies in construction
Нанотехнологии в строительстве

2026; 18 (5):
713–716

Nanobuild.ru

PUBLICATION ETHICS AND PREVENTION OF MALPRACTICE PUBLICATION

Compliance requirements of publication ethics in the preparation and publication of the journal Science Editor and Publisher apply to all members of the publishing process, i.e., authors, editors, reviewers, and the publisher of the journal. The editorial board monitors compliance with the ethics requirements based on the manuals prepared by international specialized organizations, associations and publishers, as well as the Association of Science Editors and Publishers. The main standards relied on by the journal «Nanotechnologies in construction» are those developed by the Committee on Publication Ethics (Committee on Publication Ethics) in the United Kingdom, by the publisher Elsevier (Netherlands), and other non-Russian editorial associations and information systems, as well as the declaration of «Ethical Principles of Scientific Publications», adopted by the Association of Science Editors and Publishers (Russia).

The responsibility of the authors of material for the journal «Nanotechnologies in construction»

1. The author submits materials for review, which have not been previously published. If the article is based on previously published material which are not academic articles or based on materials presented on the Internet, the author should notify the editorial staff of the journal.
2. The author does not submit the same article to different journals for review.
3. All co-authors consent to the submission of their articles to the journal.
4. The author should inform the editorial staff about a potential conflict of interest. In the case of the absence of any competing interests the author should claim that by writing «Author declare the absence of any competing interests» in the paper.
5. The author takes the necessary steps to ensure the correctness of citations in the submitted article.
6. The list of authors included only individuals who have made significant contributions to the research.
7. The author correctly cites his or her previous work as to avoid self-plagerism in the manuscript and the artificial increase of volume of publications (salami-slicing).
8. The author, who is acting as the contact with journal, informs all other co-authors of all changes and suggestions from the editorial staff, and does not make decisions regarding the article alone without the written consent of all co-authors.
9. The author properly corresponds with the reviewer through contact with the editor and responds to comments and observations if they arise.
10. If necessary, the authors either adjust the data presented in the article, or refute them.

Responsibility of the editors of the journal «Nanotechnologies in construction»

1. The editors are personally and independently responsible for the content of the materials published and recognize that responsibility. The reliability of the work in question and its scientific significance should always be the basis in the decision to publish.
2. The editors of the journal can check the materials with anti-plagiarism system «Antiplagiat» detecting borrowed fragments to provide copyright protection.
3. The editors make fair and objective decisions, regardless of any commercial considerations and provide a fair and efficient process for the independent review.
4. The editors evaluate manuscripts' intellectual content without regard to race, gender, sexual orientation, religion, origin, nationality, and/or the political preferences of the authors.
5. The editors do not work with articles for which they have a conflict of interest.
6. The editors resolve conflict situations arising during the editorial process, as well as use all available means to resolve these situations.
7. The editors of the journal publish information concerning corrections, rebuttals, and review articles in case the need arises.
8. The editors of the journal do not publish the final version of the article without the consent of the authors.

ISSN 2075-8545 (online)

The responsibility of the reviewers of the journal «Nanotechnologies in construction»

1. The reviewer evaluates his or her own availability before the examination of the manuscript and accepts materials for review only if the reviewer is able to allow for sufficient time as to ensure the quality his or her work.

2. The reviewer must use the form created by the editors and delivered with paper. The reviewer may give extended review.

3. The reviewer notifies the editorial staff of any conflict of interest (if one exists) before the start of the review of the paper.

In the case of the absence of any competing interests the reviewer should claim that by writing «The reviewer declares the absence of any competing interests» in the review.

4. The reviewer does not send information about the article and or any of the data contained within the article to any third party.

5. The reviewer does not use the information obtained from the article for any personal and or commercial purposes.

6. The reviewer does not make conclusions about the quality of the article on the basis of subjective data, e.g. the personal relationship to the author, gender, age, religion, etc.

7. The reviewer uses only proper and appropriate language and explanations in respect to the articles, avoiding any personal remarks.

The responsibility of the publisher of the journal «Nanotechnologies in construction»

1. The publisher not only supports scientific communication and invests in the process, but is also responsible for complying with all current guidelines and standards for publishing scientific work.

2. The publisher does not affect the editorial policy of the journal.

3. The publisher provides legal support to the journal if necessary.

4. The publisher provides for the timely release of futures issues of the journal.

5. The publisher publishes changes, explanations, and recalls articles that have been identified to contain scientific misconduct and or critical errors.

The responsibility of the editor-in-chief of the journal «Nanotechnologies in construction»

1. The editor-in-chief is responsible for making a decision which of submitted papers are to be published in the journal. This decision always must be based on the examination of paper reliability and its importance for scientists and readers. The editor-in-chief may be guided by methodical recommendation elaborated by the editorial board of the journal. He also may take into account legal requirements, such as exclusion of libel, infringement of copyright and plagiarism. When making decision on the publication, the editor-in-chief may consult with the members of editorial board, reviewers.

2. The editor-in-chief evaluates submitted papers by the intellectual content, regardless of the race, sex, sexual preference, religion, ethnic origins, citizenship and political views of the author.

3. The editor-in-chief, editorial staff, members of the editorial board must not disclose information on the submitted manuscript to the third person except for the author, reviewers, potential reviewers, and the publisher.

4. The information contained in the submitted paper cannot be used in the paper of the editor-in-chief, members of the editorial board without author's written permission. Confidential information or ideas obtained during review must be kept in secret and must not be used for self-profit.

5. The editor-in-chief should not review the paper if there is a conflict of the interests evolving from competition, cooperation or other relations with someone from the authors, companies and organizations which are related to the paper.

6. The editor-in-chief should ask all authors to present information on the certain competitive interests and publish corrections if the conflict of the interests has been revealed after the publication. If necessary another appropriate action such as publication of disproof or expression of a concern can be performed.

7. The editor-in-chief should take reasoned and prompt measures if he gets complaints of ethnic character in respect to the submitted manuscript or issued paper, contacting with the editors and publisher.

Complaints and appeals handling

In the case of incoming complaints and appeals a commission is formed. The commission can consist of the publisher, the editor-in-chief, deputy editor-in-chief, members of editorial council, authors and specialists which are competent in the considering subjects.

An investigation is held and the results of it are reported to all interested parties. According to laws, if it is necessary, the materials are delivered to competent state bodies.

ISSN 2075-8545 (online)

Policy of disclosure and conflicts of interest /competing interests

Unpublished data from manuscripts submitted for consideration can not be used for personal research without the expressed written consent of the author.

Information or ideas obtained through peer review and related actives, which potentially can be beneficial to any party other than the author, must be kept confidential and not be used for personal gain.

The editors and reviewers should not participate in the examination of manuscripts in the event of a conflict of interest that is a result of any competitive, cooperative, and or other interactions and relationships with any of the authors, companies, and or other organizations involved in the creation or presentation of the works.

The politics of the journal concerning data exchange and reproductibility

The journal papers (metadata of papers) are available for free access at the journal's website and at the websites of different citation systems (data bases).

The authors of the materials published in the journal permit using their content according to the license Creative Commons CC-BY «Attribution». This kind of license allows other people to distribute, edit, correct and base on the work of the authors, even with commercial purpose, while the authors mention them as co-authors. The license is recommended to distribute widely and use licensed materials.

The politics of the journal concerning data exchange and reproducibility are aimed at providing «transparent» science and transparency is a guarantee of high-quality research and innovations.

Ethical oversight of the published materials

The publisher and the editor-in-chief should deal with protection of reputation of the published materials by studying and evaluating claimed or potential delinquency (research, publications, reviews and editorial activities) jointly with scientific community.

That means interaction with the author of the manuscript and detailed consideration of the complaints or declared reclamations. To detect such delinquencies as plagiarism, the editor must use proper license software or systems.

If the editor-in-chief obtains proved evidence of delinquency, he must inform the publisher and the members of editorial council about this, as well as immediately notify the author about necessity to correct the paper or paper retraction (in dependence on the situation).

Derivation and plagiarism

During the consideration of an article, the editorial staff of the journal «Nanotechnologies in construction» may conduct a verification of the submitted materials with the help the Anti-plagiarism system. In the case of the discovery of multiple incidents of content matching, the editorial staff acts in accordance with the rules of COPE.

Intellectual property

The editors should carefully deal with the issues concerning intellectual property and interact with the publisher when settling the cases of probable delinquencies and agreements on intellectual property protection.

The editors aside from using plagiarism detecting tools can also:

– support the authors whose copyright was infringed or those who suffered from plagiarism;
– cooperate with the publisher to protect copyright and to pursue infringer (for example, by applying for paper retraction or removing materials from websites).

Discussion of the papers published in the journal. Corrections made after publication

The editors must be open for the researches that oppose the papers published earlier in the journal; to encourage and to be ready to consider valid criticism of the papers published in the journal.

The authors of the criticized works should have an opportunity to respond the criticism. The papers describing only negative results can also be published.

Preprint and postprint policy

During the submission process, the author must confirm that the article has not been published and or accepted for publication in any other journal. When citing articles published in the journal «Nanotechnologies in construction», the publisher requests the authors to provide a link (the full URL of the material) to the official website of the journal.

Articles, which have been previously posted by the author on personal and or public websites that have no relationship to any other publishers, are allowed to be submitted to the journal.

ISSN 2075-8545 (online)

On the procedure in case of abusive practice (infringement)

Publisher, editor-in-chief, each member of editorial staff member of editorial board, author, reviewer or reader must comply journal's Publication Ethics and are obliged to report any known facts concerning committed or potential infringement.

The journal's editors immediately launch investigation on all messages that state abusive practice (infringements). If the information is confirmed, the measures to eliminate claimed abusive practice (infringements) will be taken. According to legislation, all materials, if it is necessary, are referred to proper state bodies.

In response to all author's claims the editors give full and substantiated replies and make great efforts to resolve any conflicts.

Policy of using generative artificial intelligence

Generative artificial intelligence (AI) and artificial intelligence-based technologies can be used to improve the language of a manuscript, such as grammar, syntax, and spelling. In this case, no statements about the use of AI are required from the author(s).

In all other cases, the authors should disclose the use of generative AI technologies in the "Additional information" section of their manuscript. The application may be as follows: "During the preparation of the manuscript, we used [the name of the tool/service] for [a reason]. After using this tool/service, we have reviewed and edited the content as necessary and assume full responsibility for the content of the published article." This means that the use of AI-generated technologies should be accompanied by human supervision and control. Authors should carefully check and edit the results obtained, as the text generated by AI can often be erroneous, incomplete, or biased. The authors are fully responsible for the content of their work.

If the manuscript contains images created or modified using generative AI or AI-supported tools, the authors should report this in the "Additional Information" section. They should provide a detailed description of when and how these tools were used. In addition, the authors must confirm that they have obtained all permissions to use the materials.

The authorship of a manuscript can only be attributed to a person. AI and AI-enabled technologies cannot be listed as author(s) or co-author(s) due to their inability to meet the criteria of authorship. They cannot take responsibility for the work, approve publication, manage copyrights, or resolve issues related to conflicts of interest.

Personal Data Processing Policy (for Authors, Reviewers, and Readers)

The Editorial Board of the Electronic Edition «Nanotechnologies in Construction: A Scientific Internet Journal» has established its policy regarding the processing of personal data of **authors, editors, reviewers, and readers** in accordance with the Provisions of the Federal Law of the Russian Federation dated July 27, 2006, No. 152-Federal Law «On Personal Data» (hereinafter referred to as the «Personal Data Law»). This policy is aimed to ensure the protection of human and civil rights and freedoms during the personal data processing, including the protection of the right to privacy, personal privacy, and family confidentiality.

More detailed information is available on the website of the Electronic Edition «Nanotechnologies in Construction: A Scientific Internet Journal».

ISSN 2075-8545 (online)

Nanotechnologies in construction
Нанотехнологии в строительстве

2026; 18 (5):
717–722

Nanobuild.ru

AUTHOR GUIDELINES

Admission of articles

The authors submit to the editors:

- electronic manuscript by e-mail: info@nanobuild.ru;
- accompanying letter (the editors send the sample of the letter to the authors on demand).

The authors of the materials published in the journal permit using their content according to the license Creative Commons Attribution 4.0 International (CC-BY 4.0); agree to publish full texts (parts or metadata) of the paper in free access in Internet at the official website of the edition (www.nanobuild.ru), citation systems (data bases). All that authors indicate in the cover letter. More details about the license Creative Commons Attribution 4.0 International (CC-BY 4.0) are available here https://creativecommons.org/licenses/by/4.0/.

When submitting articles to the journal, it is presumed that:

- the work has not been previously published in any other journal;
- the article is not under consideration in any other journal;
- all co-authors consent to the publication of the article;
- there is implicit or explicit consent of the organization in which the study was conducted.

Information about the conflict of interest

The article should exclude any actual or potential conflict of interest. If there is no conflict of interest, you should write that «the author declares no conflict of interest.»

When submitting a manuscript to the journal, authors should ensure that the content of the paper corresponds the topic of the journal; the structure and the format of the paper meet the editorial requirements; all citations are properly formatted and the source of tables and figures are shown (unless otherwise indicated, it is assumed that the tables and figures created by the author).

Basic sections of the journal:

- construction material science;
- the study of the properties of nanomaterials;
- the results of the specialists' and scientists' researches;
- manufacturing technology for building materials and products;
- international scientific and technical cooperation;
- overview of inventions in the field of nanotechnology;
- development of new materials;
- rational use of natural sources;
- efficient use of recycled resources;
- the application of nanomaterials and nanotechnologies in construction;
- system solutions for technological problems;
- in related sectors;
- forums, exhibitions, conferences and events in the area of construction and nanoindustry.

These are the topics of the papers published in the journal: creation of new functional materials; nanostructured systems strength and penetrability formation theory development; the problems of nanomaterials and nanotechnologies implementation in construction and building materials; cement and other binders with mineral and organic additives; diagnostics of building systems nanostructures and nanomaterials; modification of building materials with nanofibers; disperse composite materials with nanocoating; formation of nanostructure coatings by means of laser sputtering; technologies aimed at studying nanomaterial properties; the systems of teaching the fundamentals of nanotechnologies; technological principles of nanostructures creation (liquid melts, sol and gel synthesis). The topics may be different, directly or indirectly related to the areas mentioned above.

The journal can also publish: original article, review article, editorial, discussion paper, individual bibliography, editorial notes, book reviews, article reviews, etc.

ISSN 2075-8545 (online)

The structure of the paper

IN ENGLISH

NAME OF THE SECTION (In English)
Original article (review article, editorial, discussion paper, individual bibliography, editorial notes, book reviews, article reviews, etc.) (In English)
https://doi.org/10.15828/2075-8545-202X-x-x-x-x

Title (In English)
Authors' First name. The first letter of the patronymic (if any) Last name (In English)
place of employment of each author, city, country (In English)
(*name of institution (organization) at which the author works or studies is given without legal form: Ltd, SOE, etc.*)
*Corresponding author: e-mail: xxxxxxxxxx

ORCID author:
first name and last name – https://orcid.org/xxxx-xxxx-xxxx-xxxx

Abstract: the source of information, which is independent on the paper and which allows Russian and foreign specialists to make conclusion about the quality of the content of the paper (extended abstracts must be informative, original, novelty, contain main results of research, structured according to IMRAD (Introduction, Methods and Materials, Results and Discussion), compact – 200–250 words) (In English):
Abstract: Introduction... Methods and Materials... Results... Discussion... Conclusion...
Keywords: (In English) They are separated from each other by commas and there are no dots placed after the last one
Acknowledgments / Sources of funding for scientific research: (In English)
For citation: (In English)

Example.
For citation: Nizin D.R., Nizina T.A., Spirin I.P., Chibulaev I.A., Pivkin N.A. The effect of the concentration of nanomodifiers and the moisture content of samples on the change in the properties of epoxy polymers. *Nanotechnologies in Construction.* 2024;16(6):499–509. https://doi.org/10.15828/2075-8545-2024-16-6-499-509. – EDN: QGYFFZ.

© authors, 2025

Text of the paper: (In English, number of words 3000–6000)
- **INTRODUCTION**
- **METHODS AND MATERIALS**
- **RESULTS**
- **DISCUSSION**
- **CONCLUSIONS**

References (In English) (according to Vancouver Style).

Example:
1. Nizin D.R., Nizina T.A., Maryanova A.V., Mironov E.B. Moisture absorption of 3D-printed PETG plastic Samples. *Bulletin of MGSU.* 2023;18(7):1078–1088. https://doi.org/10.22227/1997-0935.2023.7
2. Venkatraman V. Conventions of Scientific Authorship. Science. 16 April 2010. Available at: https://www.science.org/content/article/conventions-scientific-authorship-0 (accessed: 13.05.2024).
3. Allen L., Scott J., Brand A., Hlava M., Altman M. Publishing: Credit where credit is due. *Nature.* 2014;508(7496):312–313. https://doi.org/10.1038/508312a
4. Mekeko N., Tikhonova E. Description of Author Contributions while Submitting a Manuscript: The CREDITSystem. *Journal of Employment and Career.* 2022;1(4):5–7. (In Russ.) https://doi.org/10.56414/jeac.2022.24

Note: 1. The titles of journals, books, etc. are indicated in italics.
2. Materials published only in Russian are indicated (In Russ.)

ISSN 2075-8545 (online)

Additional information (on the use of generative artificial intelligence and artificial intelligence-based technologies) (In English)

Examples:
The authors declare that generative artificial intelligence technologies and technologies based on artificial intelligence were not used in the preparation of the article.
or
During the preparation of this article, [tool/service name] was used for [reason]. After employing this tool/service, the content has been revised and edited as needed and I take full responsibility for the content of the published article.

Information about the author (authors) (In English)
– First name The first letter of the patronymic (if any) Last name (full);
– academic degree;
– academic title;
–name of institution (organization) and its department at which the author works or studies is given without legal form: Ltd, SOE, etc.;
– address of the institution (organization), its department at which the author works or studies (city and country);
– authors' e-mail address;
– Open Researcher and Contributor ID (ORCID) (if available).
E-mail address is given without word "e-mail" and is not followed by dot. ORCID is given as an electronic address in Internet and is not followed by dot. Name of institution (organization), its address, e-mail address and ORCID of the author are separated with a comma.
The editors can give additional information about the author: position, honorary title, membership in organizations, etc.

Example.
Zhanna V. Pisarenko – Dr. Sci. (Econ.), Professor, Saint-Petersburg State University, Economic Faculty, Department of Risk Management and Insurance, Saint-Petersburg, Russian Federation,
z.pisarenko@spbu.ru, https://orcid.org/0000-0002-9082-2897

Contribution of the authors (In English):
author's First name The first letter of the patronymic (if any) Last name (full); author's personal contribution in article writing is briefly described (concept, collection of materials, analytical work, article writing, scientific editing of the text, etc.).

Example.
Marina S. Morozova – scientific management; research concept; methodology development; participation in development of curricula and their implementation; writing the draft; final conclusions.
Elena V. Bokova – participation in development of curricula and their implementation; follow-on revision of the text; final conclusions.

The authors declare no conflicts of interests.

The article was submitted XX.XX.202X; approved after reviewing XX.XX.202X; accepted for publication XX.XX.202X.

IN RUSSIAN

NAME OF THE SECTION (In Russian)
Original article (review article, editorial, discussion paper, individual bibliography, editorial notes, book reviews, article reviews, etc.) (In Russian) / (In English)
https://doi.org/10.15828/2075-8545-202X-x-x-x-x

Title (In Russian)

ISSN 2075-8545 (online)

Authors' first name and last name (In Russian)
place of employment of each author, city, country (In Russian)
(*name of institution (organization) at which the author works or studies is given without legal form: Ltd, SOE, etc.*)
* Corresponding author: e-mail: xxxxxxxxxx

ORCID author: first name and last name (In Russian) – https://orcid.org/xxxx-xxxx-xxxx-xxxx

Please note! Manuscripts without an ORCID will not be accepted. If the author does not have an ORCID, they must register at https://orcid.org/ and fill in the required information.

Abstract: the source of information, which is independent on the paper and which allows Russian and foreign specialists to make conclusion about the quality of the content of the paper (extended abstracts must be informative, original, novelty, contain main results of research, structured according to IMRAD (Introduction, Methods and Materials, Results and Discussion), compact – 200–250 words) (In Russian):
Abstract: Introduction... Methods and Materials... Results... Discussion... Conclusion...
Keywords: (In Russian)
Acknowledgments / Sources of funding for scientific research: (In English)
For citation: (In Russian)

Example.
Для цитирования: Низин Д.Р., Низина Т.А., Спирин И.П., Чибулаев И.А., Пивкин Н.А. Влияние концентрации наномодификаторов и влагосодержания образцов на изменение свойств эпоксидных полимеров. *Нанотехнологии в строительстве.* 2024;16(6):499–509. https://doi.org/10.15828/2075-8545-2024-16-6-499-509. – EDN: QGYFFZ.

Article Metadata (In English)
The title of the article (In English)
First name The first letter of the patronymic (if any) Last name of the author(s) (In English)
mandatory indication of the affiliation for each author, city, country (In English)
* Corresponding author: e-mail: xxxxxxxxxx
Abstract: Introduction… Methods and Materials… Results… Discussion…Conclusion…(In English)
Keywords: (In English)
Acknowledgments / Sources of funding for scientific research: (In English)
For citation: (In English)

© authors, 2025

Text of the paper: (In Russian, number of words 3000–6000)
- **INTRODUCTION**
- **METHODS AND MATERIALS**
- **RESULTS**
- **DISCUSSION**
- **CONCLUSIONS**

References (in the original language of the article – Russian or English) (Vancouver Style)

Example:
1. Низин Д.Р., Низина Т.А., Марьянова А.В., Миронов Е.Б. Влагопоглощение 3D-печатных образцов PETG-пластика. *Вестник МГСУ.* 2023;18(7):1078–1088. https://doi.org/10.22227/1997-0935.2023.7
2. Venkatraman V. Conventions of Scientific Authorship. Science. 16 April 2010. Available at: https://www.science.org/content/article/conventions-scientific-authorship-0 (accessed: 13.05.2024).
3. Allen L., Scott J., Brand A., Hlava M., Altman M. Publishing: Credit where credit is due. *Nature.* 2014;508(7496):312–313. https://doi.org/10.1038/508312a
4. Мекеко Н.М., Тихонова Е.В. Описание авторского вклада при подаче рукописи: система CREDIT. *Журнал Работа и Карьера.* 2022;1(4):5–7. https://doi.org/10.56414/jeac.2022.24

Note: 1. The titles of journals, books, etc. are indicated in italics.

ISSN 2075-8545 (online)

Additional information (on the use of generative artificial intelligence and artificial intelligence-based technologies) (In Russian)

> ***Examples:***
> The authors declare that generative artificial intelligence technologies and technologies based on artificial intelligence were not used in the preparation of the article.
> *or*
> During the preparation of this article, [tool/service name] was used for [reason]. After employing this tool/service, the content has been revised and edited as needed and I /we take full responsibility for the content of the published article.

Information about the author (authors) (In Russian)
– Last name First name Patronymic (if any) (full);
– academic degree;
– academic title;
– name of institution (organization) and its department at which the author works or studies is given without legal form: Ltd, SOE, etc. (affiliation);
– address of the institution (organization), its department at which the author works or studies (city and country);
– authors' e-mail address;
– Open Researcher and Contributor ID (ORCID) (if available).
E-mail address is given without word "e-mail" and is not followed by dot. ORCID is given as an electronic address in Internet and is not followed by dot. Name of institution (organization), its address, e-mail address and ORCID of the author are separated with a comma.
The editors can give additional information about the author: position, honorary title, membership in organizations, etc.

> ***Example.***
> **Писаренко Жанна Викторовна** – доктор экономических наук, профессор кафедры управления рисками и страхования экономического факультета Санкт-Петербургского государственного университета, г. Санкт-Петербург, Российская Федерация, z.pisarenko@spbu.ru, https://orcid.org/0000-0002-9082-2897

Contribution of the authors (In Russian):
author's last name and initials; author's personal contribution in article writing is briefly described (concept, collection of materials, analytical work, article writing, scientific editing of the text, etc.).

> ***Example.***
> **Морозова М.С.** – научное руководство; концепция исследования; развитие методологии; участие в разработке учебных программ и их реализации; написание исходного текста; итоговые выводы.
> **Бокова Е.В.** – участие в разработке учебных программ и их реализации; доработка текста; итоговые выводы.

The authors declare no conflicts of interests. (In Russian)

The article was submitted XX.XX.202X; approved after reviewing XX.XX.202X; accepted for publication XX.XX.202X. (In Russian)

Manuscript text

File format
The editors accept texts saved using Microsoft Word in .rtf format.

Text layout
- Use the font Times New Roman, font size – 14 pt., and 1.5 line spacing;
- Do not use an underscore in the text (for subtitles – use bold, to highlight text – use italics);
- Non-Russian languages titles (journals, organizations, etc.) should be left in the original, enclosed in quotes.

ISSN 2075-8545 (online)

Abbreviations

All abbreviations should be defined when first used. If the article contains a large number of abbreviations, a list deciphering each of them can be included before the text of the article

Tables and Figures

All tables and figures must be numbered and identified, they should be a reference in the text. The tables should not contain empty columns. Figures should be of good quality, suitable for printing. Figures should be submitted together with the article, with each figure submitted as an individual file.

One way to check the quality of the image, is to increase its size using any image manipulation software. A high quality image is not burred or distorted when enlarged.

Footnotes

If necessary, use footnotes with continuous numbering (Arabic numerals) throughout the document. Footnotes can be quotes from the works mentioned in the text, for more information.

Citations and bibliography

The journal requires the use of the Vancouver Citation Style (a reference in the text in square brackets, full bibliographic description of the source in the bibliography in the order mentioned in the text of the article).

The editorial board would like to remind the authors to take into account the citation policy of the journal when preparing the References section.

A proper citation (References) not only shows the quality of the research, but it also ensures that the cited publications will be taken into account when assessing the scientific work of the author. International indexing databases format all submitted references according to a unified structure. Therefore, strict requirements for unification and standardization apply to this section of scientific articles.

The journal uses an adapted version of Vancouver Citation Style, one of the styles recognized by international indexing databases.

References

The list of references includes sources used in the text.

References accepted for publication but not yet published articles must be labeled with the words “in press”; authors should obtain written permission to refer to these documents and evidence that they are accepted for publication. Information from unpublished sources must be marked with the words “unpublished data / documents,” the authors must also receive written confirmation of the use of such materials. The journal adopted the Vancouver style of reference design and citation.

Copyright Notice

Authors who publish in journal agree to the following:

1. Authors retain copyright of the work and provide the journal right of first publication of the work.

2. The authors retain the right to enter into certain contractual agreements relating to the non-exclusive distribution in the published version of the work here form (eg, post it to an institutional repository, the publication of the book), with reference to its original publication in this journal.

3. The authors have the right to post their work on the Internet (eg in the institute store or personal website) prior to and during the review process of its data log, as this may lead to a productive discussion and a large number of references to this work.

Privacy Statement

Specified when registering the names and addresses will be used solely for technical purposes of a contact with the Author or reviewers (editors) when preparing the article for publication. Private data will not be shared with other individuals and organizations.